

2. Type of Mathematical Model:

DOC.20030818.0006

- Process Model Abstraction Model System Model

Describe Intended Use of Model:

These abstractions define the damage to the waste package, drip shield, and cladding from seismic hazards and define the methodology for using these abstractions in the seismic scenario for TSPA-LA.

3. Title:

Seismic Consequence Abstraction

4. DI (including Rev. No. and Change No., if applicable):

MDL-WIS-PA-000003 REV 00

5. Total Attachments:

Nine (9)

6. Attachment Numbers - No. of Pages in Each:

I-8; II-10; III-12; IV-6; V-6; VI-6; VII-8; V-III-18;
plus 1 CD-ROM

	Printed Name:	Signature:	Date:
7. Originator:	Michael Gross	SIGNATURE ON FILE	8/13/03
8. CSO:	Michael Cline	SIGNATURE ON FILE	8/13/03
9. Checker:	Jim Kam	SIGNATURE ON FILE	8/13/03 8/13/03
	John Case	SIGNATURE ON FILE	
	James Knudsen	SIGNATURE ON FILE	
10. QER:	Ajulena T. Barnes	SIGNATURE ON FILE	8/14/2003
11. Responsible Manager/Lead:	Dennis W. Thomas	SIGNATURE ON FILE	8/14/03
12. Responsible Manager:	Tom W. Doering	SIGNATURE ON FILE	8.14.03

13. Remarks:

2. Title:

Seismic Consequence Abstraction

3. DI (including Rev. No. and Change No., if applicable):

MDL-WIS-PA-000003 REV 00

4. Revision / Change Number:

REV 00

5. Description of Revision/Change:

Initial Issue.

CONTENTS

	Page
1. PURPOSE.....	9
1.1 SCOPE.....	9
1.2 LIMITATIONS.....	10
2. QUALITY ASSURANCE.....	11
3. USE OF SOFTWARE.....	11
3.1 QUALIFIED SOFTWARE.....	11
3.2 EXEMPT SOFTWARE.....	12
3.2.1 Microsoft Excel.....	12
4. INPUTS.....	12
4.1 DATA AND PARAMETERS.....	12
4.2 CRITERIA.....	16
4.2.1 Project Requirements and Yucca Mountain Review Plan Acceptance Criteria.....	16
4.3 CODES AND STANDARDS.....	17
5. ASSUMPTIONS.....	17
5.1 DAMAGE THRESHOLD FROM VIBRATORY GROUND MOTION LIES BETWEEN MEAN ANNUAL EXCEEDANCE FREQUENCIES OF 10^{-4} PER YEAR AND 10^{-5} PER YEAR.....	17
5.2 PAGANY WASH AND SEVIER WASH FAULT DISPLACEMENTS.....	18
5.3 RESIDUAL STRESS ABOVE THE SEISMIC FAILURE CRITERION RESULTS IN FLOW PATHWAYS THROUGH THE WASTE PACKAGE AND DRIP SHIELD.....	19
5.4 DERIVING THE FORMULA FOR MEAN DOSE.....	20
5.5 RANDOMNESS OF SEISMIC EVENTS.....	20
5.6 MAJOR ASSUMPTIONS IN SUPPORTING CALCULATIONS.....	20
6. MODEL DISCUSSION.....	21
6.1 INTRODUCTION.....	21
6.1.1 Background.....	21
6.1.2 Information Sources and Outputs.....	22
6.1.3 Terminology.....	25
6.1.4 Corroborating Information.....	26
6.2 RELEVANT FEPS FOR THE SEISMIC SCENARIO CLASS.....	26
6.3 FAILED AREA CRITERIA FOR THE WASTE PACKAGE AND DRIP SHIELD.....	32
6.3.1 Residual Stress Damage Threshold for the Waste Package.....	32
6.3.2 Residual Stress Damage Threshold for the Drip Shield.....	33
6.4 GROUND MOTION AMPLITUDES AT THE EMPLACEMENT DRIFTS.....	34

CONTENTS (Continued)

	Page
6.5 FAILED AREA ABSTRACTION FOR THE WASTE PACKAGE	36
6.5.1 Initial Abstraction for Damage from Vibratory Ground Motion.....	36
6.5.2 Corroborating Information From The 10^{-5} Per Year Ground Motion Level	43
6.5.3 Independent Technical Review of Model Abstraction.....	44
6.5.4 Final Abstraction for Damage from Vibratory Ground Motion.....	46
6.6 FAILED AREA ABSTRACTION FOR THE DRIP SHIELD.....	46
6.6.1 Abstraction for Damage from Rockfall in the Nonlithophysal Zone.....	46
6.6.2 Damage from Rockfall in the Lithophysal Zone.....	56
6.6.3 Abstraction for Drip Shield Damage from Vibratory Ground Motion	58
6.6.4 Combined Abstraction for the Drip Shield.....	63
6.7 FAILURE ABSTRACTION FOR THE CLADDING	63
6.8 RESPONSE TO FAULT DISPLACEMENT.....	66
6.8.1 Clearance Between EBS Components and the Drift.....	66
6.8.2 Faults Intersecting Emplacement Drifts	70
6.8.3 Fault Displacement Hazards.....	72
6.8.4 Consequence for the Waste Packages	73
6.8.5 Damage Abstraction for Fault Displacement	78
6.8.6 An Alternate Conceptual Model For Damage From Fault Displacement.....	79
6.8.7 Final Abstraction for Damage from Fault Displacement	80
6.9 POST-SEISMIC CHANGES IN THE LOCAL ENVIRONMENT	80
6.10 SEISMIC SCENARIO CLASS	82
6.10.1 Computational Approach.....	83
6.10.2 Computational Algorithm.....	86
6.10.3 Limitations.....	97
6.11 DISCUSSION OF YUCCA MOUNTAIN REVIEW PLAN ACCEPTANCE CRITERIA.....	99
6.11.1 Treatment of Parameter Uncertainty	103
6.11.2 Treatment of Model Uncertainty (Alternate Conceptual Models)	106
6.12 VERIFICATION OF SCIENTIFIC ANALYSES FOR CLADDING AND FOR FAULT DISPLACEMENT	107
7. VALIDATION.....	108
8. CONCLUSIONS.....	111
9. INPUTS AND REFERENCES.....	112
9.1 DOCUMENTS CITED.....	112
9.2 CODES, STANDARDS, REGULATIONS, AND PROCEDURES.....	116
9.3 SOURCE DATA, LISTED BY DATA TRACKING NUMBER	116
9.4 PRODUCT OUTPUT, LISTED BY DATA TRACKING NUMBER.....	117
10. ATTACHMENTS.....	117

FIGURES

	Page
1. Schematic Diagram of the EBS Components in a Typical Emplacement Drift	23
2. Schematic Diagram Showing Locations of Points A and B	35
3. Hazard Curve for Point B is Generated by Scaling the Point A Hazard Curve.....	35
4. Comparison of Damage Results for the 10^{-7} per Year Ground Motion Level to the Cumulative Distribution Function for a Uniform Distribution.....	40
5. Comparison of Damage Results for the 10^{-6} per Year Ground Motion Level to the Cumulative Distribution Function for a Uniform Distribution.....	41
6. Linear Fit to Upper Bound of Damage Distribution.....	43
7. Comparison of Linear Fit to Bayesian Upper Bound of Damage Distribution at PGVs of 2.44 m/s and 5.35 m/s with the Results for the 10^{-5} per Year Ground Motions	44
8. Comparison of Upper Bounds Based on a Lognormal Distribution (Blue Curve) with the Bayesian Upper Bound	45
9. Flow chart of the Drip Shield Damage Abstraction Methodology	47
10. Comparison of Failed areas for PGV of 2.44 m/s (10^{-6} per year mean annual exceedance frequency) with the Fitted Log-Triangular Distribution.....	53
11. Comparison of Failed Areas for PGV of 5.35 m/s (10^{-7} per year mean annual exceedance frequency) with the Fitted Log-Triangular Distribution.....	53
12. Power Law Fit to the Mode of the Log-Triangular Distribution	54
13. Power Law Fit to the Fraction of Undamaged Cases	55
14. Schematic Diagram of EBS Components Illustrating the Clearances for Fault Displacement.....	67

TABLES

	Page
1. Direct Input Information for Seismic Consequence Abstractions	12
2. Corroborating Input Information for Seismic Consequence Abstractions	15
3. Direct Input Information for the Seismic Scenario Class	16
4. Included FEPs Relevant To Seismic Consequence Abstractions	27
5. Calculated Values of PGV on the Point B Hazard Curve.....	36
6. Damaged Area From Vibratory Ground Motion At The 10-6 Annual Exceedance Frequency.....	38
7. Damaged Area from Vibratory Ground Motion at the 10-7 Annual Exceedance Frequency.....	39
8. Damaged Area from Vibratory Ground Motion at the 10-5 Annual Exceedance Frequency.....	44
9. Summary of Rock Block Statistics for the 10-6 Annual Exceedance Frequency.....	49
10. Summary of Rock Block Statistics for the 10-7 Annual Exceedance Frequency.....	49
11. Characteristics of Selected Rock Blocks for the 10-6 Annual Exceedance Frequency.....	51
12. Damaged Area From Individual Rock Blocks Impacting the Drip Shield	51
13. Statistics for Damaged Area From Multiple Rockfalls on the Drip Shield at 10-6 and 10-7 Annual Exceedance Frequencies	52
14. Damaged Area From Vibratory Ground Motion At The 10-6 Annual Exceedance Frequency.....	60
15. Abstraction for Maximum Damage to the Drip Shield from Vibratory Ground Motion	61
16. Abstraction for Minimum Damage to the Drip Shield from Vibratory Ground Motion	63
17. Fuel Assembly Accelerations from Waste Package-to-Waste Package Impacts for a 450 Hertz Cutoff Frequency	64
18. Abstraction for Damage to the Cladding from Vibratory Ground Motion.....	66
19. Emplacement Drift Configuration Dimensions That Are Independent of the Waste Package	67
20. Waste Package Dimensions and Clearance Between Drip Shield and Waste Package.....	68
21. Maximum Allowable Displacement Before Waste Package Is Pinned.....	69
22. Intersections of Known Faults With Emplacement Drifts.....	71
23. Fault Displacement from Mean Hazard Curves.....	74
24. Design Basis Waste Package Dimensions and Inventory.....	75
25. Parameters for Simplified Groups of Waste Packages	75
26. Maximum Allowable Fault Displacements Before a Waste Package Group Is Pinned	76
27. Fault Exceedance Probabilities That Cause Failure in the Lower Lithophysal Zonea	77
28. Expected Number of Waste Packages Emplaced On Faults.....	77
29. Expected Waste Package Failures versus Annual Exceedance Frequency	78
30. Definition of Parameters for the Seismic Scenario Class	92
31. Comparison of Seismic Abstractions with Objective Evidence for Review Criteria	102

ACRONYMS AND ABBREVIATIONS

BWR	boiling water reactor
DHLW	defense high-level radioactive waste
DOE	U.S. Department of Energy
DTN	data tracking number
EBS	engineered barrier system
ECRB	Enhanced Characterization of the Repository Block
ENG2	Integrated Subissue for the Mechanical Disruption of Engineered Barriers
FEPs	features, events, and processes
HLW	high-level radioactive waste
IED	Information Exchange Drawing
MT	metric ton (= 1,000 kg)
NRC	U.S. Nuclear Regulatory Commission
OCRWM	Office of Civilian Radioactive Waste Management
PGA	peak ground acceleration
PGV	peak ground velocity
PWR	pressurized water reactor
RMEI	reasonably maximally exposed individual
SNF	spent nuclear fuel
TBV	To Be Verified
TSPA-LA	Total System Performance Assessment - License Application
TSPA-SR	Total System Performance Assessment - Site Recommendation
UCL	upper confidence limit

INTENTIONALLY LEFT BLANK

1. PURPOSE

The purpose of this model report is to develop abstractions for the response of engineered barrier system (EBS) components to seismic hazards at a geologic repository at Yucca Mountain, Nevada, and to define the methodology for using these abstractions in a seismic scenario class for the Total System Performance Assessment - License Application (TSPA-LA). The seismic hazards addressed herein are vibratory ground motion, fault displacement, and rockfall due to ground motion. The EBS components are the drip shield, the waste package, and the fuel cladding. The TSPA-LA is concerned with the postclosure performance of the repository. The requirements for development of the abstractions and the associated algorithms for the seismic scenario class are defined in *Technical Work Plan for: Engineered Barrier System Department Modeling and Testing FY03 Work Activities* (BSC 2003a).

The development of these abstractions will provide a more complete representation of flow into and transport from the EBS under disruptive events. The results from this development will also address portions of integrated subissue ENG2, Mechanical Disruption of Engineered Barriers, including the acceptance criteria for this subissue defined in Section 2.2.1.3.2.3 of *Yucca Mountain Review Plan, Final Report* (NRC 2003).

1.1 SCOPE

The scope of this report is limited to abstracting the mechanical response of EBS components to seismic hazards during the postclosure period and defining algorithms for the seismic scenario class. The abstractions are based on the results from structural response calculations of EBS components to vibratory ground motion, from analyses for fault displacement, and from analyses of rockfall induced by vibratory ground motion. The structural response calculations and rockfall calculations are not described in this report; rather, the results from these design calculations and scientific analyses provide the inputs that the abstractions are based on. The major design calculations and scientific analyses that provide input information for the abstractions are identified in Section 6.1.2.

The damage abstractions for EBS components include both model abstractions and scientific analyses. The abstractions for damage to the waste package and drip shield in response to vibratory ground motion and rockfall are treated as models because they rely on analyses of structural response over a range of ground motions that is wider than covered by standard engineering practices. These model abstractions have been validated to the requirements in AP-SIII.10Q, *Models*, through an independent technical review. The abstractions for damage to the cladding and for damage from fault displacement are considered scientific analyses because they are based on standard statistical techniques that bound the component response.

This report does not address the performance of naval spent nuclear fuel (SNF) during seismic events. A planned classified Naval Nuclear Propulsion Program Addendum to the License Application will provide the seismic analysis for naval SNF.

1.2 LIMITATIONS

The major limitations of the postclosure abstractions for the seismic scenario class are as follows:

- The structural response calculations include degradation of the waste package and drip shield over a 20,000-year time frame, which includes the initial 10,000-year regulatory period. The 20,000-year duration for the seismic analyses is designed to demonstrate that repository performance remains robust well after the 10,000-year regulatory period has ended. Calculations of the seismic scenario class beyond 20,000 years will require new structural response calculations with additional levels of structural degradation.
- Coupled effects from multiple seismic events are not considered because seismic hazards with the potential to have a significant impact on engineered barriers are anticipated to occur very rarely, if at all, during the 10,000-year regulatory period. More specifically, seismic hazards with the greatest potential to damage the engineered barriers correspond to large disruptive events with annual exceedance frequencies much less than 10^{-4} per year (see Sections 5 and 6 of this report), so there is only a very small probability that multiple events with the potential to induce significant damage will occur over a 10,000-year or 20,000-year period.
- Spatial variability has not been represented in the damage abstractions for EBS components under ground motion. In other words, damage to the waste package and drip shield from vibratory ground motion is assumed to be constant throughout the repository. Spatial variability for the damage abstraction for the drip shield under rockfall is limited to variability between the lithophysal and nonlithophysal zones of the repository; the damage abstraction for the drip shield from rockfall is constant throughout each zone.
- Structural response calculations for the drip shield and waste package do not include any initial backfill around the drip shield at the time of the seismic event. This representation is consistent with the present design that does not include engineered backfill but may become invalid if long-term fatigue of the tuff rock causes drift degradation and substantial collapse before the seismic hazard occurs.
- The abstraction for damage to the waste package from vibratory ground motions is based on engineering calculations that cover a range of peak ground velocity (PGV) of 1 m/s to 6 m/s and have a maximum damage of less than 2 percent of the surface area of the waste package. Similarly, the abstraction for damage to the drip shield from vibratory ground motions is valid within a range of PGV from 1 m/s to 6 m/s. This is a reasonable approach if sensitivity studies for the TSPA-LA calculations indicate that the maximum risk occurs within this range of PGV values.
- Damage to the waste package from rockfall is not included in the model abstraction for the waste package. This is a reasonable approach for the intact EBS components because an intact drip shield can deflect large rock blocks away from the waste package. However, if separation of drip shields occurs for very high amplitude ground motions and if natural backfill is not present, the shields will no longer protect the waste packages from direct

impact under rockfall during a second seismic event. Multiple hazards occur with a very low probability, as noted previously, so this is a reasonable approach for TSPA-LA.

- The potential coupling of seismic consequences with thermal processes has not been included in the model abstractions. The presence of rubble about the drip shield after drift collapse could cause changes in the thermal environment in the EBS if a seismic event occurs relatively soon after repository closure, while the waste package and drip shield are at elevated temperatures. However, the irregular and coarse nature of the rubble is expected to allow sufficient convective heat transfer that the temperature histories calculated for the nominal scenario class may reasonably be used to approximate conditions following a seismic event during the thermal period. Because potential changes in temperature due to the presence of rubble are not expected to be significant, the possible associated changes in temperature-dependent solubility and corrosion rate have not been included in TSPA-LA.

2. QUALITY ASSURANCE

The preparation of this model report and its supporting technical activities have been performed in accordance with the appropriate requirements of the quality assurance program because the abstractions and algorithms for the seismic scenario class are direct inputs for performance assessment. This document is prepared in accordance with the applicable technical work plan (BSC 2003a), which directs the work identified in work package AEBM04. The technical work plan was prepared in accordance with AP-2.27Q, *Planning for Science Activities*. All input information for this model report are identified and tracked in accordance with AP-3.15Q, *Managing Technical Product Inputs*. No qualified software is used to develop the abstractions documented in this report, so AP-SI.1Q, *Software Management*, is not applicable. The model(s) and scientific analyses in this document are not structures, systems, or components so the quality level classification from AP-2.22Q, *Classification Criteria and Maintenance of the Monitored Geologic Repository Q-List*, is not applicable. The methods used to control the electronic management of data, as required by AP-SV.1Q, *Control of the Electronic Management of Information*, are identified in Section 8 of the technical work plan.

This document is prepared in accordance with AP-SIII.10Q, *Models*, and reviewed in accordance with AP-2.14Q, *Review of Technical Products and Data*, as directed in the technical work plan.

3. USE OF SOFTWARE

3.1 QUALIFIED SOFTWARE

No qualified software is used to develop the seismic consequence abstractions. These abstractions are based on the results of rockfall calculations and structural response calculations that are performed with qualified software and that have been documented in separate scientific analyses and design calculations. This qualified software is not directly used in the abstraction process and hence is not listed here.

3.2 EXEMPT SOFTWARE

3.2.1 Microsoft Excel

Microsoft Excel for Windows, Version 97 SR-2, has been used to develop the abstractions for damage from seismic hazards. The standard functions in Excel, including its statistical package, are sufficient for all analyses. No macros, codes, or software routines are required or developed during this work. Relevant Excel files are included as attachments to this report. Microsoft Excel 97 SR-2 is an exempt software product in accordance with Sections 2.1.1 and 2.1.6 of AP-SI.1Q, *Software Management*.

The formulas, listing of inputs, and listing of outputs for the Excel spreadsheets are presented in Attachments I, II, IV, and VII of this model report.

4. INPUTS

4.1 DATA AND PARAMETERS

Table 1 presents the direct input information and Table 2 presents the corroborating information for abstraction of damage to EBS components from seismic hazards. The information in Tables 1 and 2 have been categorized into six areas that are relevant to the abstractions in this report: (1) seismic failure criteria, (2) damage to the waste package from vibratory ground motion, (3) damage to the cladding from vibratory ground motion, (4) damage to the drip shield from vibratory ground motions and from rockfall, (5) rockfall induced by ground motion, and (6) damage to the waste package and drip shield from fault displacement. Table 3 summarizes the input information for the seismic scenario class and the sources for this information. When a Data Tracking Number (DTN) is the source for a technical product input, its value is listed in Tables 1 or 3 with the same number of significant figures as in the source. The technical product inputs identified in Tables 1, 2, and 3 are appropriate for the development of model abstractions and scientific analyses for the seismic scenario class.

Section 6.11.1 identifies the uncertainties in input information and parameters for the damage analyses of EBS components and explains how these uncertainties are propagated into the abstractions for the seismic scenario class.

Table 1. Direct Input Information for Seismic Consequence Abstractions

Input Information	Value	Source
Damage to the Waste Package From Vibratory Ground Motion:		
Damage statistics for the waste package, based on a sampling of vibratory ground motions at the 10^{-6} per year hazard level	See Table 16 in BSC 2003c	BSC 2003b, Table 6.1.4-2; BSC 2003c, Table 16
Damage statistics for the waste package, based on a sampling of vibratory ground motions at the 10^{-7} per year hazard level	See Table 17 in BSC 2003c	BSC 2003b, Table 6.2.4-2; BSC 2003c, Table 17
Damage to the Cladding From Vibratory Ground Motion:		
Maximum peak acceleration of fuel assemblies due to waste package-to-waste package impacts	See Table 14 in BSC 2003e	BSC 2003d, Table 4; BSC 2003e, Table 14

Table 1. Direct Input Information for Seismic Consequence Abstractions (Continued)

Input Information	Value	Source
Average peak acceleration of fuel assemblies due to waste package-to-waste package impacts	See Table 15 in BSC 2003e	BSC 2003d, Table 5; BSC 2003e, Table 15
Damage to the Drip Shield from Vibratory Ground Motion and Rockfall:		
Damage statistics for the drip shield, based on a sampling of vibratory ground motions at the 10^{-6} per year hazard level	See Table 4 in BSC 2003f	BSC 2003f, Table 4
Damage to the drip shield due to impact by single rock blocks from the 10^{-6} per year ground motion hazard level	See Table 2 in BSC 2003f	BSC 2003g, Table 6-2; BSC 2003f, Table 2
Damage to the drip shield due to impact by the maximum rock block from the 10^{-7} per year ground motion hazard level	See Table 3 in BSC 2003f	BSC 2003g, Table 6-3; BSC 2003f, Table 3
Rockfall Induced by Ground Motion:		
Rockfall statistics in the nonlithophysal zone, based on a sampling of vibratory ground motions at the 10^{-6} per year hazard level	See Attachment XI in BSC 2003h	BSC 2003h, Attachment XI; DTN: MO0305MWDNLRKF.001
Rockfall statistics in the nonlithophysal zone, based on a sampling of vibratory ground motions at the 10^{-7} per year hazard level	See Attachment XI in BSC 2003h	BSC 2003h, Attachment XI; DTN: MO0301MWD3DE27.003
Length of the drip shield	5805 mm	BSC 2003f, Table 1
Tunnel length for rockfall calculations	25 meters	BSC 2003h, Section 6.3.1
Damage to the Waste Package and Drip Shield from Fault Displacement:		
Drift Diameter	5.5 m	BSC 2003i, Figure 1
Invert Thickness (maximum)	806 mm	BSC 2003i, Figure 2
Drip Shield Height - Exterior	2885.62 mm	BSC 2003f, Table 1
Drip Shield Height - Interior	2715.62 mm	BSC 2003f, Table 1
44-BWR Waste Package Diameter	1674 mm	BSC 2003j, Table 1
24-BWR Waste Package Diameter	1318 mm	BSC 2003j, Table 1
21-PWR Waste Package Diameter	1644 mm	BSC 2003j, Table 1
12-PWR Waste Package Diameter	1330 mm	BSC 2003j, Table 1
Naval-Long Waste Package Diameter	1949 mm	BSC 2003j, Table 1
Naval-Short Waste Package Diameter	1949 mm	BSC 2003j, Table 1
5 DHLW-Short Waste Package Diameter	2110 mm	BSC 2003j, Table 1
5 DHLW-Long Waste Package Diameter	2110 mm	BSC 2003j, Table 1
2-MCO/2-DHLW Waste Package Diameter	1814 mm	BSC 2003j, Table 1
44-BWR Waste Package Length	5165 mm	BSC 2003j, Table 1
24-BWR Waste Package Length	5105 mm	BSC 2003j, Table 1
21-PWR Waste Package Length	5165 mm	BSC 2003j, Table 1
12-PWR Waste Package Length	5651 mm	BSC 2003j, Table 1
Naval-Long Waste Package Length	6065 mm	BSC 2003j, Table 1
Naval-Short Waste Package Length	5430 mm	BSC 2003j, Table 1
5 DHLW-Short Waste Package Length	3590 mm	BSC 2003j, Table 1
5 DHLW-Long Waste Package Length	5217 mm	BSC 2003j, Table 1
2-MCO/2-DHLW Waste Package Length	5217 mm	BSC 2003j, Table 1
Emplacement Drifts Intersected by the Sundance Fault in Lower Lithophysal Zones	1-6, 1-7, and 1-8	DTN: LL030704623122.031, tspa03.mesh03-150w
Emplacement Drifts Intersected by the Drill Hole Wash Fault in Lower Lithophysal Zones	3-1, 3-2, 2-5W, 2-6W, 2-7W, 2-8W, 2-9W, and 2-10W	DTN: LL030704623122.031, tspa03.mesh03-150w

Table 1. Direct Input Information for Seismic Consequence Abstractions (Continued)

Input Information	Value	Source
Emplacement Drifts Intersected by the Drill Hole Wash Fault in Other Zones	2-9E, 2-10E, 2-11E, 2-12E, 2-13E, 2-14E, 2-15E, 2-16E, and 2-17E	DTN: LL030704623122.031, tspa03.mesh03-150w
Emplacement Drifts Intersected by the Pagany Wash Fault in Lower Lithophysal Zones	2-1W, 2-2W, 2-1E, 2-2E, 2-3E, 2-4E, and 2-5E	DTN: LL030704623122.031, tspa03.mesh03-150w
Emplacement Drifts Intersected by the Pagany Wash Fault in Other Zones	2-6E and 2-7E	DTN: LL030704623122.031, tspa03.mesh03-150w
Emplacement Drifts Intersected by the Sevier Wash Fault in Lower Lithophysal Zones	2-2E	DTN: LL030704623122.031, tspa03.mesh03-150w
Fault Displacement Hazard at Site 3 – on the Drill Hole Wash Fault	See file for data	DTN: MO0004MWDRI3M3.002, file ./displ/tot_haz/s3.frac_mean.gz
Fault Displacement Hazard at Site 5 – on the Sundance Fault	See file for data	DTN: MO0004MWDRI3M3.002, file ./displ/tot_haz/s5.frac_mean.gz
Fault Displacement Hazard at Site 7a – a generic repository location, approximately 100-meters east of the Solitario Canyon Fault, with a hypothetical small fault with 2-meter offset	See file for data	DTN: MO0004MWDRI3M3.002, file ./displ/tot_haz/s7a.frac_mean.gz
Fault Displacement Hazard at Site 8a – a generic repository location, midway between the Solitario Canyon and Ghost Dance Faults, with a hypothetical small fault with a 2-meter offset	See file for data	DTN: MO0004MWDRI3M3.002, file ./displ/tot_haz/s8a.frac_mean.gz
Fault Displacement Hazard at Sites 7b and 7c – generic repository locations, approximately 100-meters east of the Solitario Canyon Fault. Site 7b has a hypothetical shear with 10-cm offset and site 7c has a hypothetical fracture with no cumulative displacement.	See files for data	DTN: MO0004MWDRI3M3.002, files ./displ/tot_haz/s7b.frac_mean.gz and ./displ/tot_haz/s7c.frac_mean.gz
Fault Displacement Hazard at Sites 8b and 8c – generic repository locations, midway between the Solitario Canyon and Ghost Dance Faults. Site 8b has a hypothetical shear with 10-cm offset and site 8c has a hypothetical fracture with no cumulative displacement.	See files for data	DTN: MO0004MWDRI3M3.002, files ./displ/tot_haz/s8b.frac_mean.gz and ./displ/tot_haz/s8c.frac_mean.gz
Number of 21 PWR Waste Packages with Absorber Plates	4299	BSC 2003k, Table 11
Number of 21 PWR Waste Packages with Control Rods	95	BSC 2003k, Table 11
Number of 12 PWR Long Waste Packages with Absorber Plates	163	BSC 2003k, Table 11
Number of 44 BWR Waste Packages with Absorber Plates	2831	BSC 2003k, Table 11
Number of 24 BWR Waste Packages with Absorber Plates	84	BSC 2003k, Table 11
Number of 5 DHLW Short/1 DOE SNF Short Waste Package	1147	BSC 2003k, Table 11
Number of 5 DHLW Long/1 DOE SNF Long Waste Package	1406	BSC 2003k, Table 11
Number of 2 MCO/2 DHLW Waste Package	149	BSC 2003k, Table 11
Number of 5 DHLW Long/1 DOE SNF Short Waste Package	31	BSC 2003k, Table 11
Number of HLW Long Only Waste Package	679	BSC 2003k, Table 11
Number of Naval Short Waste Package	144	BSC 2003k, Table 11
Number of Naval Long Waste Package	156	BSC 2003k, Table 11

Table 2. Corroborating Input Information for Seismic Consequence Abstractions

Input Information	Value	Source
Seismic Failure Criteria:		
Residual stress threshold for initiation of stress corrosion cracking on a smooth surface of Alloy 22	90% of the yield strength of Alloy 22	BSC 2003l, Section 6.2.1, end of 3 rd paragraph
Residual stress threshold for initiation of stress corrosion cracking on a smooth surface of Titanium Grade 7	50% of the yield strength of Titanium Grade 7	BSC 2003l, Section 6.2.1, end of 3 rd paragraph
Damage to the Waste Package from Ground Motion:		
Preliminary damage statistics for the waste package, based on a sampling of vibratory ground motions at the 10 ⁻⁵ per year hazard level	See Table XI-2 in BSC 2003b	BSC 2003b, Table XI-2; BSC 2003m, Table 58
Damage to the waste package for the single vibratory ground motion at the 5×10 ⁻⁴ per year hazard level	No damage	BSC 2003b, Section 6.3, last paragraph
Damage to the Cladding from Ground Motion:		
Statistics for axial impact velocities between adjacent waste packages, based on a sampling of vibratory ground motions at the 10 ⁻⁶ per year hazard level	See Tables 6.1.2-1 through 6.1.2-15	BSC 2003b, Tables 6.1.2-1 to 6.1.2-15; BSC 2003n, Tables 28 to 42
Statistics for axial impact velocities between adjacent waste packages, based on a sampling of vibratory ground motions at the 10 ⁻⁷ per year hazard level	See Tables 6.2.2-1 through 6.2.2-15	BSC 2003b, Tables 6.2.2-1 to 6.2.2-15; BSC 2003n, Tables 43, 44, and 45; BSC 2003m, Tables 46 to 57
Axial impact velocity between adjacent waste packages for the single vibratory ground motion at the 5×10 ⁻⁴ per year hazard level	Relative displacement of waste package and pallet nodes is less than ±0.01 mm	BSC 2003b, Figures 10 and 11
Damage to the Drip Shield from Ground Motion:		
Damage statistics for the drip shield, based on a sampling of vibratory ground motions at the 10 ⁻⁷ per year hazard level	Drip shield separates for all ground motions	BSC 2003f, Calculation Results I
Damage to the drip shield for the single vibratory ground motion at the 5×10 ⁻⁴ per year hazard level	No damage	BSC 2003f, Calculation Results I
Rockfall Induced by Ground Motion:		
Rockfall statistics in the nonlithophysal zone, based on a single vibratory ground motion at the 5×10 ⁻⁴ per year level	See Table 19	BSC 2003h, Table 19
Damage statistics for a tunnel in the lithophysal zone, based on a sampling of vibratory ground motions at the 10 ⁻⁶ per year level	Tunnel collapses for all ground motions	BSC 2003h, Section 6.4.1.1
Damage to a tunnel in the lithophysal zone for the single vibratory ground motion at the 5×10 ⁻⁴ per year hazard level	No rockfall for rock mass categories 2-5; minor, low-energy rockfall for rock mass category 1	BSC 2003h, Section 6.4.1.1
Damage to the Waste Package and Drip Shield From Fault Displacement:		
Fault Displacement Hazard at Site 2 – on the Solitario Canyon Fault	See Figure 8-3 in CRWMS M&O 1998	CRWMS M&O 1998, Figure 8-3
Fault Displacement Hazard at Site 4 – on the Ghost Dance Fault	See Figure 8-5 in CRWMS M&O 1998	CRWMS M&O 1998, Figure 8-5
Fault Displacement Features of the Sevier Wash Fault and the Pagany Wash Fault	Similar to Drill Hole Wash Fault	Menges and Whitney 1996
Seismic hazard frequency for drift collapse in lower lithophysal	1e-06	BSC 2003h, Section 6.4.1.1
Subsurface facility layout and numbering of emplacement drifts	Figure 1	BSC 2003o
Alternate conceptual model for probability-weighted number of waste package failures from fault displacement	1.91×10 ⁻⁴ to 1.91×10 ⁻⁶	Waiting et al. 2003
Alternate conceptual model for number of fault intersections with emplacement drifts	191	Waiting et al. 2003
Seepage Change Due to Drift Collapse:		
Seepage abstraction if seismic hazard is large enough to collapse the drifts	See Table in DTN	DTN: LB0307SEEPDRCL.002

Table 3. Direct Input Information for the Seismic Scenario Class

Input Information	Value	Source
Horizontal PGV at Point B for the 10^{-6} per year mean annual exceedance frequency	2.44 m/s	DTN: MO0303DPGVB106.002
Horizontal PGV at Point B for the 10^{-7} per year mean annual exceedance frequency	5.35 m/s	DTN: MO0210PGVPB107.000
Mean hazard curve for horizontal PGV at Point A, a reference rock outcrop at the repository elevation	See file h_vel_extended. frac_mean in the DTN	DTN: MO03061E9PSHA1.000

4.2 CRITERIA

General programmatic requirements for this document are listed in *Technical Work Plan for: Engineered Barrier System Department Modeling and Testing FY03 Work Activities* (BSC 2003a). The technical work plan specifies that this document and all analyses described herein must adhere to the requirements of AP-SIII.10Q, *Models*. The technical work plan specifies that this document must discuss the barrier function of the EBS components (waste package, drip shield, and emplacement pallet) that may be affected by seismically induced hazards. The technical work plan also specifies that the acceptance criteria in *Yucca Mountain Review Plan, Final Report* (NRC 2003) must be addressed.

4.2.1 Project Requirements and Yucca Mountain Review Plan Acceptance Criteria

Project Requirements Document (Canori and Leitner 2003) contains the high-level technical requirements for the Yucca Mountain Project. These requirements provide a basis for criteria relevant to the seismic consequence abstractions. The requirement that pertains to this model report and its link to 10 CFR Part 63, is defined in Section 3.4 of *Project Requirements Document* (Canori and Leitner 2003) as follows:

- **PRD-002/T-015: Requirements for Performance Assessment**

10 CFR 63.114, specifies technical requirements to be used in a performance assessment to demonstrate compliance to 10 CFR 63.113. It includes requirements for calculations, including data related to site geology, hydrology, and geochemistry; the need to account for uncertainties and variabilities in model parameters, the need to consider alternative conceptual models, and technical bases for inclusion or exclusion of specific FEPs, deterioration or degradation processes of engineered barriers, and all the models used in performance assessment.

The acceptance criteria that are relevant to requirement PRD-002/T-015 for seismic consequence abstractions are found in Section 2.2.1.3.2.3 of *Yucca Mountain Review Plan, Final Report* (NRC 2003). The five general acceptance criteria in Section 2.2.1.3.2.3 follow, along with the subcriteria that are applicable to development of the seismic consequence abstractions.

- **Acceptance Criterion 1: System Description and Model Integration Are Adequate.**

The subcriteria applicable to the seismic consequence abstractions are (1), (3), (4), and (5).

- **Acceptance Criterion 2: Data Are Sufficient for Model Justification.**
Subcriteria (1), (3), and (4) are applicable to the seismic consequence abstractions.
- **Acceptance Criterion 3: Data Uncertainty Is Characterized and Propagated Through the Model Abstraction.**
Subcriteria (1), (2), and (3) are applicable to the seismic consequence abstractions.
- **Acceptance Criterion 4: Model Uncertainty Is Characterized and Propagated Through the Model Abstraction.**
Subcriteria (2), and (3) are applicable to these model abstractions.
- **Acceptance Criterion 5: Model Abstraction Output Is Supported by Objective Comparisons.**
The applicable subcriteria are (1), (2), and (3).

Section 6.11 provides a detailed discussion of how the seismic abstractions and the seismic scenario class meet the applicable acceptance criteria from *Yucca Mountain Review Plan, Final Report* (NRC 2003).

4.3 CODES AND STANDARDS

No codes and standards are applicable to the development of the seismic consequence abstractions. The regulation that is applicable to the development of these abstractions is 10 CFR Part 63, specifically 10 CFR 63.114 and 10 CFR 63.115.

5. ASSUMPTIONS

5.1 DAMAGE THRESHOLD FROM VIBRATORY GROUND MOTION LIES BETWEEN MEAN ANNUAL EXCEEDANCE FREQUENCIES OF 10^{-4} PER YEAR AND 10^{-5} PER YEAR

Assumption: There is no damage to EBS components until the repository experiences ground motions larger than those for the 10^{-4} per year annual exceedance frequency. More specifically, the abstractions for damage to the drip shield and cladding from vibratory ground motion assume that damage becomes nonzero between the 10^{-4} and 10^{-5} per year annual exceedance frequencies.

Basis: Structural analyses for the waste package and drip shield have been performed using a single set of vibratory ground motions (with two horizontal components and one vertical component) for an annual exceedance frequency of 5×10^{-4} per year. The results of these analyses demonstrate that the response of the waste package and drip shield are always in the elastic regime for the 5×10^{-4} per year ground motion (BSC 2003b, Section 6.3; BSC 2003p, Section 6.1), with no damage to the structures. There will also be no failure of the cladding because waste package displacements are very small (BSC 2003p, Section 6.3), with no impacts or significant acceleration that could fail the cladding.

The drip shield may also be damaged by tunnel collapse in the lithophysal zones or from rock blocks in the nonlithophysal zones. For the 5×10^{-4} per year ground motion, tunnels in the

lithophysal zones have no damage for higher values of rock compressive strength and only minor damage (but no collapse) at the lowest level of compressive strength (BSC 2003h, Section 6.4.1.1). For the nonlithophysal zones, a series of 25 analyses have been performed to determine the range and number of blocks ejected by the 5×10^{-4} per year ground motion (BSC 2003h, Section 6.3.1.2.5). This set of analyses is a skewed sample because it is based on the 25 fracture patterns that produce the most rockfall for the 10^{-6} per year level ground motions. Fourteen of the calculations have no rockfall (BSC 2003h, Table 19). When rockfall does occur, the median energy of the blocks is near 3,000 Joules (BSC 2003h, Figure 70), which produces very minor damage (see Table 12 in Section 6.6.1.2 of this report). Considering that 85 percent of the repository is in lithophysal rock, with no damage to the drip shield, and that the remaining 15 percent of the drifts may have only very minor damage based on a skewed sampling of fracture patterns, it is reasonable to assume that damage to the drip shield from rockfall at the 5×10^{-4} per year ground motion level is negligible.

The seismic consequence abstractions for TSPA-LA assume that damage to EBS components from vibratory ground motion becomes nonzero between the 10^{-4} and 10^{-5} per year annual exceedance frequencies.

Confirmation Status: This assumption is designated To Be Verified (TBV), pending the results from structural response calculations and rockfall calculations for ground motions at the 10^{-4} per year and 10^{-5} per year mean annual exceedance frequencies. The TBV number for this assumption is TBV-5106.

Use In Model: The abstraction for damage to the waste package in Section 6.5 uses a linear fit so that the maximum damage goes to zero for a value of PGV that lies between the 10^{-4} per year and 10^{-5} per year annual exceedance frequency. This assumption is also used in Section 6.7 to set the lower bound for damage to the cladding. The assumption for damage to the drip shield from rock blocks in the nonlithophysal zone is used in developing the abstraction in Section 6.6.1. More specifically, the abstraction for damage to the drip shield assumes that there is no damage for the 5×10^{-5} per year ground motion level (Section 6.6.1.4).

5.2 PAGANY WASH AND SEVIER WASH FAULT DISPLACEMENTS

Assumption: The fault displacement hazard curves for the Pagany Wash Fault and for the Sevier Wash Fault are identical to the fault displacement hazard curve for the Drill Hole Wash Fault.

Basis: The assumption of equivalency is justified by the results of field investigations that are summarized by Menges and Whitney (1996). The reasoning that supports the assumption of equivalency is as follows:

1. The best available field data for the three faults comes from cores on the Drill Hole Wash Fault, so it is reasonable to use the response of the Drill Hole Wash Fault as the basis for the seismic hazard.
2. None of the faults suggest displacement in Quaternary alluvial terraces, so it is appropriate to assume a low probability of significant displacement for all three faults.

3. The scale of cumulative vertical displacement is less than 5 to 10 meters for each structure, consistent with a maximum displacement of approximately 2 meters for a single low probability event.
4. Total fault length, an important factor in seismic hazard assessment, is similar for the three faults and ranges from 2 km for the Drill Hole Wash Fault to 4 km for the other faults.
5. Spatial orientation to the Solitario Canyon and Bow Ridge Faults, also an important factor in a hazard assessment, is similar for the three faults. Spatial orientation to more distant seismic sources is also similar.
6. Previous geologic studies have consolidated discussion of the three faults based on similar characteristics and apparent similarity in fault development in response to the extensional environment.

It is, therefore, reasonable to treat the Drill Hole Wash fault, the Sevier Wash fault, and the Pagany Wash fault in a similar manner with regard to the potential seismic hazard, barring any evidence to the contrary.

Confirmation Status: This assumption does not require confirmation. *Probabilistic Seismic Hazard Analyses for Fault Displacement and Vibratory Ground Motion at Yucca Mountain, Nevada* (CRWMS M&O 1998) defines fault displacement hazards at 15 faulting conditions within the immediate vicinity of Yucca Mountain. Closely spaced secondary faults are not characterized separately because their displacements during a seismic event are expected to be similar.

Use In Model: This assumption is used in Section 6.8.3.

5.3 RESIDUAL STRESS ABOVE THE SEISMIC FAILURE CRITERION RESULTS IN FLOW PATHWAYS THROUGH THE WASTE PACKAGE AND DRIP SHIELD

Assumption: If the residual stress from mechanical damage exceeds the residual stress threshold for the barrier, then the affected area(s) are considered to have failed as a barrier to flow and transport.

Basis: The seismic damage abstractions for the waste package and drip shield make use of a residual stress threshold as a failure criterion. Application of this criterion is non-mechanistic, in the sense that detailed calculations of the actual rates of general corrosion, stress corrosion cracking, or localized corrosion are not being used to determine the actual failure time after a seismic event. Rather, it is acknowledged that the potential exists for one or several of these processes to occur with such rapidity that the entire damaged area ceases to function as an effective barrier to flow and transport. Once the barrier fails, advective flow and transport and diffusive transport can occur through the damaged area.

Confirmation Status: This assumption does not require confirmation because it is a conservative, bounding approach that ignores the potential for a network of tight cracks to limit advective flow because of surface tension within a crack and because of precipitation within a crack.

Use In Model: This assumption is used in Sections 6.3 and 6.10.2.

5.4 DERIVING THE FORMULA FOR MEAN DOSE

Assumption: In deriving the formula for mean dose, the dose is assumed to be a function of the time of occurrence and the amplitude of the PGV for the seismic hazard (see Attachment VIII). The dose time histories for the reasonably maximally exposed individual at time τ from a seismic event occurring at a time, t , prior to τ depends only on the time of occurrence of the event and on PGV at the waste emplacement drifts associated with the seismic event.

Basis: This assumption simplifies the mathematical derivation for mean dose presented in Attachment VIII without being overly restrictive.

Confirmation Status: This assumption does not require confirmation.

Use In Model: This assumption is used in Attachment VIII.

5.5 RANDOMNESS OF SEISMIC EVENTS

Assumption: Seismic events occur in a random manner, following a Poisson process, over long periods of time.

Basis: The assumption that the behavior of the earth is generally random (Poisson process) is the underlying assumption in all probabilistic hazard analyses. In other words, all earthquakes are considered as independent events with regard to magnitude, time and location. Although there may be cases where sufficient data and information exists to depart from this assumption, the Poisson process is generally an effective representation of nature and represents a compromise between the complexity of natural processes, availability of information, and the sensitivity of results of engineering relevance. This assumption is identical to Assumption 6.4.2 in *Characterize Framework for Seismicity and Structural Deformation at Yucca Mountain, Nevada* (CRWMS M&O 2000a).

Confirmation Status: This assumption does not require confirmation because it is a common, engineering assumption in risk assessments and because it is an implicit assumption in the development of hazard curves.

Use In Model: This assumption is used in Section 6.10 and Attachment VIII.

5.6 MAJOR ASSUMPTIONS IN SUPPORTING CALCULATIONS

The seismic consequence abstractions are based on the results from analyses for the structural response of EBS components to vibratory ground motion and on the results from analyses of rockfall induced by vibratory ground motion. The structural response calculations and rockfall calculations are not described in this report; rather, the results from these design calculations and scientific analyses provide the input information that the abstractions are based on. These supporting calculations include several major assumptions that are not directly used in the abstraction process, but are noteworthy enough to deserve repeating here.

The structural response calculations for the waste package and drip shield incorporate assumptions for structural thickness and for material properties of Alloy 22 and of Titanium Grade 7. The thicknesses of the drip shield plates and the waste package outer shell have been reduced by 2-mm in these calculations to represent the potential degradation of these structures by general corrosion over the first 10,000 years after repository closure. The material properties of Alloy 22 and of Titanium Grade 7 have been evaluated at an elevated temperature (150°C) that provides conservative values for mechanical properties over most (97 percent) of the 10,000-year duration. The rationale for these assumptions is provided in several design calculations (BSC 2003b, Assumptions 3.20 and 3.21; BSC 2003g, Assumptions 3.7 and 3.10).

The rockfall calculations for the lithophysal and nonlithophysal zones also make several key assumptions. In the lithophysal zone, the block size distribution is assumed to be a function of the inter-lithophysal fracture density and the lithophysae spacing (BSC 2003h, Assumption 5.2.2). This assumption is relevant to the abstraction process because it limits the potential damage to the drip shield from tunnel collapse in the lithophysal zone, as discussed in Section 6.6.2 of this document.

6. MODEL DISCUSSION

6.1 INTRODUCTION

6.1.1 Background

The U.S. Department of Energy (DOE) is implementing a comprehensive seismic evaluation strategy for a geologic repository at Yucca Mountain. This strategy began during the Site Recommendation period with a probabilistic seismic hazard analysis for the repository site. In the probabilistic seismic hazard analyses, the DOE has developed (1) ground motion hazard curves for the Yucca Mountain site, and (2) fault displacement hazard curves for fifteen faulting conditions mapped within the immediate vicinity of Yucca Mountain (CRWMS M&O 1998, Sections 7 and 8).

The results from *Probabilistic Seismic Hazard Analyses for Fault Displacement and Vibratory Ground Motion at Yucca Mountain, Nevada* (CRWMS M&O 1998) were used to support screening decisions for features, events, and processes (FEPs) relevant to potential seismic effects on the repository. With the exception of seismic ground motion effects on fuel rod cladding, FEPs related to ground motion were screened out of the Total System Performance Assessment for the Site Recommendation (TSPA-SR) on the basis of median ground motion hazard (CRWMS M&O 2000b, Section 6.2.6). A key assumption for the TSPA-SR screening decision was that the median hazard curve, rather than the mean hazard curve, was appropriate for the analysis. The ground motions and fault displacement amplitudes from the median hazard curves were low enough that their expected damage to the engineered barriers was not significant, even down to the lowest annual exceedance frequency of 10^{-8} per year. This result supported the decision to screen out seismic effects, except for fuel rod cladding, from TSPA-SR.

The Nuclear Regulatory Commission (NRC) subsequently expressed concern about the potential impacts of larger (less frequent) earthquakes on EBS components during the postclosure period. These concerns resulted in agreements that were reached between the NRC staff and the DOE during the NRC/DOE Technical Exchange and Management Meeting on the Key Technical Issue of Structural Deformation and Seismicity, October 11–12, 2000 (Gardner 2000).

The DOE's seismic analysis approach for the License Application is outlined in a letter report, *Approach to Postclosure Seismic Analyses for a Potential Geologic Repository at Yucca Mountain, Nevada* (Brocoum 2001, enclosure). The strategy outlined in the letter report responds to the NRC's concerns on seismic issues. Specifically, the DOE agreed to either provide technical justification for the use of median fault displacement and ground motion hazard curves as the basis for screening seismic FEPs for the TSPA-LA, or to adopt mean values as the basis for screening seismic FEPs, or to evaluate and implement an alternative approach. The DOE has adopted mean hazard curves for vibratory ground motion and for fault displacement in screening FEPs for TSPA-LA and in developing the seismic consequence abstractions for TSPA-LA.

6.1.2 Information Sources and Outputs

This report presents the abstractions for damage to EBS components due to seismic hazards. These abstractions are the output from this model report. The intended use of this output is to define the abstractions and associated computational algorithms for the seismic scenario class for TSPA-LA. The report includes discussion of:

- The criteria for determining the failed areas of the waste package and drip shield under vibratory ground motions
- The abstraction of these failed areas as a function of the seismic hazard
- Damage to EBS components from fault displacement
- The abstraction of cladding failure in response to waste package impacts
- The algorithms for including the damage abstractions in the seismic scenario class
- Post-seismic event changes in seepage due to tunnel collapse and in EBS flow pathways due to accelerated localized corrosion of Alloy 22.

Figure 1 illustrates the major components of the EBS in a typical emplacement drift.

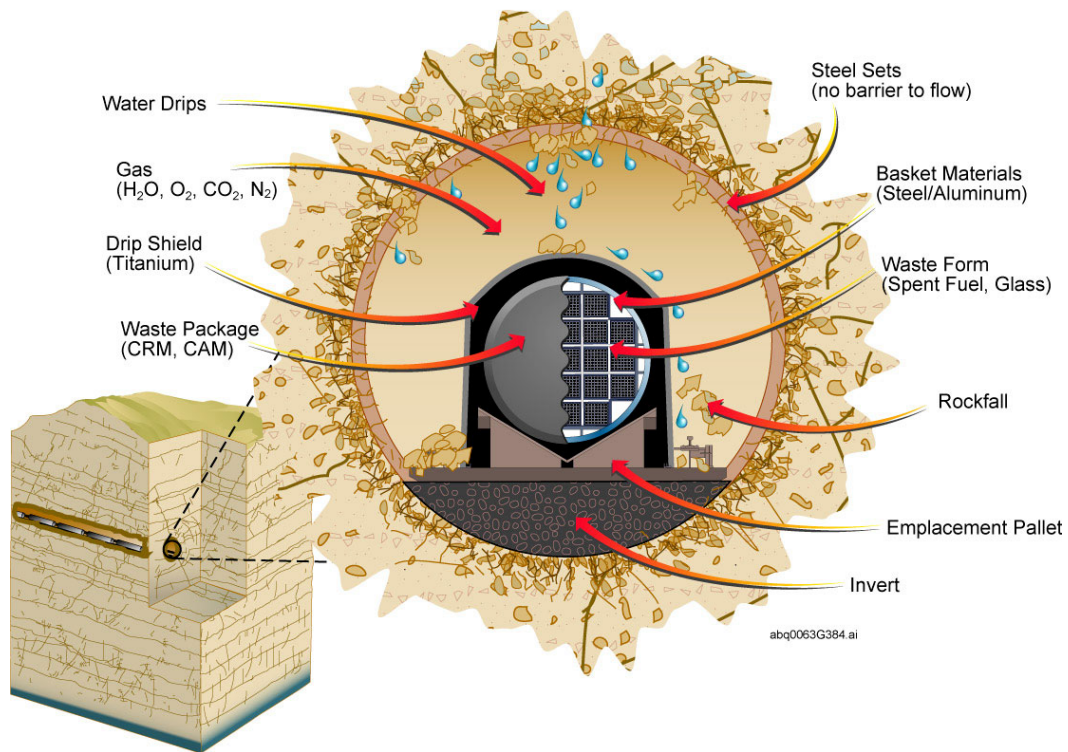


Figure 1. Schematic Diagram of the EBS Components in a Typical Emplacement Drift

Mathematically, the hazards included in the seismic scenario class can be represented by the following vector:

$$\vec{A} = (t, v, \vec{d}, fWPA_{|V}, fDSA_{|V}, fDSARF_{|V}, fCLD_V, nPWRFD_{|D}, aPWRFD, nBWRFD_{|D}, aBWRFD, nHLWFD_{|D}, aLHLWFD, cSPFLX_V, cSPFLX_I), \quad (\text{Eq. 1})$$

Where t is the time (year) after repository closure when the seismic hazard occurs;
 v is the amplitude of the ground motion, measured as horizontal PGV (m/s);
 \vec{d} is a vector of displacements for faults that intersect emplacement drifts (m);
 $fWPA_{|V}$ is the fraction of waste package surface area damaged by ground motion. The abstraction for damage to the waste package is defined in Section 6.5, based on information in *Structural Calculations of Waste Package Exposed to Vibratory Ground Motion* (BSC 2003b);
 $fDSA_{|V}$ is fraction of drip shield surface area damaged by ground motion. The abstraction for damage to the drip shield from ground motion is defined in Section 6.6.3, based information in *Structural Calculations of Drip Shield Exposed to Vibratory Ground Motion* (BSC 2003p);

- $fDSARF|_V$ is the fraction of drip shield surface area damaged by rockfall in the nonlithophysal zone. The abstraction for damage to the drip shield from rockfall (induced by ground motion) is defined in Section 6.6.1, based on information in *Drift Degradation Analysis* (BSC 2003h) and in *Drip Shield Structural Response to Rock Fall* (BSC 2003g);
- $fCLD_V$ is the fraction of cladding perforated by the vibratory ground motion. The abstraction for damage to the cladding is defined in Section 6.7, based on information in *Maximum Accelerations on the Fuel Assemblies of a 21-PWR Waste Package During End Impacts* (BSC 2003d) and in *Structural Calculations of Waste Package Exposed to Vibratory Ground Motion* (BSC 2003b);
- $nPWRFD|_D$ is the number of PWR waste packages failed due to fault displacement. The abstraction for the number of failed waste packages is defined in Section 6.8, based on information from design and from the mean hazard curves in the probabilistic seismic hazard analyses (CRWMS M&O 1998; DTN: MO0004MWDRIFM3.002);
- $aPWRRD$ is the failed area (m^2) on PWR waste packages and their associated drip shield and cladding resulting from fault displacement. The abstraction for failed area and for damage to drip shield and cladding is defined in Section 6.8.5;
- $nBWRFD|_D$ is the number of BWR waste packages failed due to fault displacement. The abstraction for the number of failed waste packages is defined in Section 6.8, based on information from design and from the mean hazard curves in the probabilistic seismic hazard analyses (CRWMS M&O 1998; DTN: MO0004MWDRIFM3.002);
- $aBWRRD$ is the failed area (m^2) on BWR waste packages and their associated drip shields and cladding resulting from fault displacement. The abstraction for failed area and for damage to drip shield and cladding is defined in Section 6.8.5;
- $nHLWFD|_D$ is the number of HLW waste packages failed due to fault displacement. The abstraction for the number of failed waste packages is defined in Section 6.8, based on information from design and from the mean hazard curves in the probabilistic seismic hazard analyses (CRWMS M&O 1998; DTN: MO0004MWDRIFM3.002);
- $aHLWRD$ is the failed area (m^2) on HLW waste packages and their associated drip shields resulting from fault displacement. The abstraction for failed area and for damage to drip shields is defined in Section 6.8.5;
- $cSPFLX_V$ is an indicator variable (-) for the change in seepage flux in the lithophysal zone after the seismic hazard; and
- $cSPFLX_t$ is an indicator variable for the change in flux splitting on the waste package (i.e., the fraction of seepage flux that enters a waste package after passing through an opening in the drip shield) after the seismic hazard.

In the above notation, a subscript “|V” or “|D” indicates a parameter that has a distribution that is conditional on (i.e., is a function of) v or \vec{d} , respectively. The subscripts “v” and “t” indicate variables that are functions of v and t , respectively.

The levels of ground motion and fault displacement are based on the mean hazard curves defined in *Probabilistic Seismic Hazard Analyses for Fault Displacement and Vibratory Ground Motion at Yucca Mountain, Nevada* (CRWMS M&O 1998). The response of the EBS components incorporates an allowance for corrosion and degradation of the waste package and drip shield over the 10,000-year regulatory period for the repository. The seismic scenario class has been designed to adequately represent the seismic hazards that cause significant structural damage, and considers hazards with an annual exceedance probability of 10^{-8} per year or greater, per 10 CFR 63.114(d).

6.1.3 Terminology

The terminology for the seismic hazard curves, for the suite of ground motions corresponding to a given exceedance frequency, and for a comparison of the damage abstractions in this report with a response surface requires a brief explanation.

A mean hazard curve defines the relationship between the mean estimate of the annual frequency of exceedance and the amplitude of the vibratory ground motion (measured by PGV) or the amplitude of the fault displacement (measured by a vertical displacement). The mean annual exceedance frequency represents the mean value with which a seismic event will exceed a given value of the PGV or fault displacement.

The mean annual exceedance frequency spans many orders of magnitude, from a minimum of 10^{-8} per year to a maximum of 1 per year (or greater). The mean frequency is defined as the number of observed events, divided by the time interval of observation. It varies randomly from one observation to the next. We use the mean of this random number as a measure of how likely it is over the next year. When the mean annual exceedance frequency is much less than 1, the mean annual exceedance frequency and the annual exceedance probability are essentially equal. This report uses the term exceedance frequency because it is more general, although the exceedance frequency and exceedance probability are interchangeable for the seismic hazards considered in this study. All hazard curves in this report are based on the mean annual exceedance frequency.

A suite of 15 three-component ground motions have been developed for the 10^{-6} per year (mean) annual exceedance frequency to support the postclosure performance assessment. This suite of ground motions has been sampled in order to represent the temporal variability and uncertainty from the ground motions in the structural response calculations and rockfall calculations that support the damage abstractions for the seismic scenario class. These ground motions are collectively referred to as the ground motions at the 10^{-6} per year mean annual exceedance frequency, or more simply the 10^{-6} ground motion level. Similarly, the suite of 15 three-component ground motions at the 10^{-7} per year (mean) annual exceedance frequency is referred to as the 10^{-7} ground motion level.

Finally, the damage abstractions for EBS components are defined in a different manner than the typical response surface for a seismic fragility analysis. A typical response surface represents the mean damage (or mean probability of failure) and its standard deviation, often as normal or lognormal distributions whose parameters are functions of the amplitude of the ground motion or fault displacement. The damage abstractions for the seismic scenario class are often uniform

distributions that provide a conditional distribution of the range of damage as a function of the seismic amplitude. Typically, the upper bound of the uniform distribution is a function of the amplitude of the ground motion and the lower bound of the uniform distribution is usually zero damage. While the use of a uniform distribution is not typical for fragility analyses, this approach does provide a simple and transparent approach for representing the variability and uncertainty in seismically induced damage via Monte Carlo sampling for TSPA-LA.

6.1.4 Corroborating Information

The abstractions for damage to EBS components from seismic hazards are based on the direct input information in Tables 1 and 3 of Section 4.1 and on the corroborating information in Table 2 of Section 4.1.

6.2 RELEVANT FEPS FOR THE SEISMIC SCENARIO CLASS

The development of a comprehensive list of features, events, and processes (FEPs) potentially relevant to post-closure performance of the potential Yucca Mountain repository is an ongoing, iterative process based on site-specific information, design, and regulations. The approach for developing an initial list of FEPs, in support of *Total System Performance Assessment for the Site Recommendation* (CRWMS M&O 2000c), was documented by Freeze et al. (2001). The initial FEP list contained 328 FEPs, of which 176 were included in TSPA-SR models (CRWMS M&O 2000c, Tables B-9 through B-17). To support TSPA-LA, the FEP list was re-evaluated in accordance with Section 3.2 of *The Enhanced Plan for Features, Events, and Processes (FEPs) at Yucca Mountain* (BSC 2002).

The seismic scenario class is based on a single modeling case, with a single seismic event that occurs at a randomly chosen time in each realization of the TSPA-LA. The focus here is on seismic events with frequencies less than 10^{-4} per year because the associated ground motions and fault displacements have the potential to cause damage to the EBS components (see Assumption 5.1). The response of the drip shield, waste package, and cladding to this single seismic event is represented through damage abstractions for the EBS components under vibratory ground motion and fault displacement. The failed areas on the EBS components define pathways for flow and transport through the engineered barriers. Once radionuclides are released from the EBS, flow and transport in the unsaturated zone and the saturated zone are based on the same models and algorithms as for the nominal scenario class, with the exception of the seepage model in the lithophysal zones of the repository and the flux splitting for the waste package if accelerated localized corrosion can occur. Biosphere calculations and parameters for the seismic scenario class are also unchanged from those for the nominal scenario class.

The damage abstractions for the drip shield, waste package and cladding provide the representation for TSPA-LA of the FEPs that can cause damage to the engineered barriers from seismic hazards. Table 4 identifies the TSPA-LA FEPs that are relevant to the seismic scenario class and the seismic consequence abstractions. Table 4 also identifies how these FEPs are represented in TSPA-LA.

Table 4. Included FEPs Relevant to Seismic Consequence Abstractions and Their Disposition in TSPA-LA

FEP #	FEP Name	Summary TSPA-LA Disposition
1.2.02.03.0A	Fault Displacement Damages EBS Components	<p>Damage to the waste package from fault displacement is included in the seismic scenario class for TSPA-LA. The expected numbers of damaged waste packages on four secondary faults are evaluated for a range of annual exceedance frequencies, based on the mean hazard curves for the Sundance Fault, the Drill Hole Wash, the Pagany Wash Fault, and the Sevier Wash Fault, on the clearances between various types of waste packages and the drip shield, and on the expected numbers of waste packages that lie on these four faults. The clearances between the waste package packages and drip shield are based on a simple representation for damage to the invert from fault displacement. The approximation is made that the emplacement pallet collapses into the invert on the elevated side of the fault. No credit is taken for the potential increase in clearances due to further shifting of the ballast in the invert or due to failure of the steel framework in the invert. Further details are provided in Section 6.8.1.</p> <p>Damage to the waste package is sampled from a uniform distribution with a lower bound of 0% and an upper bound given by the area of the waste package lid. The uniform distribution is a simple approximation to the upper and lower damage bounds in lieu of detailed structural response calculations. The upper bound is a reasonable estimate for a severely crimped waste package that loses its lid because of cracking in the welds holding the lid in place. The lower bound is a reasonable estimate for a waste package this is minimally damaged, either because fault displacement slightly exceeds the available clearance or because the shear occurs at the opposite end of the waste package from the lid.</p> <p>Crimping is viewed as the main damage mechanism for the waste package because the package is a very robust, thick-walled cylinder that will not be damaged by tilting or minor displacements. In addition, the ability of the waste package to move on the pallet makes it unlikely that a large enough bending moment or torsion can be applied to result in failure.</p> <p>Damage to a drip shield from fault displacement is 100% if it surrounds a damaged waste package or 0 if it does not. Similarly, cladding in a waste package is 100% perforated if it is in a damaged waste package or undamaged if its waste package is not affected by fault displacement.</p> <p>Section 6.8 defines the damage abstraction for the EBS components in response to fault displacement. Step 8 in Section 6.10.2 provides an algorithmic description and definition of output parameters for the fault displacement damage abstraction for the EBS components. Table 30 summarizes the 20 output parameters for TSPA-LA that specifically relate to damage from fault displacement.</p>

Table 4. Included FEPs Relevant to Seismic Consequence Abstractions and Their Disposition in TSPA-LA (Continued)

FEP #	FEP Name	Summary TSPA-LA Disposition
1.2.03.02.0A	Seismic Ground Motion Damages EBS Components	<p>Damage to the waste package, the drip shield, and the cladding is included in the seismic scenario class for TSPA-LA. Structural response calculations for the waste package and drip shield are the basis for predicting failed areas for advective flow and transport. The criteria for failure are based on a residual stress threshold of between 80% and 90% of the yield strength for Alloy 22 and of 50% of the yield strength for Titanium Grade 7. The residual stress thresholds are based on an analysis of experimental data for stress corrosion cracking, as described in <i>Stress Corrosion Cracking of the Drip Shield, the Waste Package Outer Barrier, and the Stainless Steel Structural Material</i> (BSC 2003I, Section 6.2.1); this analysis is summarized and extended in Section 6.3 of this report. Failed areas occur in response to impact of the waste package on the emplacement pallet and to end-to-end impacts of adjacent waste packages. Because damage to the waste package is always much less than 100%, the failed areas are abstracted as a uniform distribution with a lower bound of 0 and an upper bound that is a function of PGV. The uniform distribution has also been compared to an alternate conceptual model based on a lognormal distribution of damage. This alternate conceptual model provides insights into the conservatism or nonconservatism of the original uniform distribution. In fact, the upper bound of the uniform distribution has been increased to ensure conservatism with respect to the lognormal distribution over a PGV range of 1 m/s to 6 m/s.</p> <p>To determine the functional dependence on PGV, vibratory ground motions are defined at annual exceedance frequencies of 10^{-6} per year, 10^{-7} per year, and 5×10^{-4} per year. Fifteen sets of three-component ground motions are sampled to capture the variability in the temporal details of the ground motions at the 10^{-6} per year and 10^{-7} per year PGV levels. A single set of three-component ground motions, originally developed for preclosure design, represents ground motion at the 5×10^{-4} per year level. The variability in the ground motions is a major uncertainty for structural response.</p> <p>The structural response calculations do not represent the dynamic response of the invert to the ground motion. The invert is represented as an elastic body whose surface responds instantaneously and uniformly to the given ground motion. This is a reasonable approach for small amplitude ground motions because the invert is compacted under the weight of the waste packages and drip shield and because any remaining steel framework in the invert will tend to provide some integrity, resulting in an invert that tends to move as a single unit. For high amplitude ground motions, the ballast is likely to be thrown up and redistributed, allowing the heavy EBS components to settle on the bottom of the drift, directly in contact with the rock floor. In this case, applying the ground motions directly to the surface of the invert is again a reasonable approach.</p> <p>Sections 6.5.1 and 6.6.3 define the damage abstractions for the waste package and drip shield, respectively, in response to vibratory ground motion. Steps 3 and 4 in Section 6.10.2 provide an algorithmic description and definition of output parameters, for the damage abstractions for these two barriers.</p> <p>Table 30 summarizes the 4 output parameters for TSPA-LA that specifically relate to damage to the waste package and the 4 output parameters for TSPA-LA that relate to damage to the drip shield from vibratory ground motion.</p> <p>Damage to the cladding is also included in the seismic scenario class for TSPA-LA. Structural response calculations for end-to-end impacts of adjacent waste packages define the axial loads on fuel assemblies. These loads are compared to fuel rod failure criteria based on Euler buckling for various fuel pin designs. Comparison of axial loads with the failure criteria indicates that most if not all fuel pins will fail under vibratory ground motions at the 10^{-6} per year and the 10^{-7} per year levels. Cladding will not fail from the vibratory ground motion at the 5×10^{-4} per year level.</p> <p>Section 6.7 defines the damage abstraction for the cladding under vibratory ground motion. Step 7 in Section 6.10.2 defines the algorithm for the damage abstraction for cladding in TSPA-LA. Table 30 identifies the single output parameter for the abstraction of cladding damage.</p>

Table 4. Included FEPs Relevant to Seismic Consequence Abstractions and Their Disposition in TSPA-LA (Continued)

FEP #	FEP Name	Summary TSPA-LA Disposition
1.2.03.02.0B	Seismic Induced Rockfall Damages EBS Components	<p>Damage to EBS components from seismically induced rockfall is included in the seismic scenario class for TSPA-LA. Vibratory ground motions can cause failure of the host rock around the emplacement drifts. In the nonlithophysal zones, large rock blocks can be ejected from the walls of the drift at high velocity. Rock blocks are ejected for the 10^{-6} per year and the 10^{-7} per year ground motion levels; relatively few blocks are ejected at the 5×10^{-4} per year ground motion level. The damage to the drip shield from large rock blocks is abstracted for TSPA-LA as a function of the PGV. The effects of large rock blocks on the drip shield are discussed in FEP 2.1.07.01.0A.</p> <p>Structural response calculations for the drip shield are the basis for predicting failed areas for advective flow. The criteria for failure are based on a residual stress threshold of 50% of the yield strength for Titanium Grade 7. The residual stress threshold is based on the analysis of experimental data for stress corrosion cracking, as described in <i>Stress Corrosion Cracking of the Drip Shield, the Waste Package Outer Barrier, and the Stainless Steel Structural Material</i> (BSC 2003i, Section 6.2.1); this analysis is summarized in Section 6.3 of this report. Failed areas occur in response to the combined impacts of the rock blocks on the drip shield.</p> <p>In the lithophysal zones, the rock mass can shatter into small fragments, completely collapsing the drift for the 10^{-6} per year and the 10^{-7} per year ground motion levels; the probability of collapse is small at the 5×10^{-4} per year ground motion level, with a small volume of rubble generated by rockfall. The effects of drift collapse on EBS components are discussed in FEP 2.1.07.02.0A.</p> <p>Sections 6.6.1 and 6.6.2 define the damage abstraction for the drip shield in response to rockfall induced by vibratory ground motion. Step 5 in Section 6.10.2 provides an algorithmic description and definition of output parameters for the damage abstraction from rockfall. Table 30 summarizes the 6 output parameters for TSPA-LA that specifically relate to drip shield damage from rockfall in the nonlithophysal zones.</p> <p>Rockfall induced by vibratory ground motion can alter the hydrologic and thermal environment in the drifts after the seismic event. The collapse of drifts from high amplitude ground motion in the lithophysal zones can fill the drifts with rubble, altering the hydrologic and thermal environment around the EBS components. The change in the seepage abstraction in response to drift collapse in the lithophysal zones is based on results from <i>Abstraction of Drift Seepage</i> (BSC 2003q, Section 6.5.1.5). There is no change in the seepage abstraction in the nonlithophysal zones because the rockfall does not completely fill the tunnels at the ground motion levels of interest.</p> <p>The presence of rubble about the drip shield could cause changes in the thermal environment in the EBS if a seismic event occurs relatively soon after repository closure, while the waste package and drip shield are at elevated temperatures. However, the irregular and coarse nature of the rubble is expected to allow sufficient convective heat transfer that the temperature histories calculated for the nominal scenario class may reasonably be used to approximate conditions following a seismic event during the thermal period. If the seismic event occurs when the conditions are satisfied for initiating accelerated localized corrosion on the waste package, then the flux splitting algorithm for the waste package is modified in an appropriate manner (see Section 6.9). Because potential changes in temperature due to the presence of rubble are not expected to be significant, the possible associated changes in temperature-dependent solubility and corrosion rate have not been included in TSPA-LA.</p>

Table 4. Included FEPs Relevant to Seismic Consequence Abstractions and Their Disposition in TSPA-LA (Continued)

FEP #	FEP Name	Summary TSPA-LA Disposition
2.1.07.01.0A	Rockfall (Large Blocks)	<p>Damage to the drip shield from large rock blocks in the nonlithophysal zones is included in the seismic scenario class for TSPA-LA. Rockfall calculations define the ranges in mass, velocity, and frequency of rock blocks that are ejected from the tunnel walls. The rockfall analysis considers the uncertainties associated with fracture geometry and vibratory ground motions. To determine the functional dependence on PGV, vibratory ground motions have been defined at annual exceedance frequencies of 10^{-6} per year, 10^{-7} per year, and 5×10^{-4} per year. Fifteen sets of three-component ground motions have been sampled to capture the variability in the temporal details of the ground motions at the 10^{-6} per year and 10^{-7} per year PGV levels. A single set of three-component ground motions, originally developed for preclosure design purposes, represents the 5×10^{-4} per year level.</p> <p>Structural response calculations for the drip shield are the basis for predicting failed areas for advective flow. (There is no transport through the drip shields because they are upgradient from the waste packages.) The criterion for failure is based on a residual stress threshold of 50% of the yield strength for Titanium Grade 7. The residual stress threshold is based on an analysis of experimental data for stress corrosion cracking in <i>Stress Corrosion Cracking of the Drip Shield, the Waste Package Outer Barrier, and the Stainless Steel Structural Material</i> (BSC 2003I, Section 6.2.1); this analysis is summarized in Section 6.3 of this report. Failed areas are calculated for individual rock blocks that span the range of mass, energy, and impact location (top, side and corner) observed in the rockfall calculations. The damaged area for a complex sequence of rock blocks is then evaluated by interpolation and summation of the damage values for individual rock blocks.</p> <p>Damage is abstracted as two stochastic parameters: (1) a probability that no damage occurs, and (2) a log-triangular distribution if damage does occur. The probability that no damage occurs and the mode of the log-triangular distribution are functions of PGV.</p> <p>Section 6.6.1 defines the damage abstraction for the drip shield due to rock blocks in the nonlithophysal zones. Step 5 in Section 6.10.2 provides an algorithmic description and definition of output parameters for the damage abstraction for the drip shield in the nonlithophysal zones. Table 30 summarizes the 6 output parameters for TSPA-LA that specifically relate to drip shield damage from rockfall in the nonlithophysal zones.</p> <p>Damage to the waste package or cladding from rock blocks is screened out of the seismic scenario class for TSPA-LA. The drip shield remains intact until a seismic event occurs during the first 10,000 to 20,000 years after repository closure. In its intact state, the drip shield will deflect blocks away from the waste package without collapsing, even for the largest blocks. Hence damage to the waste package or cladding from rock blocks is negligible and this damage mechanism is screened out of TSPA-LA.</p>

Table 4. Included FEPs Relevant to Seismic Consequence Abstractions and Their Disposition in TSPA-LA (Continued)

FEP #	FEP Name	Summary TSPA-LA Disposition
2.1.07.02.0A	Drift Collapse	<p>Damage to the EBS components from drift collapse is included in the seismic scenario class for TSPA-LA. The direct effects from drift collapse in the lithophysal zones on EBS components are not included in abstractions for TSPA-LA. In the lithophysal zones, the rock mass is relatively weak and often permeated with large void spaces. This weak rock mass can collapse into small fragments under the load imposed by a large vibratory ground motion. These smaller fragments have little capability to damage the drip shield, either from individual impacts or from their static load, as discussed in Section 6.6.2. Damage to the waste package and cladding will also be insignificant because the drip shield remains intact until a major seismic event occurs, deflecting the rock away from the waste package.</p> <p>The indirect effects from drift collapse may be more significant for EBS performance in lithophysal zones after the seismic event. Drift collapse alters the shape of the drift and fills it with a natural backfill. These indirect changes can affect a variety of processes:</p> <ul style="list-style-type: none"> (i) Seepage may increase because of the irregular drift shape; (ii) Temperature of the drip shield and waste package will increase (relative to an unfilled drift) because the backfill provides an insulating blanket on top of the drip shield; (iii) The general corrosion rate, glass dissolution rate, and some radionuclide solubility limits will increase with increasing temperature. <p>The indirect effect on seepage is included in the seismic abstractions by modifying the seepage flux after a seismic event in the lithophysal zone, based on results from <i>Abstraction of Drift Seepage</i> (BSC 2003q, Section 6.5.1.5) (see Section 6.9 of this report). The indirect effect from accelerated localized corrosion is included in TSPA-LA by modifying the flux splitting algorithm on the waste package if the waste package temperature is above the threshold for accelerated corrosion at the time of the seismic event. The indirect effects from thermal changes are screened out of TSPA-LA because the temperature histories calculated for the nominal scenario class may reasonably be used to approximate conditions following a seismic event during the thermal period, as discussed under FEP 1.2.03.02.0B.</p>

The FEPs in Table 4 differ from the FEP list in *Technical Work Plan for: Engineered Barrier System Department Modeling and Testing FY03 Work Activities* (BSC 2003a). The differences are as follows:

- The title of FEP 1.2.02.03.0A has been changed from *Fault Movement Shears Waste Container* to *Fault Displacement Damages EBS Components*. This FEP has been redefined to address the potential for a variety of failure mechanisms for EBS components due to fault movement, rather than limiting discussion to shear failure of waste containers.
- The description of FEP 1.2.03.01.0A, Seismic Activity, is redundant with other seismic-related FEPs, and has been deleted for TSPA-LA.
- The title of FEP 1.2.03.02.0A has been changed from *Seismic Vibration Causes Container Failure* to *Seismic Ground Motion Damages EBS Components*. The FEP description is split to separately address the effects of ground motion and rockfall on all of the EBS components, in addition to the waste packages.

- A new FEP, 1.2.03.02.0B, *Seismic-Induced Rockfall Damages EBS Components*, is added for TSPA-LA. The description of FEP 1.2.03.02.0A is split to address ground motion and rockfall separately and to identify damage to all of the EBS components.

6.3 FAILED AREA CRITERIA FOR THE WASTE PACKAGE AND DRIP SHIELD

Mechanical processes that occur during a seismic event can result in permanent structural deformation and residual stress in EBS components. These mechanical processes include impacts between adjacent waste packages, between the waste package and its emplacement pallet, between the waste package and the drip shield, between the drip shield and emplacement pallet, and between the drip shield and invert. The presence of residual stress may result in local barrier degradation from enhanced general corrosion, enhanced stress corrosion cracking, and/or enhanced localized corrosion (pitting and/or crevice corrosion). Once the barriers degrade, seepage can flow through the drip shield and into the waste package, resulting in advective flow and transport through the EBS. If seepage is not present, diffusive transport will occur from the waste package into the unsaturated zone.

If the residual stress from mechanical damage exceeds the residual stress threshold for the barrier, then the affected area(s) are considered to have failed as a barrier to flow and transport. Application of this criterion is non-mechanistic, in the sense that detailed calculations of the actual rates of general corrosion, stress corrosion cracking, or localized corrosion are not used to determine the actual failure time after a seismic event. Once the barrier fails, advective flow and transport and diffusive transport can occur through the damaged area (see Assumption 5.3). This is a conservative approach because surface tension can limit advective flow through a network of tight cracks and because precipitation of dissolved salts has the potential to reduce the flow area through these cracks, if not seal them entirely.

The residual stress thresholds for seismic response are similar to the criteria for initiation of stress corrosion cracking on smooth surfaces of Alloy 22 and Titanium Grade 7 (BSC 20031, Section 6.2.1). The use of a stress corrosion cracking initiation criterion is appropriate for seismic analysis because regions where the residual stress from mechanical damage exceeds the failure criterion are expected to be severely cold-worked and, hence, potentially subject to enhanced general and localized corrosion in addition to stress corrosion cracking. If detailed models of stress corrosion cracking initiation, stress corrosion cracking propagation, and enhanced local and general corrosion are developed and applied, not only would failures occur at a later time than the seismic event, but the failed openings would be smaller than those resulting from this simplified failure criterion. A conservative approach is used here because: (a) it is consistent with other failure criteria (BSC 20031, Section 6.2.1), (b) the residual stress failure criterion is transparent, and (c) it is easily applied to the output from detailed structural response calculations.

6.3.1 Residual Stress Damage Threshold for the Waste Package

The residual stress threshold for failure of the waste package is represented by a uniform distribution with a lower bound of 80 percent of the yield strength of Alloy 22 and an upper bound of 90 percent of the yield strength of Alloy 22. The upper bound of 90 percent is based on experimental data and incorporates a safety factor of 2.2 because of the very long lifetime of the

waste package (BSC 20031, Section 6.2.1, third paragraph). The lower bound of 80 percent is introduced to evaluate the sensitivity of damaged area to residual stress threshold for the seismic scenario class. Alloy 22 is the outer shell material for the waste package, where most of the mechanical damage would occur.

This residual stress criterion (80 to 90 percent of the yield strength) is consistent with the failure criterion for stress corrosion cracking initiation in other waste package analyses. For example, the same criterion is used for the initiation of stress corrosion cracking in *FY 01 Supplemental Science and Performance Analyses, Volume 1: Scientific Bases and Analyses* (BSC 2001a, Section 7.3.3.3.3).

In practice, the damage to the waste package has been evaluated at the extremes of the uniform distribution. The results from each structural response calculation are post-processed to determine the elements in the outer shell of the waste package whose residual stress exceeds 80 percent of the yield strength of Alloy 22 and to determine the elements in the outer shell of the waste package whose residual stress exceeds 90 percent of the yield strength of Alloy 22. The failed elements are then converted into a failed area and the failed areas for both the 80 and 90 percent criteria are reported in Section 6.5. The failed areas at intermediate values of the residual stress threshold can then be defined by linear interpolation between the extremes. The elements that exceed 90 percent of the yield strength are always a subset of the elements that exceed 80 percent of the yield strength. In other words, the damaged area for the 90 percent residual stress threshold is always less than or equal to the damaged area for the 80 percent residual stress threshold.

6.3.2 Residual Stress Damage Threshold for the Drip Shield

For the drip shield barrier, the residual stress threshold for failure is represented by a fixed lower bound of 50 percent of the yield strength of the drip shield plate material (Titanium Grade 7) (BSC 20031, Section 6.2.1, third paragraph). The following discussion is abridged from this report. References to the experimental data and technical basis for this threshold can be found in *Stress Corrosion Cracking of the Drip Shield, the Waste Package Outer Barrier, and the Stainless Steel Structural Material* (BSC 20031).

There is a significant experimental data base for Titanium Grade 7 that justifies the use of 50 percent of yield strength as a stress corrosion cracking initiation criterion. These data include long-term constant load tests in a concentrated J-13 brine environment (~15 percent Basic Saturated Water) at 105°C with specimens loaded to stresses of 110 to 140 percent of the yield strength. Some specimens failed relatively early (≤ 168 hours) at applied stresses in excess of 110 percent of yield strength. At 110 percent of yield strength, there is a mixture of failure and non-failure runout times from about 200 hours for first failure to greater than 7,000 hours without failure. These data are consistent with a failure threshold that is less than 110 percent of yield strength.

A second source of information regarding the stress corrosion cracking initiation criterion for Titanium Grade 7 comes from U-bend tests. Initiation of stress corrosion cracking is not observed in fixed deflection U-bend tests on Titanium Grade 7 exposed for one year and Titanium Grade 16 (an analogous titanium/palladium alloy) exposed for five years to a range of

relevant aqueous environments at 60 and 90°C in the Lawrence Livermore National Laboratory Long Term Corrosion Test Facility. These U-bend tests are more representative of secondary residual stress loading that might result from deformation following seismic loadings. These U-bend specimens are deflected and then restrained to give apex strains (cold work level) of greater than 10 percent, which results in sustained stress levels significantly over yield strength. A very conservative value of 50 percent of yield strength is selected as a threshold criterion for Titanium Grade 7, even though the initiation of stress corrosion cracking is not observed for residual stresses greater than yield strength.

6.4 GROUND MOTION AMPLITUDES AT THE EMPLACEMENT DRIFTS

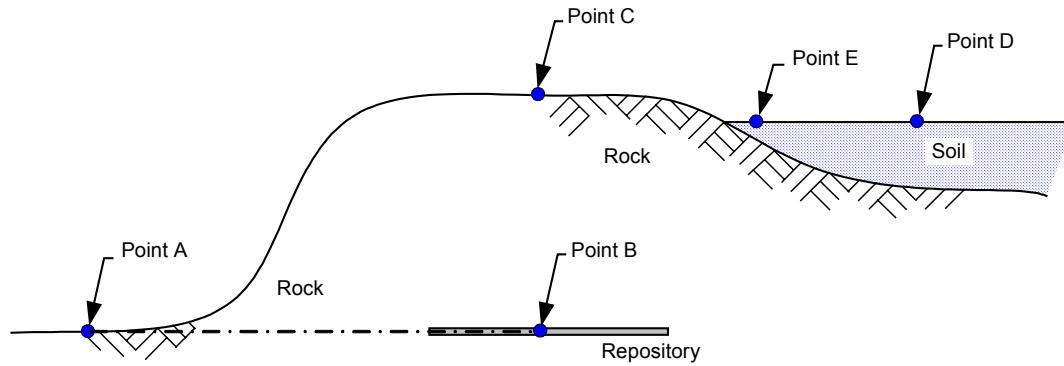
Structural damage from a seismic effect, such as vibratory ground motion, is usually abstracted as a function of the level or amplitude of the ground motion, rather than its annual exceedance frequency. The amplitude of the ground motion is often expressed as PGV or as peak ground acceleration (PGA). This approach has the advantage that the damage abstraction can be defined independently of the geologic properties that influence the propagation and attenuation of ground motions at a specific site. Stated differently, the damage abstraction is independent of the hazard curve at a specific site.

The choice of PGV or PGA for the magnitude of the ground motion is based on engineering judgment as to which parameter will more closely correlate with structural damage. The abstractions in this document use the horizontal PGV as the measure of the amplitude of the ground motion. PGV is appropriate for the response of a rock mass to dynamic loading because the change in stress across a weak compression wave is directly proportional to the particle velocity. PGV is also appropriate for structural damage caused by sliding or impact under earthquake loads (Newmark and Rosenblueth 1971, Sections 11.3.5 and 11.4). As a result, PGV has been selected as the appropriate measure for these abstractions.

The horizontal PGV values have been calculated for the 10^{-6} per year and 10^{-7} per year mean annual exceedance frequencies at the emplacement drifts (called Point B in the probabilistic seismic hazard analyses). The horizontal PGV value for the 10^{-6} per year ground motions is 2.44 m/s (DTN: MO0303DPGVB106.002). The horizontal PGV value for the 10^{-7} per year ground motions is 5.35 m/s (DTN: MO0210PGVPB107.000). The location of Point B is illustrated in Figure 2.

TSPA requires a mean hazard curve at the emplacement drifts (Point B) for a wide range of exceedance frequencies. The two values of horizontal PGV that are available at Point B are insufficient to define the hazard curve over its full range, which is typically 10^{-4} per year to 10^{-8} per year. A solution to this problem is to scale the Point A (a reference rock outcrop at the repository elevation, as shown in Figure 2) hazard curve so that it minimizes the sum of the squares of the residuals with respect to the two known values at Point B. This approach, known as a least square fit, is reasonable because it preserves the shape of the Point A hazard curve while reproducing the known values at Point B within a small error. The shape of the hazard curves at Points A and B will be approximately the same if the deaggregation of earthquake sources over the frequency range of interest remains similar at the two points. This is a reasonable approximation over the frequency range of interest.

The scaling analysis is presented in Attachment I, based on the Point A hazard curve defined by the probabilistic seismic hazard analyses expert elicitation (DTN: MO03061E9PSHA1.000, file h_vel_extended.frac_mean). A scaling factor of 0.7963 results in an error of +7.6 and -1.7 percent with respect to the two known values at Point B. The scaled hazard curve at Point B is illustrated in Figure 3. PGV values at other annual exceedance frequencies can be determined by interpolation, with the resulting values shown in Table 5.



LEGEND

- Point "A" - Reference rock outcrop
- Point "B" - Repository elevation
- Point "C" - At rock surface
- Point "D" - At surface of significant soil layer over rock
- Point "E" - At surface of shallow soil layer over rock

Modified from CRWMS M&O 1998

Figure 2. Schematic Diagram Showing Locations of Points A and B

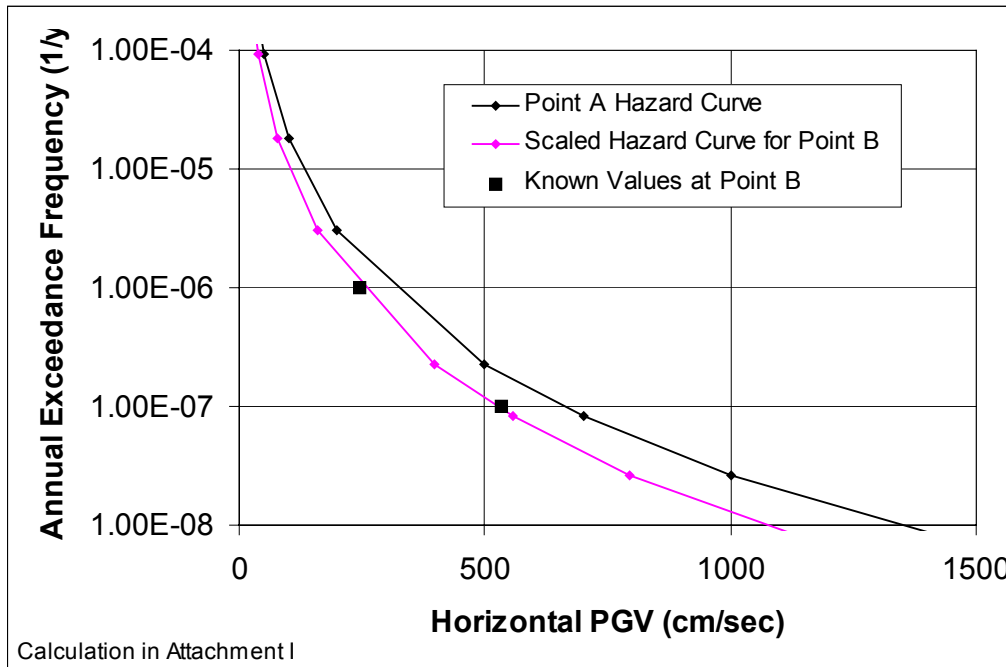


Figure 3. Hazard Curve for Point B is Generated by Scaling the Point A Hazard Curve

Table 5. Calculated Values of PGV on the Point B Hazard Curve

Annual Frequency of Occurrence (1/yr)	Horizontal PGV ^a (cm/s)
5×10^{-4}	18.1
10^{-4}	38.8
5×10^{-5}	55.0
10^{-5}	106.7
10^{-6}	262.4 ^b
10^{-7}	525.8 ^b
10^{-8}	1073.

NOTES: ^a All values calculated in Attachment I.

^b These calculated values have an error of +7.6 and -1.7 percent with respect to the known values at Point B of 244 cm/s for 10^{-6} per year and 535 cm/s for 10^{-7} per year, respectively.

6.5 FAILED AREA ABSTRACTION FOR THE WASTE PACKAGE

6.5.1 Initial Abstraction for Damage from Vibratory Ground Motion

This abstraction defines the damage to the waste package from vibratory ground motion. To this end, structural response calculations have been performed to determine the damage from impact(s) between the waste package and emplacement pallet and from impact(s) between adjacent waste packages. The potential for damage from impacts between the waste package and drip shield is included in the analysis, but produces negligible damage because the drip shield is unrestrained and can move freely.

In this section, the term “damage” is synonymous with a failed area that exceeds the residual stress threshold for Alloy 22, allowing advective flow through the waste package and radionuclide transport from the waste package. Permanent structural deformation does not always result in “damage” because the residual stress may be below the threshold for Alloy 22. No damage is equivalent to 0 percent failed area on the surface of the package, so there is no flow through or transport from the waste package. Full damage is equivalent to 100 percent failed area, wherein all the incident flux passes through the waste package.

6.5.1.1 Structural Response Calculations

A set of 15 calculations for dynamic waste package structural response are performed for the suite of ground motions with a PGV of 2.44 m/s, corresponding to the 10^{-6} per year mean annual exceedance frequency at Point B. A similar set of calculations is also performed for a PGV of 5.35 m/s, corresponding to the 10^{-7} per year mean annual exceedance frequency at Point B (BSC 2003b). The stochastic (uncertain) input parameters for the 15 simulations are the 15 sets of three-component ground motion time histories, the metal-to-metal friction coefficient, and the metal-to-rock friction coefficient. A Monte Carlo sampling scheme defines the appropriate combinations of ground motion and friction coefficients (BSC 2003r, Section 6.4) for each PGV level. The same sets of ground motion time histories (accelerograms) are also used for the analyses of drip shield damage from vibratory ground motions described in Section 6.6.1 and for the analyses of rockfall induced by vibratory ground motion.

The structural response calculations do not represent the dynamic response of the invert to the ground motion. The invert is represented as an elastic body whose surface responds instantaneously and uniformly to the given ground motion. In other words, the ground motion time histories for the three components of motion are applied directly to the surface of the invert. This is a reasonable approach for small amplitude ground motions because the invert is compacted under the weight of the waste packages and drip shield and because any remaining steel framework in the invert will tend to provide some integrity. These effects will result in an invert that tends to move as a single unit. For high amplitude ground motions, the invert ballast is likely to be thrown up and redistributed, allowing the heavy EBS components to settle on the bottom of the drift, directly in contact with the rock floor. In this case, applying the ground motions directly to the surface of the invert is again a reasonable approach.

The damage to the waste package is determined by comparing the residual first principal stress on the waste package outer shell to the failure criterion defined in Section 6.3. More specifically, two residual stress thresholds are used to define the damaged area on the outer shell of the waste package. The two stress thresholds are 80 and 90 percent of the yield strength of Alloy 22. These values correspond to the lower and upper bound of the uniform distribution for the residual stress threshold defined in Section 6.3. The area on the outer shell of the waste package for which the residual first principal stress exceeds the residual stress threshold is referred to as the “damaged area” or “failed area” throughout this document.

6.5.1.2 Waste Package Damage

The damaged areas for 14 different realizations at an annual frequency of occurrence of 10^{-6} per year are summarized in Table 6 (BSC 2003b, Table 6.1.4-2; BSC 2003c, Table 16). The results for realization 8 are not presented in Table 6 because an input error was discovered for this calculation during the checking process. The mean damage and standard deviation of the damage is also presented in this table. The mean damage for the 80 percent residual stress threshold is approximately twice as large as the mean damage for the 90 percent residual stress threshold. Note also that the variability in damage (i.e., the ratio of the maximum damage to the minimum damage for a given ground motion level) from the ground motions is approximately a factor of 10 at a given residual stress threshold. The uncertainty in damage is dominated by the uncertainty in ground motion, rather than the uncertainty in the residual stress threshold.

The results in Table 6 also demonstrate that the cumulative damage area is dominated by the contribution from end-to-end impacts of adjacent waste packages. In particular, the damaged area from waste package to pallet impacts is much smaller than the damage due to the end-to-end impacts of adjacent waste packages, with the exception of realization number 14. The damage from end-to-end impacts is the dominant contribution to total damage because the adjacent waste package is conservatively represented as an essentially rigid wall anchored to the invert. The rigid wall is used for computational simplicity, but results in overestimating the damage from end-to-end impacts. The damage from multiple end-to-end impacts may also be overestimated because the potential for stress waves caused by a late impact to relax the residual stress generated by earlier impacts is ignored in estimated to total damaged area.

The damaged areas for 14 different realizations at an annual frequency of occurrence of 10^{-7} per year are summarized in Table 7 (BSC 2003b, Table 6.2.4-2; BSC 2003c, Table 17). The results

for realization 2 are not presented in Table 7 because the kinematics of the waste package are such that the impacts between package and pallet occur outside the finely meshed region of the outer shell. The mean damage for the 80 percent residual stress threshold is again approximately twice as large as the mean damage for the 90 percent residual stress threshold. The variability in damage from the ground motions is the dominant uncertainty because it is more than a factor of 10 at a given residual stress threshold. Finally, the damaged area from waste package to pallet impacts is much smaller than the damage due to the end-to-end impacts of adjacent waste packages, with the exception of realization numbers 1, 4, and 14.

Table 6. Damaged Area from Vibratory Ground Motion at the 10^{-6} Annual Exceedance Frequency

Realization Number†	Ground Motion Number	Damaged Area on the Waste Package					
		Waste Package to Pallet Interaction (m^2 ; % of total OS area)		Waste Package to Waste Package Interaction (m^2 ; % of total OS area)		Cumulative (m^2 ; % of total OS area)	
		80% Yield Strength	90% Yield Strength	80% Yield Strength	90% Yield Strength	80% Yield Strength	90% Yield Strength
1	7	0.0029; 0.010	0.0014; 0.0050	0.023; 0.082	0.012; 0.043	0.026; 0.092	0.013; 0.046
2	16††	0; 0	0; 0	0.017; 0.060	0.0089; 0.032	0.017; 0.060	0.0089; 0.032
3	4	0.0050; 0.018	0; 0	0.19; 0.67	0.083; 0.29	0.20; 0.71	0.083; 0.29
4	8	0.030; 0.11	0.0064; 0.023	0.12; 0.43	0.061; 0.22	0.15; 0.53	0.067; 0.24
5	11	0.0015; 0.0053	0; 0	0.15; 0.53	0.066; 0.23	0.15; 0.53	0.066; 0.23
6	1	0.025; 0.089	0.0028; 0.0099	0.15; 0.53	0.063; 0.22	0.18; 0.64	0.066; 0.23
7	2	0.017; 0.060	0; 0	0.11; 0.39	0.057; 0.20	0.13; 0.46	0.057; 0.20
9	10	0.0035; 0.012	0; 0	0.12; 0.43	0.062; 0.22	0.12; 0.43	0.062; 0.22
10	9	0; 0	0; 0	0.014; 0.050	0.0071; 0.025	0.014; 0.050	0.0071; 0.025
11	5	0.012; 0.043	0.0037; 0.013	0.074; 0.26	0.032; 0.11	0.086; 0.30	0.036; 0.13
12	6	0.0039; 0.014	0; 0	0.073; 0.26	0.036; 0.13	0.077; 0.27	0.036; 0.13
13	12	0; 0	0; 0	0.032; 0.11	0.016; 0.057	0.032; 0.11	0.016; 0.057
14	14	0.010; 0.035	0.0043; 0.015	0.0056; 0.020	0.0029; 0.010	0.016; 0.057	0.0072; 0.026
15	3	0.0078; 0.028	0.0015; 0.0053	0.020; 0.071	0.010; 0.035	0.028; 0.099	0.012; 0.043
Mean Value‡						0.310%	0.136%
Standard Deviation‡						0.237%	0.097%
Minimum Value‡						0.050%	0.025%
Maximum Value‡						0.710%	0.136%

Source: BSC 2003c, Table 16

NOTES: † Only 14 realizations are presented in this table. Results for realization 8 are not presented because of an error in the input file for this calculation.

†† Calculations are performed with 15 ground motions numbered 1, 2, 3, ..., 14, and 16. Time history 15 is not used because it has an anomalous response spectrum.

‡ Mean, standard deviation, minimum and maximum damage areas are calculated in Attachment II.

OS = outer surface of waste package.

Table 7. Damaged Area from Vibratory Ground Motion at the 10^{-7} Annual Exceedance Frequency

Realization Number†	Ground Motion Number	Damaged Area on the Waste Package					
		Waste Package to Pallet Interaction (m^2 ; % of total OS area)		Waste Package to Waste Package Interaction (m^2 ; % of total OS area)		Cumulative (m^2 ; % of total OS area)	
		80% Yield Strength	90% Yield Strength	80% Yield Strength	90% Yield Strength	80% Yield Strength	90% Yield Strength
1	7	0.20; 0.71	0.17; 0.60	0.16; 0.57	0.086; 0.30	0.36; 1.28	0.26; 0.92
3	4	0.096; 0.34	0.083; 0.29	0.42; 1.49	0.17; 0.60	0.52; 1.84	0.25; 0.89
4	8	0.12; 0.43	0.096; 0.34	0.11; 0.39	0.050; 0.18	0.23; 0.82	0.15; 0.53
5	11	0.093; 0.33	0.071; 0.25	0.18; 0.64	0.080; 0.28	0.27; 0.96	0.15; 0.53
6	1	0.046; 0.16	0.024; 0.085	0.42; 1.49	0.15; 0.53	0.47; 1.67	0.17; 0.60
7	2	0.038; 0.13	0.028; 0.099	0.32; 1.13	0.14; 0.50	0.36; 1.28	0.17; 0.60
8	13	0.095; 0.34	0.068; 0.24	0.32; 1.13	0.14; 0.50	0.42; 1.49	0.21; 0.74
9	10	0.0052; 0.018	0.0035; 0.012	0.034; 0.12	0.017; 0.060	0.039; 0.14	0.021; 0.074
10	9	0.16; 0.57	0.14; 0.50	0.33; 1.17	0.15; 0.53	0.49; 1.74	0.29; 1.03
11	5	0.0016; 0.0057	0; 0	0.30; 1.06	0.11; 0.39	0.30; 1.06	0.11; 0.39
12	6	0.062; 0.22	0.041; 0.15	0.10; 0.35	0.044; 0.16	0.16; 0.57	0.085; 0.30
13	12	0.027; 0.096	0.018; 0.064	0.12; 0.43	0.053; 0.19	0.15; 0.53	0.071; 0.25
14	14	0.020; 0.071	0.016; 0.057	0.0077; 0.027	0.0040; 0.014	0.028; 0.099	0.020; 0.071
15	3	0.0045; 0.016	0; 0	0.29; 1.03	0.14; 0.50	0.29; 1.03	0.14; 0.50
Mean Value‡						1.036%	0.530%
Standard Deviation‡						0.560%	0.298%
Minimum Value‡						0.099%	0.071%
Maximum Value‡						1.84%	1.03%

Source: BSC 2003c, Table 17

NOTES: † Only 14 realizations are presented in this table. Results for realization 2 are not presented because the kinematics of the waste package are such that the impacts between package and pallet occur outside the finely meshed region of the outer shell.

‡ Mean, standard deviation, minimum and maximum damage calculated in Attachment II.

OS = outer surface of waste package.

6.5.1.3 Initial Abstraction for Waste Package Damage

The failure criterion for Alloy 22 is defined as a uniform distribution between 80 and 90 percent of the yield strength (see Section 6.3.1). In other words, there is uncertainty in the value of the appropriate residual stress threshold for Alloy 22. Tables 6 and 7 present damage values at the two extremes (80 and 90 percent) of the residual stress threshold. Since the failed area is defined by the elements of the finite-element grid whose residual stress exceeds the value of the residual stress threshold, it follows that the failed area for the 90 percent threshold is always less than or equal to the failed area for the 80 percent threshold.

The residual stress threshold could be retained as a stochastic parameter whose value is sampled for TSPA-LA. In this situation, the damage at intermediate values of the residual stress

threshold could be defined by linear interpolation between the damage at the extreme values. However, the uncertainty in damaged area is dominated by the ground motions, rather than the residual stress threshold, as discussed above. In this situation, it is reasonable to simplify the damage abstraction for the waste package by averaging the failed areas at the two extremes (80 and 90 percent). In effect, this corresponds to a failure criterion for the average (85 percent) value of the residual stress thresholds. The use of the average or mean value is consistent with the release limits for the repository at Yucca Mountain, which are expressed in terms of the mean of the distribution of projected dose to the reasonably maximally exposed individual, per 10 CFR 63.303 and 63.311. The average damage values are calculated in Attachment II.

A number of distributions are considered as potential fits to the damage area for the 14 realizations with damage information. A normal distribution provides a reasonable fit to the results at the 10^{-7} per year annual exceedance frequency, although it must be truncated for the 10^{-6} per year annual exceedance frequency because the mean and standard deviation are approximately equal. The magnitude of the mean is only 30 to 40 percent greater than the standard deviation, implying a significant fraction of negative damage values for a normal distribution.

A uniform distribution provides an excellent description of the damage, is simple to implement in a Monte Carlo sampling scheme, and does not need to be truncated. Figure 4 compares the damage results for the 10^{-7} per year ground motion level to the cumulative distribution function for a uniform distribution, which is simply a straight line. In comparing the damage results to the cumulative distribution function, the damage values have been sorted in ascending order and each point is assigned equal probability.

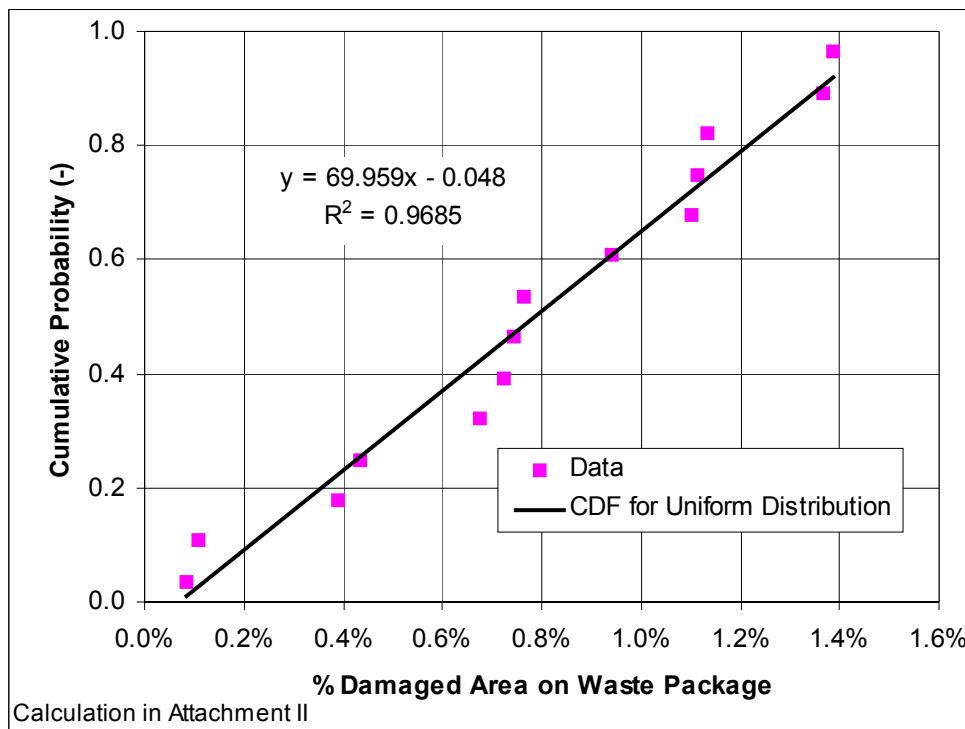


Figure 4. Comparison of Damage Results for the 10^{-7} per Year Ground Motion Level to the Cumulative Distribution Function for a Uniform Distribution

The straight line for the least squares fit to the results has been determined by Excel’s statistical package. This straight line provides an excellent fit to the results, judging by the fact that the square of the residuals, r^2 , is 0.9685. As a reminder, an r^2 value of 1.0 is a perfect correlation and a value of 0.0 is no correlation. The fact that a straight line provides an excellent fit to the results confirms that a uniform distribution is a reasonable representation for the damage abstraction.

A uniform distribution also provides a very good description of the damage results for the 10^{-6} per year ground motion level. Figure 5 compares the damage results for the 10^{-6} per year ground motion level to the straight line for the least squares fit. The square of the residuals with the straight line, 0.946, is slightly less than that in Figure 4 but still quite close to 1.0. Again, a uniform distribution is a reasonable representation of these damage results.

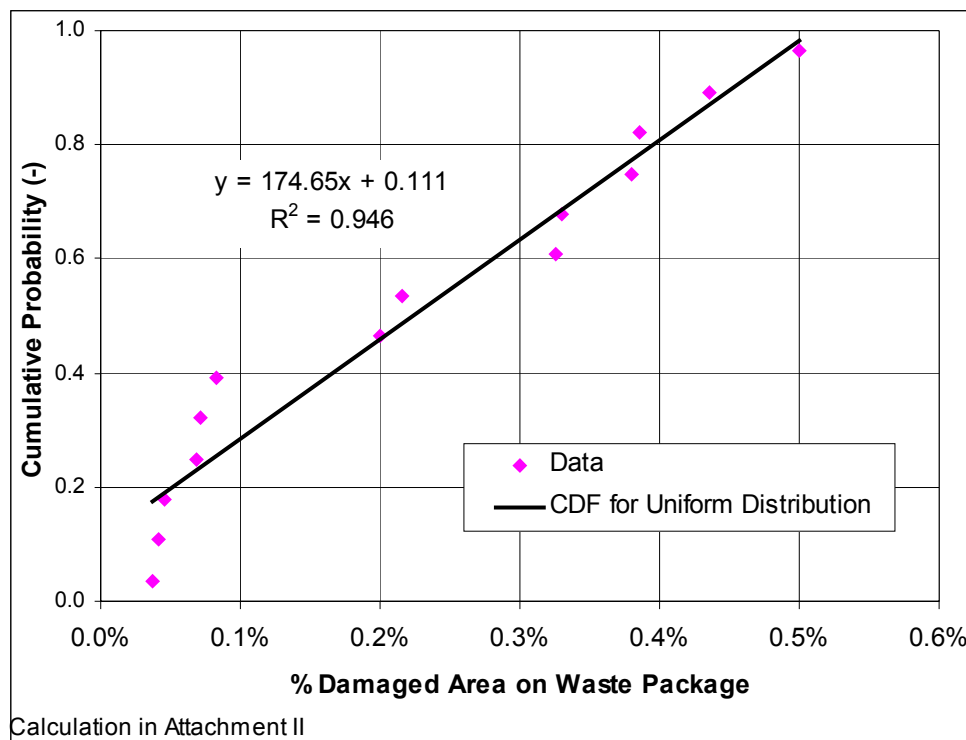


Figure 5. Comparison of Damage Results for the 10^{-6} per Year Ground Motion Level to the Cumulative Distribution Function for a Uniform Distribution

The upper and lower bounds of the uniform distribution must span the range of damage values shown in Figures 4 and 5. Estimation of the upper bound of a uniform distribution from sampled results (especially when the number of samples is small) requires careful consideration. Rossman et al. (1998) describe a Bayesian procedure for calculating the 95 percent upper confidence limit (UCL) for the upper bound of a uniform distribution as follows:

$$95\%UCL = \alpha^{-\frac{1}{n-1}} \max(X) \tag{Eq. 2}$$

where α is the significance level (i.e., 0.05 at the 95 percent confidence level), n is the sample size, and X is the uncertain quantity of interest (i.e., the damaged area). Using Equation 2, the Bayesian upper bound for the uniform distribution of damaged area is calculated to be 0.630 percent at the 10^{-6} per year hazard level and 1.744 percent at the 10^{-7} per year hazard level. This formula for calculating the Bayesian upper bound uses the so-called flat prior, which indicates maximal uncertainty about the upper bound based on the sampled values. Other prior distributions tend to represent increased prior certainty about the value of the parameter, and thus produce lower posterior estimates (Rossman et al. 1998). The selection of the flat prior can thus be justified as a conservative choice.

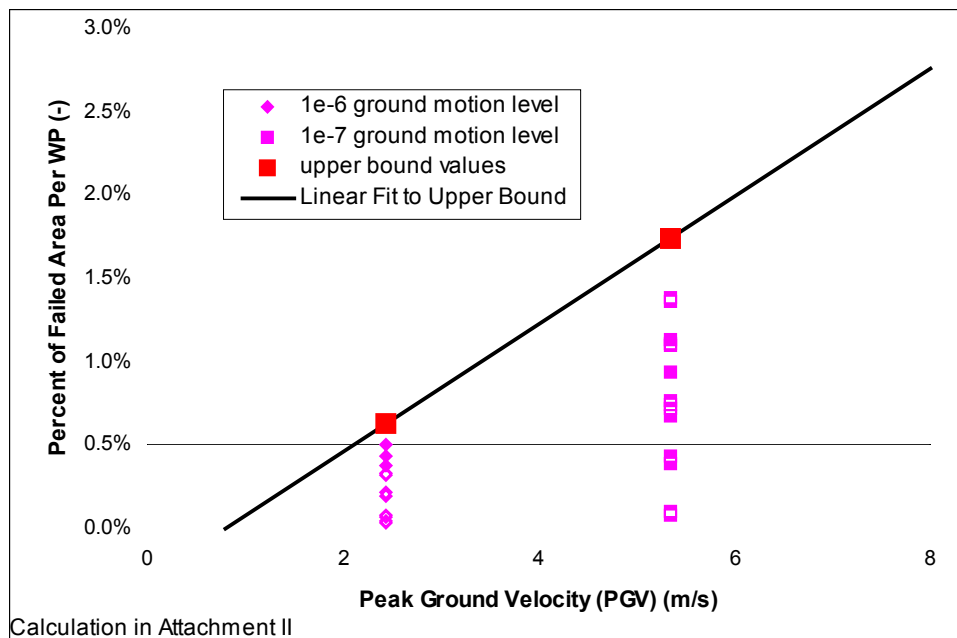
Estimation of the lower bound of the uniform distribution also must be considered carefully. Figure 4 shows that the least squares fit for the 10^{-7} per year ground motion level has a minimum damage value of less than 0.1 percent at a cumulative probability of 0.0. This minimum damage value is about a factor of 15 less than the damage of 1.5 percent at a cumulative probability of 1.0. Figure 5 shows that the least squares fit for the 10^{-6} per year ground motion level has a negative damage at a cumulative probability of 0.0. This is physically impossible, and is probably caused by the cluster of six points with damage values between 0.0 and 0.1 percent.

In this situation, it is reasonable to set the lower bound of the uniform distribution at 0 percent at all ground motion levels. Zero percent is clearly the minimum value for the least squares fit at the 10^{-6} per year ground motion level. A zero percent minimum value produces a minor error in the minimum value for the least squares fit at the 10^{-7} per year ground motion level. Zero percent is also a reasonable lower bound for the preliminary damage results at the 10^{-5} per year ground motion level presented in the next section (Section 6.5.2). However, it is difficult to extrapolate the behavior for ground motions significantly greater than those at the 10^{-7} per year ground motion level.

The damage abstraction for the TSPA-LA calculations is a relationship between the Bayesian upper bound and the corresponding seismic hazard level, as measured by horizontal PGV. The PGV levels corresponding to the 10^{-6} and 10^{-7} per year hazard levels are 2.44 m/s and 5.35 m/s, respectively (see Section 6.4). A linear fit to the Bayesian upper bounds calculated earlier and these PGV values produces the following linear relationship:

$$D_{ub} = \text{MAX}(0.0, 0.383 \times PGV - 0.305) \quad (\text{Eq. 3})$$

where D_{ub} = Bayesian upper bound of the uniform distribution of the percent of damaged area on the surface of the waste package at a given PGV. The MAX function ensures that the value of D_{ub} cannot be less than 0 percent. These calculations are documented in Attachment II. Figure 6 compares the results for percent damaged area on the surface of the waste package with the linear fit to the Bayesian upper bound at the 95 percent confidence limit from Equation 3.



NOTE: The lower bound is 0 percent.

Figure 6. Linear Fit to Upper Bound of Damage Distribution

The damage to the waste package is applied to all waste packages in the repository, except for those packages that experience a juvenile failure. There is no spatial variability for damage to the waste package.

6.5.2 Corroborating Information from the 10^{-5} Per Year Ground Motion Level

Three simulations have been performed using approximate ground motions for the 10^{-5} per year annual exceedance frequency, corresponding to a PGV value of 1.067 m/s. These simulations provide added confirmation that the upper bound for the damage, as shown in Figure 7, is tending to zero in a linear fashion. The approximate ground motions are created by scaling the three acceleration components of each 10^{-6} per year ground motions by the ratio of the PGV for the 10^{-5} per year level to the PGV for the 10^{-6} per year level. This procedure is not exact because the deaggregation of seismic sources for the 10^{-5} and 10^{-6} per year ground motion levels is different. However, it provides a reasonable approach for calculations that can corroborate the abstraction in Figure 6. The scaling factor, 0.4066, is calculated in Attachment I of this report.

Ground motions number 1, 2, and 10, corresponding to realizations 6, 7, and 9, respectively, are scaled for these calculations. These three ground motions are characterized by the highest intensity (energy) among the set of 15 10^{-6} per year ground motions and have high levels of damage, although not the maximum damage (for example, see Table 6). The damage results for these three ground motions (BSC 2003b, Table XI-2; BSC 2003m, Table 58) are summarized in Table 8.

The damage results for these three additional points, at a PGV of 1.067 m/s corresponding to the 10^{-5} per year ground motion level (see Table 5), can be added to the abstraction in Figure 6. The Bayesian upper bound at the 95 percent confidence limit can also be calculated for the three

points in Table 8, and results in a value of 0.114 percent. Figure 7 shows that the linear equation for the upper bound, based on the results at PGVs of 2.44 m/s and 5.35 m/s, is a reasonable fit at the 10^{-5} per year ground motion level, and that a lower bound of 0 percent damage is reasonable at this level. While there are only three results at a PGV of 1.067 m/s, these points do provide additional confidence in the extrapolation of the abstraction for waste package damage to values of PGV of 1 m/s and below.

Table 8. Damaged Area from Vibratory Ground Motion at the 10^{-5} Annual Exceedance Frequency

Realization Number	Ground Motion Number	Damaged Area (m^2 ; % of total OS area)		
		80% Yield Strength	90% Yield Strength	Average Yield Strength
6	1	0.0060; 0.021	0; 0	0.0030; 0.0105
7	2	0; 0	0; 0	0; 0
9	10	0.0106; 0.038	0.0037; 0.013	0.00715; 0.0255

Source: BSC 2003b, Attachment XI, Table XI-2; BSC 2003m, Table 58
OS = outer surface of waste package.

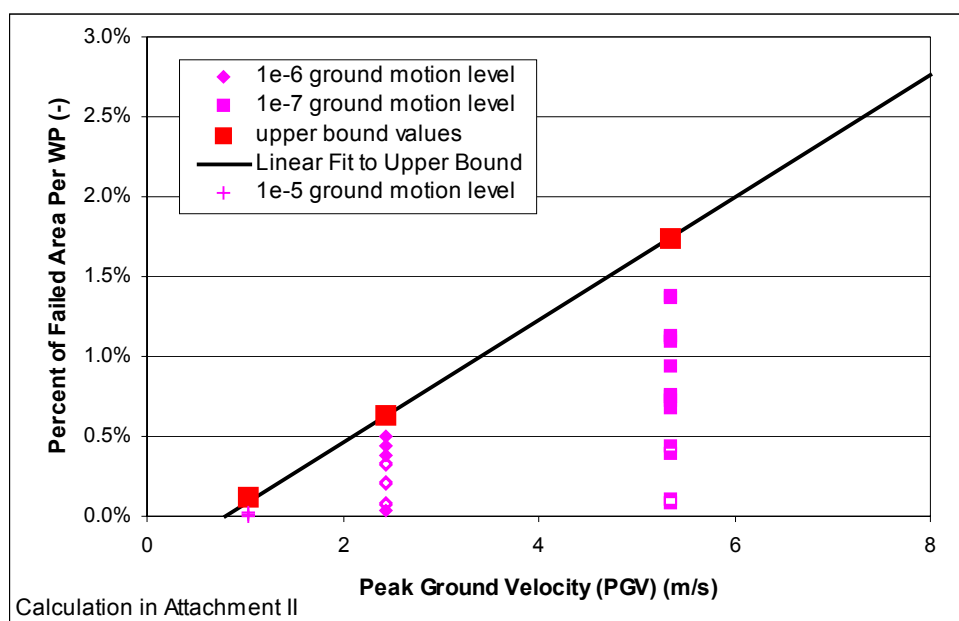


Figure 7. Comparison of Linear Fit to Bayesian Upper Bound of Damage Distribution at PGVs of 2.44 m/s and 5.35 m/s with the Results for the 10^{-5} per Year Ground Motions

6.5.3 Independent Technical Review of Model Abstraction

An independent technical review of this model abstraction has been performed by Dr. Robert P. Kennedy of RPK Structural Mechanics Consulting. The result of Dr. Kennedy’s review is presented in Attachment III and briefly summarized here.

Dr. Kennedy presents an alternate analysis of the damage information for the waste package. This alternative analysis is structured around a fragility approach. In a fragility approach, one often asks: “What is the exceedance probability that the damage will exceed a given level for a

given value of PGV?” Following this approach, a lognormally distributed approximation of the damage surface is fit by trial and error. The following lognormal distribution provides a good fit to the damage results in terms of exceedance probability (Equation III-9 in Attachment III):

$$\begin{aligned} \text{Median:} & \quad PGV_{50} = (5.7 \text{ m/s})D^{0.5} \\ \text{Log. Std. Dev.:} & \quad \beta = 0.28D^{-0.5} \leq 0.8 \\ \text{Truncation Point:} & \quad EP = 1 \% \end{aligned}$$

A comparison of the lognormal distribution at PGV of 2.44 m/s and 5.35 m/s with the uniform distribution in Section 6.5.1 identifies values of D (in the units of percent damaged area) where the uniform distribution is nonconservative with respect to the lognormal distribution. For a PGV of 5.35 m/s, the uniform damage surface provides a good approximation for D less than about 1.67 percent. Above this damage level the uniform damage surface estimate of exceedance probability becomes seriously nonconservative. For a PGV of 2.44 m/s, the uniform damage surface significantly overestimates exceedance probability (is conservative) for damage between 0.06 and 0.56 percent. However, a more significant issue is that the uniform damage surface significantly underestimates exceedance probability for damage greater than 0.60 percent.

The nonconservatism at higher damage values can be easily corrected by changing Equation 2 to slightly increase the linear upper bound for damage, D_{ub} . The nonconservatism can be eliminated if D_{ub} is defined as:

$$D_{ub} = 0.436(PGV) - 0.305 \tag{Eq. 4}$$

instead of using Equation 3. D_{ub} has the units of percent damage, so that a PGV of 5.35 m/s results in damage of 2.0 percent. Details of the comparison between the lognormal distribution and the uniform distribution are presented in Attachment III. Figure 8 compares the modified upper bound for the lognormal fit to the original upper bound for the uniform distribution.

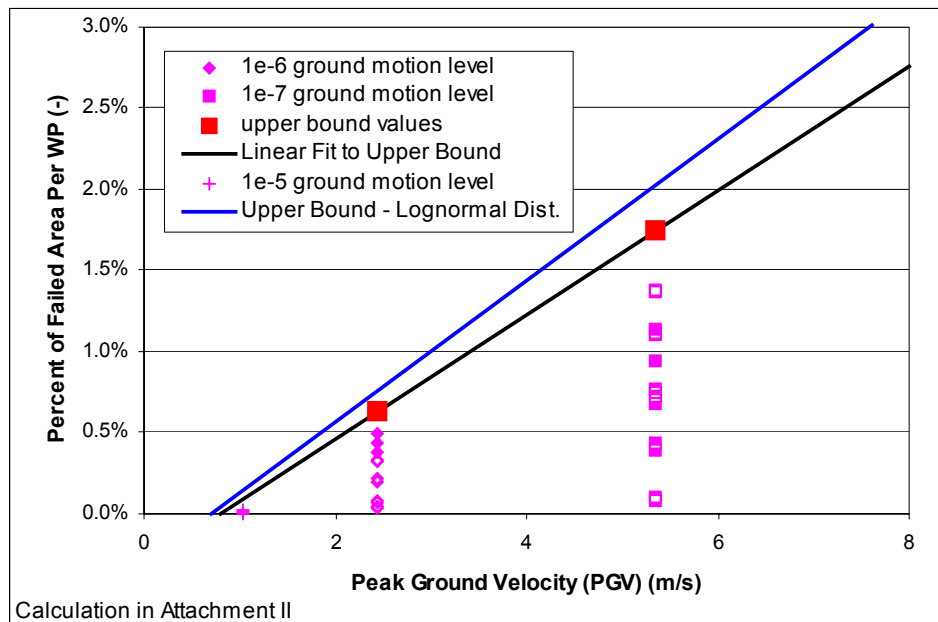


Figure 8. Comparison of Upper Bounds Based on a Lognormal Distribution (Blue Curve) with the Bayesian Upper Bound

6.5.4 Final Abstraction for Damage from Vibratory Ground Motion

Without additional data for PGV values below 2.44 m/s or above 5.35 m/s, it is prudent to choose the more conservative fit (Equation 3) for the upper bound of the uniform distribution for waste package damage for TSPA-LA. Additional structural response calculations at a PGV of 1 m/s (corresponding to the 10^{-5} per year ground motion level) can provide additional insight into the appropriateness of a uniform versus a lognormal distribution for the damage to the waste package. In addition, activities related to defining the maximum amplitude ground motion that can propagate through Yucca Mountain will also assist in bounding the potential damage at PGV values greater than 6 m/s.

6.6 FAILED AREA ABSTRACTION FOR THE DRIP SHIELD

Vibratory ground motion has the potential to damage the drip shield as a barrier to flow. This damage may occur due to the mechanical response of the drip shield to impacts from the waste package, emplacement pallet or invert. Damage may also occur due to the mechanical response of the drip shield to impacts from rock blocks or rockfall that are induced by the ground motions. In addition to damage caused by impact, it is also possible that adjacent drip shields will be separated during a high amplitude ground motion. Separated drip shields could allow seepage to fall directly on a waste package(s), and therefore have the same effect as damage caused by impact. Both mechanisms (damage due to impact and separation) have been observed in the structural response calculations for ground motions at the 10^{-6} per year and 10^{-7} per year levels.

In this section, the term “damaged area” is synonymous with a failed area that exceeds the residual stress threshold for Titanium Grade 7, allowing advective flow through the drip shield. Permanent deformation of the drip shield does not always result in “damage” if the residual stress is below the threshold. No damage is equivalent to 0 percent failed area on the surface, so there is no flow through the drip shield. Full damage is equivalent to 100 percent failed area, wherein all the incident flux passes through the drip shield.

6.6.1 Abstraction for Damage from Rockfall in the Nonlithophysal Zone

Vibratory ground motions have the potential to eject large rock blocks in the nonlithophysal zone. The mechanical response of the drip shield to impact by a large rock block has the potential to damage the drip shield as a barrier to flow. This damage could also occur because of separation between two adjacent drip shields from vibratory ground motions.

Development of an abstraction for damage to the drip shield due to rockfall induced by vibratory ground motion in the nonlithophysal zone involves the following steps. Figure 9 presents a flowchart of these steps, which are described in detail in the following sections.

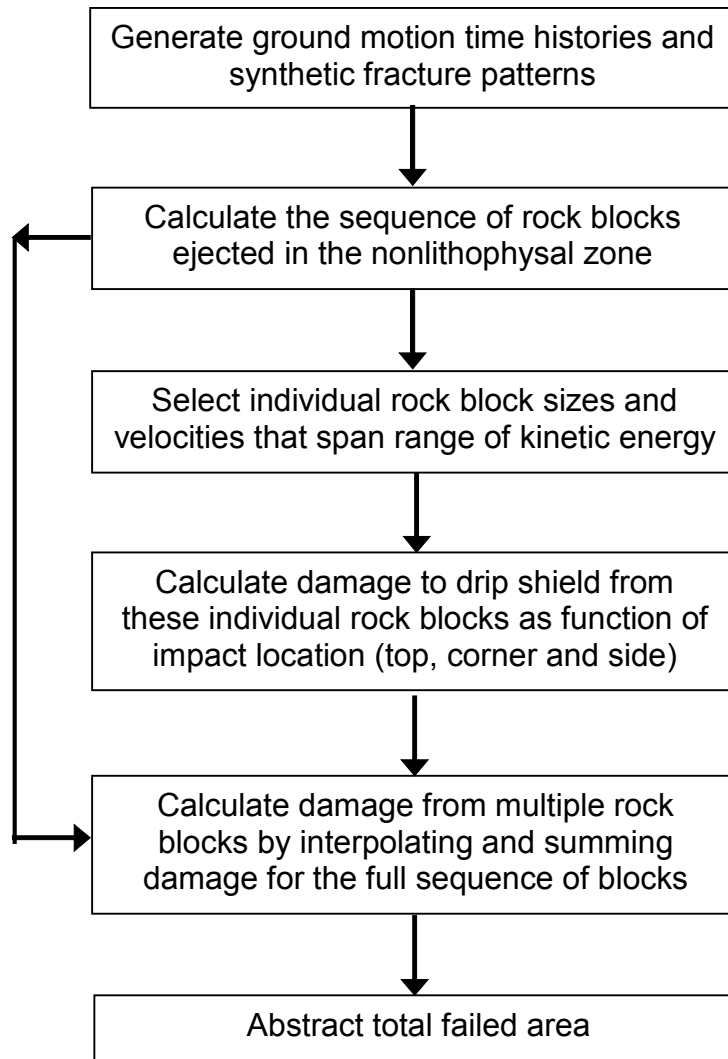


Figure 9. Flow chart of the Drip Shield Damage Abstraction Methodology

- Rockfall calculations have been performed for 15 ground motion time histories at each annual exceedance frequency (10^{-6} per year and 10^{-7} per year), sampling a suite of 105 synthetic fracture patterns.
- Potential results of the rockfall calculations are summarized in terms of the block mass, relative impact velocity, impact angle, impact momentum, and impact energy associated with each individual block that impacts the drip shield.
- A set of representative rocks that span the block energy distribution and impact location are selected in order to optimize the structural response calculations. For each representative block and impact location, a structural response calculation is performed to determine the damage to the drip shield. The residual stress from these calculations is interpreted as a failed area on the drip shield, and collated into a catalog of damage areas as a function of block energy and impact location.

- This catalog is used as the basis for estimating (by interpolation) the impact from multiple rockfall events at intermediate kinetic energy values and impact locations. The damage from a multi-block rockfall is estimated as the sum of the effects from individual blocks.
- The distribution of failed area (caused by the 15 ground motion time histories and synthetic fracture patterns) is generated for the 10^{-6} and 10^{-7} per year annual exceedance frequencies. This distribution is parameterized in terms of a log-triangular distribution, and also characterized in terms of the fraction of no-fail cases.
- The resulting damage abstractions for: (a) mode of log-triangular distribution of the failed area as a function of PGV, and (b) fraction of no-fail cases, as a function of PGV are characterized in terms of best-fit curves. The parameters of these curves are the abstractions for drip shield failure due to rockfall induced by vibratory ground motion.

6.6.1.1 Rockfall Calculations

Analysis of rockfall in the nonlithophysal zone requires ground motion time histories, fracture geometries, and fracture properties as input parameters or boundary conditions for the calculations. To ensure adequate representation of uncertainty and variability, individual rockfall calculations are sampled from 15 ground motions at each probability level (10^{-6} and 10^{-7} per year) and from 105 synthetic fracture patterns. The synthetic fracture patterns (BSC 2003h, Section 6.1.6) are based on a random sampling of 105 centroid locations within a cube of rock that is 100-meters on a side. A Monte Carlo sampling scheme provides the appropriate combinations of ground motion and synthetic fracture pattern (BSC 2003r, Sections 6.1 and 6.2).

A total of 76 3DEC simulations are performed for the 10^{-6} per year annual exceedance frequency (BSC 2003h, Section 6.3.1.2.3 and Attachment XI; DTN: MO0305MWDNLRKF.001). Approximately 33 percent of the simulations predict no rockfall. A total of 281 rock blocks, with a total volume of 101.8 m^3 , have been identified from the analyses. The associated impact parameters for these rock blocks include the following:

- Rock block volume falling on the drip shield
- Relative impact velocity of rock block to the drip shield
- Impact location.

The impact momentum and impact energy, both functions of block mass and impact velocity, are also calculated as functions of the block mass and impact velocity. Summary statistics for these parameters are provided in Table 9. The maximum predicted mass of an individual rock block is 21.42 tons, while the median block mass is 0.23 tons. The predicted results all show large variance and high skewness with the exception of impact velocity.

Table 9. Summary of Rock Block Statistics for the 10^{-6} Annual Exceedance Frequency

	Block Mass (MT)‡	Relative Impact Velocity (m/s)	Impact Angle (degree)	Impact Momentum (kg × m/s)	Impact Energy (Joules)
Mean	0.87	3.39	132	2747	5267
Median	0.23	3.49	120	663	902
Standard Deviation	1.97	1.61	81	6209	12941
Skewness	6.04	0.04	1.12	6.23	7.52
Range	21.39	7.54	355	68836	163083
Minimum	0.02	0.02	5	4	0
Maximum	21.42	7.56	360	68840	163083
Sum	245.55	NA†	NA†	771861	1479888

Source: BSC 2003h, Table 14

NOTES: † Not Applicable; ‡ MT = Metric Ton = 1,000 kg.

A similar number of 3DEC simulations are also performed for the 10^{-7} per year exceedance frequency (BSC 2003h, Section 6.3.1.2.4). Approximately 21 percent of the simulations predict no rockfall. A total of 380 blocks (with a total volume of 151.2 m^3) have been identified from the analyses. As before, information about individual rockfall events (e.g., rock block volume falling on the drip shield, relative impact velocity of rock block to the drip shield, impact location, impact momentum and impact energy) are documented in DTN: MO0301MWD3DE27.003.

Summary statistics for these parameters are provided in Table 10 (BSC 2003h, Table 16). The maximum rockfall block mass predicted is 21.42 tonnes, same as predicted for the 10^{-6} annual exceedance frequency ground motions. The median block size is 0.23 tonnes, also the same as predicted for the 10^{-6} per year exceedance frequency. The median impact momentum and energy predicted for rockfall impact on the drip shield for the 10^{-7} annual exceedance frequency are approximately two times the values predicted for those parameters at the 10^{-6} annual exceedance frequency.

Table 10. Summary of Rock Block Statistics for the 10^{-7} Annual Exceedance Frequency

	Block Mass (MT)‡	Relative Impact Velocity (m/s)	Impact Angle (degree)	Impact Momentum (kg × m/s)	Impact Energy (Joules)
Mean	0.96	5.03	139	4169	11459
Median	0.23	4.63	127	980	2440
Standard Deviation	2.04	2.78	87	8489	27461
Skewness	5.01	1.00	1.06	4.64	6.73
Range	21.39	17.67	356	89485	348170
Minimum	0.02	0.07	1	18	4
Maximum	21.42	17.74	357	89502	348174
Sum	364.58	NA†	NA†	1584186	4354385

Source: BSC 2003h, Table 16

NOTES: † Not Applicable; ‡ MT = Metric Ton = 1,000 kg.

A minor discrepancy has been found between the final version of *Drift Degradation Analysis* (BSC 2003h, Attachment XI; DTN: MO0305MWDNLRKF.001) and the rockfall information used in Attachment IV of this report. For rockfall from ground motions at the 10^{-6} per year level, two blocks associated with case #42 are missing from the “rockfall 1e-6” and “impact information” worksheets in Attachment IV of this report. The material impact of this omission on the abstractions for drip shield damage due to rockfall is negligible. The rationale for this viewpoint is as follows:

- Only 2 out of 281 rockfall events are inadvertently missing from the analysis.
- The rock masses for these two blocks are 0.69 MT (metric tons) and 0.04 MT. By way of comparison, the mean of the entire distribution of 281 blocks is 0.87 MT, the median is 0.23 MT, and the minimum is 0.02 MT (see Table 9).
- The kinetic energy for these two blocks is 10,654 Joules and 307 Joules, whereas the 95th percentile for the entire distribution of 281 events is 24,052 Joules, the median is 902 Joules, and the 5th percentile is 42 Joules.
- Because kinetic energy is directly related to failed area, the two additional points in the failed area distribution should be located between the 5th and 50th percentiles (for the 0.04 MT rock) and between the 50th and 95th percentiles for the 0.69 MT rock.

Given this rationale, the deletion of these two blocks from the original distribution of 279 points is not expected to have any significant impact on the statistics of the distribution because only two blocks are involved and the mass and kinetic energy of both blocks lie well within the typical ranges for rockfall. In this situation, no significant impact is anticipated for the resulting abstraction for damage to the drip shield from rockfall.

6.6.1.2 Drip Shield Damage - Single Block Impact

In order to minimize the number of structural response calculations, a set of five representative blocks and three representative impact locations are selected to span the range of blocks. The idea behind this approach is to perform a limited set of calculations that span the range of rock sizes, rock velocities, rock impact angles and rock impact points on the drip shield. This limited set of calculations then provides the basis for estimating the response of the drip shield when multiple blocks are ejected from drift walls during a ground-motion-induced event. This limited set of calculations is referred to as a “catalog of results” or simply a “catalog.”

The selection of representative rocks is based on their kinetic energy since the impact energy of a rock block should provide a direct correlation with damage. The impact energies associated with the selected rocks correspond to the minimum, maximum, median (50th-percentile), 5th-percentile and 95th-percentile of the sorted impact energies for the 10^{-6} per year exceedance frequency (BSC 2003h, Attachment XI; DTN: MO0305MWDNLRKF.001). Other characteristics of these rock blocks are given in Table 11. Note that the variability in ejection velocity from the host rock sometimes leads to small blocks, with less mass, having a higher kinetic energy than larger blocks.

Table 11. Characteristics of Selected Rock Blocks for the 10^{-6} Annual Exceedance Frequency

Rock Block Mass (MT)	Kinetic Energy (J)	Vertical Velocity (m/s)	Lateral Velocity (m/s)
14.5	163083	4.69	0.656
3.3	24712	3.75	0.0824
0.15	902	3.09	0.955
0.11	42	0.202	0.383
0.25	~0	0.0137	0.0103

DTN: MO0305MWDNLRKF.001

An examination of the rockfall results for the 10^{-7} per year ground motion level (DTN: MO0301MWD3DE27.003) reveals that the range of rocks considered in Table 11 would be adequate for spanning the impact energy range, provided one rock block representing the maximum possible impact energy level for 10^{-7} is added to this set. The parameters for this additional rock block are: block mass = 11.5 MT, kinetic energy = 348174 Joules, vertical velocity = 7.77 m/s, and lateral velocity = 0.295 m/s.

Damage to the drip shield from impact of individual rock blocks is determined by structural response calculations. The objective of these calculations is to determine the areas on the drip shield where the residual stress exceeds the threshold value (50 percent of yield strength) for Titanium Grade 7. The six representative rock sizes impact the drip shield from three different angles: vertically downward onto the top of the drip shield, at a 60° angle (with the horizontal) onto the transition region between the top and side of the drip shield, and horizontally into the side wall. Table 12 shows the results for the 10^{-6} and 10^{-7} per year rockfall on drip shield (BSC 2003g, Section 5.5.1).

Table 12. Damaged Area from Individual Rock Blocks Impacting the Drip Shield

Rock Mass and Kinetic Energy (MT and Joules)	Failed Area (m ²) and Failed Area as a % of Total Drip Shield Surface Area		
	Vertical Rockfall (90° from horizontal)	Rockfall Onto Drip Shield Corner (60° from horizontal)	Rockfall Onto Drip Shield Side-Wall (40° from horizontal)
11.5 MT Rock (348174 J)	4.304 (11.25%)	2.835 (7.41%)	1.126 (2.94%)
14.5 MT Rock (163083 J)	3.508 (9.17%)	0.612 (1.60%)	0.079 (0.21%)
3.3 MT Rock (24712 J)	0.548 (1.43%)	0.416 (1.09%)	0.0 (0.00%)
0.15 MT Rock (902 J)	0.0015 (0.00%)	0.0091 (0.02%)	0.0 (0.00%)
0.11 MT Rock (42 J)	0.0 (0.00%)	0.0 (0.00%)	0.0 (0.00%)
0.25 MT Rock (~0 J)	0.0 (0.00%)	0.0 (0.00%)	0.0 (0.00%)

Source: BSC 2003f, Tables 2 and 3

6.6.1.3 Drip Shield Damage - Multiple Block Impacts

Using the catalog of damage results for individual rock blocks in Table 12, the failed areas for multi-block rockfalls at the 10^{-6} per year and 10^{-7} per year ground motion levels are calculated by interpolation. In other words, the information presented in Table 12 is used to estimate the damage caused for all of the single or multi-rockfall events summarized in Table 9 and Table 10. In the interpolation process, the impact angle associated with individual rockfall events is converted to an indicator variable representing either a vertical rockfall, a rockfall into the transition region between top and side, or a rockfall into the sidewall. The details of the interpolation process are explained in Attachment IV. Thus, impact energy is the only interpolating variable. Furthermore, the impact from a multi-block fall is estimated as the sum of the effects from individual rock blocks. Summary statistics for the failed area corresponding to these hazard levels are derived in sheet “impact information by case” of Attachment IV of this document and given in Table 13.

Table 13. Statistics for Damaged Area from Multiple Rockfalls on the Drip Shield at 10^{-6} and 10^{-7} Annual Exceedance Frequencies

	Failed Area at the 10^{-6} Level (%)	Failed Area at the 10^{-7} Level (%)
Mean	1.698	3.405
Median	0.049	0.941
Standard Deviation	5.165	9.322
Minimum	0	0
Maximum	32.245	63.568

NOTE: Calculation in Attachment IV, sheet “impact information by case.”

The spread in the failed area reflects: (a) the uncertainty associated with the ground motion time histories corresponding to a given annual exceedance probability, and (b) the geologic uncertainty regarding the exact configuration of the fracture system near the emplacement drifts. This uncertainty is represented in the rockfall calculations through the synthetic fracture pattern.

The distribution of the failed area for the 10^{-6} annual exceedance frequency is presented in Figure 10. Approximately 25 percent of the cases do not have any damage (i.e., 0 percent failed area). A log-triangular fit to the damage distribution is also shown in Figure 10, where the lower bound is fixed at 0.001 percent (as the logarithm of zero is undefined) and the upper bound is fixed at 100 percent. The most-likely value (mode) is obtained using a least-squares regression as 0.197 percent (see Attachment IV). Although fits of similar quality could be obtained using more complicated distributional forms such as the gamma or extreme value distributions, a log-triangular distribution is chosen for its simplicity and because it provides a good fit to the results.

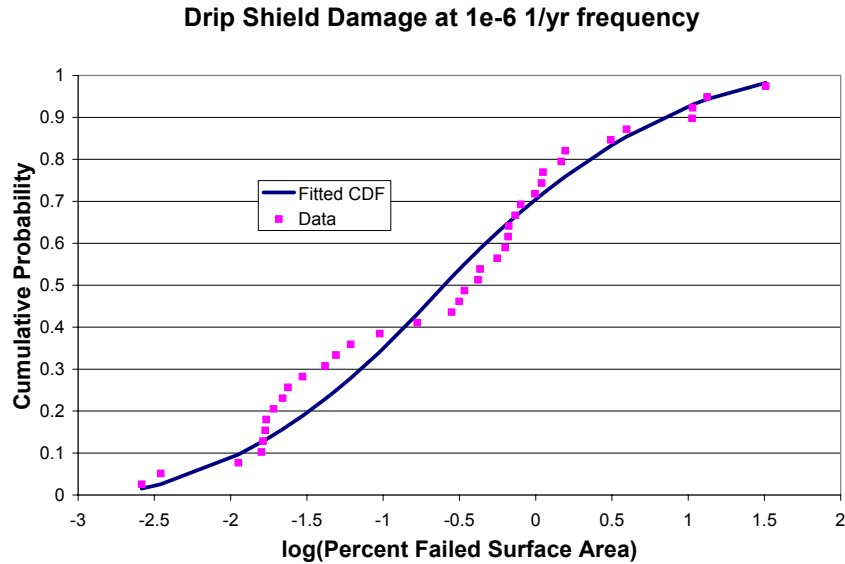


Figure 10. Comparison of Failed Areas for PGV of 2.44 m/s (10^{-6} per year mean annual exceedance frequency) with the Fitted Log-Triangular Distribution

The distribution of the failed area for the 10^{-7} annual exceedance frequency is presented in Figure 11. Approximately 20 percent of the cases do not have any damage (i.e., 0 percent failed area). A log-triangular fit to the damage distribution is also shown in Figure 11, where the lower bound is fixed at 0.001 percent (as the logarithm of zero is undefined) and the upper bound is fixed at 100 percent. The most-likely value (mode) is obtained using least-squares regression as 5.83 percent (see Attachment IV). A log-triangular distribution is chosen because it provides a good fit to the results with a simple distribution type, although fits of similar quality could be obtained using more complicated distributional forms such as the gamma or extreme value distribution.

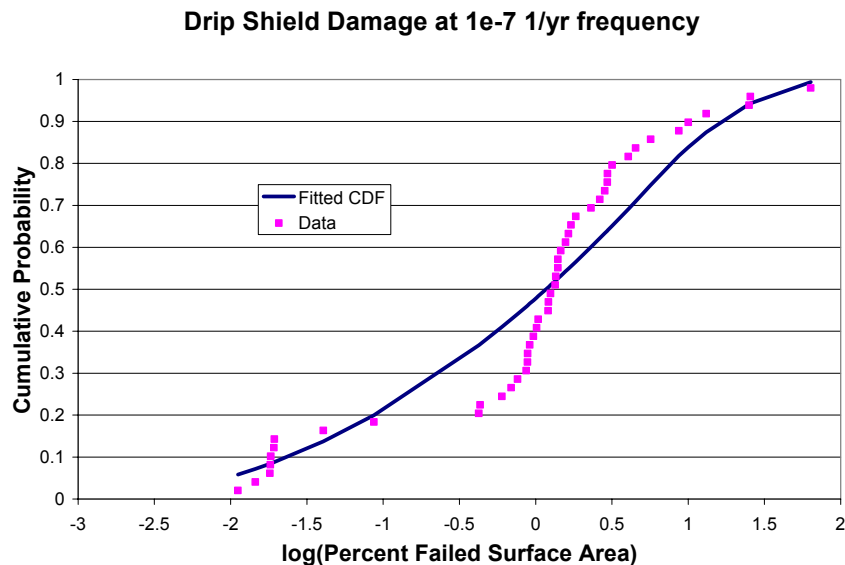


Figure 11. Comparison of Failed Areas for PGV of 5.35 m/s (10^{-7} per year mean annual exceedance frequency) with the Fitted Log-Triangular Distribution

6.6.1.4 Abstraction for Drip Shield Damage from Rockfall

Figure 12 shows the abstraction for the mode of the percent failed surface area as a function of PGV, based on a log-triangular distribution. Figure 13 shows the abstraction for the fraction of cases with no damage, again as a function of the PGV. The results of the calculations for PGVs of 2.44 m/s and 5.35 m/s (10^{-6} and 10^{-7} per year mean annual exceedance frequencies, respectively) have been supplemented by an additional point representing the 5×10^{-5} per year exceedance frequency with a PGV of 0.55 m/s. This is consistent with Assumption 5.1, in that the threshold of damage lies between 10^{-4} and 10^{-5} per year exceedance frequencies. For this latter case, there is zero damage to the drip shield. Thus, the mode is taken to be the same as the lower bound (i.e., 0.001 percent), and the fraction of no-failure cases is taken to be 1.0.

A power law fit to the mode, M , of the log-triangular distribution is given by the following relationship:

$$M = 0.0088 \times (PGV)^{3.7767} \tag{Eq. 5}$$

The numerical parameters in this fit are determined by the Excel fitting function, and are shown in Figure 12. Similarly, a power law fit to the fraction of cases with no damage is given by:

$$F = \text{MIN}(1.0, 0.601 \times (PGV)^{-0.735}) \tag{Eq. 6}$$

where F is the fraction of rockfall cases without failure. The numerical parameters in this fit are again determined on the Excel fitting function, and are shown in Figure 13. The MIN function ensures that the value of F cannot be greater than 1.0.

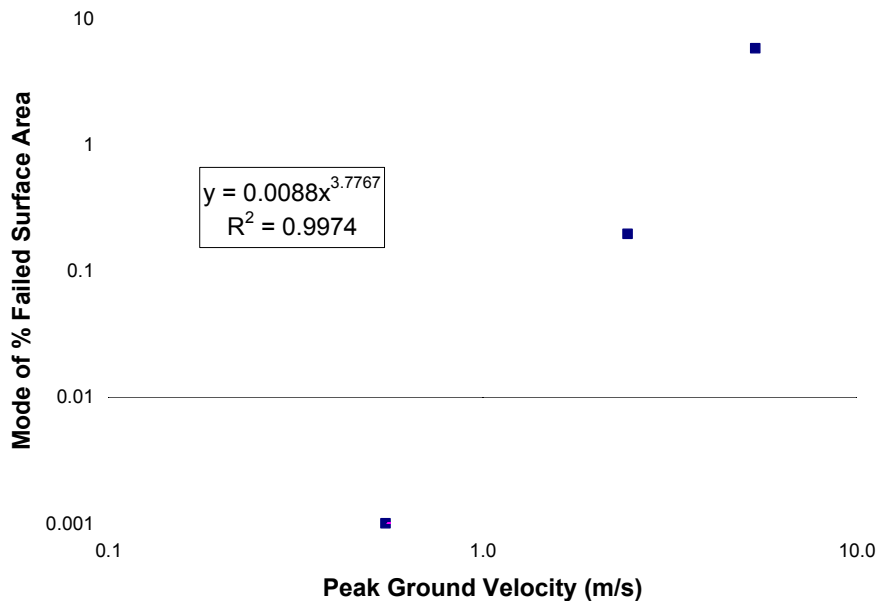


Figure 12. Power Law Fit to the Mode of the Log-Triangular Distribution

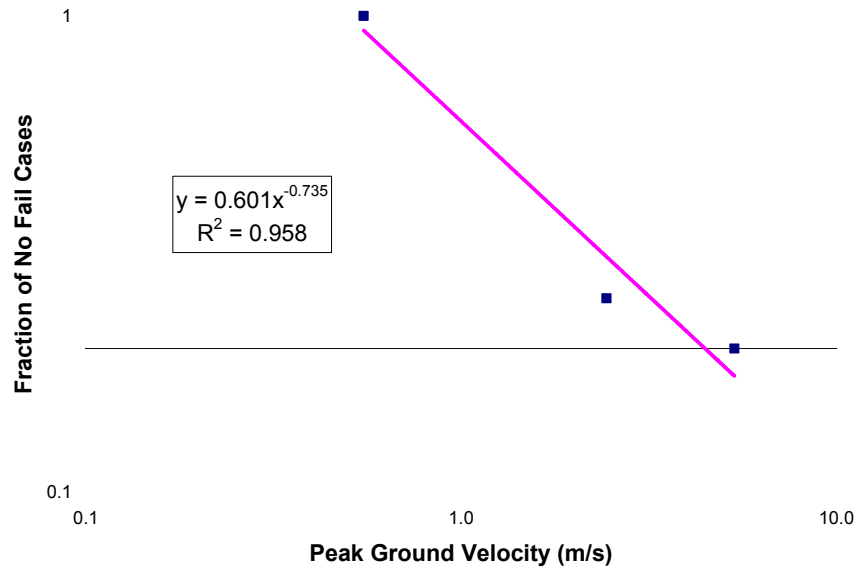


Figure 13. Power Law Fit to the Fraction of Undamaged Cases

6.6.1.5 Damage Abstraction for Multiple Drip Shields

The rockfall calculations in the nonlithophysal zone are based on a tunnel length of 25 meters (BSC 2003h, Section 6.3.1). Since the length of an individual drip shield is 5805 mm (BSC 2003f, Table 1), the damage from multiple block impacts will be shared between $25/5.805 = 4.31$ drip shields, rather than being applied to a single drip shield. Note that the overlap between adjacent drip shields is ignored in this calculation because it is a relatively small length compared to the overall length of the drip shield. Given the presence of multiple drip shields, it is necessary to reconsider the damage abstraction in Equations 4 and 5.

The power law fit to the fraction of cases with no damage (Equation 6) is unchanged by the effective number of drip shields exposed to the rock fall. On the other hand, the mode of the log-triangular distribution (Equation 5) needs to be modified because this damage is distributed among 4 to 5 drip shields. As a first approximation, it is reasonable to reduce the mode by a factor of 4.31 to represent the mean damage to each drip shield in the 25-meter length of tunnel. That is,

$$M = (0.0088/4.31) \times (PGV)^{3.7767} \quad (\text{Eq. 7})$$

$$M = 0.00204 \times (PGV)^{3.7767} \quad (\text{Eq. 8})$$

represents the mode of the log triangular distribution for the damage to each drip shield in the nonlithophysal zones. The fixed upper and lower bounds of the log-triangular distribution, 0.001 and 100 percent, are not being changed because these bounds are limiting values.

6.6.1.6 Independent Technical Review of Model Abstraction

An independent technical review of this model abstraction has been performed by Dr. Robert P. Kennedy of RPK Structural Mechanics Consulting. The result of Dr. Kennedy's review is presented in Attachment V and briefly summarized here.

Dr. Kennedy's major recommendations are as follows:

- A constant residual stress threshold of 50 percent for failure of Titanium Grade 7 is unduly conservative; a distribution for the residual stress threshold is desirable to represent this uncertainty in the damaged areas.
- The abstraction for damage at a PGV of 2.44 m/s has good agreement with the percent damaged surface area for values between zero and 30 percent. The abstraction for damage at a PGV of 5.35 m/s also has good agreement with the percent damaged surface area for values up to 1.5 percent and becomes very conservative above this value. This could lead to a significant overestimation of the annual probability of exceeding higher damage values.
- So long as this potential conservatism is acceptable, the damage abstraction is more than adequate within a range of PGV values between 1.5 m/s and 6 m/s.

Given these recommendations, the TSPA-LA will use the model abstraction defined in Section 6.6.1.5.

6.6.2 Damage from Rockfall in the Lithophysal Zone

Vibratory ground motions can cause failure of the host rock around the emplacement drifts. In the nonlithophysal zones, large rock blocks can be ejected from the walls of the drift at high velocities. The damage to the drip shield from large rock blocks in the nonlithophysal zones is discussed and abstracted in Section 6.6.1.

In the lithophysal zones, the static loads from a collapsed drift using continuum or discontinuum representations of the host rock are not expected to collapse the drip shield from the mean value of the rock mass pressure predicted for the drip shield. Damage to the drip shield from rockfall in the lithophysal zone is neglected for TSPA-LA on this basis. However, structural response calculations have not been performed for the most extreme pressures or for the nonuniform loading predicted by the rock mechanics codes.

In the lithophysal zones, the rock mass has very low compressive strength and is permeated with void spaces of varying size. Average joint spacing is less than 1 meter, and at certain locations this spacing is much smaller, on the order of 0.1 meters (BSC 2003h, Section 6.1.4.1). This weak rock mass is expected to collapse into small fragments under the load imposed by a large vibratory ground motion. Rockfall calculations demonstrate that drifts in the lithophysal zones would collapse under the 10^{-6} per year (and by inference the larger, 10^{-7} per year) vibratory ground motions (BSC 2003h, Section 6.4.1.1).

The small fragments from lithophysal failure have little capability to damage the drip shield because the small mass and energy of the individual fragments cannot cause permanent deformation of the drip shield. Consider a fragment that (for simplicity) is a cube 0.1-meter (4-inches) on a side. The volume of this fragment is 0.001 m^3 and its mass is approximately 2 kg, assuming a tuff density of approximately $2,000 \text{ kg/m}^3$. The velocity of this fragment is 7.7 m/s for a 3-meter drop under gravitational acceleration, and the associated kinetic energy is 59 Joules. Table 13 shows that a 0.11 MT rock with 42 J of kinetic energy does not produce a failed area on the surface of the drip shield. A comparison of the mass and kinetic energy of the 0.1-meter fragment with the block in Table 13 indicates that there should be no damage from the impact of this fragment on the drip shield.

A cubic fragment that is 0.3-meters (12 inches) on a side has a mass of 54 kg and a kinetic energy of 1600 Joules. This fragment is approximately equivalent to the 0.15 MT (150 kg) rock with 902 Joules of kinetic energy in Table 13. This rock produces no damage for the top and side impacts, and very small damage (0.02 percent) for the corner impact. Again, the damage for impact of a cubic fragment 1-foot on a side should be negligible. In summary, the drip shield will not be damaged by direct impact of small rock fragments in the lithophysal zone.

It is also worth noting that rockfall in the lithophysal zone does not damage the waste package and cladding. The waste package and cladding are not damaged because the drip shield remains intact until a seismic event occurs, deflecting any rockfall away from the waste package. If the duration of the seismic scenario class extends beyond 20,000 years, then the drip shield may be significantly degraded before the seismic event occurs and may not protect the waste package from rock blocks or drift collapse.

Drift collapse in the lithophysal zones can impose a static load on the drip shield from the weight of the natural backfill that fills the drifts as a result of the collapse. The structural response of the drip shield to the static load from a hypothetical engineered backfill and fallen host rock generated by tunnel collapse has been evaluated with structural response calculations. The layer of engineered backfill in these calculations is taken to be 0.9 meters thick or 1.1 meters thick. The fallen host rock is 5.5 meters thick. The applied pressure from these materials is 143 kPa if the hypothetical engineered backfill is 0.9-meters thick and 146 kPa if the engineered backfill is 1.1 meters thick (BSC 2003s, Table 5.2-1 and Section 5.2).

The maximum stress in all components of the drip shield is always less than the yield strength for this combined load (BSC 2003s, Section 6 and Table 6.2). At room temperature, the highest stress in the drip shield is 43 percent of the yield strength for Titanium Grade 7. At 150°C , the highest stress in the drip shield is 68 percent of the yield strength for Titanium Grade 7. In addition, the average stress in the large support beams (the peripheral bulkheads) of the drip shield is far enough below the yield strength of Titanium Grade 24 to alleviate any concern of buckling. (The drip shield plates are fabricated from Grade 7, while the supporting structure is fabricated from Grade 24.)

It is important to differentiate between dynamic and static failure of the drip shield. For dynamic loading of the drip shield due to seismic hazards, an area fails as a flow barrier when the residual stress exceeds 50 percent of the yield strength of Titanium Grade 7. This failure is a combined chemical-mechanical response of a cold worked material to dynamic impacts. For static loading,

as discussed in the above paragraph, the failure of the drip shield is determined by mechanical collapse of the drip shield. In this situation, a local stress of 68 percent of the yield strength of Titanium Grade 7 does not imply structural failure.

The potential rock loads in the lithophysal zones after complete collapse of the emplacement drift have been analyzed for 5 cases using a discontinuum representation of the host rock (BSC 2003h, Section 6.4.2.4 and Table 40). The mean pressure on the top of the drip shield is 145 kPa, with a maximum value of 179.2 kPa. The mean pressure on the right side of the drip shield is 85 kPa, with a single outlier at 220.8 kPa. The mean pressure on the left side of the drip shield is 86 kPa, with a maximum value of 142.7 kPa. The elastic response of the drip shield for an applied pressure of 146 kPa clearly indicates that the drip shield will not fail from these mean rock loads. It is also likely that the drip shield will not fail from the maximum load on the top of the drip shield, 179.2 kPa. However, the single outlier on the right side of the drip shield, at 220.8 kPa, may require additional analysis. In addition, the pressure contours on individual segments of the drip shield are quite nonuniform (BSC 2003h, Figure 139), which is not included in the structural response calculations.

An alternate conceptual representation of the potential rock loads can be based on a continuum approach. The potential rock loads after the complete collapse of the emplacement drift from 15 ground motions at the 10^{-6} per year level have been analyzed for the lithophysal rock (BSC 2003h, Section 6.4.1.1 and Table 38). The mean pressure on the top of the drip shield is 178 kPa, slightly greater than the value of 146 kPa for the static load calculation. This increase, on the order of 22 percent, is still well below the threshold for yielding.

The largest pressure on the top of the drip shield is 317.1 kPa and the largest pressure on the side of the drip shield is 507.1 kPa for the 15 cases. This latter value is not realistic because it is due to a single elastic block of rock that is wedged in place. In reality, this level of stress will fracture or crush the rock, invalidating the elastic assumption. Local deformation of the drip shield plates will also reduce the lateral pressure.

6.6.3 Abstraction for Drip Shield Damage from Vibratory Ground Motion

The mechanical response of the drip shield to vibratory ground motions has the potential to damage the drip shield as a barrier to flow. This loss of integrity could occur because of impacts between the drip shield and the waste package, emplacement pallet or invert or because of separation between two adjacent drip shields. In fact, all these mechanisms are observed in the structural response calculations that are performed for ground motions at the 10^{-6} per year and 10^{-7} per year levels.

The structural response calculations do not represent the dynamic response of the invert to the ground motion. The invert is represented as an elastic body whose surface responds instantaneously and uniformly to the given ground motion. In other words, the ground motion time histories for the three components of motion are applied directly to the surface of the invert. This is a reasonable approach for small amplitude ground motions because the invert is compacted under the weight of the waste packages and drip shield and because any remaining steel framework in the invert will tend to provide some integrity. These effects will result in an invert that tends to move as a single unit. For high amplitude ground motions, the invert ballast is likely to be thrown up and redistributed, allowing the heavy EBS components to settle on the

bottom of the drift, directly in contact with the rock floor. In this case, applying the ground motions directly to the surface of the invert is again a reasonable approach.

The results of the structural response calculations for ground motions at the 5×10^{-4} per year, at the 10^{-6} per year and at the 10^{-7} per year ground motion levels are summarized as follows (BSC 2003p):

- One simulation performed at the 5×10^{-4} per year ground motion level indicates that there is no damage to the drip shield (BSC 2003f, Calculation Results I). More specifically, no area of the drip shield exceeds the residual stress threshold of 50 percent of the yield strength of Titanium Grade 7. The residual stress threshold is 104.5 MPa at 150°C for Titanium Grade 7.
- Fourteen simulations are performed at the 10^{-6} per year ground motion level using the set of three-component ground motion time histories. Table 14 identifies the realization number, the associated ground motion number, and the drip shield area exceeding the residual stress threshold for the 14 simulations (BSC 2003f, Table 4).

The mean percent damaged area in Table 14 is 0.70 percent and the maximum percent damaged area is 2.13 percent. This latter value is an outlier, in the sense that the second greatest percent damaged area is 1.25 percent, or more than 40 percent below the maximum damage value. There is no indication of separation of drip shields in the calculations for the 10^{-6} per year ground motion level.

- Five simulations performed at the 10^{-7} per year ground motion level indicate separation of adjacent drip shields (BSC 2003f, Calculation Results I). Separation occurs between adjacent drip shields because of plastic deformation of the drip shield and because of the large magnitude of the ground motions. In fact, each of the five simulations demonstrates that a drip shield rides over its adjacent neighbor, implying that a separation must occur somewhere in the emplacement drift. The degree to which the drip shield rides over its neighbor is substantial, on the order of 10 to 25 percent of the length of the drip shield.

A uniform distribution has been selected to represent the damaged area on the drip shield from vibratory ground motion. The motivation for selection of a uniform distribution is twofold. First, there are only five realizations for the 10^{-7} per year ground motion level, and a uniform distribution is a reasonable representation of the upper and lower bounds with a very limited number of samples. Second, the use of a uniform distribution is conservative for damage at the 10^{-6} per year ground motion level because a uniform distribution samples the high damage end more than a normal or log-normal distribution that incorporates the single outlier at 2.13 percent.

Table 14. Damaged Area from Vibratory Ground Motion at the 10^{-6} Annual Exceedance Frequency

Realization Number †	Ground Motion Number	Damaged Area (m ² ; % of Total Area)
1	7	0.113; 0.30
2	16‡	0.055; 0.14
3	4	0.248; 0.65
4	8	0.105; 0.27
5	11	0.257; 0.67
6	1	0.427; 1.12
7	2	0.479; 1.25
8	13	0.100; 0.26
9	10	0.814; 2.13
10	9	0.192; 0.50
11	5	0.456; 1.19
12	6	0.376; 0.98
14	14	0.0456; 0.12
15	3	0.0989; 0.26

Source: BSC 2003f, Table 4

NOTES: †Only 14 realizations are presented in this table. Results for realization 13 are not presented because a numerical instability occurred during this calculation. ‡Calculations are performed with 15 ground motions numbered 1, 2, 3, ..., 14, and 16. Time history 16 is used in place of 15 because because 15 has an anomalous response spectrum.

The upper bound of the uniform distribution at the 10^{-6} per year ground motion level is based on the damage results in Table 14. The 95 percent UCL for the upper bound of a uniform distribution can be defined using a Bayesian procedure (Rossman et al. 1998):

$$\begin{aligned}
 95\%UCL &= \alpha^{-\frac{1}{n-1}} \max(X), \\
 &= (0.05)^{-\frac{1}{13}} (2.13\%), \\
 &= 2.68\%.
 \end{aligned}
 \tag{Eq. 9}$$

where α is the significance level (i.e., $\alpha = 0.05$ at the 95 percent confidence level), n is the sample size (i.e., $n = 14$ entries in Table 14), and X is the uncertain quantity of interest (i.e., the percent damaged area).

The upper bound of the uniform distribution at the 10^{-7} per year ground motion level or higher amplitude ground motions is 50 percent. The rationale for this value is as follows. The five structural response calculations at the 10^{-7} per year level demonstrate that a drip shield can cover or overlap its neighbor by a substantial amount. In an extreme case, each pair of drip shields in the emplacement drifts could be reduced to one-half their original length if one member of the pair completely covers the other member of the pair. In this situation, the total length of drip shield in a drift would be reduced by 50 percent. While more extreme situations are possible, such as a stack of three or four drip shields that cover one another, these situations seem extremely improbable. First, a tall pile of drip shields will probably be less stable than a 2-high

stack under vibratory ground motions. Second, increasing structural deformations are required to add a third or fourth drip shield to a stack that is 2-high. Deformation must increase because the inner width of the third drip shield in a stack must be greater than the outer width of the second drip shield, and so on. The complex dynamics of the EBS components in response to ground motions make these arrangements improbable, given that ground motions are usually coherent over 10's of meters.

The lower bound of the uniform distribution is defined as 0 percent at all ground motion levels. In reality, the lower bound around the 10^{-6} per year level is a small non-zero value that changes with the ground motion level. Setting the lower bound for damage to 0 percent provides a reasonable simplification based on the available computational results. The lower bound at the 10^{-7} per year level is highly uncertain because there is substantial uncertainty in the degree of separation between adjacent drip shields. This uncertainty is represented in TSPA-LA by defining the lower bound as 0 percent at the 10^{-7} per year ground motion level. This choice provides a range of damage between 0 and 50 percent at the 10^{-7} per year level, bounding the potential variability in overlap between adjacent drip shields and passing this uncertainty into TSPA-LA for sensitivity studies.

Finally, the maximum damage is assumed to go to zero at the 5×10^{-5} per year ground motion level. This approach is consistent with Assumption 5.1, whereby damage from vibratory ground motion first begins between the 10^{-4} and 10^{-5} per year ground motion levels. In other words, the ground motions greater than those at the 10^{-4} per year level are required to damage the drip shield. This approach is also consistent with the zero damage state chosen for the damage abstraction for the drip shield from rockfall (see Section 6.6.1.4).

In terms of PGV, the abstraction for the upper bound of the uniform distribution is a simple look-up table defined by the five points in Table 15. The mean annual exceedance frequencies of 10^{-6} and 10^{-7} per year have been replaced with the corresponding PGV values in the emplacement drifts, 2.44 m/s and 5.35 m/s, respectively. The mean annual exceedance frequency for 5×10^{-5} per year is replaced with 0.55 m/s, based on the scaled hazard curve for Point B in Table 5.

Table 15. Abstraction for Maximum Damage to the Drip Shield from Vibratory Ground Motion

PGV Value (m/s)	Damage to Drip Shield (%)
0.0	0
0.55	0
2.44	2.68
5.35	50
20	50

6.6.3.1 Independent Technical Review of Model Abstraction

An independent technical review of this model abstraction has been performed by Dr. Robert P. Kennedy of RPK Structural Mechanics Consulting. The result of Dr. Kennedy's review is presented in Attachment VI and briefly summarized here.

Dr. Kennedy presents an alternate analysis of the damage information for the drip shield. This alternative analysis is structured around a fragility approach. Following this approach, the

damage data at the 10^{-6} per year ground motion level (PGV = 2.44 m/s) has been fit with a lognormal distribution. A lognormal distribution with the following parameters provides an excellent fit to the damage results at 10^{-6} per year (Equation VI-4 in Attachment VI):

$$\begin{array}{ll} \text{Median:} & D_{50} = 0.55\% \\ \text{Log. Std. Dev.:} & \beta = 0.85 \end{array}$$

A comparison of this lognormal distribution with the uniform distribution in Section 6.6.3 shows that the uniform distribution is very conservative for percent damage areas of 0.50 percent and greater. This could lead to a significant overestimation of the annual probability of exceeding the percent damage when the damage is greater than 0.50 percent with a normal distribution.

Dr. Kennedy notes that there are only 5 data points for the damage from ground motions at the 10^{-7} per year level (PGV = 5.35 m/s). One knows that damage will be large, but it is difficult to estimate exceedance probability for various percent damage values. He also states that the upper bound of 50 percent for damage is probably reasonable for PGV = 5.35 m/s; however, the lower bound should probably be in excess of 10 percent at this level. Given limited data, his primary conclusion is that the drip shields are likely to be severely damaged at a PGV of 5.35 m/s or greater.

6.6.3.2 Final Abstraction for Damage from Vibratory Ground Motion

Without additional damage data for PGV values at or above 5.35 m/s, it is prudent to choose the uniform distribution with an upper bound defined in Table 15 because it is more conservative than the lognormal distribution. The maximum damage of 50 percent for PGV values of 5.35 m/s or greater is considered a reasonable upper bound. The rationale for this bound is twofold: (1) the five simulations for the PGV level of 5.35 m/s (10^{-7} per year) demonstrate that a drip shield rides over its adjacent neighbor by 10 percent to 25 percent of its axial length, well below the recommended maximum of 50 percent, and (2) the value of 50 percent corresponds to an extreme case in which each and every pair of drip shields through the repository is reduced to one-half of its original length.

However, Dr. Kennedy notes that using a lower bound of zero for the uniform distribution does not seem conservative for PGV values of 5.35 m/s or greater. In this situation, it seems appropriate to define a lower bound that is a function of PGV. This lower bound is zero for all values of PGV that are less than or equal to 2.44 m/s, as discussed in Section 6.6.3. For values of PGV between 2.44 m/s and 5.35 m/s, there is a linear interpolation between 0 percent damage and 10 percent damage, respectively. The value of 10 percent is selected because it is the minimum value for the 5 simulations at the PGV level of 5.35 m/s, and this minimum is appropriate for a uniform distribution. For values of PGV greater than 5.35 m/s, the lower bound is based on a linear extrapolation of the damage at 2.44 and 5.35 m/s. In other words, damage continues to increase with PGV. The data points for the abstraction are summarized in Table 16.

Table 16. Abstraction for Minimum Damage to the Drip Shield from Vibratory Ground Motion

PGV Value (m/s)	Damage to Drip Shield (%)
0.0	0
2.44	0
5.35	10%

6.6.4 Combined Abstraction for the Drip Shield

The combined abstraction for damage to the drip shield is a function of the host rock:

- In the lithophysal zone, the damage to the drip shield from vibratory ground motion is determined by the abstraction in Section 6.6.3.2. The damage from vibratory ground motion is given by a uniform distribution with a lower bound defined by Table 16 and an upper bound given in Table 15.
- In the nonlithophysal zone, the damage to the drip shield is determined by the sum of the damage abstraction for rockfall, as described in Section 6.6.1.4, and the damage abstraction for vibratory ground motion, as defined in Section 6.6.3.2. The total damage cannot be greater than 100 percent.

These levels of damage are applied to all drip shields in the lithophysal zone and to all drip shields in the nonlithophysal zone. There is no spatial variability within each of these zones.

6.7 FAILURE ABSTRACTION FOR THE CLADDING

The mechanical response of the waste package to vibratory ground motions can produce dynamic impacts between adjacent waste packages, between the waste package and its emplacement pallet, and between the waste package and the drip shield. During each of these impacts, the waste package may experience very high acceleration in the axial and lateral directions. These accelerations can be “transmitted” to the the fuel rod assemblies and fuel rods. The assemblies and fuel rods may impact the lid of a waste package due to the end-on (axial) impact of adjacent waste packages, or the fuel rods may be pushed sideways, toward the sidewall of the waste package, during impact with the emplacement pallet or drip shield. Either of these impacts has the potential to fail the cladding.

As noted in Section 6.5.1.2, the end-on impact between two adjacent waste packages accounts for 87 percent of the mean damage to the waste package at the 10^{-6} per year ground motion level and 92 percent of the mean damage to the waste package at the 10^{-7} per year ground motion level. These results imply that the end-on impact of adjacent waste packages produces much more severe forces and accelerations than the side-on impact between a waste package and the emplacement pallet or drip shield. These results are consistent with the conservative approach to the end-on impact calculations, which are based on a waste package impacting an almost rigid plane of symmetry located midway between two adjacent waste packages.

The maximum waste package velocities from end-on impacts with the 15 ground motions at the 10^{-6} per year level vary between 1.4 to 4.5 m/s (BSC 2003b, Tables 6.1.2-1 through 6.1.2-15;

BSC 2003n, Tables 28 through 42). In other words, all realizations for the 10^{-6} per year ground motions have an impact velocity of at least 1.4 m/s. Similarly, the maximum waste package velocities for end-on impacts at the 10^{-7} per year level vary between 1.3 and 6.5 m/s (BSC 2003b, Tables 6.2.2-1 through 6.2.2-15; BSC 2003m, Tables 46 through 57; BSC 2003n, Tables 43, 44, and 45). That is, all realizations for the 10^{-7} per year ground motions have an impact velocity of at least 1.3 m/s. (The minimum value for the 10^{-7} per year ground motions is less than that for the 10^{-6} per year ground motions because of the stochastic variability in the 15 ground motions.)

The resulting fuel assembly accelerations due to this range of impact velocities have been analyzed using a finite-element representation of the fuel assemblies. The maximum peak acceleration and the average peak acceleration for all assemblies in a waste package are reported in Tables 4 and 5 of *Maximum Accelerations on the Fuel Assemblies of a 21-PWR Waste Package During End Impacts* (BSC 2003d) and Tables 14 and 15 of *Repository Design Project, RDP/PA IED Typical Waste Package Components Assembly (4)* (BSC 2003e). The peak and average accelerations in this reference have been evaluated for cutoff frequencies of 450 Hertz, 600 Hertz, and 1,000 Hertz. The accelerations for a cutoff frequency of 450 Hertz are repeated in Table 17.

The finite-element calculations for the fuel assembly accelerations do not include any damping. Impact calculations with no damping often produce highly transient time histories with peak accelerations that are influenced by the spatial and temporal discretization of the calculations. In this situation, the output is typically filtered through a low-pass, Butterworth filter to determine a more realistic acceleration time history. The cutoff frequency for the filter is a compromise between damping the extraneous numerical noise while leaving the fundamental modes of the structure intact. Filtering the output below 400 Hertz dampens the fundamental modes of waste package and fuel assembly, potentially leading to erroneous results. Filtering the output at greater than 1,000 Hertz preserves computational noise and can also lead to misleading results. A cutoff frequency of 450 Hertz dampens the numerical noise but has minimal impact on the fundamental modes of fuel assembly and waste package (BSC 2003d, Attachment VIII).

Table 17. Fuel Assembly Accelerations from Waste Package-to-Waste Package Impacts for a 450 Hertz Cutoff Frequency

Parameter	Initial Impact Velocity (m/s)				
	0.5	1	2	4	6
Maximum Peak Acceleration (g's)	75	144	263	323	506
Average Peak Acceleration (g's)	35	72	115	155	194

Source: BSC 2003d, Tables 4 and 5

The minimum impact velocity for the 10^{-6} per year and the 10^{-7} per year ground motions is 1.3 m/s, as noted above. Interpolating on the results in Table 17 for impact velocities of 1 m/s and 2 m/s, the maximum peak acceleration is 180 g's and the average peak acceleration is 85 g's at 1.3 m/s with a 450 Hertz cutoff frequency. With a cutoff frequency of 600 Hertz, the average peak accelerations for 1 m/s and 2 m/s are 99 g's and 147 g's, respectively (BSC 2003d, Table 4). The interpolated value for the average peak acceleration at 1.3 m/s is then 113 g's for the 600 Hertz cutoff.

The integrity of fuel rod cladding during cask drop or tipover incidents has been extensively studied for zircalloy-clad light water reactor spent fuel assemblies (Chun et al. 1987; Sanders et al. 1992). The work by Chun et al. (1987) is more useful here because it explicitly calculates g-loads for axial buckling and for yielding due to side drops. The range of g-loads for failure due to axial buckling varies between 82 g's for the Westinghouse 17×17 fuel assembly to 252 g's for the Combustion Engineering 16×16 fuel assembly (Chun et al. 1987, Table 4). The range of g-loads for yielding due to side drops varies between 63 g's for a Westinghouse 17×17 fuel assembly to 211 g's for a Combustion Engineering 16×16 fuel assembly (Chun et al. 1987, Table 4). The actual g-loads for failure may be lower because: (1) the weight of the fuel pellets is not transferred to the cladding (Chun et al. 1987, p. 2), and (2) the potential effects of cladding defects or existing failures are not included in the analysis. These effects increase the inertial mass or weaken the clad, possibly causing failure at lower g-loads.

Based on Table 17, end-on impacts of adjacent waste packages result in average fuel assembly accelerations of 85 g's at the lowest impact velocity, and often much greater values for higher impact velocities. The use of a 600 Hertz cutoff filter increases this minimum value to 113 g's. Simple fuel rod failure criteria indicate that clad failure occurs between 82 and 252 g's, depending on the type of fuel rod (Chun et al. 1987, Table 4). In this situation, 100 percent perforation of the cladding is reasonable when a ground motion event with an annual exceedance frequency less than or equal to 10^{-6} per year occurs.

One calculation is available for the structural response of the waste package to a ground motion with an annual exceedance frequency of 5×10^{-4} per year (BSC 2003b, Section 6.3). There is no damage to the cladding for this ground motion because there is no appreciable motion of the waste package and no impact between adjacent waste packages. As explained in Assumption 5.1 (see Section 5.1), it is reasonable to expect that there will be no impact between adjacent waste packages for the 10^{-4} per year seismic hazard, and therefore no cladding damage for this hazard. However, the potential exists for more significant displacements and impacts at the 10^{-5} per year ground motion level.

The cladding damage for ground motion at the 10^{-5} per year mean annual exceedance frequency (or less) is conservatively set to 100 percent. In addition, the cladding damage is assumed to go to zero at the 5×10^{-5} per year ground motion level. This approach is consistent with Assumption 5.1, whereby damage from vibratory ground motion first begins between the 10^{-4} and 10^{-5} per year ground motion levels. In other words, ground motions greater than those at the 10^{-4} per year level are required to damage the drip shield. This approach is also consistent with the zero damage state chosen for the abstraction for damage to the drip shield from rockfall (see Section 6.6.1.4) and from vibratory ground motion (see Section 6.6.3)

In terms of PGV, the abstraction for damage to the cladding is a simple look-up table with a linear interpolation between the four points in Table 18. The mean annual exceedance frequencies of 5×10^{-5} per year and 10^{-5} per year have been replaced with the corresponding PGV values in the emplacement drifts, 0.55 and 1.067 m/s, respectively, based on the scaled hazard curve for Point B in Table 5.

Table 18. Abstraction for Damage to the Cladding from Vibratory Ground Motion

PGV Value (m/s)	Damage to Cladding (%)
0.0	0
0.55	0
1.067	100
20	100

There is no uncertainty in this abstraction because the abstraction represents a conservative, bounding estimate for cladding response at all values of PGV.

6.8 RESPONSE TO FAULT DISPLACEMENT

In addition to inducing severe ground motion/acceleration as discussed in the previous sections, seismic events can also result in fault displacements within the emplacement drifts. Fault displacement could impact key EBS components in two ways:

- Separation between adjacent drip shields can allow a pathway for seepage to contact the waste packages thereby potentially accelerating corrosion-induced waste package failure.
- Mechanical damage to the waste packages caused directly by the fault displacement.

Potential faulting within the emplacement drifts that have a reasonable likelihood of slipping over the 10,000-year regulatory period generally have very small displacements associated with the faults. With the exception of the Solitario Canyon fault and the Ghost Dance fault, which are immediately outside the western and eastern boundaries of the emplacement drifts, a fault displacement of greater than 0.1 cm requires an annual frequency of occurrence of less than 10^{-5} per year. For such low-probability events, there is significant uncertainty in the expected magnitude of the fault displacement, and the estimates that have been developed are necessarily quite conservative. Given the lack of precision in the estimated fault displacement magnitudes at low probability, a highly detailed calculation of drip shield and waste package response to such events is not warranted. Thus, the response calculations presented herein are intentionally quite simplistic and conservative.

For a fault displacement that occurs along an emplacement drift, a sudden discontinuity in the floor and roof of the tunnel may occur. This would result in one portion of the tunnel being displaced vertically relative to the adjacent section. Such a discontinuity in the tunnel axis could cause separation of adjacent drip shields, and if severe enough, could cause shearing of a waste package at that location. The discussion in this section identifies the conditions under which these damage mechanisms could occur.

6.8.1 Clearance Between EBS Components and the Drift

To determine the response of the drip shield and waste package to a fault displacement, consider the layout within the emplacement drift, shown schematically in Figure 14. The tunnel itself is 5500 mm in diameter. Within the tunnel, the steel support beams and associated ballast form a level invert whose top surface is 806 mm above the lowest part of the tunnel floor. Sitting on this invert floor is the waste package emplacement pallet, which raises the waste package off the

invert floor. While the actual elevation difference between the invert floor and the bottom of the waste package varies depending on the specific diameter of the waste package, the exact value is not important for this analysis. As indicated in the discussion that follows, this elevation difference is not actually used in the analysis.

The drip shield is also sitting on the invert floor. The drip shield has an external height of 2886 mm (BSC 2003f, Table 1). The internal height of the drip shield, defined as the distance from the invert floor to the lowest point on the underside of the top of the drip shield, is 2716 mm (BSC 2003f, Table 1). There is then a clearance of 1808 mm between the top of the drip shield and the tunnel roof. A summary of these parameters, which are independent of waste package design, along with the source of the values, is provided in Table 19.

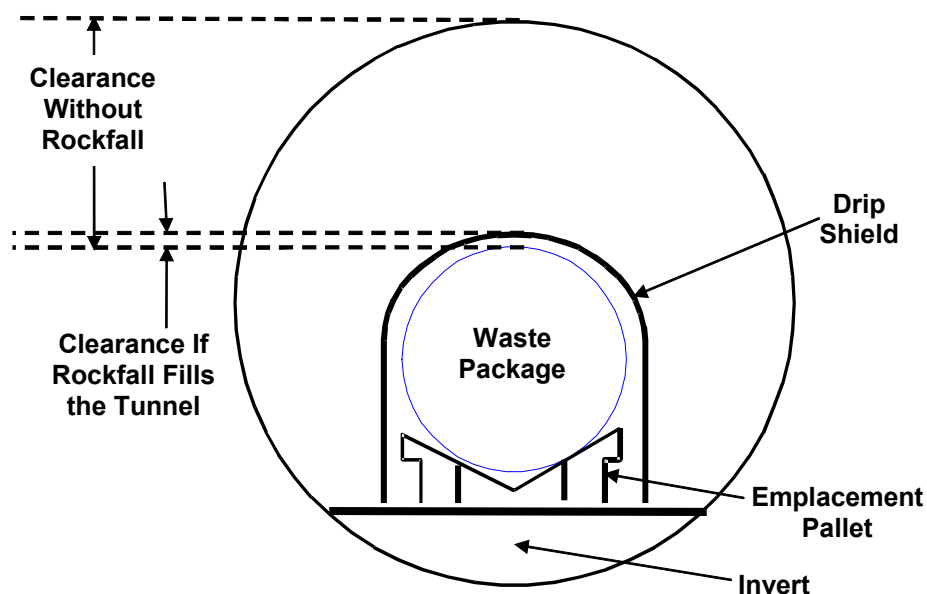


Figure 14. Schematic Diagram of EBS Components Illustrating the Clearances for Fault Displacement

Table 19. Emplacement Drift Configuration Dimensions that Are Independent of the Waste Package

Description	Value	Source
Drift Diameter	5.5 m	BSC 2003i, Figure 1
Invert Thickness (maximum)	806 mm	BSC 2003i, Figure 2
Drip Shield Height - Exterior	2886 mm	BSC 2003f, Table 1
Drip Shield Height - Interior	2716 mm	BSC 2003f, Table 1
Clearance Between Top of Drip Shield and Roof of Tunnel	1808 mm	Calculated (5500 - 806 - 2886 = 1808)

Table 20 summarizes the exterior dimensions of the various waste package designs (BSC 2003j, Table 1). The most important parameter for the analyses presented herein is the waste package diameter, which is seen to vary between 1,318 mm and 2,110 mm. Also shown in Table 20 is the calculated clearance between the top of the waste package and the underside of the drip shield in the undisturbed state. This clearance is defined as the interior height of drip shield less the package diameter. The elevation of the package above the invert is ignored in calculating the clearance, as explained below. This clearance varies between 606 mm and 1398 mm, depending on waste package type.

Table 20. Waste Package Dimensions and Clearance Between Drip Shield and Waste Package

Package Type	Diameter (mm)	Length (mm)	Clearance (mm)
44-BWR	1674	5165	1042
24-BWR	1318	5105	1398
21-PWR	1644	5165	1072
12-PWR	1330	5651	1386
Naval-Long	1949	6065	767
Naval-Short	1949	5430	767
5 DHLW/DOE SNF -Short	2110	3590	606
5 DHLW/DOE SNF -Long	2110	5217	606
2-MCO/2-DHLW	1814	5217	902

Source: BSC 2003j, Table 1 for diameter and length

NOTE: Clearance is calculated as the interior height of the drip shield minus waste package diameter.

The clearance between the top of the drip shield and the roof of the tunnel (Table 19) and the clearance between the top of the waste package and the bottom of the drip shield (Table 20) are measures of how much fault displacement could occur before the waste packages are potentially degraded through a shearing mechanism. However, the clearance above the drip shield is only relevant if tunnel collapse does not occur. Once a tunnel collapses, the space surrounding the drip shield will be filled with rock fragments (previously called “natural backfill”) that prevent free motion of the drip shield in all directions. For those tunnels in the lower lithophysal zone of the repository, tunnel collapse is calculated to occur for ground motion hazards with an annual occurrence frequency of 10^{-6} per year or less (BSC 2003h, Section 6.4.1.1).

The actual response of the EBS components to a fault displacement scenario is complicated. As a conservative simplification, the fault displacement is analyzed considering:

- The fault is perpendicular to the tunnel axis with the displacement being purely vertical
- The fault displacement occurs at a discrete point, creating a “knife-edge” discontinuity.

Vertical faulting is consistent with the faults investigated at the site. As part of the exploratory studies of the site, the Enhanced Characterization of the Repository Block (ECRB) Cross-Drift was dug through a representative part of the repository footprint to obtain visual evidence of both rock stratigraphy and faulting. The results of this investigation (Mongano et al. 1999, pp. 51 to 59) found evidence for four faults along the length of the ECRB Cross-Drift between the two major north/south faults (Ghost Dance and Solitario Canyon) that bound the location of the emplacement drifts. One of these was the Sundance fault, the other three are unnamed faults that showed between one and a few meters of cumulative faulting. In each of these cases, the measured displacements were characterized as vertical, which is consistent with the assumption made herein. By treating the faults as perpendicular to the tunnel axis, no credit is taken for sideways movement of the waste packages that could lessen the degree to which fault displacement could cause damage.

An actual fault zone has a finite width over which the displacement could occur. However, based on the observations reported in the investigation of the ECRB Cross-Drift (Mongano et al. 1999, pp. 51 to 59), the width of the fault disturbed zone varied between just under a meter to a little over 2 meters. Thus, the width of the zone is in all cases less than the length of a typical

waste package. If during a single seismic faulting event, the total displacement were to be distributed over a sufficiently wide zone, a single waste package could potentially see less than the total fault displacement, resulting in a decreased likelihood of failure. By treating the displacement as a sharp discontinuity in the tunnel floor/roof, the likelihood of damage to the waste package is increased. Thus, the overall treatment is conservative.

A sudden discontinuity in the tunnel floor would tend to raise one end of a drip shield and waste package. However, the other EBS components, specifically the invert and emplacement pallet, would also be affected. A significant amount of the invert (ballast) from the elevated portion of the tunnel is expected to fall into the lower tunnel segment. In addition, the steel supports in the invert and the emplacement pallet are likely to collapse at the plane of displacement, further degrading the integrity of the invert.

The exact details of these events are difficult to predict. As a simplification, the approximation is simply made that the emplacement pallet collapses into the invert on the elevated side of the fault. No credit is taken for any further shifting of the ballast in the invert. Using this approximation, the total available free height that the waste package can move through before contacting the underside of the drip shield can be calculated as the clearance between waste package and drip shield, without consideration for the elevation of the package above the invert (see Table 20). In those cases where drift collapse has occurred, the drip shield would be effectively held in place, so this free height represents the maximum allowable (vertical) fault displacement before the waste package could be damaged (waste package shearing is assumed at this point).

In those cases where drift collapse does not occur from the seismic hazard or from gradual degradation of the drift and host rock, waste package displacement beyond that required for contact with the underside of the drip shield is possible without damage. Further displacement would cause the drip shield to lift since there is no tunnel debris to hold it in place. Such lifting would occur until the drip shield contacts the roof of the drift. Thus, the clearance between the top of the drip shield and the roof of the drift (1,809 mm; see Table 19) is also available, and the maximum allowable fault displacement prior to waste package damage is increased by this amount. These calculated results are summarized in Table 21.

Table 21. Maximum Allowable Displacement Before Waste Package Is Pinned

Package Type	Maximum Allowable Displacement With Tunnel Collapse (mm)	Maximum Allowable Displacement Without Tunnel Collapse (mm)
44-BWR	1042	2850
24-BWR	1398	3206
21-PWR	1072	2880
12-PWR	1386	3194
Naval-Long	767	2575
Naval-Short	767	2575
5 DHLW/DOE SNF -Short	606	2414
5 DHLW/DOE SNF -Long	606	2414
2-MCO/2-DHLW	902	2710

NOTES: Maximum allowable displacement with tunnel collapse = clearance in Table 20
Maximum allowable displacement without tunnel collapse = clearance in Table 20 + 1808 mm

The values in Table 21 represent the failure criteria for waste packages and drip shield under fault displacement. Any fault displacement in excess of these values is conservatively considered to fail the waste package, the overlying drip shield, and the internal cladding through direct shearing.

Failure of the drip shields could also occur without direct waste package damage. One mechanism for this is lifting of one drip shield relative to its neighbor, thereby creating a pathway for ingress of seepage water onto the waste package. However, drip shield failure without waste package damage will have low consequence for performance assessment, so it will be screened out from TSPA-LA based on low consequence and is not considered further herein.

6.8.2 Faults Intersecting Emplacement Drifts

The location, likelihood, and magnitude of potential fault displacements within the emplacement drift footprint must be analyzed to determine the potential impacts of fault displacement on the Yucca Mountain repository. Such fault displacements could occur at known faults that intersect the emplacement drifts (based on surface mapping), or at other locations within the repository.

6.8.2.1 Location of Known Faults

Information on known faults intersecting the emplacement drift is obtained from two sources. The actual location of known faults relative to the repository location is provided in Figure 7 of *Site Recommendation Subsurface Layout* (BSC 2001b). A more detailed mapping of each emplacement drift tunnel, indicating locations of known fault zones intersecting each tunnel, as well as whether those locations occur in the lower lithophysal zone, is provided as part of the output from the multiscale thermo-hydrologic model (DTN: LL030704623122.031, tspa03.mesh03-150w). From these two sources of information, the known faults that intersect the drifts, the specific tunnels impacted, and whether the specific location is in the lower lithophysal zone or not can be determined. This information is summarized in Table 22, where tunnels are identified by panel number and tunnel number, plus a designation for east or west when appropriate (see the standard subsurface facilities layout shown in BSC 2003o).

As can be seen from Table 22, there are 19 locations in the lower lithophysal zones where a known fault intersects an emplacement drift, plus another 11 locations where such an intersection occurs in the nonlithophysal zones. This information, along with the probability of a fault displacement of sufficient magnitude to cause waste package failure at these locations, can be used to determine the likelihood and consequence of waste package failure.

Table 22. Intersections of Known Faults with Emplacement Drifts

Fault Designator	Tunnels in Lower Lithophysal Zones	Tunnels in Nonlithophysal Zones
Sundance Fault	1-8	-
	1-7	-
	1-6	-
Drill Hole Wash Fault	3-2	2-17E
	3-1	2-16E
	2-10W	2-15E
	2-9W	2-14E
	2-8W	2-13E
	2-7W	2-12E
	2-6W	2-11E
	2-5W	2-10E
	-	2-9E
	Pagany Wash Fault	2-2W
2-1W		2-6E
2-5E		-
2-4E		-
2-3E		-
2-2E		-
Sevier Wash Fault	2-1E	-
	2-2E	-

Source: DTN: LL030704623122.031, tspa03.mesh03-150w

6.8.2.2 Faulting Other Than At Known Faults

During a major seismic event, faulting could occur not only coincident with the location of well-characterized, known faults, but also elsewhere in the repository. In characterizing the potential magnitude of fault displacement elsewhere in the repository (see Section 6.8.3), rock conditions ranging from intact rock to the presence of existing small faults with ~2 meters of cumulative offset are considered. As is discussed in Section 6.8.3, the likelihood of significant fault displacement (>10 cm) is low, even for 10^{-8} probability events, except where an existing fault is located with cumulative displacement of ~2 meters. However, the exact location and number of such small faults is not known at this time, because they are not readily identified through surface mapping. Thus, it is necessary to estimate the density of such smaller faults based on either existing site data or natural analogues.

One means of quantifying the likelihood of such smaller faults is through use of the data obtained from the characterization of the ECRB Cross-Drift (Mongano et al. 1999, pp. 51 to 59). The ECRB Cross-Drift extends through the repository footprint near its north/south midpoint and spans the approximate east/west extent of the repository. Over the length of this tunnel, three small faults with cumulative displacement of between ~1 and a few meters were identified. If we assume that this is representative of the density of small faults throughout the repository, one can make an estimate of the number of such small faults that might intersect the emplacement drifts. In reviewing the repository layout (BSC 2003o), it can be seen that there are 46 emplacement drifts that span the entire north to south extent of the repository (designated 2-1W through 2-23W, 1-1 through 1-8, and 5-1 through 5-15). While in several cases these tunnels are much

shorter than the ECRB Cross-Drift, for conservatism it is assumed that there exist three unknown small faults that intersect the repository footprint along its entire north to south extent. Thus, it is estimated that there are 138 locations (3 times 46) where small faults intersect the emplacement drifts.

Since the exact location of these potential faults is unknown, one cannot determine with certainty whether they would intersect the emplacement drifts in the lower lithophysal zone or not. To estimate what fraction of these intersections correspond to the lower lithophysal zone, we use the fact that the estimated fraction of the overall repository in the lithophysal zone is 85 percent (Section 5.1). This fractional distribution is applied to the 138 small fault intersections to get a probability-weighted distribution of fault intersections versus rock stratigraphy.

- 117.3 Small fault intersections with drifts in lower lithophysal zone
- 20.7 Small fault intersections with drifts other than in lower lithophysal zone.

6.8.3 Fault Displacement Hazards

Magnitudes of fault displacements along two of these known faults (Sundance and Drill Hole Wash) as a function of probability are obtained from *Probabilistic Seismic Hazard Analyses for Fault Displacement and Vibratory Ground Motion at Yucca Mountain, Nevada* (CRWMS M&O 1998; DTN: MO0004MWDRIFM3.002). In Section 8 of that document, the DOE has developed fault displacement hazard curves for fifteen faulting conditions mapped within the immediate vicinity of Yucca Mountain. Mean fault displacement curves are used in all the following analyses. The faulting conditions relevant to this abstraction are as follows:

- Site 2 - Solitario Canyon Fault.
- Site 3 - Drill Hole Wash Fault.
- Site 4 - Ghost Dance Fault.
- Site 5 - Sundance Fault.
- Site 7 - A generic location within the repository, approximately 100-meters east of the Solitario Canyon fault. The ground conditions at the generic location include intact rock (7d), a hypothetical fracture with no cumulative displacement (7c), a hypothetical shear with 10-cm of offset (7b) and a hypothetical small fault with 2-meter offset (7a).
- Site 8 - A generic location within the repository, midway between the Solitario Canyon fault and the Ghost Dance fault. The ground conditions at the generic location include intact rock (8d), a hypothetical fracture with no cumulative displacement (8c), a hypothetical shear with 10-cm of offset (8b) and a hypothetical small fault with 2-meter offset (8a).

Four named secondary faults intersect the emplacement areas of the repository. These four faults are the Drill Hole Wash fault, the Sundance fault, the Pagany Wash fault, and the Sevier Wash

fault. It is assumed that displacements on the Pagany Wash and Sevier Wash faults are identical to those on the Drill Hole Wash fault (see Assumption 5.2).

The generic locations designated Site 7 and Site 8 apply throughout the repository. The estimated 138 intersections between the emplacement drifts and various small faults (~2 meter offset) identified in Section 6.8.2.2 correspond to locations 7a and/or 8a.

Table 23 provides the fault displacement values from the mean hazard curves as a function of the mean annual exceedance frequency (or probability) (DTN: MO0004MWDRIFM3.002). The first two faults (Solitario Canyon and Ghost Dance) in Table 23 are directly adjacent to the repository block and are not considered further because no waste packages lie on these faults. Locations 7 and 8 have essentially the same estimated displacements relative to the accuracy of the results in *Probabilistic Seismic Hazard Analyses for Fault Displacement and Vibratory Ground Motion at Yucca Mountain, Nevada* (CRWMS M&O 1998; DTN: MO0004MWDRIFM3.002). Thus, the distinction between 7a and 8a for the 138 small fault intersections described in Section 6.8.2.2 is not relevant.

6.8.4 Consequence for the Waste Packages

A comparison of Table 23 with Table 21 shows that all the waste packages would survive even a 10^{-8} frequency fault displacement at locations 7a, b, c and 8a, b, c because the maximum displacement at these sites (9 cm = 90 mm) is always less than the available clearances in Table 21. However, several of the waste package designs could potentially fail due to fault displacement for hazards near the 10^{-8} per year level if they are directly over any of the four known faults (Drill Hole Wash, Sundance, Pagany Wash, and Sevier Wash) intersecting the emplacement drifts. Further, the waste packages containing DHLW would potentially fail when placed over a small displacement fault (designated 7a and 8a). Thus, the likelihood of waste package failure at a given fault location is a function of the clearance for the specific type of waste package emplaced there.

Waste package distribution by type is available in the design basis inventory. This inventory is repeated in Table 24, along with the waste package dimensions. *Repository Design Project, RPD/PA IED Typical Waste Package Components Assembly, 1 of 9* (BSC 2003j), the source document for the waste package dimensions, does not provide information for the 5 DHLW Long/1 DOE SNF Short or the 5 DHLW Long Only waste package configurations. This is because these two configurations use the same waste package as the 5 DHLW Long/1 DOE SNF Long configuration with different assemblies loaded. Thus, the waste package exterior dimensions are the same for all three configurations.

Table 23. Fault Displacement from Mean Hazard Curves

	Mean Annual Exceedance Frequency (1/yr)				
	10^{-4} ^c	10^{-5} ^c	10^{-6} ^d	10^{-7} ^d	10^{-8} ^d
Site Number and Fault Name	Displacement (cm)				
2 - Solitario Canyon	<0.1	32.0	190	500	>1000
4- Ghost Dance	<0.1	<0.1	13	58	160
3 - Drill Hole Wash ^a	<0.1	<0.1	17	80	240
5 - Sundance	<0.1	<0.1	6	42	~145
7a - small fault with 2-m offset	<0.1	<0.1	2	20	~75
7b - shear with 10-cm offset	<0.1	<0.1	1	6	9
7c - fracture with no displacement	<0.1	<0.1	0.1	<1	<1
7d - intact rock ^b	<0.1	<0.1	<0.1	<0.1	<0.1
8a - small fault with 2-m offset	<0.1	<0.1	2	20	~75
8b - shear with 10-cm offset	<0.1	<0.1	1	6	9
8c - fracture with no displacement	<0.1	<0.1	0.1	<1	<1
8d - intact rock ^b	<0.1	<0.1	<0.1	<0.1	<0.1

DTN: MO0004MWDRIFM3.002

- NOTES: ^a Also representative of Pagany Wash and Sevier Wash faults.
^b Zero displacement at Sites 7d and 8d is documented in DTN: MO0004MWDRIFM3.002. See also CRWMS M&O 1998, Section 8.2.1.
^c See DTN: MO0004MWDRIFM3.002 for displacement hazards at Sites 3, 5, 7a-c and 8a-c for the 10^{-4} and 10^{-5} per year annual exceedance frequencies. See also CRWMS M&O 1998, Table 8-1 for displacement hazards at 10^{-4} and 10^{-5} annual exceedance frequencies.
^d See DTN: MO0004MWDRIFM3.002 for displacement hazards at Sites 3, 5, 7a-c and 8a-c for the 10^{-6} , 10^{-7} , and 10^{-8} per year annual exceedance frequencies. See CRWMS M&O 1998, Figures 8-3 and 8-5 for displacement hazards at Sites 2 and 4 for the 10^{-6} , 10^{-7} , and 10^{-8} per year annual exceedance frequencies.

To simplify the analysis, the inventory of waste packages is split into four groups. Waste packages of similar design (similar waste type) are grouped together, and the maximum diameter for all included waste packages is conservatively assigned to the group. These groupings are chosen to facilitate consequence assessment for the waste package groupings in TSPA-LA. The four groupings are as follows.

- PWR: includes **21-PWR with absorber plates**, **21-PWR with control rods**, and the 12-PWR Long with absorber plates.
- BWR: includes **44-BWR with absorber plates** and 24-BWR with absorber plates.
- Naval: includes **Naval-Long** and **Naval-Short**.
- HLW: includes **5 DHLW/1 DOE SNF – Short**, **5 DHLW/1 DOE SNF – Long**, and all other HLW designs.

The waste package designs in bold letters are the ones with the largest diameter in the group, and thus are chosen to represent the diameter for all packages in that group. While the inclusion of the 12 PWR design with the PWR group, the 24 BWR design with the BWR group, and the 2-MCO/2-DHLW design with the HLW group conservatively accounts for the likelihood of failure for those waste package designs (by overestimating diameter), the impact of this approximation is small because in each case the number of such packages is small relative to the total number of packages in the group.

Table 24. Design Basis Waste Package Dimensions and Inventory

Waste Package Configuration	Waste Package Length (m)	Waste Package Diameter (m)	Nominal Quantity
21-PWR with Absorber Plates	5.165	1.644	4299
21-PWR with Control Rods	5.165	1.644	95
12-PWR with Absorber Plates - Long	5.651	1.330	163
44-BWR with Absorber Plates	5.165	1.674	2831
24-BWR with Absorber Plates	5.105	1.318	84
5 DHLW Short/1 DOE SNF - Short	3.590	2.110	1147
5 DHLW Long/1 DOE SNF - Long	5.217	2.110	1406
5 DHLW Long/1 DOE SNF - Short	5.217	2.110	31
5 HLW Long Only	5.217	2.110	679
2-MCO/2-HLW	5.217	1.814	149
Naval-Short	5.430	1.949	144
Naval-Long	6.065	1.949	156

Source: BSC 2003j, Table 1 for length and diameter
BSC 2003k, Table 11 for nominal quantity

NOTES: The diameter of DHLW packages and HLW package is taken to be that of the DHLW packages in Table 20.
The length of the DHLW Short package is taken to be that of the 5 DHLW/DOE SNF - Short package in Table 20.
The length of the DHLW Long and HLW Long packages is taken to be that of the 5 DHLW/DOE SNF - Long package in Table 20.

The percentage of the inventory of the waste packages for each group is calculated based on the total length of that waste package type versus the total length of all emplaced waste packages. Length is the appropriate parameter here because it more accurately represents the probability that a waste package will lie on a fault. These results are shown in Table 25. The average length per package type is shown for information only. It is used to calculate the fraction of waste packages by waste package type.

Table 25. Parameters for Simplified Groups of Waste Packages

Waste Package Group	Average Waste Package Length (m)	Maximum Waste Package Diameter (m)	Waste Package Surface Area ^a (m ²)	Nominal Quantity (-)	Effective Waste Package Length for Group ^b (m)	Fraction of Waste Packages (% of Total Length)
PWR	5.1824	1.644	31.01	4557	23616	41.9
BWR	5.1633	1.674	31.55	2915	15051	26.7
Naval	5.760	1.949	41.24	300	1728	3.1
HLW	4.670	2.110	37.95	3412	15934	28.3

NOTES: ^a Surface Area = $(\pi/2)(D_{\max})^2 + \pi D_{\max}L_{\text{avg}}$.

^b Effective Length = (Average Length) × (Nominal Quantity).

Using the maximum waste package diameter in Table 25 and the calculated maximum fault displacements before the waste package is pinned in Table 21, the following maximum fault displacement values (to cause waste package damage) are used in the analysis.

Table 26. Maximum Allowable Fault Displacements Before a Waste Package Group Is Pinned

Waste Package Group	Maximum Allowable Displacement With Tunnel Collapse (mm)	Maximum Allowable Displacement Without Tunnel Collapse (mm)
PWR	1072	2880
BWR	1042	2850
Naval	767	2575
HLW	606	2414

A determination of waste package failure is made by comparing the maximum allowable displacements in Table 26 with the fault displacement hazard curve in Table 23. As a reminder, the Solitario Canyon and Ghost Dance faults are not included in this analysis because these faults lie outside the emplacement areas of the repository.

Consider the case where tunnel collapse has not occurred. As can be seen from Table 26, the HLW/Naval waste package design is subject to potential failure when the fault displacement exceeds the maximum allowable displacement of 2,414 mm. However, as can be seen from Table 23, the maximum fault displacement for any of the faults that intersect the emplacement drifts is 230 cm = 2,300 mm, which corresponds to a 10^{-8} fault displacement along the Drill Hole Wash fault. (The Solitario Canyon fault has larger displacements, but no drifts in the current repository layout intersect this known fault.) Thus, since the maximum fault displacement is less than the allowable displacement of 2,414 mm, no damage to EBS components would be predicted without tunnel collapse. The same conclusion is valid for the other waste package designs, with even greater margin.

Now consider the case where tunnel collapse has occurred, as is expected in the lower lithophysal zones for seismic hazards with an annual exceedance frequency of 10^{-6} or less. First, it is evident from a comparison of Tables 25 and 22 that all BWR, PWR, and Naval waste packages will survive a fault displacement event for Sites 7a and 8a, even in the lower lithophysal zones. The maximum fault displacement in Table 23 for Sites 7 and 8 is 75 cm = 750 mm, slightly less than the allowable fault displacement of 767 mm for the Naval group with drift collapse in the lower lithophysal units. Again, the same conclusion is valid for the BWR and PWR waste package designs, with even greater margin.

However, at mean annual exceedance frequencies between 10^{-7} per year and 10^{-8} per year, waste package failure may occur for any of the waste packages placed directly over the four known secondary faults intersecting the emplacement drifts, as well as for the HLW packaged placed over faults characterized by location 7a and 8a. In those cases, the fault displacement values in Table 23 exceed the maximum allowable displacements summarized in Table 26 for the case of drift collapse.

The probability of a fault displacement event severe enough to cause waste package failure is a function of both the specific fault (different fault displacements for a given probability) as well as the specific waste package design (different allowable displacements). (The exceedance frequency is equal to the exceedance probability for values much less than one per year.) To determine the probability associated with a fault displacement event severe enough to cause waste package damage, the fault displacement hazard curves from the *Probabilistic Seismic*

Hazard Analyses for Fault Displacement and Vibratory Ground Motion at Yucca Mountain, Nevada (CRWMS M&O 1998; DTN: MO0004MWDRIFM3.002) are used. The relevant information is provided in file `./displ/tot-haz/s3.frac_mean.gz` of the DTN for the Drill Hole Wash fault, in file `./displ/tot_haz/s5.frac_mean.gz` for the Sundance fault, and in files `./displ/tot-haz/s7a.frac_mean.gz` and `./displ/tot-haz/s8a.frac_mean.gz` of the DTN for locations 7a and 8a. These curves show the predicted fault displacement as a function of probability of the event (a graphical presentation of the results in Table 23). Using the maximum allowable displacements from Table 26 (for each waste package design), the associated event probabilities are determined from the hazard curves in DTN: MO0004MWDRIFM3.002. The resulting fault exceedance probabilities that would cause waste package failure are summarized in Table 27. As previously stated, the Pagany Wash and Sevier Wash faults are assumed to be represented by the Drill Hole Wash fault (see Assumption 5.2). Again, these results only apply to the lower lithophysal zone, which is predicted to collapse from seismic hazards at these annual exceedance frequencies.

Table 27. Fault Exceedance Probabilities That Cause Failure in the Lower Lithophysal Zone^a

Fault	HLW	Naval	BWR	PWR
Sundance	$< 5 \times 10^{-8}$	$< 4 \times 10^{-8}$	$< 3 \times 10^{-8}$	$< 3 \times 10^{-8}$
Drill Hole Wash	$< 2 \times 10^{-7}$	$< 1 \times 10^{-7}$	$< 6 \times 10^{-8}$	$< 6 \times 10^{-8}$
Pagany Wash	$< 2 \times 10^{-7}$	$< 1 \times 10^{-7}$	$< 6 \times 10^{-8}$	$< 6 \times 10^{-8}$
Sevier Wash	$< 2 \times 10^{-7}$	$< 1 \times 10^{-7}$	$< 6 \times 10^{-8}$	$< 6 \times 10^{-8}$
7a/8a	$< 2 \times 10^{-8}$	N/A	N/A	N/A

NOTE: ^a Tunnels in the lithophysal zones are predicted to collapse from ground motions at these mean annual exceedance frequencies, so the maximum allowable displacement is based on Table 21 with tunnel collapse.

As expected, the highest probability fault displacement events leading to waste package failure are associated with the HLW waste packages, which have the largest diameter.

There are three locations where the Sundance fault intersects the emplacement drifts in the lower lithophysal zone (from Table 22), 16 locations where either the Drill Hole Wash, Pagany Wash, or Sevier Wash faults intersect the emplacement drifts in the lower lithophysal zone (see Table 22), and 117.3 locations (probability-weighted) where additional small faults intersect the emplacement drifts in the lower lithophysal zone (Section 6.8.2.2). Combining this information with the probability of finding a particular waste package group at a given point in the repository (see Table 25), one can estimate the expected number of each type of waste package found at the four secondary faults. This result is shown in Table 28. Note that the number of waste packages is not an integral number because it represents an average expectation of finding a particular waste package along a particular fault. The Pagany Wash, Sevier Wash and Drill Hole Wash faults have been combined in Table 28 because they have the same fault displacement hazard curves.

Table 28. Expected Number of Waste Packages Emplaced on Faults

	PWR Group	BWR Group	Naval Group	HLW Group	Total
Sundance	1.26	0.80	.09	0.85	3
Drill Hole Wash, etc.	6.71	4.28	.49	4.53	16
7a/8a	49.18	31.34	3.60	33.18	117.3

6.8.5 Damage Abstraction for Fault Displacement

The expected number of waste package failures as a function of annual exceedance frequency can be calculated by combining the results in Tables 26 and 27. These results are shown in Table 29. A spreadsheet with the details of this calculation is provided as Attachment VII.

Table 29. Expected Waste Package Failures versus Annual Exceedance Frequency

Annual Exceedance Probability (1/yr)	Expected Number of Waste Package Failures				
	PWR	BWR	Naval	HLW	Total
$> 2 \times 10^{-7}$	0	0	0	0	0
1×10^{-7} to 2×10^{-7}	0	0	0	4.53	4.53
6×10^{-8} to 1×10^{-7}	0	0	0.49	4.53	5.02
5×10^{-8} to 6×10^{-8}	6.71	4.28	0.49	4.53	16.00
4×10^{-8} to 5×10^{-8}	6.71	4.28	0.49	5.37	16.85
3×10^{-8} to 4×10^{-8}	6.71	4.28	0.58	5.37	16.94
2×10^{-8} to 3×10^{-8}	7.97	5.08	0.58	5.37	19.00
1×10^{-8} to 2×10^{-8}	7.97	5.08	0.58	38.56	52.18

NOTE: Total values are based on the spreadsheet in Attachment VII. Sums of the contributions by waste package type are not exact because of roundoff.

When a waste package fails by fault displacement, the failed area on the waste package is determined by sampling a uniform distribution with a lower bound of 0 m² and an upper bound equal to the area of the waste package lid, as explained below. The area of the lid for the PWR, BWR, Naval, and HLW groups is 2.123 m², 2.201 m², 2.983 m² and 3.497 m², respectively, based on the maximum waste package diameter in Table 25. The total failed area from a faulting event is based on the weighted sum of the damage to each type of waste package.

The lower bound is appropriate for annual exceedance probabilities near 10⁻⁷ per year because a waste package that is minimally pinned from fault displacement should only have minor crimping with a very small damaged area. The upper bound is appropriate for a fault that shears a waste package near its lid. In this case, the lid welds can fracture, separating the lid from the package and potentially exposing the entire waste form to seepage and release. The use of a uniform distribution is appropriate here because reasonable upper and lower bounds can be defined and because the use of this type of distribution maintains the uncertainty in the damaged area for this abstraction.

When a waste package fails from fault displacement, the associated drip shield and fuel rod cladding also fail as barriers to flow and transport. A sheared drip shield will allow all seepage to pass through it; that is, the failed area is taken as the total surface area of the drip shield so there is no flux splitting (diversion of seepage) on the drip shield. Similarly, cladding becomes 100 percent perforated in response to a fault displacement that can shear a waste package. These changes represent conservative, bounding approximations, particularly for annual exceedance frequencies near 10⁻⁷ per year.

6.8.6 An Alternate Conceptual Model For Damage From Fault Displacement

The analysis of waste package failure due to fault displacement presented herein provides a basis for estimating the number of potentially damage-inducing faults that intersect the emplacement drifts. This analysis uses the known location of larger faults (e.g., Sundance fault, Ghost Dance fault, etc.) relative to the planned location of the emplacement drifts, as well as an estimate of the density of smaller-displacement faults based on the observed fault density along the exploratory tunnel. The maximum allowable fault displacement before waste package damage is assumed to occur was shown to vary between 606 mm and 1072 mm depending on waste package design (Table 26). Using this site-specific information, it is shown that there are 30 locations where known faults intersected the planned emplacement drifts (Table 22) plus an estimated 138 locations where unmapped faults could intersect the drifts (Section 6.8.2.2) for a total of 168 fault intersections. Of these, there are a maximum of 52.2 locations (probability weighted by waste package type and location within the repository footprint) that are calculated to cause waste package damage (Table 29) with an occurrence frequency between 2×10^{-7} per year and 10^{-8} per year.

As an alternate conceptual model, we consider work published in “Methodologies for the Evaluation of Faulting at Yucca Mountain, Nevada” (Waiting et al. 2003). This paper presents an assessment of the consequences of fault displacement at Yucca Mountain based on historical earthquake activity in the Western United States. Four historic rupture events were considered to arrive at a median value for fault rupture density (length of faulting per unit area of surface). A conservative median value of 20 km/km^2 was obtained from this analysis of the four events considered. Using this value, along with a representative angle of 50 degrees between the typical tunnel orientation and the orientation of the faults and an 80-meter drift spacing, the authors determined that there would be 191 waste package locations where a fault would intersect an emplacement drift at Yucca Mountain. This result compares favorably to the 168 fault intersections calculated in this report.

The specific analog event considered by the authors for purposes of quantification was the Borah Peak earthquake from 1983. Prior analysis of this event had shown that the maximum displacement for the Borah Peak earthquake was 2.7 meters, with an average displacement of approximately 1 meter. Given the fact that the mean annual exceedence probability for 1 meter of displacement at Yucca Mountain ranges from $\sim 10^{-6}/\text{yr}$ for the Solitario Canyon fault to $\sim 10^{-8}/\text{yr}$ for the Sundance fault, the probability-weighted number of waste package failures is calculated to be between 1.91×10^{-4} to 1.91×10^{-6} . It should be noted that the upper end of this range applies only to the Solitario Canyon fault. As shown in Section 6.8.2.1, no drifts intersect the Solitario Canyon fault for the current repository footprint. The largest fault displacement would be expected to correspond to the Drill Hole Wash fault. The mean annual exceedence probability for one meter of displacement for this fault is on the order of $10^{-7}/\text{yr}$. Thus, the probability-weighted number of waste package failures would be between 1.91×10^{-5} to 1.91×10^{-6} .

The results presented herein in Table 29 are not quoted in terms of probability-weighted number of waste package failures. Thus, a direct comparison with the results of the alternate model is not possible. However, it is straightforward to recast the Table 29 results in a compatible form. If for each probability range we consider the number of incremental waste packages that are

calculated to fail, then the product of the annual exceedence probability (using the upper end of the range) and the number of incremental waste packages calculated to fail represents the probability-weighted number of waste package failures for that exceedence interval. If we sum this result for all exceedence probability ranges, one arrives at the equivalent total number of probability-weighted waste package failures. This is shown in the following calculation:

<u>Exceedence Probability</u>	<u># Incremental WP Failures</u>	<u>Probability Weighted WP Failures</u>
2×10^{-7}	4.53	0.91×10^{-6}
1×10^{-7}	0.49	0.05×10^{-6}
6×10^{-8}	10.98	0.66×10^{-6}
5×10^{-8}	0.85	0.04×10^{-6}
4×10^{-8}	0.09	0.00×10^{-6}
3×10^{-8}	2.06	0.06×10^{-6}
<u>2×10^{-8}</u>	<u>33.18</u>	<u>0.66×10^{-6}</u>
Totals	52.18	2.38×10^{-6}

So the probability-weighted number of waste package failures for the model in this report is 2.38×10^{-6} . This value is within the range of results provided by the alternate conceptual model, 1.91×10^{-5} to 1.91×10^{-6} . Thus, the alternate conceptual model based on the use of analog data provides results that are consistent with the results of the model presented in this report for both the probability-weighted number of waste package failures and the number of fault intersections with the emplacement drifts. This provides added confidence in the validity of the results presented herein.

6.8.7 Final Abstraction for Damage from Fault Displacement

The seismic scenario class for TSPA-LA will use the abstraction described in Section 6.8.5 as the basis for damage to EBS components from fault displacement.

6.9 POST-SEISMIC CHANGES IN THE LOCAL ENVIRONMENT

A large seismic event, involving both vibratory ground motion and/or fault displacement, can change the local environment around the emplacement drifts. The most obvious physical change is that the emplacement drifts in the lithophysal zone are predicted to collapse as a result of the 10^{-6} per year ground motion level, and by inference at greater ground motion levels. Drift collapse can alter the shape of the drift and fill it with a natural backfill, resulting in the following potential process-level changes in and around the engineered barrier system:

- Seepage may increase because of the irregular drift shape and because of a loosening of the fractures around the drift.
- Temperature of the drip shield and waste package may increase relative to an unfilled drift because the backfill provides an insulating blanket on top of the drip shield. General corrosion may increase because of increased temperature and because of rock and water contact with the drip shield or waste package.

- Glass dissolution rate and some radionuclide solubility limits will increase with increasing temperature.

A change in the seepage flux into the emplacement drifts in the lithophysal zones is being incorporated into the seismic abstractions for TSPA-LA. The seepage into the emplacement drifts in the lithophysal zones will be determined in analogy with ambient seepage by using the seepage table for degraded drifts as provided in DTN: LB0307SEEPDRCL.002. This table is invoked after a seismic hazard occurs, provided the hazard is large enough to collapse the drifts. The seepage fluxes provided in this table are considered conservative but not unrealistic. If a more realistic model for seepage after drift collapse becomes available through *Abstraction of Drift Seepage* (BSC 2003q) or through related work, then this new information should be incorporated into TSPA-LA.

For TSPA-LA, all ground motions with mean annual exceedance frequency of 10^{-4} per year or less will be considered large enough to collapse the drifts. This threshold for change is consistent with the fact that tunnels in the lithophysal zone do not collapse for the 5×10^{-4} per year ground motion, except for very minor damage at the lowest level of compressive strength (BSC 2003h, Section 6.4.1.1).

There is no change in the seepage flux into the emplacement drifts in the nonlithophysal zones. The seepage abstraction already includes an enhancement factor for limited collapse of the emplacement drifts, and this enhancement factor is deemed adequate because the rockfall calculations show only limited collapse of the emplacement drifts in the nonlithophysal zones

A second seepage-related change can occur for seismic hazards that occur during the rewetting period. The flux splitting algorithm for the waste package and drip shield is unchanged from that for the nominal scenario class, with one exception. If the seismic hazard occurs at a time when the conditions for the existence of accelerated localized corrosion of Alloy 22 are satisfied, then all seepage that enters the drip shield will flow into the waste package without any flux splitting. This is a reasonable change because enhanced localized corrosion on the waste package will generate corroded areas directly beneath the seeps through the drip shield. Once these corroded areas penetrate the outer and inner shells of the waste package, the seeps will fall directly onto the waste package internals, without diversion by the surface of the waste package.

The presence of rubble about the drip shield after drift collapse could cause changes in the thermal environment in the EBS if a seismic event occurs relatively soon after repository closure, while the waste package and drip shield are at elevated temperatures. However, the irregular and coarse nature of the rubble is expected to allow sufficient convective heat transfer that the temperature histories calculated for the nominal scenario class may reasonably be used to approximate conditions following a seismic event during the thermal period. Because potential changes in temperature due to the presence of rubble are not expected to be significant, the possible associated changes in temperature-dependent solubility and corrosion rate have not been included in TSPA-LA.

6.10 SEISMIC SCENARIO CLASS

The impact of seismic hazards on repository performance is being represented in a separate scenario, called the seismic scenario, for TSPA-LA. The rationale for defining a separate scenario is based on several key observations:

- **Seismic events with annual frequencies down to 10^{-8} per year must be considered by TSPA-LA.**

10 CFR 63.114, Requirements for Performance Assessment, states that:

Any performance assessment used to demonstrate compliance with §63.113 must: . . . (d) Consider only events that have at least one chance in 10,000 of occurring over 10,000 years.

Very large seismic hazards (i.e., ground motions and/or fault displacements) with annual probability of occurrence down to 10^{-8} per year must be considered by TSPA-LA, even though their probability is very low during the 10,000-year regulatory period.

- **The nominal scenario class cannot determine the impact of low probability seismic events in a computationally efficient manner. A separate scenario for seismic hazards is desirable.**

Events with very small annual probabilities of occurrence cannot be represented in the nominal scenario class in a computationally efficient fashion. Accurate representation of events with annual probability of occurrence down to 10^{-8} per year would require millions of realizations in the nominal scenario class, which is not computationally feasible. The alternative is to define a separate scenario for seismic hazards that determines dose in a probability-weighted manner, as explained below.

- **The mean dose time history is the main parameter for compliance determinations.**

Radionuclide release limits for the repository are expressed in terms of the mean of the distribution of projected doses to the reasonably maximally exposed individual, per 10 CFR 63.303 and 63.311. Calculation of releases from the seismic scenario class must generate mean dose for consistency with the nominal scenario class.

- **Damage from seismic events is expressed as a failed area on the surfaces of the drip shield, the waste package, and the cladding.**

The damage from seismic events is expressed as a failed area for advective flow on the surfaces of the drip shield, the waste package, and the cladding. These failed areas are a function of the amplitude of the seismic event. For example, the amplitude of a ground motion is defined through the horizontal PGV. The individual damage abstractions for the waste package, the drip shield, and the cladding are based on the results from structural response calculations and rockfall calculations, as discussed in Sections 6.5 through 6.9.

The seismic scenario class is based on a single seismic hazard that occurs at a randomly chosen time in each realization of the TSPA-LA. That is, the conditional probability of a seismic event is 1 for each realization. The damage from this single event is based on the damage abstractions for the drip shield, the waste package and the cladding. The damaged areas on the EBS components define pathways for flow and transport through the EBS. The seepage flux for the emplacement drifts in the lithophysal zones changes after a seismic hazard occurs, and there is no flux splitting on the waste package if the seismic event occurs when conditions for accelerated localized corrosion are satisfied. Once radionuclides are released from the EBS, flow and transport in the unsaturated zone and the saturated zone are based on the same models and algorithms as for the nominal scenario class. Biosphere calculations and parameters for the seismic scenario class are also unchanged from the nominal scenario class.

Each realization of the seismic scenario class determines an annual dose time history for a single seismic hazard with mean annual exceedance frequency λ_i . These dose time histories do not represent the mean dose, as called for in 10 CFR 63.303, because a single hazard always occurs in each realization. A mean dose time history is calculated using a probability-weighted sum and average of all the realizations for the seismic scenario class. The weighting factor for each realization corrects for the expected number of seismic events in each realization and for the logarithmic sampling of the hazard curve for PGV.

6.10.1 Computational Approach

The mean dose for the seismic scenario class is calculated using a two-step approach: (1) in the first step, TSPA-LA generates a set of R realizations that have robust sampling of all levels of seismic hazards with the potential to generate releases from the EBS, and (2) in the second step, the mean or expected dose time history is calculated using a weighted sum and average of the dose time histories from the R realizations evaluated during the first step. Additional post-processing can present results as cumulative distribution functions, as complementary cumulative distribution functions, or can evaluate the variability of the dose time histories, if necessary.

The mathematical basis for calculating the mean dose as a weighted sum and average of the individual dose time histories is presented in Attachment VIII. The following discussion explains how these two steps are implemented in a Monte Carlo computational procedure.

6.10.1.1 Description of the First Step

The first step generates R realizations of future performance with the TSPA-LA model for the seismic scenario class for all seismic hazards. This suite of R realizations represents the epistemic and aleatory uncertainty in the TSPA-LA model for the seismic scenario class. Epistemic uncertainty is captured by all those stochastic parameters that represent the “lack of knowledge” uncertainty in various processes. Aleatory uncertainty is captured by the stochastic parameters that represent the randomness of processes, such as the uncertainty in the timing and amplitude of seismic hazards.

The TSPA-LA model for the seismic scenario class is very similar to the TSPA-LA model for the nominal scenario class, with two major exceptions: (1) failed areas on the drip shield, waste

package or cladding are determined by sampling stochastic parameters in abstractions for damage to EBS components, rather than by the waste package degradation (WAPDEG) model for corrosion processes; and (2) a single seismic event occurs at a random time during each realization. The output from each these R realizations is a time history of dose to the reasonably maximally exposed individual.

For each realization, the annual exceedance frequency of the seismic hazard, λ_i , and the time of occurrence of the seismic hazard, T_i , are determined by a Monte Carlo process that samples appropriate distributions for these parameters. (Each realization has a single seismic hazard that occurs at a randomly selected time during the calculation.) The type of distribution for λ_i and T_i are determined as follows.

The sampling for the annual exceedance frequency uses a logarithmic, rather than a linear, scale to ensure robust sampling throughout all frequency ranges. More specifically, λ_i is determined by sampling a log-uniform distribution with lower bound λ_{min} and upper bound λ_{max} . The bounds must be chosen to encompass all seismic exceedance frequencies with the potential to release significant radionuclides from the EBS. Typical values of λ_{max} and λ_{min} for the seismic scenario class are 10^{-4} per year and 10^{-8} per year, respectively, because this range spans the response of the system, from no damage at 10^{-4} per year (see Assumption 5.1) to the regulatory limit at 10^{-8} per year.

The time of the seismic event, t_i , is determined by sampling a log-uniform distribution between T_{min} and T_{max} . Typical values of T_{max} will be 10,000 years, the regulatory period, or 20,000 years. As noted in Section 1.2, the 20,000-year duration for the seismic analyses is designed to demonstrate that repository performance remains robust well after the 10,000-year regulatory period. The value for T_{min} will be determined through sensitivity studies with the TSPA-LA model.

Once the value of the annual exceedance frequency (λ_i) is determined for the i^{th} realization, the corresponding values of the peak ground velocity (PGV_i) is calculated. The relationship between PGV and λ is called a hazard curve, and is site- and location-specific. The mean hazard curve for the Yucca Mountain site at Point A, a reference rock outcrop at the repository elevation, is defined in *Probabilistic Seismic Hazard Analyses for Fault Displacement and Vibratory Ground Motion at Yucca Mountain, Nevada* (CRWMS M&O 1998; DTN: MO03061E9PSHA1.000, file h_vel_extended.frac_mean), based on the results of an expert elicitation.

The TSPA-LA requires a mean hazard curve at Point B, corresponding to the emplacement drifts. The derivation of the PGV hazard curve at Point B is explained in Section 6.4, with the calculations documented in Attachment I. Figure 3 in Section 6.4 illustrates the scaled hazard curve for Point B. The PGV hazard curve at Point B provides the basis for determining the value of PGV_i for the i^{th} realization. Once the value for PGV_i is known, the distributions for the failed areas on the waste package, drip shield, and cladding are sampled. For example, the damaged area on the waste package is represented as a uniform distribution whose upper bound is a function of the value of PGV for the i^{th} realization. Once the value of PGV_i is known, the upper bound is calculated and the uniform distribution sampled to determine the damaged area on the waste package for this realization. This approach explicitly includes the variability from the structural response calculations in the TSPA-LA model by sampling this distribution.

Damage from fault displacement occurs simultaneously with damage from vibratory ground motion. The value of λ_i determines the number of damaged waste packages by type, based on the abstraction in Table 28. The damaged area from fault displacement is determined by sampling a distribution with a lower bound of 0 and an upper bound based on the lid area for each type of waste package.

Simultaneous damage from fault displacement and vibratory ground motion is a reasonable approach for the seismic scenario class. Damage from fault displacement only occurs for the largest seismic hazards, with an annual exceedance frequency of 2×10^{-7} per year or less (see Table 28). Such a large seismic hazard is always accompanied by vibratory ground motion, so fault displacement and ground motion are not considered independent processes for TSPA-LA.

It is reasonable to expect that 50 to 100 realizations in each decade (i.e., from 10^{-5} to 10^{-6}) of the hazard curve are sufficient to provide robust sampling for this scenario. If the hazard spans three decades (such as 10^{-5} to 10^{-8} per year), then the simulation requires 150 to 300 realizations. In practice, the variability of the mean dose is used to determine an adequate number of realizations. In this approach, a comparison of TSPA-LA calculations with 300 and 500 realizations is used as a test to determine when the mean dose has “converged” within acceptable limits.

6.10.1.2 Description of the Second Step

Each of the R realizations generates a time history of dose to the reasonably maximally exposed individual, conditional upon the occurrence of a single seismic event. However, “compliance is based upon the mean of the distribution of projected doses of DOE’s performance assessments which project the performance of the Yucca Mountain disposal system for 10,000 years after disposal,” as noted in 10 CFR 63.303.

The mean annual dose is calculated using a weighted sum and average of the R realizations performed during the first step. The weighting factors for each realization are derived in Attachment VIII. The weighting factors for each realization correct for the number of expected seismic events in each realization and for the log-uniform distributions for the annual frequency of occurrence and for the sampling on time. The mean dose, as derived in Section 2 of Attachment VIII, is given by Equation VIII.2.12 as:

$$\bar{D}(t) = \frac{1}{R} \ln\left(\frac{\lambda_{max}}{\lambda_{min}}\right) \ln\left(\frac{T_{max}}{T_{min}}\right) \sum_{i=1}^R t_i \lambda_i D_i\{t | t_i, PGV_i\}, \quad (\text{Eq. 10})$$

where

$D_i\{t | t_i, PGV_i\}$ is the dose at time t for the i^{th} realization, which has a seismic event of magnitude PGV_i occurring at time t_i

$\bar{D}(t)$ is the mean dose for the scenario at time t

R is the number of realizations in the scenario

λ_{max} is the maximum value for the occurrence frequency

λ_{min} is the minimum value for the occurrence frequency

T_{max} is the maximum time (duration) of the scenario

T_{min} is the minimum time in the log-uniform sampling for the event time

6.10.2 Computational Algorithm

The first step in the computational algorithm for the seismic scenario class, as described in Section 6.10.1.1, generates R realizations of future performance with the TSPA-LA model. The computational algorithm has been split into 12 simple operations to document the procedure for this scenario class. The first nine operations define the constant parameters, the stochastic parameters, and the formulas that represent the epistemic and aleatory uncertainty for the TSPA-LA model. Each realization of the TSPA-LA model is based on a single sampling of the stochastic parameters from the first nine operations. Repeated samplings of the stochastic parameters generate a full suite of R realizations of the TSPA-LA model. The second step in the computational algorithm (see Section 6.10.1.2) evaluates the mean dose from these R realizations, using the formula and parameters defined in the tenth operation.

The modifications for post-seismic event response are summarized in Operations 11 and 12. While these operations are part of the TSPA-LA model calculations in the first step, the parameter values are defined by reference rather than by analysis in this model report. These modifications are listed last in the procedure to emphasize this difference.

A list of the 12 operations in the computational procedure is indicated below. The parameters for the computational procedure are listed in Table 30.

1. Determine the mean annual exceedance frequency, λ_i , for the i^{th} realization.

The value of λ is sampled from a log-uniform distribution between λ_{min} and λ_{max} . A log-uniform distribution ensures robust sampling in each decade of the distribution. The values of λ_{min} , λ_{max} , and λ_i are represented by the parameters LAMBDA_MIN, LAMBDA_MAX, and LAMBDA, respectively, in Table 30.

2. Determine the corresponding value of PGV_i through the hazard curve, $\lambda = \lambda(PGV)$.

The value of PGV_i is determined by a table lookup, using the scaled PGV hazard curve for Point B. The scaled hazard curve is calculated in Attachment I and tabulated in Table I-1. The interpolation between points in this table is based on a linear interpolation using the value of $\log(\lambda)$ at individual points. This is referred to as a log-linear interpolation scheme in Table 30. The value of PGV_i is the parameter PGV in Table 30.

3. Determine the fraction of failed waste package surface area due to vibratory ground motion for each realization.

The percent of failed waste package area is a random variable with distribution parameters that are functions of PGV_i . This damage abstraction is defined by a uniform distribution with a lower bound of 0 percent failed area and an upper bound that is a linear function of PGV_i . The fraction of failed surface area is applied to all packages in the repository (i.e., there is no spatial variability).

- The upper bound of the uniform distribution is defined by:

$$\text{MAX}(0.0, 0.436 \times PGV_i - 0.305) \quad (\text{Eq. 11})$$

in units of % damage. The value of this function is represented in Table 30 by the parameter WP_DAMAGE_MAX.

- The lower bound of the uniform distribution is 0 percent. This value is represented by the parameter WP_DAMAGE_MIN in Table 30.
- The sampled value of the uniform distribution (for each realization) is denoted as WP_DAMAGE%.
- The fraction of failed surface area is denoted as WP_DAMAGE and calculated as:

$$\text{WP_DAMAGE} = \text{WP_DAMAGE\%/100} \quad (\text{Eq. 12})$$

This failed area allows advective flow and advective and diffusive transport from the waste package, per Assumption 5.3.

4. Determine the fraction of failed drip shield surface area due to vibratory ground motion for each realization. This damage abstraction is defined by a uniform distribution with a lower bound of 0 percent failed area and an upper bound that is a linear function of PGV_i. The fraction of failed surface area is applied to all drip shields in the repository (i.e., there is no spatial variability).

- The upper bound of the uniform distribution, DS_DAMAGE_MAX, is a function of PGV and defined in Table 15 with a linear interpolation between the points.
- The lower bound of the uniform distribution, DS_DAMAGE_MIN, is a function of PGV and defined in Table 16 with a linear interpolation/extrapolation between the points.
- The sampled value of the uniform distribution is denoted as DS_DAMAGE%_GM.
- The fraction of failed surface area is denoted as DS_DAMAGE_GM and calculated as:

$$\text{DS_DAMAGE_GM} = (\text{DS_DAMAGE\%_GM})/100 \quad (\text{Eq. 13})$$

5. Determine the fraction of failed drip shield surface area due to rockfall in the nonlithophysal zones for each realization. The probability of no drip shield damage from rockfall follows a simple power law. The non-zero damage to the drip shield from rockfall is represented as a log-triangular distribution, with minimum 0.001 percent and maximum 100 percent; the value of the mode follows a simple power law in PGV. The fraction of failed surface area is applied to all drip shields in the nonlithophysal zones of the repository (i.e., there is no spatial variability within the nonlithophysal zones).

- The log-triangular distribution is denoted by DS_DAMAGE_LOGTRI in Table 30.
- The upper bound of the log-triangular distribution, is 100 percent. The lower bound of the log-triangular distribution is 0.001 percent. The mode of the log-triangular distribution is denoted by DS_MODE and is given by:

$$DS_MODE = 0.00204 \times (PGV)^{3.7767} \quad (\text{Eq. 14})$$

- The probability of zero damage is represented by DS_NODAMAGE and is given by:

$$DS_NODAMAGE = \text{MIN}(1.0, 0.601 \times (PGV)^{-0.735}) \quad (\text{Eq. 15})$$

- The sampling algorithm draws a random number between 0 and 1, denoted by RANDOM in Table 30. If the random number is less than DS_NODAMAGE then there is no damage from rockfall for this realization (DS_DAMAGE%_RF = 0). If the random number is greater than or equal to DS_NODAMAGE, then the log-triangular distribution is sampled to determine the damage to the drip shield from rockfall for this realization. That is, DS_DAMAGE%_RF = DS_DAMAGE_LOGTRI, as shown in Table 30.
- The fraction of failed surface area is denoted as DS_DAMAGE_RF and calculated as:

$$DS_DAMAGE_RF = (DS_DAMAGE\%_RF)/100 \quad (\text{Eq. 16})$$

6. Determine the total fraction of drip shield damage due to vibratory ground motion and rockfall in each waste package group.

- In the nonlithophysal zone, the fraction of total damage is given by the sum of DS_DAMAGE_GM and DS_DAMAGE_RF, with an upper limit of 1.0:

$$DS_DAMAGE_TOTAL_NONLITH = \text{MIN}(1.0, DS_DAMAGE_GM + DS_DAMAGE_RF). \quad (\text{Eq. 17})$$

The fraction of total damage in the nonlithophysal zone is applied to all drip shields in this zone (i.e., there is no spatial variability within the nonlithophysal zone).

- In the lithophysal zone, the fraction of total damage is given by DS_DAMAGE_GM:

$$DS_DAMAGE_TOTAL_LITH = DS_DAMAGE_GM \quad (\text{Eq. 18})$$

The lithophysal zone does not include the contribution from rockfall because the lithophysal is expected to shatter into small fragments that cannot produce significant damage to the drip shield. The fraction of total damage in the lithophysal zone is applied to all drip shields in the lithophysal zone (i.e., there is no spatial variability within the lithophysal zone).

- Waste package groups for TSPA-LA may include packages in both the lithophysal and nonlithophysal zones. If this is the case, an appropriately weighted average should be used to determine the damage to all packages in each group. The calculation of this weighted average is not shown in Table 30.
- The total failed area on the drip shield allows advective flow, per Assumption 5.3.

7. Cladding does not fail if the mean annual exceedance frequency of the seismic hazard is 5×10^{-5} per year or greater (see Assumption 5.1). Cladding experiences complete failure (i.e., 100 percent of the cladding is perforated) at the time of the seismic event if the annual exceedance frequency is less than or equal to 10^{-5} per year. The abstraction for cladding failure is defined in Table 18 with a linear interpolation for the percent damage to the cladding between the appropriate values of PGV. In other words, cladding damage is (1) always zero for PGV values less than 0.55 m/s (corresponding to annual exceedance frequencies greater than 5×10^{-5} per year), (2) always 100 percent for PGV values greater than 1.067 m/s (corresponding to annual exceedance frequencies less than 10^{-5} per year), and (3) based on a linear interpolation on PGV for values between 0.55 m/s, with 0 percent damage, and 1.067 m/s, with 100 percent damage.

This parameter is denoted by CLAD_DAMAGE in Table 30. There is no uncertainty in this damage abstraction because it is a bounding estimate for cladding failure. The percent of failed cladding is applied to all fuel assemblies in the repository (i.e., there is no spatial variability).

8. Determine the percent failed area on the waste package due to fault displacement. The expected number of waste packages that fail, as a function of annual exceedance probability, is defined in Table 29.
 - The expected number of waste packages that fail from fault displacement is a very small fraction of the total packages in the repository because very few waste packages are located on secondary faults. In addition, these failures only occur for a small fraction of the realizations in the seismic scenario class because there are no failures from fault displacement for an annual frequency of occurrence greater than 2×10^{-7} per year. In this situation, a special waste package group, such as the juvenile failure group, should be used to represent the failures from fault displacement.
 - When a waste package fails by fault displacement, the failed area on each waste package is determined by sampling a uniform distribution with a lower bound of 0 m^2 and an upper bound equal to the area of the waste package lid. These sampled distributions are denoted by FAILED_AREA_PWR, FAILED_AREA_BWR, FAILED_AREA_NAVAL, and FAILED_AREA_HLW in Table 30.
 - The area of the lid for the PWR, BWR, Naval, and HLW groups is 2.123 m^2 , 2.201 m^2 , 2.983 m^2 , and 3.497 m^2 , respectively, based on the maximum waste package diameter in Table 25. These areas are denoted as LID_AREA_PWR, LID_AREA_BWR, LID_AREA_NAVAL, and LID_AREA_HLW in Table 30.
 - The surface area of a package in the PWR, BWR, Naval, and HLW groups is 31.01 m^2 , 31.55 m^2 , 41.24 m^2 , and 37.95 m^2 , respectively. The values of the surface areas are based on the average waste package lengths and maximum waste package diameters for each of the four groups, as listed in Table 25. These areas are denoted as SURF_AREA_PWR, SURF_AREA_BWR, SURF_AREA_NAVAL, and SURF_AREA_HLW in Table 30.

- The fraction of failed area for the PWR waste package type is calculated as:

$$\text{FRACTION_FAILED_PWR} = \text{LID_AREA_PWR}/\text{SURF_AREA_PWR} \quad (\text{Eq. 19})$$

with similar equations for the BWR, Naval, and HLW waste package types. This failed area allows advective flow and advective and diffusive transport, per Assumption 5.3.

- The expected number of package failures for the three waste package types are denoted by NO_PWR_FAILURES, NO_BWR_FAILURES, NO_NAVAL_FAILURES, and NO_HLW_FAILURES in Table 30.
 - The damage to drip shields from a fault displacement with annual exceedance probability less than 2×10^{-7} per year is taken to be 100 percent. The number of impacted drip shields is identical to the total number of waste packages that will be damaged by the fault displacement.
 - Cladding that is impacted by a fault displacement with annual exceedance probability less than 2×10^{-7} will be 100 percent perforated. The impacted cladding is associated with the fuel assemblies in the number of waste packages that are damaged by the fault displacement.
9. Determine the time of the seismic event for each realization.

The time of the event, EVENT_TIME, is determined by sampling a log-uniform distribution with a lower bound denoted by TIME_MIN and an upper bound denoted by TIME_MAX in Table 30. A typical value of TIME_MAX is 10,000 or 20,000 years. Appropriate values for TIME_MIN will be determined through sensitivity studies with the TSPA-LA model.

10. Calculate the mean dose for all realizations, $i = 1, 2, \dots, R$.

The weighting factor for each realization corrects for the expected number of seismic events in each realization and for the log-uniform sampling for the exceedance frequency, λ_i . The appropriate formula for calculating the mean or expected dose with uniform sampling for the event time and log-uniform sampling for the annual exceedance frequency, λ_i , is:

$$\begin{aligned} \bar{D}(t) &= \frac{1}{R} \ln\left(\frac{\lambda_{max}}{\lambda_{min}}\right) \ln\left(\frac{T_{max}}{T_{min}}\right) \sum_{i=1}^R t_i \lambda_i D_i\{t | t_i, PGV_i\}, \\ &= \frac{1}{R} \sum_1^R \text{WEIGHTED_DOSE}_i \\ &= \text{Mean}(\text{WEIGHTED_DOSE}_i) \end{aligned}$$

where $\bar{D}(t)$ is the expected (mean) dose, $D_i\{t | t_i, PGV_i\}$ is the dose from the i^{th} realization with a seismic hazard of amplitude PGV_i occurring at time t_i , and R is the total number of

realizations. The term $t_i\lambda_i$ is denoted by EVENT_WEIGHT in Table 30. The term $\ln\left(\frac{T_{max}}{T_{min}}\right)\ln\left(\frac{\lambda_{max}}{\lambda_{min}}\right)$ is represented as the parameter SAMPLE_WEIGHT in Table 30. The term WEIGHTED_DOSE is the product of EVENT_WEIGHT, SAMPLE_WEIGHT, and the DOSE at any given time.

11. Modify the seepage in the lithophysal zones after the seismic event.

The seepage into the emplacement drifts in the lithophysal zones is determined by the seepage table for degraded drifts provided in DTN: LB0307SEEPDRCL.002. This table is invoked after a seismic hazard occurs, provided the hazard is large enough to collapse the drifts. If a more realistic model for seepage after drift collapse becomes available through *Abstraction of Drift Seepage* (BSC 2003q) or through related work, then this new information should be incorporated into TSPA-LA.

For TSPA-LA, all ground motions with mean annual exceedance frequency of 10^{-4} per year or less (equivalent to a PGV greater than 0.388 m/s) are large enough to collapse the drifts in the lithophysal zones. There is no change in the seepage flux into nonlithophysal zones because complete collapse of the drifts is not predicted for this type of host rock.

12. Modify the flux into the waste package after the seismic event if accelerated localized corrosion can occur.

The flux splitting algorithm for the waste package and drip shield is identical to that for the nominal scenario, with one exception. If the seismic hazard occurs at a time when the conditions for the existence of accelerated localized corrosion of Alloy 22 are satisfied, then all seepage that passes through the drip shield flows into the waste package without any flux splitting.

Table 30. Definition of Parameters for the Seismic Scenario Class

Parameter Name	Description, Units, and Type	Definition																				
EVENT_TIME	Distribution for the time when the seismic event occurs in this realization Units: {yr} Type: Distribution sampled once per realization	Log-Uniform Distribution: Minimum Value: TIME_MIN Maximum Value: TIME_MAX																				
TIME_MAX	Duration of the seismic scenario class Units: {yr} Type: Data	Typical values are 10,000 years or 20,000 years.																				
TIME_MIN	Minimum value of the log-uniform distribution for event time Units: {yr} Type: Data	The appropriate value for TIME_MIN will be determined by sensitivity studies with the TSPA-LA model.																				
LAMBDA	Distribution of annual exceedance frequency for the seismic scenario class Units: {1/yr} Type: Distribution sampled once per realization	Log-Uniform Distribution: Minimum Value: LAMBDA_MIN Maximum Value: LAMBDA_MAX																				
LAMBDA_MIN	Minimum annual exceedance frequency Units: {1/yr} Type: Data	1×10^{-8} per year																				
LAMBDA_MAX	Maximum annual exceedance frequency Units: {1/yr} Type: Data	1×10^{-4} per year																				
PGV	Hazard curve for horizontal PGV as a function of LAMBDA Units: {m/s} Type: 1D table, function of LAMBDA	1D table lookup as a function of the value of LAMBDA for this realization. Use log-linear interpolation between λ values: <table border="1"> <thead> <tr> <th>λ (1/yr)</th> <th>PGV (m/s)</th> </tr> </thead> <tbody> <tr> <td>6.26×10^{-4}</td> <td>0.159</td> </tr> <tr> <td>2.78×10^{-4}</td> <td>0.239</td> </tr> <tr> <td>9.30×10^{-5}</td> <td>0.398</td> </tr> <tr> <td>1.84×10^{-5}</td> <td>0.796</td> </tr> <tr> <td>3.07×10^{-6}</td> <td>1.59</td> </tr> <tr> <td>2.28×10^{-7}</td> <td>3.98</td> </tr> <tr> <td>8.15×10^{-8}</td> <td>5.57</td> </tr> <tr> <td>2.60×10^{-8}</td> <td>7.96</td> </tr> <tr> <td>6.56×10^{-9}</td> <td>11.9</td> </tr> </tbody> </table>	λ (1/yr)	PGV (m/s)	6.26×10^{-4}	0.159	2.78×10^{-4}	0.239	9.30×10^{-5}	0.398	1.84×10^{-5}	0.796	3.07×10^{-6}	1.59	2.28×10^{-7}	3.98	8.15×10^{-8}	5.57	2.60×10^{-8}	7.96	6.56×10^{-9}	11.9
λ (1/yr)	PGV (m/s)																					
6.26×10^{-4}	0.159																					
2.78×10^{-4}	0.239																					
9.30×10^{-5}	0.398																					
1.84×10^{-5}	0.796																					
3.07×10^{-6}	1.59																					
2.28×10^{-7}	3.98																					
8.15×10^{-8}	5.57																					
2.60×10^{-8}	7.96																					
6.56×10^{-9}	11.9																					
WP_DAMAGE	Fraction of failed surface area on the waste package Units: {-} Type: Function	WP_DAMAGE%/100																				
WP_DAMAGE%	Distribution of percent failed area on the waste package Units: {%} Type: Distribution sampled once per realization	Uniform Distribution: Minimum Value: WP_DAMAGE_MIN Maximum Value: WP_DAMAGE_MAX																				

Table 30. Definition of Parameters for the Seismic Scenario Class (Continued)

Parameter Name	Description, Units, and Type	Definition												
WP_DAMAGE_MAX	Maximum value of percent failed area on the waste package for this realization Units: {%} Type: Function of PGV	$MAX(0.0, 0.436*(PGV) - 0.305)$												
WP_DAMAGE_MIN	Minimum value of percent failed area on the waste package for this realization. Units: {%} Type: Constant	0%												
DS_DAMAGE_GM	Fraction of failed surface area on the drip shield from ground motion Units: {-} Type: Function	$DS_DAMAGE\%_GM/100$												
DS_DAMAGE%_GM	Distribution of percent failed area on the drip shield from vibratory ground motion Units: {%} Type: Distribution sampled once per realization	Uniform Distribution: Minimum Value: DS_DAMAGE_MIN Maximum Value: DS_DAMAGE_MAX												
DS_DAMAGE_MAX	Maximum value of percent failed area on the drip shield from ground motion for this realization Units: {%} Type: Table Look-up as function of PGV with linear interpolation between points	1D table lookup as a function of the value of PGV for this realization. <table border="1"> <thead> <tr> <th>PGV (m/s)</th> <th>Damage (%)</th> </tr> </thead> <tbody> <tr> <td>0</td> <td>0</td> </tr> <tr> <td>0.55</td> <td>0</td> </tr> <tr> <td>2.44</td> <td>2.68</td> </tr> <tr> <td>5.35</td> <td>50</td> </tr> <tr> <td>20</td> <td>50</td> </tr> </tbody> </table>	PGV (m/s)	Damage (%)	0	0	0.55	0	2.44	2.68	5.35	50	20	50
PGV (m/s)	Damage (%)													
0	0													
0.55	0													
2.44	2.68													
5.35	50													
20	50													
DS_DAMAGE_MIN	Minimum value of percent failed area on the drip shield from ground motion for this realization. Units: {%} Type: Table Look-up as a function of PGV, with linear interpolation between points & linear extrapolation for PGV > 5.35 m/s.	1D table lookup as a function of the value of PGV for this realization. <table border="1"> <thead> <tr> <th>PGV (m/s)</th> <th>Damage (%)</th> </tr> </thead> <tbody> <tr> <td>0</td> <td>0</td> </tr> <tr> <td>2.44</td> <td>0</td> </tr> <tr> <td>5.35</td> <td>10%</td> </tr> </tbody> </table>	PGV (m/s)	Damage (%)	0	0	2.44	0	5.35	10%				
PGV (m/s)	Damage (%)													
0	0													
2.44	0													
5.35	10%													
DS_NODAMAGE	Probability of no damage to the drip shield from rockfall in the nonlithophysal zones of the repository. Units: {-} Type: Function of PGV	$MIN(1.0, 0.601(PGV)^{-0.735})$												
RANDOM	Random number between 0 and 1 for determining if rockfall damages the drip shield. Units: {-} Type: Distribution sampled once per realization	Uniform distribution: Minimum Value: 0 Maximum Value: 1												

Table 30. Definition of Parameters for the Seismic Scenario Class (Continued)

Parameter Name	Description, Units, and Type	Definition										
DS_DAMAGE_LOGTRI	Log-triangular distribution defining the percent failed area on the drip shield due to rockfall in the nonlithophysal zone. This distribution is used for the non-zero damage cases. Units: {%} Type: Distribution sampled once per realization	Log-triangular distribution in PGV Minimum Value: 0.001% Maximum Value: 100% Mode: DS_MODE (function of PGV)										
DS_MODE	Mode of the percent failed area of the drip shield due to rockfall in the nonlithophysal zones. Units: {%} Type: Function of PGV	$(0.00204)(PGV)^{3.7767}$										
DS_DAMAGE%_RF	Percent failed area on the drip shield from rockfall in the nonlithophysal zones Units: {%} Type: If-Then-Else Logical Operator	If(RANDOM<DS_NODAMAGE) Then DS_DAMAGE%_RF = 0, Else DS_DAMAGE%_RF = DS_DAMAGE_LOGTRI										
DS_DAMAGE_RF	Fraction of failed surface area on the drip shield from rockfall in the nonlithophysal zones Units: {-} Type: Function	DS_DAMAGE%_RF/100										
DS_DAMAGE_TOTAL_NONLITH	Total fraction of failed surface area on the drip shield in the nonlithophysal zones Units: {-} Type: Function	MIN(1.0, DS_DAMAGE_RF + DS_DAMAGE_GM)										
DS_DAMAGE_TOTAL_LITH	Total fraction of failed surface area on the drip shield in the lithophysal zones Units: {-} Type: Function	DS_DAMAGE_GM										
CLAD_DAMAGE	Percent perforated cladding from vibratory ground motion Units: {%} Type: Table look-up as function of PGV	1D table lookup as a function of the value of PGV for this realization. <table border="1"> <thead> <tr> <th>PGV {m/s}</th> <th>Damage {%}</th> </tr> </thead> <tbody> <tr> <td>0</td> <td>0</td> </tr> <tr> <td>0.55</td> <td>0</td> </tr> <tr> <td>1.067</td> <td>100</td> </tr> <tr> <td>20</td> <td>100</td> </tr> </tbody> </table>	PGV {m/s}	Damage {%}	0	0	0.55	0	1.067	100	20	100
PGV {m/s}	Damage {%}											
0	0											
0.55	0											
1.067	100											
20	100											
LID_AREA_PWR	Lid area of the PWR waste package group for fault displacement Units: {m ² } Type: Data	2.123 m ²										
LID_AREA_BWR	Lid area of the BWR waste package group for fault displacement Units: {m ² } Type: Data	2.201 m ²										

Table 30. Definition of Parameters for the Seismic Scenario Class (Continued)

Parameter Name	Description, Units, and Type	Definition
LID_AREA_NAVAL	Lid area of the Naval waste package group for fault displacement Units: {m ² } Type: Data	2.983 m ²
LID_AREA_HLW	Lid area of the HLW waste package group for fault displacement Units: {m ² } Type: Data	3.497 m ²
FAILED_AREA_PWR	Distribution of failed area on the PWR waste package group for fault displacement Units: {m ² } Type: Distribution sampled once per realization	Uniform Distribution: Minimum Value: 0.0 Maximum Value: LID_AREA_PWR
FAILED_AREA_BWR	Distribution of failed area on the BWR waste package group for fault displacement Units: {m ² } Type: Distribution sampled once per realization	Uniform Distribution: Minimum Value: 0.0 Maximum Value: LID_AREA_BWR
FAILED_AREA_NAVAL	Distribution of failed area on the Naval waste package group for fault displacement Units: {m ² } Type: Distribution sampled once per realization	Uniform Distribution: Minimum Value: 0.0 Maximum Value: LID_AREA_NAVAL
FAILED_AREA_HLW	Distribution of failed area on the HLW waste package group for fault displacement Units: {m ² } Type: Distribution sampled once per realization	Uniform Distribution: Minimum Value: 0.0 Maximum Value: LID_AREA_HLW
SURF_AREA_PWR	Surface area for a waste package in the PWR group for fault displacement Units: {m ² } Type: Data	31.01 m ²
SURF_AREA_BWR	Surface area for a waste package in the BWR group for fault displacement Units: {m ² } Type: Data	31.55 m ²
SURF_AREA_NAVAL	Surface area for a waste package in the Naval group for fault displacement Units: {m ² } Type: Data	41.24 m ²
SURF_AREA_HLW	Surface area for a waste package in the HLW group for fault displacement Units: {m ² } Type: Data	37.95 m ²

Table 30. Definition of Parameters for the Seismic Scenario Class (Continued)

Parameter Name	Description, Units, and Type	Definition																		
FRACTION_FAILED_A REA_PWR	Fraction of failed surface area on PWR waste package group from fault displacement Units: {-} Type: Function	FAILED_AREA_PWR/SURF_AREA_PWR																		
FRACTION_FAILED_A REA_BWR	Fraction of failed surface area on BWR waste package group from fault displacement Units: {-} Type: Function	FAILED_AREA_BWR/SURF_AREA_BWR																		
FRACTION_FAILED_A REA_NAVAL	Fraction of failed surface area on Naval waste package group from fault displacement Units: {-} Type: Function	FAILED_AREA_NAVAL/SURF_AREA_NAVAL																		
FRACTION_FAILED_A REA_HLW	Fraction of failed surface area on HLW waste package group from fault displacement Units: {-} Type: Function	FAILED_AREA_HLW/SURF_AREA_HLW																		
NO_PWR_FAILURES	Number of failed PWR waste packages from fault displacement Units: {-} Type: Step function of annual exceedance frequency, λ	1D table lookup as a function of the value of λ for this realization. <table border="1"> <thead> <tr> <th>λ (1/yr)</th> <th># Failures (-)</th> </tr> </thead> <tbody> <tr> <td>$> 2 \times 10^{-7}$</td> <td>0</td> </tr> <tr> <td>1×10^{-7} to 2×10^{-7}</td> <td>0</td> </tr> <tr> <td>6×10^{-8} to 1×10^{-7}</td> <td>0</td> </tr> <tr> <td>5×10^{-8} to 6×10^{-8}</td> <td>6.71</td> </tr> <tr> <td>4×10^{-8} to 5×10^{-8}</td> <td>6.71</td> </tr> <tr> <td>3×10^{-8} to 4×10^{-8}</td> <td>6.71</td> </tr> <tr> <td>2×10^{-8} to 3×10^{-8}</td> <td>7.97</td> </tr> <tr> <td>1×10^{-8} to 2×10^{-8}</td> <td>7.97</td> </tr> </tbody> </table>	λ (1/yr)	# Failures (-)	$> 2 \times 10^{-7}$	0	1×10^{-7} to 2×10^{-7}	0	6×10^{-8} to 1×10^{-7}	0	5×10^{-8} to 6×10^{-8}	6.71	4×10^{-8} to 5×10^{-8}	6.71	3×10^{-8} to 4×10^{-8}	6.71	2×10^{-8} to 3×10^{-8}	7.97	1×10^{-8} to 2×10^{-8}	7.97
λ (1/yr)	# Failures (-)																			
$> 2 \times 10^{-7}$	0																			
1×10^{-7} to 2×10^{-7}	0																			
6×10^{-8} to 1×10^{-7}	0																			
5×10^{-8} to 6×10^{-8}	6.71																			
4×10^{-8} to 5×10^{-8}	6.71																			
3×10^{-8} to 4×10^{-8}	6.71																			
2×10^{-8} to 3×10^{-8}	7.97																			
1×10^{-8} to 2×10^{-8}	7.97																			
NO_BWR_FAILURES	Number of failed BWR waste packages from fault displacement Units: {-} Type: Step function of annual exceedance frequency, λ	1D table lookup as a function of the value of λ for this realization. <table border="1"> <thead> <tr> <th>λ (1/yr)</th> <th># Failures (-)</th> </tr> </thead> <tbody> <tr> <td>$> 2 \times 10^{-7}$</td> <td>0</td> </tr> <tr> <td>1×10^{-7} to 2×10^{-7}</td> <td>0</td> </tr> <tr> <td>6×10^{-8} to 1×10^{-7}</td> <td>0</td> </tr> <tr> <td>5×10^{-8} to 6×10^{-8}</td> <td>4.28</td> </tr> <tr> <td>4×10^{-8} to 5×10^{-8}</td> <td>4.28</td> </tr> <tr> <td>3×10^{-8} to 4×10^{-8}</td> <td>4.28</td> </tr> <tr> <td>2×10^{-8} to 3×10^{-8}</td> <td>5.08</td> </tr> <tr> <td>1×10^{-8} to 2×10^{-8}</td> <td>5.08</td> </tr> </tbody> </table>	λ (1/yr)	# Failures (-)	$> 2 \times 10^{-7}$	0	1×10^{-7} to 2×10^{-7}	0	6×10^{-8} to 1×10^{-7}	0	5×10^{-8} to 6×10^{-8}	4.28	4×10^{-8} to 5×10^{-8}	4.28	3×10^{-8} to 4×10^{-8}	4.28	2×10^{-8} to 3×10^{-8}	5.08	1×10^{-8} to 2×10^{-8}	5.08
λ (1/yr)	# Failures (-)																			
$> 2 \times 10^{-7}$	0																			
1×10^{-7} to 2×10^{-7}	0																			
6×10^{-8} to 1×10^{-7}	0																			
5×10^{-8} to 6×10^{-8}	4.28																			
4×10^{-8} to 5×10^{-8}	4.28																			
3×10^{-8} to 4×10^{-8}	4.28																			
2×10^{-8} to 3×10^{-8}	5.08																			
1×10^{-8} to 2×10^{-8}	5.08																			

Table 30. Definition of Parameters for the Seismic Scenario Class (Continued)

Parameter Name	Description, Units, and Type	Definition																		
NO_NAVAL_FAILURES	Number of failed Naval waste packages from fault displacement Units: {-} Type: Step function of annual exceedance frequency, λ	1D table lookup as a function of the value of λ for this realization. <table border="1"> <thead> <tr> <th>λ (1/yr)</th> <th># Failures (-)</th> </tr> </thead> <tbody> <tr> <td>$> 2 \times 10^{-7}$</td> <td>0</td> </tr> <tr> <td>1×10^{-7} to 2×10^{-7}</td> <td>0</td> </tr> <tr> <td>6×10^{-8} to 1×10^{-7}</td> <td>0.49</td> </tr> <tr> <td>5×10^{-8} to 6×10^{-8}</td> <td>0.49</td> </tr> <tr> <td>4×10^{-8} to 5×10^{-8}</td> <td>0.49</td> </tr> <tr> <td>3×10^{-8} to 4×10^{-8}</td> <td>0.58</td> </tr> <tr> <td>2×10^{-8} to 3×10^{-8}</td> <td>0.58</td> </tr> <tr> <td>1×10^{-8} to 2×10^{-8}</td> <td>0.58</td> </tr> </tbody> </table>	λ (1/yr)	# Failures (-)	$> 2 \times 10^{-7}$	0	1×10^{-7} to 2×10^{-7}	0	6×10^{-8} to 1×10^{-7}	0.49	5×10^{-8} to 6×10^{-8}	0.49	4×10^{-8} to 5×10^{-8}	0.49	3×10^{-8} to 4×10^{-8}	0.58	2×10^{-8} to 3×10^{-8}	0.58	1×10^{-8} to 2×10^{-8}	0.58
λ (1/yr)	# Failures (-)																			
$> 2 \times 10^{-7}$	0																			
1×10^{-7} to 2×10^{-7}	0																			
6×10^{-8} to 1×10^{-7}	0.49																			
5×10^{-8} to 6×10^{-8}	0.49																			
4×10^{-8} to 5×10^{-8}	0.49																			
3×10^{-8} to 4×10^{-8}	0.58																			
2×10^{-8} to 3×10^{-8}	0.58																			
1×10^{-8} to 2×10^{-8}	0.58																			
NO_HLW_FAILURES	Number of failed HLW packages from fault displacement Units: {-} Type: Step function of annual exceedance frequency, λ	1D table lookup as a function of the value of λ for this realization. <table border="1"> <thead> <tr> <th>λ (1/yr)</th> <th># Failures (-)</th> </tr> </thead> <tbody> <tr> <td>$> 2 \times 10^{-7}$</td> <td>0</td> </tr> <tr> <td>1×10^{-7} to 2×10^{-7}</td> <td>4.53</td> </tr> <tr> <td>6×10^{-8} to 1×10^{-7}</td> <td>4.53</td> </tr> <tr> <td>5×10^{-8} to 6×10^{-8}</td> <td>4.53</td> </tr> <tr> <td>4×10^{-8} to 5×10^{-8}</td> <td>5.37</td> </tr> <tr> <td>3×10^{-8} to 4×10^{-8}</td> <td>5.37</td> </tr> <tr> <td>2×10^{-8} to 3×10^{-8}</td> <td>5.37</td> </tr> <tr> <td>1×10^{-8} to 2×10^{-8}</td> <td>38.56</td> </tr> </tbody> </table>	λ (1/yr)	# Failures (-)	$> 2 \times 10^{-7}$	0	1×10^{-7} to 2×10^{-7}	4.53	6×10^{-8} to 1×10^{-7}	4.53	5×10^{-8} to 6×10^{-8}	4.53	4×10^{-8} to 5×10^{-8}	5.37	3×10^{-8} to 4×10^{-8}	5.37	2×10^{-8} to 3×10^{-8}	5.37	1×10^{-8} to 2×10^{-8}	38.56
λ (1/yr)	# Failures (-)																			
$> 2 \times 10^{-7}$	0																			
1×10^{-7} to 2×10^{-7}	4.53																			
6×10^{-8} to 1×10^{-7}	4.53																			
5×10^{-8} to 6×10^{-8}	4.53																			
4×10^{-8} to 5×10^{-8}	5.37																			
3×10^{-8} to 4×10^{-8}	5.37																			
2×10^{-8} to 3×10^{-8}	5.37																			
1×10^{-8} to 2×10^{-8}	38.56																			
EVENT_WEIGHT	Expected number of events in this realization Units: {-} Type: Function	LAMBDA \times EVENT_TIME																		
SAMPLE_WEIGHT	Correction for sampling of log-uniform distributions for time of the event and for annual exceedance frequency Units: {-} Type: Function	LN(TIME_MAX/TIME_MIN) \times LN(LAMBDA_MAX/LAMBDA_MIN)																		
WEIGHTED_DOSE	The probability-weighted dose for this realization Units: {mrem/yr} Type: Function	EVENT_WEIGHT \times SAMPLE_WEIGHT \times DOSE, where DOSE is the time dependent (unweighted) dose for this realization.																		

6.10.3 Limitations

There are five important limitations for the seismic scenario class for TSPA-LA: the duration of the calculations, the possibility of rockfall in the drifts before the seismic event, and coupling of seepage and thermal conditions with rockfall, the range of validity of the model abstraction for waste package damage, and the potential for rockfall to damage the waste package.

The seismic scenario class for TSPA-LA is designed for a duration of 20,000 years, twice the length of the established regulatory period of interest. This design limitation arises from two factors. The first factor relates to the parameters for the structural response calculations, namely structural thicknesses and mechanical properties for the drip shield and waste package. The thicknesses of the drip shield and waste package have been reduced to (conservatively) represent the potential degradation of these structures by general corrosion over the first 10,000 years to

20,000 years after repository closure. The mechanical properties of Alloy 22 and of Titanium Grade 7 have been evaluated at an elevated temperature that provides conservative values for over 97 percent of the 10,000-year regulatory period for the high temperature operating model and for 100 percent of the time for the low temperature operating mode. This approach is highly conservative from a risk assessment viewpoint because it is conservative for almost all the realizations in the TSPA-LA. The definition of structural thickness and material properties should be reevaluated and new abstractions developed if the duration of the seismic scenario class is extended beyond 20,000 years.

The second factor for the design limitation related to the duration of the seismic scenario class is that coupled effects from multiple seismic events are not considered because seismic hazards with the potential to have a significant impact on engineered barriers are anticipated to occur very rarely during the 20,000-year period. This is a reasonable approach for events which occur with an annual frequency of 10^{-5} per year or less over a 10,000 year or 20,000 year period. This is also a reasonable approach for annual exceedance frequencies between 10^{-4} and 10^{-5} per year if the corresponding ground motions and fault displacements produce negligible damage to EBS components (as is true for these abstractions).

The second limitation is related to the condition of the drifts at the time of the seismic event. Structural response calculations for the drip shield and waste package do not include any initial backfill around the drip shield at the time of the seismic event. This representation is consistent with the present design that does not include engineered backfill but may become invalid if long-term fatigue of the tuff rock causes drift degradation and substantial collapse before the seismic hazard occurs.

If natural backfill is present, the kinematics of the waste package and drip shield will be altered, leading to changes in the impacts between and associated failed areas on both EBS components. For the waste package, there may be less damage from end-to-end impacts if the fixed drip shield restricts the motion of the waste package. However, damage may increase from side-on impacts in comparison to the no backfill case. The change in damage area for the drip shield may be substantial because the damage from impact of large blocks of rock ejected from the nonlithophysal zone will be mitigated.

The third limitation relates to the potential for a tunnel collapse caused by a seismic event to alter the temperature of the EBS components because of the presence of natural backfill. The presence of rubble about the drip shield after drift collapse could cause changes in the thermal environment in the EBS if a seismic event occurs relatively soon after repository closure, while the waste package and drip shield are at elevated temperatures. However, the irregular and coarse nature of the rubble is expected to allow sufficient convective heat transfer that the temperature histories calculated for the nominal scenario class may reasonably be used to approximate conditions following a seismic event during the thermal period. Because potential changes in temperature due to the presence of rubble are not expected to be significant, the possible associated changes in temperature-dependent solubility and corrosion rate have not been included in TSPA-LA.

The fourth limitation relates to the range of validity for the waste package damage abstraction. The abstraction for damage to the waste package from ground motions is based on data that

cover a range of PGV of 1 m/s to 6 m/s and have a maximum damage of less than 2 percent of the surface area of the waste package; there is no spatial variability in this damage abstraction. This is a reasonable approach if sensitivity studies for the TSPA-LA calculations indicate that the maximum risk occurs within this range of PGV values.

A fifth limitation relates to waste package damage from rockfall. Damage to the waste package from rockfall is not included in the abstraction for the waste package. This is a reasonable approach for intact EBS components because an intact drip shield can deflect large rock blocks away from the waste package. However, if separation of drip shields occurs for very high amplitude ground motions and if natural backfill is not present, the shields will no longer protect the waste packages from rockfall during a second seismic event. Multiple hazards occur with a very low probability, as noted previously, so this is a reasonable approach for TSPA-LA.

6.11 DISCUSSION OF YUCCA MOUNTAIN REVIEW PLAN ACCEPTANCE CRITERIA

The acceptance criteria that are relevant to requirement PRD-002/T-015 (Canori and Leitner 2003, Section 3.4) for the seismic abstractions are found in Section 2.2.1.3.2.3 of *Yucca Mountain Review Plan, Final Report* (NRC 2003). The manner in which the seismic consequence abstractions meet the five acceptance criteria are summarized in the following bulletized list. More detailed discussions of issues related to uncertainty in input parameters, to the propagation of uncertainty into TSPA, and to model uncertainty (alternate conceptual models) are provided in the following sections.

The features of the seismic consequence abstractions that meet these five general acceptance criteria are identified in the following list, along with the subcriteria that are relevant to each feature.

- Acceptance Criterion 1: System Description and Model Integration Are Adequate
 - The abstractions for damaged areas on the waste package, drip shield, and cladding are based on a statistically robust sampling of uncertain parameters, including the ground motion time histories, rock fracture patterns, and friction coefficients. The abstractions are based on calculations that use consistent assumptions and consistent material properties. (Subcriteria (1), (3), and (4))
 - All results are based on the mean hazard curves for ground motion and fault displacement. (Subcriteria (1), (3) and (4))
 - Degradation of the drip shield and waste package is addressed for the first 10,000 to 20,000 years after repository closure. (Subcriteria (1), (3), and (4))
 - Material properties for structural response calculations are based on a temperature of 150°C, resulting in conservative values for 97 percent of the first 10,000 years after closure for the high temperature operating mode. This choice is even more conservative over the first 20,000 years after repository closure. (Subcriteria (1), (3), and (4))

- Drip shield damage from rockfall induced by vibratory ground motion in the lithophysal and nonlithophysal zones is included in the abstractions. Rockfall is analyzed with state-of-the-art computer codes that are used for other drift degradation calculations. (Subcriterion (1) and (3))
- The seismic-related FEPs in Table 4 are directly considered in these abstractions. Damage to EBS components from ground motion, rockfall, drift collapse, and shear due to fault displacement have been considered in the abstractions for the seismic scenario class or in the structural response calculations that support the abstractions. (Subcriteria (1) and (5))
- The description of rockfall and structural response are based on state-of-the-art computer codes using nonlinear constitutive relations that describe material yield and failure. These computer codes are also used for the design of other repository structures and components. (Subcriterion (3))
- The residual stress threshold for failure of Alloy 22 is also used as the threshold for initiation of stress corrosion cracking in the representation of corrosion processes on the waste package. (Subcriterion (3))
- Acceptance Criterion 2: Data Are Sufficient For Model Justification
 - The residual stress failure criteria are based on experimental data for Alloy 22 and for Titanium Grade 7 (BSC 2003I, Section 6.2.1). (Subcriteria (1) and (3))
 - The constitutive models for Alloy 22 and for Titanium Grade 7 are based on material properties in the published literature. (Subcriteria (1), (3), and (4))
 - Hazard curves are based on the results of an expert elicitation (CRWMS M&O 1998; DTN: MO0004MWDRIFM3.002). (Subcriteria (1))
- Acceptance Criterion 3: Data Uncertainty Is Characterized And Propagated Through The Model Abstraction
 - Rockfall models and structural response calculations use parameter values and parameter ranges that are defensible and account for variabilities in rock properties and fracture patterns and uncertainties in ground motion time histories and friction coefficients. (Subcriteria (1), (2), and (3))
 - A major uncertainty in the response of the lithophysal zone is the rock compressive strength. This parameter is sampled from 5 levels for the rockfall calculations. (Subcriteria (1) and (3))
 - A major uncertainty in the response of the nonlithophysal zone is the fracture geometry and fracture properties. These uncertainties are represented by the use of numerous synthetic joint fracture patterns that are generated in a statistically sound manner and incorporated into the rockfall calculations for the nonlithophysal zones. (Subcriteria (2) and (3))

- Material properties for structural response calculations are based on a temperature of 150°C, which is conservative over 97 percent of the time for the first 10,000 years after closure. This choice is even more conservative for the first 20,000 years after repository closure. (Subcriteria (1) and (3))
 - Thicknesses of the waste package outer shell and drip shield plates have been reduced by 2-mm to conservatively account for general corrosion over the first 10,000 years to 20,000 years after closure. (Subcriterion (3))
 - Uncertainty and variability in damaged areas of the waste package and drip shield are represented in the abstractions as a sampled distribution. This uncertainty is directly incorporated into the abstractions for TSPA-LA.
- Acceptance Criterion 4: Model Uncertainty Is Characterized and Propagated Through The Model Abstraction
 - Grid convergence studies and alternate finite element representations have been evaluated for the rockfall models and for the structural response calculations. Calculations have been performed with the most appropriate numerical representations, so this particular source of model uncertainty is not propagated through the damage abstractions for TSPA-LA. (Subcriteria (2) and (3))
 - Alternative modeling approaches have been evaluated for the conceptual and computational models of lithophysal and nonlithophysal rock. (Subcriteria (2) and (3))
 - Alternate distributions have been considered in abstracting the damage results for the waste package and drip shield into model abstractions. (Subcriterion (3))
- Acceptance Criterion 5: Model Abstraction Output Is Supported By Objective Comparisons
 - Objective comparisons between the calculated damage to EBS components and the corresponding abstractions for TSPA-LA are described in Table 31. (Subcriteria (1), (2), and (3))

Table 31. Comparison of Seismic Abstractions with Objective Evidence for Review Criteria

Abstraction	Objective Comparison
Damage to Waste Package from Ground Motion	The abstraction for damage to the waste package is based on a uniform distribution. Figures 6 and 7 compare the upper bound of this uniform distribution with the calculated damage from ground motions with a PGV of 1.067 m/s, 2.44 m/s, and 5.35 m/s. The lower bound of this distribution is zero. Figures 6 and 7 demonstrate that the calculated damage to the waste package is bounded by the upper and lower bounds of this uniform distribution, providing objective evidence of its adequacy. An independent technical review has also been performed for this damage abstraction to provide increased confidence in the model abstraction.
Damage to Drip Shield from Rockfall	Figures 10 and 11 compare the calculated damage from rockfall induced by ground motions for PGVs of 2.44 and 5.35 m/s with the damage abstraction based on a log-triangular distribution. These figures demonstrate that the log-triangular distribution provides a reasonable fit to the calculated damage at these two PGV levels. Figure 12 compares the mode of this log-triangular distribution as a function of PGV, demonstrating that it is a reasonable fit to the value of the mode over a range of PGV from 0.55 m/s to 5.35 m/s. Collectively, these three figures provide objective evidence that the abstraction is an accurate representation of the computational results. An independent technical review has also been performed for this damage abstraction to provide increased confidence in the model abstraction.
Damage to Drip Shield from Ground Motion	The abstraction for damage to the drip shield from ground motion is based on a uniform distribution. The upper limit of this uniform distribution provides an upper bound for the calculated damage from ground motions with a PGV of 0.55 m/s, 2.44 m/s, and 5.35 m/s, providing objective evidence of its adequacy.
Damage to Cladding from Ground Motion	The abstraction for damage to the cladding assumes that 100 percent of the cladding perforates after a ground motion with PGV of 1.067 m/s or larger occurs. This scientific analysis is based on a conservative, bounding approach that can be verified through the checking process for model reports.
Damage to Waste Package and Drip Shield from Fault Displacement	The abstraction for damage to the waste package and drip shield from fault displacement is based on the hazard curves for displacement of secondary faults in the repository block and available clearances for EBS components. The analysis of fault displacement demonstrates that there is only damage from fault displacement with a 2×10^{-7} per year annual exceedance frequency, or less (see Table 29). In this situation, damage from fault displacement is a very low probability occurrence. In addition, a maximum of 53 packages is affected by fault displacement (see Table 29). In this situation, it is appropriate to verify this scientific analysis through the normal checking process for model reports.

6.11.1 Treatment of Parameter Uncertainty

Data uncertainty is explicitly included in the seismic abstractions for TSPA-LA. Uncertainty has been directly represented through the use of sampled input parameters for the structural response calculations for the drip shield and waste package under vibratory ground motions, and in the rockfall analyses. The uncertainty in these input parameters and its propagation into TSPA-LA is discussed in the next three sections, followed by a discussion of model uncertainty (i.e., alternate conceptual models).

6.11.1.1 Uncertainty in Input Parameters for Structural Response

The structural response calculations for the waste package response and drip shield under vibratory ground motions include three major sources of uncertainty: (1) the ground motion time histories, (2) the metal-to-metal friction coefficient, and (3) the metal-to-rock friction coefficient:

- Fifteen sets of three-component ground motion time histories are used to represent the uncertainty in the seismic hazard at a given annual exceedance frequency (i.e., 10^{-6} per year or 10^{-7} per year). Although these fifteen ground motions are scaled to have the same horizontal PGV, the PGA and the duration of the time histories span a wide range of response. For example, the PGA for the first horizontal ground motion component at the 10^{-6} per year hazard level ranges from about 1.5 g to 7 g.
- The metal-to-metal friction coefficient between the waste package and emplacement pallet varies from 0.2 to 0.8. The friction coefficient affects the onset of sliding and dissipation of energy for the EBS components as a function of the amplitude of the ground motion. However, the importance of friction is anticipated to diminish with increasing ground motion level because the EBS components begin to slide almost immediately for high amplitude ground motions.
- The metal-to-rock friction coefficient between the emplacement pallet and the invert or between the drip shield and the invert varies from 0.2 to 0.8. Again, the friction coefficient affects the onset of sliding and dissipation of energy for the unanchored EBS components as a function of the amplitude of the ground motion. However, the importance of friction is anticipated to diminish with increasing amplitude of the ground motions.

The selection of friction coefficients as major sources of uncertainty, in addition to the ground motions, is based on engineering judgment. Variability in ground motions is often the most significant uncertainty in structural response calculations for nuclear plant components. Variability of friction coefficients may be important if damage varies significantly with the relative motions or impacts between adjacent structures.

The variations of these uncertain input parameters are simultaneously included in the fifteen structural response calculations at each seismic hazard level. This is accomplished by a Monte Carlo procedure that ensures robust sampling of the uncertain parameters over their full ranges. The Monte Carlo procedure and the sampled values of the three uncertain input parameters are described and documented in *Sampling of Stochastic Input Parameters for Rockfall and Structural Response Calculations Under Vibratory Ground Motion* (BSC 2003r).

The results from the structural response calculations are postprocessed to determine the damaged areas on the drip shield or waste package. The seismic damage abstractions for the waste package and drip shield make use of a residual stress threshold as a failure criterion. If the residual stress from mechanical damage exceeds the stress threshold for the barrier, then the affected area(s) are considered to have failed as a barrier to flow and transport. The residual stress threshold for the waste package is based on a uniform distribution between 80 and 90 percent of the yield strength for Alloy 22 (see Section 6.2). Postprocessing of the output from waste package calculations has determined the damaged areas corresponding to both 80 and 90 percent of the yield strength of Alloy 22 (BSC 2003b, Tables 6.4.1-2 and 6.4.2-2). The residual stress threshold for titanium is (very) conservatively set to a constant value of 50 percent of the yield strength of Titanium Grade 7, so no uncertainty is propagated into TSPA-LA for damaged area on the drip shield from vibratory ground motion.

6.11.1.2 Uncertainty in Input Parameters for Rockfall Calculations

All rockfall calculations include the ground motion time histories as a major source of uncertainty. Fifteen ground motions again represent the uncertainty in the seismic hazard at each annual exceedance frequency. In the lithophysal units, the rock compressive strength is an uncertain input parameter that is represented as five discrete levels of rock strength, ranging from low (5 MPa) to high (30 MPa). In the nonlithophysal units, the synthetic fracture pattern is an uncertain input parameter. The synthetic fracture pattern is a representation of the fracture system geometry in three dimensions. Approximately 70 synthetic fracture patterns are used in the rockfall calculations for the nonlithophysal units. The variations in these uncertain parameters are simultaneously included in the rockfall analyses at each seismic hazard level (BSC 2003r).

The stochastic input parameters for the rockfall calculations are based on engineering judgment. For example, the rock compressive strength is a key parameter for tunnel failure in a continuum material, while the fracture geometry is a key parameter for identifying the size and location of rock blocks that can be ejected from the walls of a tunnel. Fracture properties can also be important in the nonlithophysal units, but are conservatively represented rather than being incorporated into the stochastic sampling scheme.

The results from the rockfall calculations are not direct inputs to TSPA-LA. Rockfall calculations for lithophysal units predict drift collapse at seismic hazard levels of 10^{-6} and 10^{-7} per year; however, the strong seismic waves are predicted to shatter the lithophysal rock into small fragments that cannot fail the drip shield or waste package as a flow barrier.

Rockfall calculations for the nonlithophysal units predict a wide range of block sizes and velocities that can be ejected from the tunnel walls and impact the drip shield. More specifically, each rockfall calculation for the nonlithophysal unit predicts a complex, time-dependent sequence of rock blocks that impact the drip shield at varying locations and velocities. These impacts can cause damage if the block has enough mass and kinetic energy.

Numerous rockfall calculations are performed for the nonlithophysal zone, so it is impractical from a computational viewpoint to perform a structural response calculation for each time-dependent sequence of rock blocks. Instead, structural response calculations are performed for a

single block impacting the drip shield over a range of block sizes/velocities and impact points. A range of six block kinetic energies and three impact points (crown, corner, and side) span the range of response observed for the 10^{-6} and 10^{-7} per year seismic hazards. The damaged areas for these 18 cases provide a basis for determining the total damage from a time-dependent sequence of rock blocks by interpolation and summation of damaged areas for the individual impacts.

This approach (interpolation and summation) preserves the variability in the damaged areas of the drip shield due to the uncertainties in the quantity and velocity of rock blocks striking the drip shield.

6.11.1.3 Propagation of Uncertainty into Abstractions for TSPA-LA

The calculations of damaged areas on the waste package and drip shield due to vibratory ground motions and rockfall induced by vibratory ground motions exhibit substantial variability induced by the uncertainties in seismic ground motions and other input parameters. This variability has been directly represented in TSPA-LA by defining stochastic parameters that are sampled during each realization of the seismic scenario class. For example:

- For a given value of PGV, damage to the waste package from vibratory ground motion is represented as a uniform distribution that is sampled for each realization of the seismic scenario class. The lower bound of this distribution is zero damage for all values of PGV. The upper bound of this distribution is a linear function of PGV. This function represents the maximum damage with a 95 percent confidence limit, based on the damage results for the 10^{-6} and 10^{-7} per year hazard levels. The upper range of this uniform distribution is illustrated in Figures 6, 7, and 8.
- The uncertainty in the residual stress threshold for Alloy 22 has not been propagated into the abstraction for TSPA-LA. The damage states for the waste package are based on an average of the damage areas using the 80 and 90 percent Alloy 22 failure criteria. This is an accurate representation for the mean damage area due to the variability in the uniformly distributed residual stress threshold. This approach is reasonable because the variability in damaged area due to the uncertainty in failure criterion is approximately a factor of 2, while the variability in damaged area due to the ground motions at a given value of PGV is more than an order of magnitude (see Tables 6 and 7). In this situation, it is reasonable to ignore the variability in damaged area due to failure criterion because the variability from ground motions is the dominant effect on uncertainty.
- For a given value of PGV, damage to the drip shield from vibratory ground motion is represented as a uniform distribution for annual exceedance frequencies less than 10^{-6} per year. This distribution is sampled for each realization of the seismic scenario class. The lower bound of this distribution is zero damage. The upper bound of this distribution is a linear function of PGV that rises from zero damage to 50 percent damage between 10^{-6} and 10^{-7} per year, and then remains constant at 50 percent below 10^{-7} per year.
- Damage to the drip shield from rock blocks in the nonlithophysal units depends on two distributions that are sampled in each realization. The first distribution determines the

probability of no damage at a given level of PGV (see Figure 13). If damage occurs, its value is determined by sampling a log-triangular distribution whose mode is a function of PGV (see Figure 12).

The abstraction for cladding does not propagate uncertainty into TSPA-LA because it is based on a simplified response that is bounded with two damage states: zero damage or 100 percent damage.

6.11.2 Treatment of Model Uncertainty (Alternate Conceptual Models)

The seismic consequence abstractions have considered alternate conceptual models, primarily through different representations of the mean damage and the distribution of damage about the mean.

In Section 6.3, the maximum damage to the waste package is represented as a linear function of PGV. This is equivalent to a linear function for the mean because damage is represented as a uniform distribution from zero to its maximum value. This linear function is consistent with Assumption 5.1 because it results in zero damage at the 2×10^{-5} per year hazard level or for greater values of the exceedance frequency. An alternate formulation is to represent the mean damage as a power law function of PGV. However, this alternate formulation has been eliminated because it results in substantially greater damage than calculated for the 10^{-5} per year ground motions, while the linear function is an excellent fit to the damage data at this ground motion level.

The distribution of damaged areas on the waste package has been analyzed for the 10^{-7} and 10^{-6} per year ground motion levels. At the 10^{-7} per year level, the damage values can be represented by either a normal distribution or a uniform distribution. At the 10^{-6} per year level, the damage becomes bimodal. These points can be represented with a normal distribution that is truncated at a small, nonzero damage value, or again with a uniform distribution. The uniform distribution is selected for the abstraction for several reasons. First, it is conservative relative to a normal distribution for high values of damage because it will be sampled uniformly across its range, rather than being skewed towards sampling around the mean. Second, the normal distribution at 10^{-6} produces negative damage values because its mean and standard deviation are approximately equal. Extrapolating this behavior to lower ground motions, say at the 10^{-5} per year level, is highly uncertain without additional calculations. Third, a uniform distribution is a reasonable representation for the computational results for damage.

The damage to the drip shield from rockfall is based on similar considerations. The damage to the drip shield at 10^{-6} per year and 10^{-7} per year ground motion levels (remember that the rockfall is induced by the ground motions) follows a bimodal pattern for the zero and non-zero damage points. The probability of zero damage is represented as a linear function of PGV. The non-zero damage to the drip shield is represented as a log-triangular distribution with a mode that is a linear function of PGV. A single distribution did not produce a reasonable match to all the damage values at the two ground motion levels. The log-triangular distribution provides a simple representation of the computational results for damage.

6.12 VERIFICATION OF SCIENTIFIC ANALYSES FOR CLADDING AND FOR FAULT DISPLACEMENT

The abstractions for cladding damage from vibratory ground motions and for the EBS damage from fault displacement are stochastic distributions whose parameters are a function of the amplitude or the exceedance frequency of the ground motion. These abstractions are considered scientific analyses because they are based on standard statistical techniques that bound the component response, rather than the results from detailed engineering calculations or other scientific analyses. Since these abstractions are not models, they are not validated per AP-SIII.10Q, *Models*. However, the abstractions still require verification, defined as providing objective evidence that the abstractions are an accurate representation of the variability and uncertainty in damage to the EBS components.

- **Damage to Cladding from Vibratory Ground Motion**

The abstraction for damage to the cladding assumes that 100 percent of the cladding perforates after a ground motion with PGV of 1.067 m/s or larger occurs. This is a conservative, bounding approach that does not require further verification.

- **Damage to EBS Components from Fault Displacement**

The abstraction for damage to the waste package and drip shield from fault displacement is based on the mean hazard curves for displacement of secondary faults in the repository block and on the available clearances between EBS components. The analysis of damage from fault displacement demonstrates that there is no damage from faulting until an annual exceedance frequency less than 2×10^{-7} per year is reached. In other words, only the largest fault displacements can damage the EBS components.

Once damage can occur, the failed area on the waste package is defined as a uniform distribution with a lower bound of 0 and an upper bound given by the lid area. The lower bound represents a situation with minor crimping of the waste package; the upper bound represents a situation in which the welds fail and the lid completely separates from the waste package. These damage states are intended to be bounding conditions because there is high uncertainty in the state of the drift, the invert, and the EBS components after a major fault displacement.

The failed area on the drip shield is assumed to be 100 percent for a fault displacement that damages the waste package. This total damage state is clearly a bounding condition because some fault displacements produce minimal crimping between the waste package and drip shield. Similarly, the cladding is assumed to be 100 percent perforated for a fault displacement that damages the waste package.

The damage abstraction for fault displacement has been compared to an alternate conceptual model proposed by (Waiting et al. 2003). There is reasonable agreement between the damage abstraction in this report and the alternate conceptual model, considering that the alternate model is based on historical data for fault displacement in the western United States and that the damage abstraction is based on hazard curves specific to

Yucca Mountain. For example, the number of fault intersections predicted by the damage abstraction is 168, versus 191 for the alternate conceptual model. Similarly, the probability weighted number of waste package failures is predicted to be 2.4×10^{-6} for the damage abstraction, within the range of 1.9×10^{-6} to 1.9×10^{-5} for the alternate conceptual model. This agreement provides added confidence in the damage abstraction for fault displacement.

7. VALIDATION

The abstractions for waste package response to vibratory ground motions and for drip shield response to vibratory ground motions and rockfall are stochastic distributions whose parameters (i.e., the upper and lower bounds for a uniform distribution or the mode and bounds of a log-triangular distribution) are a function of the amplitude of the ground motion. These distributions, also called damage abstractions, are based on information from detailed structural response calculations and from rockfall calculations. These distributions are model abstractions because they represent this detailed computational information in a simplified manner for TSPA-LA. The underlying information for the model abstractions are created by models that have been validated under SP-SIII.10Q and by engineering calculations with software qualified under AP-SI.1Q. The status of the engineering calculations for structural response, of the rockfall models and analyses, and of the failure criteria are discussed next, followed by a discussion of the validation of the individual model abstractions.

Structural calculations for the response of large engineered components (e.g., waste package, drip shield, or cladding) due to impact and vibration is a well-established technology. The deformation of these types of structures can be evaluated with standard, commercially available finite-element programs. As a result, there is high confidence in the results from the computational process because of the extensive testing of commercial software on a wide variety of problems, including impact calculations. In addition, each computational study is based on a mesh refinement analysis and other supporting calculations that provide additional confidence in the results. No changes to the finite-element software are needed for these calculations. These engineering codes have been qualified for their intended use under AP-SI.1Q and the engineering calculations are performed under AP-3.12Q.

The results from the engineering calculations are considered appropriate for their intended use for several reasons. First, the calculations are based on standard, commercially available software that has demonstrated the capability to accurately analyze impact processes. Second, the finite-element representation of EBS components is designed (via mesh refinement studies) to accurately represent the potential damage from the impact processes. And lastly, the ground motions for the calculations are based on state-of-the-art techniques for representing seismic phenomena.

The seismic failure criteria for Alloy 22 and Titanium Grade 7 have been selected in a conservative manner. The failure criteria are based on considerations of accelerated corrosion due to residual stress, rather than the ultimate tensile stress of Alloy 22 or Titanium Grade 7. In fact, none of the structures reached ultimate tensile failure in any of the structural calculations. The rationale for selection of the residual stress thresholds for failure is documented in

Section 6.3, based on information in *Stress Corrosion Cracking of the Drip Shield, the Waste Package Outer Barrier, and the Stainless Steel Structural Material* (BSC 2003i, Section 6.2.1). The conservative approach to defining the residual stress thresholds for failure provides ample safety margin, helping to enhance confidence in the seismic failure criteria. The failure criteria are considered appropriate for their intended use because they are a conservative interpretation of the experimental data for the corrosion of Alloy 22 and Titanium Grade 7 under conditions relevant to Yucca Mountain.

The rockfall calculations are also performed with commercially available software, although it is necessary to modify the software for computational efficiency, for the representation of fractures with short or intermittent trace lengths, and for constitutive models for tuff. Because of these modifications, the rock mechanics codes are qualified and the models validated for their intended application to lithophysal and nonlithophysal tuffs. This model validation is documented in Section 7 of *Drift Degradation Analysis* (BSC 2003h).

The model abstractions for waste package response to vibratory ground motions and for drip shield response to vibratory ground motions and rockfall are simple numerical fits to the percent failed surface area as a function of PGV. The fits involve selecting the most appropriate distribution to represent the variability of damage as a function of PGV. The appropriate distributions and functional fits have been developed and documented in Microsoft Excel spreadsheets. The numerical values in these spreadsheets have been verified during the checking process for this model report. These spreadsheets are found in Attachments II, IV, and V of this report, as well as electronically on a CD-ROM. Details of the validation process for the model abstractions are as follows:

- **Abstraction for Damage to the Waste Package from Ground Motion**

The abstraction for damage to the waste package is based on a uniform distribution. The selection of a uniform distribution is justified by the comparisons shown in Figures 4 and 5 of Section 6.5.1.3. Figure 6 (also in Section 6.5.1.3) compares the upper bound of this uniform distribution with the calculated damage from ground motions with PGVs of 1.067 m/s, 2.44 m/s, and 5.35 m/s. The lower bound of this distribution is zero. Figure 8 provides an alternate upper bound, based on a lognormal distribution. The discussion in Section 6.5.3 and Attachments II and III explains how the calculated damage to the waste package is bounded by the upper and lower limits of the uniform distribution, providing objective evidence of its adequacy.

The model abstraction for damage to the waste package from vibratory ground motion has been validated through an independent technical review. This review is documented in Attachment III. The recommendations of the review have been incorporated into the waste package abstraction, as discussed in Section 6.5.4.

- **Abstraction for Damage to the Drip Shield from Rockfall**

Figures 9 and 10 in Section 6.6.1.3 compare the calculated damage from rockfall for PGVs of 2.44 and 5.35 m/s with the damage abstraction based on a log-triangular distribution. These figures demonstrate that the log-triangular distribution provides a reasonable fit to

the calculated damage at these two PGV levels. Figure 12 in Section 6.6.1.4 compares the mode of this log-triangular distribution as a function of PGV, demonstrating that it is a reasonable fit to the value of the mode over a range of PGV from 0.55 m/s to 5.35 m/s. Collectively, these three figures provide objective evidence that the abstraction is an accurate representation of the underlying data.

The model abstraction for damage to the drip shield from rockfall has been validated through an independent technical review. This review is documented in Attachment V. The recommendations of the review confirmed the model abstraction, as discussed in Section 6.6.1.6.

- **Abstraction for Damage to the Drip Shield from Direct Ground Motion**

The abstraction for damage to the drip shield from ground motion is based on a uniform distribution. Section 6.6.3 defines the upper bound of this uniform distribution with the calculated damage from ground motions with a PGV of 0.55 m/s, 2.44 m/s, and 5.35 m/s. The lower bound of this distribution is zero. The calculated damage to the drip shield is bounded by the upper and lower bounds of this uniform distribution for a PGV value of 2.44 m/s. The 50 percent upper bound at a PGV of 5.35 is based on the maximum estimate, as explained in Section 6.6.3. In this situation, there is again objective evidence of the adequacy of the abstraction, based on the fact that the calculated damage is bounded by the upper and lower limits of the uniform distribution.

The technical approach for this model abstraction is identical to that for the other model abstractions for seismic damage. Namely, a simple distribution is fit to the available information for structural damage. However, this model abstraction is unique in the sense that damaged areas are only available for a PGV of 2.44 m/s. In particular, the damaged area at a PGV of 5.35 m/s is conservatively bounded by 50 percent, while the damaged area at a PGV of 0.55 m/s is set to 0, based on Assumption 5.1. The technical approach here is consistent with the methodology confirmed by the independent technical review for the other two model abstractions, although this model abstraction is essentially a bounding analysis for the low probability, high amplitude seismic events. In this situation, the model abstraction is considered validated because it is based on a methodology that is identical to that confirmed by the independent technical review and because it is a bounding representation of the damage for low probability seismic events.

8. CONCLUSIONS

The purpose of this work is to develop abstractions for the response of EBS components to seismic hazards at a geologic repository at Yucca Mountain, Nevada, and to define the methodology for using these abstractions in a seismic scenario class for the TSPA-LA. The seismic hazards are vibratory ground motion, fault displacement, and rockfall due to ground motion. The EBS components are the drip shield, the waste package, and the fuel cladding. The following abstractions for seismically induced damage have been developed:

- Damage to the waste package from vibratory ground motions
- Damage to the drip shield from vibratory ground motions
- Damage to the drip shield from rockfall induced by vibratory ground motions in the nonlithophysal zones
- Damage to the cladding from end-to-end impacts of adjacent waste packages
- Damage to the waste package, drip shield and cladding from fault displacement.

The recommended implementation of these abstractions and their associated input parameters for TSPA-LA is defined in Section 6.10.2 and Table 30. This computational algorithm can also be referenced through DTN: MO0308SPACALSS.002.

Damage to the drip shield from rockfall in the lithophysal zones is not abstracted for TSPA-LA because the lithophysal zone is expected to shatter into small fragments that cannot produce failed areas on the drip shield.

The seismic scenario class is designed to efficiently determine the mean dose for seismic events with annual frequencies down to 10^{-8} per year. The seismic scenario class is based on a single seismic hazard occurring at a randomly chosen time in each realization of the TSPA-LA. That is, the conditional probability of a seismic event is 1 for each realization. The damage from this single event is based on the abstractions for the drip shield, the waste package and the cladding. The damaged areas on the EBS components define pathways for flow and transport through the EBS. Once radionuclides are released from the EBS, flow and transport in the unsaturated zone and the saturated zone are based on the same models and algorithms as for the nominal scenario class. Biosphere calculations and parameters for the seismic scenario class are also unchanged from the nominal scenario class.

Each realization of the seismic scenario class will determine an annual dose time history for a single seismic hazard with mean annual exceedance frequency λ_i . These dose time histories do not represent the mean dose, as called for in 10 CFR 63.303, because a single hazard always occurs in each realization. However, a mean dose time history can be calculated using a probability-weighted sum and average of all the realizations for the seismic scenario class. The weighting factor for each realization corrects for the expected number of seismic events in each realization and for the logarithmic sampling of the hazard curve for PGV and of the time of the seismic event.

9. INPUTS AND REFERENCES

9.1 DOCUMENTS CITED

Brocoum, S. 2001. "Transmittal of Report Addressing Key Technical Issues (KTI) Structural Deformation and Seismicity (SDS)." Letter from S. Brocoum (DOE/YMSCO) to C.W. Reamer (NRC), October 25, 2001, OL&RC:TCG-0140, with enclosure. ACC: MOL.20020304.0297; MOL.20030714.0094.

BSC (Bechtel SAIC Company) 2001a. *FY 01 Supplemental Science and Performance Analyses, Volume 1: Scientific Bases and Analyses*. TDR-MGR-MD-000007 REV 00 ICN 01. Las Vegas, Nevada: Bechtel SAIC Company. ACC: MOL.20010801.0404; MOL.20010712.0062; MOL.20010815.0001.

BSC 2001b. *Site Recommendation Subsurface Layout*. ANL-SFS-MG-000001 REV 00 ICN 02. Las Vegas, Nevada: Bechtel SAIC Company. ACC: MOL.20010411.0131.

BSC 2002. *The Enhanced Plan for Features, Events, and Processes (FEPs) at Yucca Mountain*. TDR-WIS-PA-000005 REV 00. Las Vegas, Nevada: Bechtel SAIC Company. ACC: MOL.20020417.0385.

BSC 2003a. *Technical Work Plan for: Engineered Barrier System Department Modeling and Testing FY03 Work Activities*. TWP-MGR-MD-000015 REV 03. Las Vegas, Nevada: Bechtel SAIC Company. ACC: DOC.20030225.0001.

BSC 2003b. *Structural Calculations of Waste Package Exposed to Vibratory Ground Motion*. 000-00C-EBS0-00300-000-00B. Las Vegas, Nevada: Bechtel SAIC Company. ACC: ENG.20030520.0003.

BSC 2003c. *Repository Design Project, RDP/PA IED Typical Waste Package Components Assembly (5)*. 800-IED-WIS0-00205-000-00A. Las Vegas, Nevada: Bechtel SAIC Company. ACC: ENG.20030707.0001.

BSC 2003d. *Maximum Accelerations on the Fuel Assemblies of a 21-PWR Waste Package During End Impacts*. 000-00C-DSU0-01100-000-00A. Las Vegas, Nevada: Bechtel SAIC Company. ACC: ENG.20030327.0002.

BSC 2003e. *Repository Design Project, RDP/PA IED Typical Waste Package Components Assembly (4)*. 800-IED-WIS0-00204-000-00A. Las Vegas, Nevada: Bechtel SAIC Company. ACC: ENG.20030702.0004.

BSC 2003f. *Repository Design Project, Repository/PA IED Interlocking Drip Shield and Emplacement Pallet*. 800-IED-WIS0-00401-000-00A. Las Vegas, Nevada: Bechtel SAIC Company. ACC: ENG.20030730.0004.

BSC 2003g. *Drip Shield Structural Response to Rock Fall*. 000-00C-TED0-00500-000-00A. Las Vegas, Nevada: Bechtel SAIC Company. ACC: ENG.20030327.0001.

BSC 2003h. *Drift Degradation Analysis*. ANL-EBS-MD-000027 REV 02. Las Vegas, Nevada: Bechtel SAIC Company. ACC: DOC.20030709.0003.

BSC 2003i. *Repository Design Project, Repository/PA IED Emplacement Drift Committed Materials (2)*. 800-IED-WIS0-00302-000-00A. Las Vegas, Nevada: Bechtel SAIC Company. ACC: ENG.20030627.0004.

BSC 2003j. *Repository Design Project, RPD/PA IED Typical Waste Package Components Assembly 1 of 9*. 800-IED-WIS0-00201-000-00A. Las Vegas, Nevada: Bechtel SAIC Company. ACC: ENG.20030702.0001.

BSC 2003k. *Repository Design Project, RPD/PA IED Typical Waste Package Components Assembly (2)*. 800-IED-WIS0-00202-000-00A. Las Vegas, Nevada: Bechtel SAIC Company. ACC: ENG.20030702.0002.

BSC 2003l. *Stress Corrosion Cracking of the Drip Shield, the Waste Package Outer Barrier, and the Stainless Steel Structural Material*. ANL-EBS-MD-000005 REV 01. Las Vegas, Nevada: Bechtel SAIC Company. ACC: DOC.20030717.0001.

BSC 2003m. *Repository Design Project, RDP/PA IED Typical Waste Package Components Assembly (8)*. 800-IED-WIS0-00208-000-00A. Las Vegas, Nevada: Bechtel SAIC Company. ACC: ENG.20030707.0004.

BSC 2003n. *Repository Design Project, RDP/PA IED Typical Waste Package Components Assembly (7)*. 800-IED-WIS0-00207-000-00A. Las Vegas, Nevada: Bechtel SAIC Company. ACC: ENG.20030707.0003.

BSC 2003o. *Repository Design Project, Repository/PA IED Subsurface Facilities*. 800-IED-WIS0-00101-000-00Ad. Las Vegas, Nevada: Bechtel SAIC Company. ACC: MOL.20030730.0337. TBV-5310

BSC 2003p. *Structural Calculations of Drip Shield Exposed to Vibratory Ground Motion*. 000-00C-PEC0-00100-000-00A. Las Vegas, Nevada: Bechtel SAIC Company. ACC: ENG.20030618.0009.

BSC 2003q. *Abstraction of Drift Seepage*. MDL-NBS-HS-000019 REV 00C. Las Vegas, Nevada: Bechtel SAIC Company. ACC: MOL.20030728.0198. TBV-5280

BSC 2003r. *Sampling of Stochastic Input Parameters for Rockfall and Structural Response Calculations Under Vibratory Ground Motion*. ANL-EBS-PA-000009 REV00. Las Vegas, Nevada: Bechtel SAIC Company. ACC: DOC.20030707.0003.

BSC 2003s. *Drip Shield Statically Loaded by Backfill and Loose Rock Mass*. 000-00C-TED0-00300-000-00A. Las Vegas, Nevada: Bechtel SAIC Company. ACC: ENG.20030224.0004.

Canori, G.F. and Leitner, M.M. 2003. *Project Requirements Document*. TER-MGR-MD-000001 REV 01. Las Vegas, Nevada: Bechtel SAIC Company. ACC: DOC.20030404.0003.

Chun, R.; Witte, M.; and Schwartz, M. 1987. *Dynamic Impact Effects on Spent Fuel Assemblies*. UCID-21246. Livermore, California: Lawrence Livermore National Laboratory. ACC: HQX.19881020.0031.

CRWMS M&O (Civilian Radioactive Waste Management System Management and Operating Contractor) 1998. *Probabilistic Seismic Hazard Analyses for Fault Displacement and Vibratory Ground Motion at Yucca Mountain, Nevada*. Milestone SP32IM3, September 23, 1998. Three volumes. Las Vegas, Nevada: CRWMS M&O. ACC: MOL.19981207.0393.

CRWMS M&O 2000a. *Characterize Framework for Seismicity and Structural Deformation at Yucca Mountain, Nevada*. ANL-CRW-GS-000003 REV 00. Las Vegas, Nevada: CRWMS M&O. ACC: MOL.20000510.0175.

CRWMS M&O 2000b. *Features, Events, and Processes: Disruptive Events*. ANL-WIS-MD-000005 REV 00 ICN 1. Las Vegas, Nevada: CRWMS M&O. ACC: MOL.20001218.0007.

CRWMS M&O 2000c. *Total System Performance Assessment for the Site Recommendation*. TDR-WIS-PA-000001 REV 00 ICN 01. Las Vegas, Nevada: CRWMS M&O. ACC: MOL.20001220.0045.

DOE 2002. *Yucca Mountain Science and Engineering Report*. DOE/RW-0539, Rev. 1. Washington, D.C.: U.S. Department of Energy, Office of Civilian Radioactive Waste Management. ACC: MOL.20020404.0042. [155943]

DOE 2002. *Yucca Mountain Site Suitability Evaluation*. DOE/RW-0549. Washington, D.C.: U.S. Department of Energy, Office of Civilian Radioactive Waste Management. ACC: MOL.20020404.0043. [156958]

Freeze, G.A.; Brodsky, N.S.; Swift, P.N 2001. *The Development of Information Catalogued in REV00 of the YMP FEP Database*. TDR-WIS-MD-000003 REV 00 ICN 01. Las Vegas, Nevada: Bechtel SAIC Company. ACC: MOL.20010301.0237.

Gardner, D. 2000. "Meeting Summary, NRC/DOC Technical Exchange on Structural Deformation and Seismicity KTI, October 11-12, 2000." E-mail from D. Gardner to C. Hanlon, October 13, 2002, with attachment. ACC: MOL.20001102.0041; MOL.20001102.0042.

Hahn, G.J. and Shapiro, S.S. 1967. *Statistical Models in Engineering*. New York, New York: John Wiley & Sons. TIC: 247729. [146529]

Helton, J.C. 1994. "Treatment of Uncertainty in Performance Assessments for Complex Systems." *Risk Analysis*, 14, (4), 483-511. New York, New York: Plenum Press. TIC: 245848. [107739]

Helton, J.C. 1997. "Uncertainty and Sensitivity Analysis in the Presence of Stochastic and Subjective Uncertainty." *Journal of Statistical Computation and Simulation*, 57, (1-4), 3-76. New York, New York: Gordon and Breach Science Publishers. TIC: 245958. [107496]

Helton, J.C. and Davis, F.J. 2000. *Sampling-Based Methods for Uncertainty and Sensitivity Analysis*. SAND99-2240. Albuquerque, New Mexico: Sandia National Laboratories. TIC: 251256. [156572]

Helton, J.C. and Davis, F.J. 2002. *Latin Hypercube Sampling and the Propagation of Uncertainty in Analyses of Complex System*. SAND2001-0417. Albuquerque, New Mexico: Sandia National Laboratories. TIC: 254367. [163475]

Kaplan, S. and Garrick, B.J. 1981. "On the Quantitative Definition of Risk." *Risk Analysis*, 1, (1), 11-27. New York, New York: Plenum Press. TIC: 241205. [100557]

McKay, M.D.; Beckman, R.J.; and Conover, W.J. 1979. "A Comparison of Three Methods for Selecting Values of Input Variables in the Analysis of Output from a Computer Code." *Technometrics*, 21, (2), 239-245. Alexandria, Virginia: American Statistical Association. TIC: 221741.[127905]

Menges, C.M. and Whitney, J.W. 1996. "Distribution of Quaternary Faults in the Site Area." Chapter 4.2 of *Seismotectonic Framework and Characterization of Faulting at Yucca Mountain, Nevada*. Whitney, J.W., ed. Milestone 3GSH100M. Denver, Colorado: U.S. Geological Survey. TIC: 237980. ACC: MOL.19970129.0041.

Mongano, G.S.; Singleton, W.L.; Moyer, T.C.; Beason, S.C.; Eatman, G.L.W.; Albin, A.L.; and Lung, R.C. 1999. *Geology of the ECRB Cross Drift - Exploratory Studies Facility, Yucca Mountain Project, Yucca Mountain, Nevada*. Deliverable SPG42GM3. Denver, Colorado: U.S. Geological Survey. ACC: MOL.20000324.0614.

Newmark, N.M. and Rosenblueth, E. 1971. *Fundamentals of Earthquake Engineering*. Civil Engineering and Engineering Mechanics Series. Englewood Cliffs, New Jersey: Prentice-Hall. TIC: 248548.

NRC (U.S. Nuclear Regulatory Commission) 2003. *Yucca Mountain Review Plan, Final Report*. NUREG-1804, Rev. 2. Washington, D.C.: U.S. Nuclear Regulatory Commission, Office of Nuclear Material Safety and Safeguards. TIC: 254568.

Paté-Cornell, M.E. 1996. "Uncertainties in Risk Analysis: Six Levels of Treatment." *Reliability Engineering and System Safety*, 54, 95-111. New York, New York: Elsevier. TIC: 245961. [107499]

Rossman, A.J.; Short, T.H.; and Parks, M.T. 1998. "Bayes Estimators for the Continuous Uniform Distribution." *Journal of Statistic Education*. Alexandria, Virginia: American Statistical Association. Accessed April 7, 2003. TIC: 254033.
<http://www.amstat.org/publications/jse/v6n3/rossman.html>

Rubinstein, R.Y. 1981. *Simulation and the Monte Carlo Method*. New York, New York: John Wiley & Sons. TIC: 254563. [163476]

Sanders, T.L.; Seager, K.D.; Rashid, Y.R.; Barrett, P.R.; Malinauskas, A.P.; Einziger, R.E.; Jordan, H.; Duffey, T.A.; Sutherland, S.H.; and Reardon, P.C. 1992. *A Method for Determining*

the Spent-Fuel Contribution to Transport Cask Containment Requirements. SAND90-2406. Albuquerque, New Mexico: Sandia National Laboratories. ACC: MOV.19960802.0116.

Waiting, D.J.; Stamatakos, J.A.; Ferrill, D.A.; Sims, D.W.; Morris, A.P.; Justus, P.S.; and Ibrahim, A.K. 2003. "Methodologies for the Evaluation of Faulting at Yucca Mountain, Nevada." *Proceedings of the 10th International High-Level Radioactive Waste Management Conference (IHLRWM), March 30-April 2, 2003, Las Vegas, Nevada.* Pages 377-387. La Grange Park, Illinois: American Nuclear Society. TIC: 254559.

9.2 CODES, STANDARDS, REGULATIONS, AND PROCEDURES

10 CFR Part 63. Energy: Disposal of High-Level Radioactive Wastes in a Geologic Repository at Yucca Mountain, Nevada. Readily available.

AP-2.14Q, Rev. 2, ICN 2. *Review of Technical Products and Data.* Washington, D.C.: U.S. Department of Energy, Office of Civilian Radioactive Waste Management. ACC: DOC.20030206.0001.

AP-2.22Q, Rev. 0, ICN 1. *Classification Criteria and Maintenance of the Monitored Geologic Repository Q-List.* Washington, D.C.: U.S. Department of Energy, Office of Civilian Radioactive Waste Management. ACC: DOC.20030422.0009.

AP-2.27Q, Rev. 1, ICN 1. *Planning for Science Activities.* Washington, D.C.: U.S. Department of Energy, Office of Civilian Radioactive Waste Management. ACC: DOC.20030724.0001.

AP-3.12Q, Rev. 2, ICN 0. *Design Calculations and Analyses.* Washington, D.C.: U.S. Department of Energy, Office of Civilian Radioactive Waste Management. ACC: DOC.20030403.0003.

AP-3.15Q, Rev. 4, ICN 2. *Managing Technical Product Inputs.* Washington, D.C.: U.S. Department of Energy, Office of Civilian Radioactive Waste Management. ACC: DOC.20030627.0002.

AP-SI.1Q, Rev. 5, ICN 1. *Software Management.* Washington, D.C.: U.S. Department of Energy, Office of Civilian Radioactive Waste Management. ACC: DOC.20030708.0001.

AP-SIII.10Q, Rev. 1, ICN 2. *Models.* Washington, D.C.: U.S. Department of Energy, Office of Civilian Radioactive Waste Management. ACC: DOC.20030627.0003.

AP-SV.1Q, Rev. 0, ICN 3. *Control of the Electronic Management of Information.* Washington, D.C.: U.S. Department of Energy, Office of Civilian Radioactive Waste Management. ACC: MOL.20020917.0133.

9.3 SOURCE DATA, LISTED BY DATA TRACKING NUMBER

MO0004MWDRIFM3.002. Results of the Yucca Mountain Probabilistic Seismic Hazard Analysis (PSHA). Submittal date: 04/14/2000.

MO0210PGVPB107.000. Design Peak Ground Velocity for the Repository Level (Point B) at 10-7 Annual Exceedance Probability. Submittal date: 10/17/2002.

MO0301MWD3DE27.003. Results from 3DEC Nonlithophysal Rockfall Analyses with 10-7 Ground Motion Level. Submittal date: 01/23/2003.

MO0303DPGVB106.002. Design Peak Ground Velocity for the Repository Level (Point B) at 10-6 Annual Exceedance Probability. Submittal date: 03/10/2003.

MO0305MWDNLRKF.001. Results from 3DEC Nonlithophysal Rockfall Analyses with 10-6 Ground Motion Level. Submittal date: 05/27/2003.

MO03061E9PSHA1.000. Spectral Acceleration and Velocity Hazard Curves Extended to 1E-9 Based on the Results of the PSHA for Yucca Mountain. Submittal date: 06/09/2003.

LB0307SEEPDRCL.002. Seepage Into Collapsed Drift: Data Summary. Submittal Date: 07/21/2003.

LL030704623122.031. NUFT Input File Data Development to support LA Multi-Scale Analyses. Submittal Date: 07/23/2003.

TBV-5106: Assumption 5.1 – MDL-WIS-PA-000003 REV 00 – No damage from ground motions hazards with exceedance frequencies greater than 10^{-4} per year.

9.4 PRODUCT OUTPUT, LISTED BY DATA TRACKING NUMBER

MO0305SPASFEGM.000. Scaling Factor for Estimating the 10-5 Per Year Ground Motions.

MO0308SPACALSS.002. Computational Algorithm of the Seismic Scenario for TSPA. Submittal Date: 08/13/2003.

10. ATTACHMENTS

Attachment	Title
-------------------	--------------

- | | |
|-----|---|
| I | Spreadsheet for Point B Hazard Curve (8 pages) |
| II | Spreadsheet for Waste Package Damage Abstraction (10 pages) |
| III | Review Comments on Response Surface for Waste Package Damage from Vibratory Ground Motion, by R. P. Kennedy (12 pages) |
| IV | Spreadsheet for Drip Shield Damage Abstraction from Rockfall (6 pages) |
| V | Review Comments on Response Surface for Drip Shield Damage from Rockfall In Nonlithophysal Zone, by R. P. Kennedy (6 pages) |

- VI Review Comments on Response Surface for Drip Shield Damage from Vibratory Ground Motion, by R. P. Kennedy (6 pages)
- VII Spreadsheet for Fault Displacement Damage Abstraction (8 pages)
- VIII Representation of Aleatory and Epistemic Uncertainty in the Calculation of Expected Dose from Seismic Events at the Proposed Yucca Mountain Facility for the Disposal of High-Level Waste, by J. C. Helton (18 pages)

Electronic copies of Attachments I, II, IV, and VII are available on CD-ROM.

ATTACHMENT I

SPREADSHEET FOR POINT B HAZARD CURVE

List of Inputs

DTN: MO0004MWDRIFM3.002. Results of the Yucca Mountain Probabilistic Seismic Hazard Analysis (PSHA). Submittal date: 04/14/2000.

DTN: MO0303DPGVB106.002. Design Peak Ground Velocity for the Repository Level (Point B) at 10⁻⁶ Annual Exceedance Probability. Submittal date: 03/10/2003.

DTN: MO0210PGVPB107.000. Design Peak Ground Velocity for the Repository Level (Point B) at 10⁻⁷ Annual Exceedance Probability. Submittal date: 10/17/2002.

Relevant Formulas

The PGV hazard curve at Point A is defined by the points ($PGV_{Point A,i}$, $\lambda_{Point A,i}$) for $i = 1, 2, \dots, n$, where PGV is the peak ground velocity and λ is the annual exceedance frequency. The scaled hazard curve for point B is defined by the following formulas:

$$\begin{aligned} PGV_{Point B,i} &= a(PGV_{Point A,i}) \\ \lambda_{Point B,i} &= \lambda_{Point A,i}, \end{aligned} \quad (\text{Eq. I-1})$$

for $i = 1, 2, \dots, n$. Note that the values of the exceedance frequency remain unchanged in Equation 1, and can be denoted more simply as λ_i . The quantity a is a constant, 0.7736, that minimizes the error with the known PGV values at Point B for the 10⁻⁶ per year and 10⁻⁷ per year annual exceedance frequencies. The value of a is determined by trial and error, using the spreadsheet to calculate the error with the known values at Point B for varying values of a .

The values of PGV between the n points defined by Equation 1 are calculated with a log-linear interpolation scheme. For a given value of λ such that $\lambda_k < \lambda < \lambda_{k+1}$, the interpolation is given by:

$$PGV = PGV_{Point B,k} + \frac{PGV_{Point B,k+1} - PGV_{Point B,k}}{\log(\lambda_{k+1}) - \log(\lambda_k)} (\log(\lambda) - \log(\lambda_k)) \quad (\text{Eq. I-2})$$

Output Information

Table I-1 defines the points for the scaled PGV hazard curve at Point B.

Table I-1. Scaled Points for the PGV Hazard Curve at Point B

Scaled PGV At Point B (cm/s)	Annual Exceedance Frequency (1/yr)
15.9	6.26×10^{-4}
23.9	2.78×10^{-4}
39.8	9.30×10^{-5}
79.6	1.84×10^{-5}
159	3.07×10^{-6}
398	2.28×10^{-7}
557	8.15×10^{-8}
796	2.60×10^{-8}
1190	6.56×10^{-9}

The interpolated values of PGV for various values of the annual exceedance frequency are given in Table I-2. Note that the errors of the scaled hazard curve with the known values at Point B for the 10^{-6} per year and 10^{-7} per year annual exceedance frequencies are +7.5 percent and -1.7 percent, respectively.

Table I-2. Interpolated Values on the Scaled PGV Hazard Curve for Point B

Annual Exceedance Frequency (1/yr)	Interpolated PGV at Point B (cm/s)	Comments
5×10^{-4}	18.1	
10^{-4}	38.8	
5×10^{-5}	55.0	
10^{-5}	106.7	
10^{-6}	262.4	Error of +7.5% relative to the exact value of 244 cm/s
10^{-7}	525.8	Error of -1.7% relative to the exact value of 535 cm/s
1×10^{-8}	1073	

Finally, the ratio of the PGV values at Point B for annual exceedance frequencies of 10^{-5} per year to 10^{-6} per year is given by:

$$\frac{PGV \text{ at } 10^{-5}}{PGV \text{ at } 10^{-6}} = \frac{106.7 \text{ cm/s}}{262.4 \text{ cm/s}} = 0.4066. \quad (\text{Eq. I-3})$$

This ratio has been used to generate approximate ground motions for the 10^{-5} per year hazard level. It is available as a product output in DTN: MO0305SPASFEGM.000.

The spreadsheet defining the values in Tables I-1 and I-2 follows.

DEFINE THE MEAN HORIZONTAL PGV HAZARD CURVE AT POINT B (THE EMPLACEMENT DRIFTS) AND USE THIS CURVE TO ESTIMATE THE HORIZONTAL PGV VALUES AT ANNUAL EXCEEDANCE FREQUENCIES BETWEEN 5E-04 PER YEAR AND 1E-08 PER YEAR.

This calculation estimates the mean hazard curve for horizontal PGV at Point B (the emplacement drifts), based on the mean hazard curve for PGV at Point A, a reference rock outcrop at the repository elevation, and the known PGV values at Point B for the 10^{-6} per year and 10^{-7} per year annual exceedance probabilities. More specifically, the two known PGV values at point B are the basis for defining a scaling factor that minimizes the least squares differences with respect to these two points. This approach preserves the shape of the Point A hazard curve.

The scaling factor, 0.7963, minimizes the sum of the squared errors, based on a least squares analysis. The small magnitude of the errors, +8% and -2%, between the scaled Point A hazard curve and the known Point B values confirms that this is a reasonable approach.

PGV values at Point B for various annual exceedance probabilities are calculated using a log-linear interpolation for the annual exceedance frequency between the scaled points defining the new hazard curve for Point B.

Input Data for the mean horizontal PGV hazard curve at Point A:

DTN: MO03061E9PSHA1.000.

PGV values are in cm/sec.

Input Data for mean horizontal PGV values at Point B:

Horizontal PGV value at Point B for the 10^{-6} mean annual exceedance probability, 2.44 m/s, is from DTN: MO0303DPGVB106.002.

Horizontal PGV value at Point B for the 10^{-7} mean annual exceedance probability, 5.35 m/s, is from DTN: MO0210PGVPB107.000.

First, define the PGV value at Point A for the annual exceedance frequency of 1e-06, based on a log-linear interpolation scheme.

Annual Exceedance Frequency (1/yr)	Point A Horizontal PGV (cm/sec)	Interpolated Value At Point A
3.07E-06	2.00E+02	3.30E+02
2.28E-07	5.00E+02	

Second, define the PGV value at Point A for the annual exceedance frequency of 1e-07, based on a log-linear interpolation scheme.

Annual Exceedance Frequency (1/yr)	Point A Horizontal PGV (cm/sec)	Interpolated Value At Point A
2.28E-07	5.00E+02	6.60E+02
8.15E-08	7.00E+02	

Third, use the Excel equation solver to find the value of the Scale Factor that minimizes the sum of the square of the residuals with the known values at Point B.

Scale Factor 0.796294795

Annual Exceedance Frequency (1/yr)	Known Point A Horizontal PGV (cm/sec)	Scaled Value for Horizontal PGV (cm/sec)	Known Point B Horizontal PGV (cm/sec)	Square of the Residuals (cm ² /sec ²)	Percent Error (%)
1.00E-06	3.30E+02	2.62E+02	2.44E+02	339.1	7.55%
1.00E-07	6.60E+02	5.26E+02	5.35E+02	84.5	-1.72%
Sum:				423.6	

Define the New Points for the Scaled PGV Hazard Curve at Point B:

PGV Scaling Factor 0.7963

Point A Horizontal PGV (cm/sec)	Scaled Horiz. PGV for Point B (cm/sec)	Annual Exceedance Frequency (1/yr)
1.00E+01	7.96E+00	2.19E-03
2.00E+01	1.59E+01	6.26E-04
3.00E+01	2.39E+01	2.78E-04
5.00E+01	3.98E+01	9.30E-05
1.00E+02	7.96E+01	1.84E-05
2.00E+02	1.59E+02	3.07E-06
5.00E+02	3.98E+02	2.28E-07
7.00E+02	5.57E+02	8.15E-08
1.00E+03	7.96E+02	2.60E-08
1.50E+03	1.19E+03	6.56E-09

Interpolation for horizontal PGV values at Point B at 5×10^{-04} , 10^{-04} , 5×10^{-05} , 10^{-05} , 10^{-06} , 10^{-07} , and 10^{-08} per year. The interpolation is linear in the $\log(\lambda)$, where λ is the annual exceedance probability.

Value of Annual Exceedance Frequency (1/yr)	Points on the Point B Curve Bracketing This Value		Interpolated Value of PGV (cm/sec)	% Error With Known Values At Point B for 10^{-6} and 10^{-7}
	Annual Exceedance Frequency (1/yr)	Scaled Horizontal PGV for Point B (cm/sec)		
5.00E-04	6.26E-04	1.59E+01	18.1	
	2.78E-04	2.39E+01		
1.00E-04	2.78E-04	2.39E+01	38.8	
	9.30E-05	3.98E+01		
5.00E-05	9.30E-05	3.98E+01	55.0	
	1.84E-05	7.96E+01		
1.00E-05	1.84E-05	7.96E+01	106.70	
	3.07E-06	1.59E+02		
1.00E-06	3.07E-06	1.59E+02	262.42	7.55%
	2.28E-07	3.98E+02		
1.00E-07	2.28E-07	3.98E+02	525.8	-1.72%
	8.15E-08	5.57E+02		
1.00E-08	2.60E-08	7.96E+02	1073	
	6.56E-09	1.19E+03		
Ratio of PGV at 10^{-5} to PGV at 10^{-6}:			0.4066	

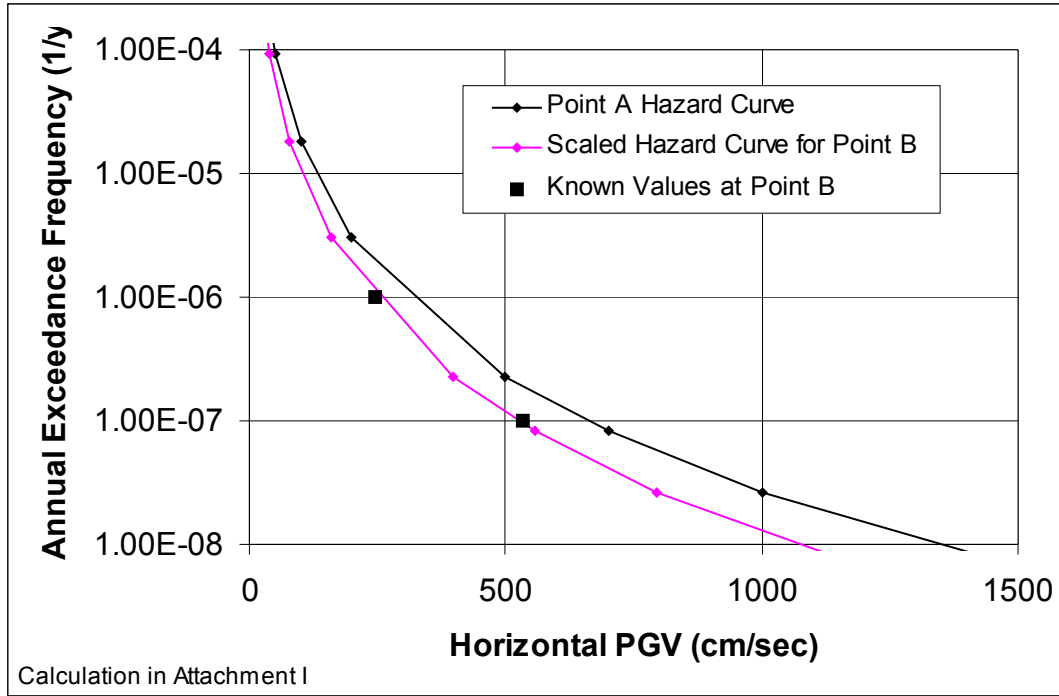


Figure I-1. Scaled Hazard Curve for Point B

INTENTIONALLY LEFT BLANK

ATTACHMENT II

SPREADSHEET FOR WASTE PACKAGE DAMAGE ABSTRACTION

This spreadsheet contains the calculations that produce the waste package damage abstraction described in Section 6.5.1.

The following worksheets are included:

- (1) results_80% YS
- (2) results_90% YS
- (3) fit_80%_90%_vs_Uniform_Dist
- (4) fit_80%_90%_Upper_Bound

The inputs, outputs, and formulas used in each worksheet are described below.

(1) results_80% YS

This worksheet is a copy of the results presented in Tables 6 and 7 (see column labeled Cumulative Damaged area expressed as % of total area) for the damaged areas from vibratory ground motion for 80% of yield strength (YS) failure threshold. Minimum, maximum, mean, and standard deviation of the damaged areas are calculated for the results.

The PGV values are from DTN: MO0303DPGVB106.002 and DTN: MO0210PGVPB107.000. The damaged areas are from BSC 2003b Table 6.1.4-2; BSC 2003c, Table 16.

(2) results_90% YS

This worksheet is a copy of the results presented in Tables 6 and 7 (see column labeled Cumulative Damaged area expressed as % of total area) for the damaged areas from vibratory ground motion for 90% of yield strength (YS) failure threshold. Minimum, maximum, mean, and standard deviation of the damaged areas are calculated for the results.

The PGV values are from DTN: MO0303DPGVB106.002 and DTN: MO0210PGVPB107.000. The damaged areas are from BSC 2003b, Table 6.2.4-2; BSC 2003c, Table 17.

3) Avg_80%_90%_vs_Uniform_Dist

In this worksheet, the cumulative % damage area is computed as the average of the 80% YS and 90% YS results given in worksheets (1) and (2).

These average values are shown in column B.

The average values are then sorted in ascending order in column C.

The cumulative probability is computed for each point in column D.

Finally, the points are compared with a least squares fit to a straight line determined by Excel's fitting routine for PGV of 2.44 m/s and for the PGV of 5.35 m/s.

The equation of the straight line and the r² value for the fit is also shown.

(4) Avg_80%_90%_Upper_Bound

In this worksheet, the cumulative % damage area is computed as the average of the 80% YS and 90% YS results given in worksheets (1) and (2).

These average values are shown in columns B and D.

Then, the 95% upper confidence limit associated with this value is computed

Using $95\% \text{ UCL} = (\alpha)^{-1/(n-1)} \times \max\{\text{observed value}\}$

where $\alpha = 0.05$ is the level of significance and UCL = upper confidence limit.

This is shown in Row 26 for PGV of 2.44 m/s and 5.35 m/s.

These formulas are by Rossman et al. (1998).

Also shown in this worksheet are three graphs of percent failed area versus PGV.

The magenta squares and diamonds are the computed % cumulative damage.

The red squares are the Bayesian 95% UCL in Row 26 of this worksheet.

Three graphs then present (1) comparison of the Bayesian upper bound with the damaged areas for PGV of 2.44 m/s and 5.35 m/s, (2) a comparison of the upper bound with the results for PGV of 2.44 m/s, 5.35 m/s, and 1.067 m/s, and (3) a comparison of the upper bound for the lognormal distribution, derived in Attachment III, with the upper bound for the uniform distribution.

(1) results_80% YS

PGV (m/s)	Cum. % Damage at 1E-06 1/yr for 80% of Yield	PGV (m/s)	Cum. % Damage at 1E-07 1/yr for 80% of Yield
2.44	0.092%	5.35	1.280%
2.44	0.060%	5.35	1.840%
2.44	0.710%	5.35	0.820%
2.44	0.530%	5.35	0.960%
2.44	0.530%	5.35	1.670%
2.44	0.640%	5.35	1.280%
2.44	0.460%	5.35	1.490%
2.44	0.430%	5.35	0.140%
2.44	0.050%	5.35	1.740%
2.44	0.300%	5.35	1.060%
2.44	0.270%	5.35	0.570%
2.44	0.110%	5.35	0.530%
2.44	0.057%	5.35	0.099%
2.44	0.099%	5.35	1.030%
min	0.050%		0.099%
max	0.710%		1.840%
mean	0.310%		1.036%
std, dev.	0.237%		0.560%
confidence	95%		95%
alpha	5%		5%
upper conf limit	0.894%		2.317%

Ref: Rossman et al.
1998

(2) results_90% YS

PGV (m/s)	Cum. % Damage at 1E-06 1/yr for 90% of Yield	PGV (m/s)	Cum. % Damage at 1E-07 1/yr for 90% of Yield
2.44	0.046%	5.35	0.920%
2.44	0.032%	5.35	0.890%
2.44	0.290%	5.35	0.530%
2.44	0.240%	5.35	0.530%
2.44	0.230%	5.35	0.600%
2.44	0.230%	5.35	0.600%
2.44	0.200%	5.35	0.740%
2.44	0.220%	5.35	0.074%
2.44	0.025%	5.35	1.030%
2.44	0.130%	5.35	0.390%
2.44	0.130%	5.35	0.300%
2.44	0.057%	5.35	0.250%
2.44	0.026%	5.35	0.071%
2.44	0.043%	5.35	0.500%
min	0.025%		0.071%
max	0.290%		1.030%
mean	0.136%		0.530%
stnd, dev.	0.097%		0.298%
confidence	95%		95%
alpha	5%		5%
upper conf limit	0.365%		1.297%

Ref: Rossman et al.
1998

(3) Avg_80%_90%_vs_Uniform_Dist

PGV (m/s)	Cum. % Damage at 1E-06 1/yr for Average YS	Sorted % Damage	Cumulative Probability (-)
2.44	0.069%	0.038%	0.036
2.44	0.046%	0.042%	0.107
2.44	0.500%	0.046%	0.179
2.44	0.385%	0.069%	0.250
2.44	0.380%	0.071%	0.321
2.44	0.435%	0.084%	0.393
2.44	0.330%	0.200%	0.464
2.44	0.325%	0.215%	0.536
2.44	0.038%	0.325%	0.607
2.44	0.215%	0.330%	0.679
2.44	0.200%	0.380%	0.750
2.44	0.084%	0.385%	0.821
2.44	0.042%	0.435%	0.893
2.44	0.071%	0.500%	0.964

PGV (m/s)	Cum. % Damage at 1E-07 1/yr for Average YS	Sorted % Damage	Cumulative Probability (-)
5.35	1.100%	0.085%	0.036
5.35	1.365%	0.107%	0.107
5.35	0.675%	0.390%	0.179
5.35	0.745%	0.435%	0.250
5.35	1.135%	0.675%	0.321
5.35	0.940%	0.725%	0.393
5.35	1.115%	0.745%	0.464
5.35	0.107%	0.765%	0.536
5.35	1.385%	0.940%	0.607
5.35	0.725%	1.100%	0.679
5.35	0.435%	1.115%	0.750
5.35	0.390%	1.135%	0.821
5.35	0.085%	1.365%	0.893
5.35	0.765%	1.385%	0.964

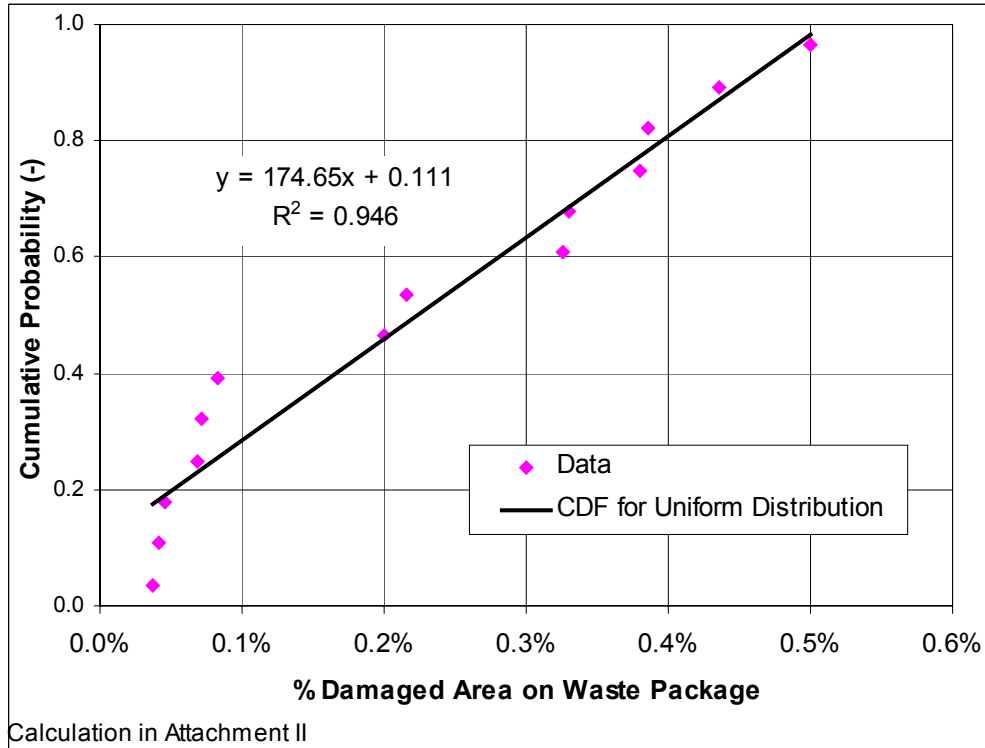


Figure II-1. Comparison of Damage Results for 10^{-6} per Year Ground Motions with a Uniform Distribution

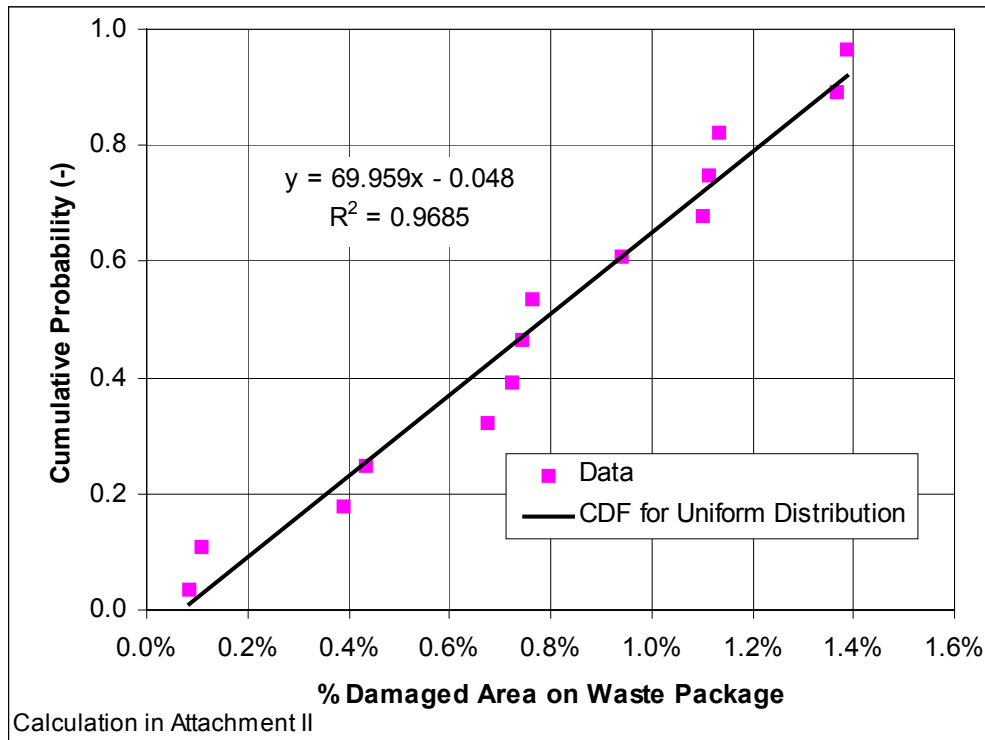


Figure II-2. Comparison of Damage Results for 10^{-7} per Year Ground Motions with a Uniform Distribution

(4) Avg_80%_90%_Upper_Bound

PGV (m/s)	Cum. % Damage at 1E-06 1/yr for Average	PGV (m/s)	Cum. % Damage at 1E-07 1/yr for Average	PGV (m/s)	Cum. % Damage at 1E-05 1/yr for Average
2.44	0.069%	5.35	1.100%	1.067	0.0105%
2.44	0.046%	5.35	1.365%	1.067	0.0000%
2.44	0.500%	5.35	0.675%	1.067	0.0255%
2.44	0.385%	5.35	0.745%		
2.44	0.380%	5.35	1.135%		
2.44	0.435%	5.35	0.940%		
2.44	0.330%	5.35	1.115%		
2.44	0.325%	5.35	0.107%		
2.44	0.038%	5.35	1.385%		
2.44	0.215%	5.35	0.725%		
2.44	0.200%	5.35	0.435%		
2.44	0.084%	5.35	0.390%		
2.44	0.042%	5.35	0.085%		
2.44	0.071%	5.35	0.765%		
Minimum	0.038%		0.085%		0.000%
Maximum	0.500%		1.385%		0.026%
Mean	0.223%		0.783%		0.012%
Standard Deviation	0.166%		0.420%		0.013%

Calculation of Bayesian Maximum:

Confidence	95%	95%	95%
Alpha	5%	5%	5%
Upper Conf Limit	0.630%	1.744%	1.067
			0.114%

Ref: Rossman et al. 1998

Plot the Straight Line Through the Bayesian Maxima:

PGV (m/s)	Upper Limit (%)	Plot the Linear Fit:	
2.44	0.63%	Slope	0.003829389
5.35	1.74%	y-intercept	-0.00305
		x-intercept	0.795932203
		PGV	0.7959322
		Damage	0
			8 0.02758718

Plot Maximum of Lognormal Distribution (Attachment III, Eq. III-9):

PGV	Damage
0.7	0.0002%
7.6	3.01%

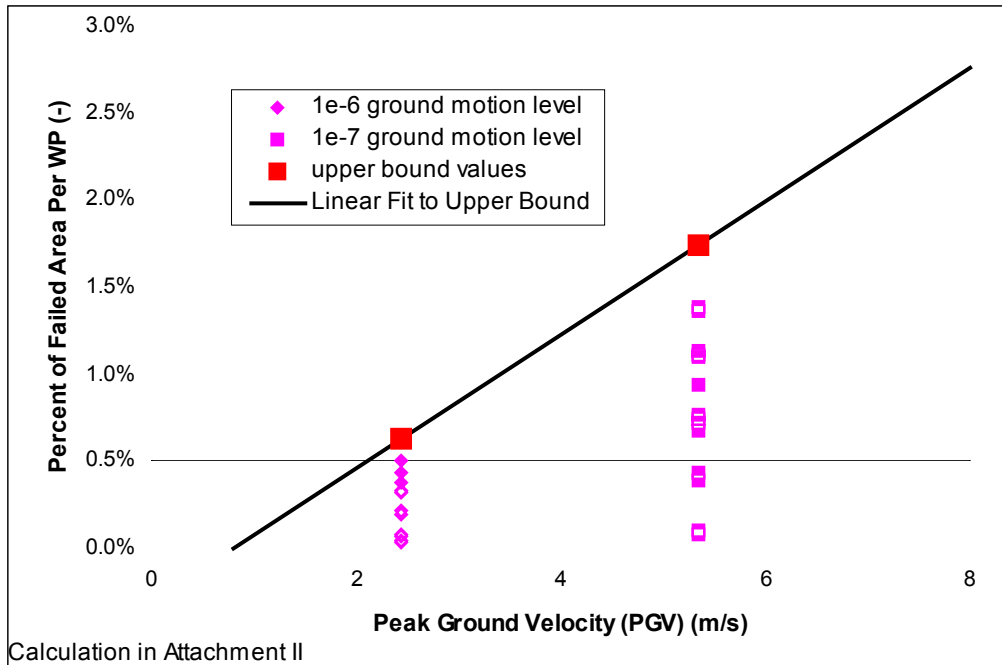


Figure II-3. Linear Fit to Bayesian Upper Bound of Damage Distribution

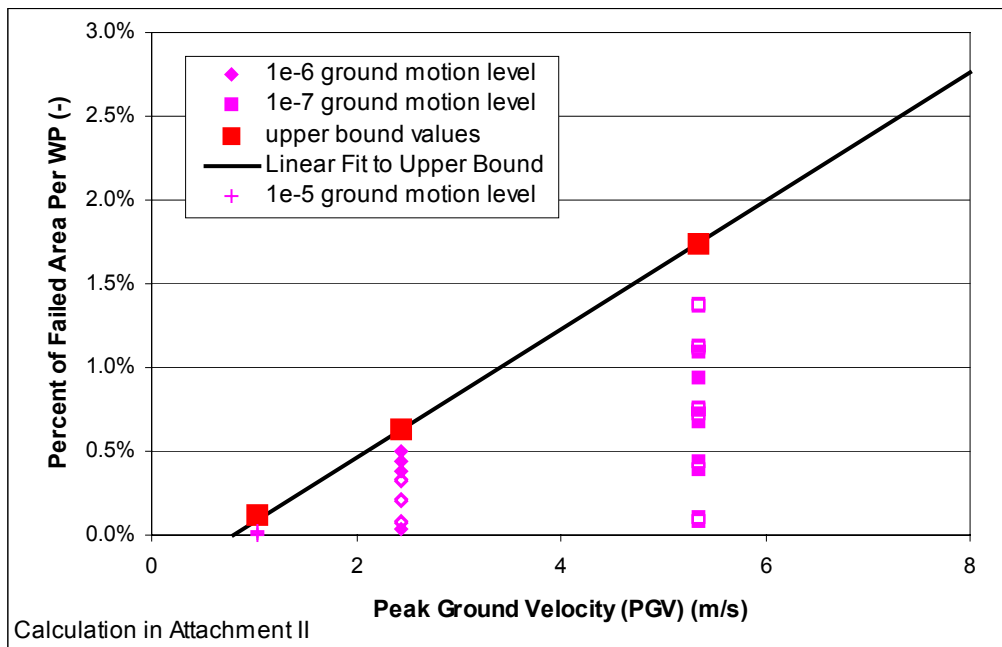


Figure II-4. Comparison of Linear Fit to Bayesian Upper Bound of Damage Distribution with the Damage Results for the 10^{-5} per Year Ground Motions

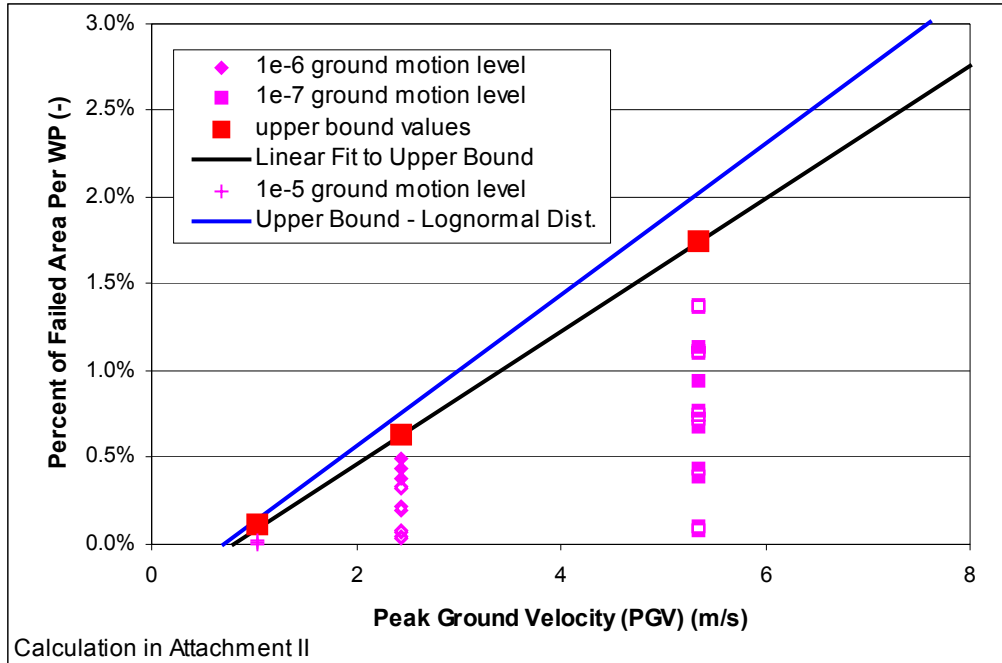


Figure II-5. Comparison of Upper Bounds Based on a Lognormal Distribution (Blue Curve) with the Bayesian Upper Bound

INTENTIONALLY LEFT BLANK

ATTACHMENT III

**REVIEW COMMENTS ON RESPONSE SURFACE FOR WASTE PACKAGE DAMAGE
FROM VIBRATORY GROUND MOTION**

by R. P. Kennedy

Review Comments on Response Surface for Waste Package Damage from Vibratory Ground Motion¹

R.P. Kennedy
June 2003

III.1. Introduction

This report presents my review comments on the response surface for waste package damage from vibratory ground motion developed and presented in Section 6.5.1 of Ref. III.1.

Damage is defined in terms of the percentage of damaged area D . The response surface defines the exceedance probability EP that the defined percentage of damaged area D might be exceeded as a function of the peak ground velocity PGV ,

III.1.1 Symbols and Units Used Herein

D	=	Percentage of damaged area (%)
D_{UB}	=	Upper bound on D (%) as a function of PGV
D_{80}	=	Value of D obtained using 80% yield criteria
D_{90}	=	Value of D obtained using 90% yield criteria
EP	=	Exceedance Probability (%)
NEP	=	Non-Exceedance Probability (%)
PGV	=	Peak ground velocity (m/sec)
U	=	Uniform damage surface defined by Eqns. (III-1) and (III-2)
LN	=	Lognormal damage surface defined by Eqn. (III-9)

III.1.2 Response Surface Recommended in Ref. III.1

Ref. III.1 defines an upper bound D_{UB} (%) on D as a function of PGV (m/sec) by:

$$D_{UB} = 0.383(PGV) - 0.305 \quad (III-1)$$

At any given PGV , Ref. III.1 assumes the percentage of damaged area D (%) is uniformly distributed between zero and D_{UB} . Thus, the exceedance probability EP (%) for any specified D conditional on the given PGV is defined by:

$$EP = \left[1 - \frac{D}{D_{UB}} \right] (100\%) \quad (III-2)$$

¹ Section numbers, table numbers, equation numbers, and reference numbers have been changed by adding a "III" to distinguish this attachment from the main body of the text. No other changes have been made to the content of this independent review, beyond these editorial changes.

Representation of the damage response surface by Eqns. (III-1) and (III-2) is attractive because it is very easy to use. However, several conservatisms and unconservatisms are embedded into the development of the damage surface represented by Eqns. (III-1) and (III-2). It is not intuitively obvious whether Eqns. (III-1) and (III-2) provide an adequate representation of the damage surface. It is also questionable as to how far this damage surface can be extrapolated beyond the limited data base. Over what range of PGV values and what range of D values is it reasonable to express the damage surface by Eqn. (III-1) and (III-2)?

The damage surface defined by Eqns. (III-1) and (III-2) will be called herein the “Uniform” damage surface and will be represented in the attached tables by the symbol U.

III.1.3 Scope of Review

Starting with the same data base defined in Tables 6 and 7 of Ref. III.1, I have developed in Section III.2 a more complex description of the damage surface. This more complex damage surface attempts to correct the unconservatisms and conservatisms described subsequently associated with the U damage surface. This more complex damage surface is defined by lognormally distributed exceedance probabilities EP as a function of both D and PGV, and will be called herein the “Lognormal” damage surface and will be represented in the attached tables by the symbol LN.

Exceedance probability EP results computed using this LN damage surface will be compared with those computed for the U damage surface. Recommendations concerning both the LN and U damage surface representations are presented in Section III.3.

III.1.4 Data Base Used to Develop Damage Surface Representations

Nonlinear time history analyses were performed for the following two ground motion levels:

$$\begin{aligned} \text{PGV} &= 2.44 \text{ m/sec} \\ \text{PGV} &= 5.35 \text{ m/sec} \end{aligned} \tag{III-3}$$

The results are reported in Tables 6 and 7 of Ref. III.1. A total of 14 analyses for PGV = 2.44 m/sec are summarized in Table 6 of Ref. III.1. A total of 14 analyses for PGV = 5.35 m/sec are summarized in Table 7 of Ref. III.1. Two damage thresholds are used to compute the percentage of damaged area D for each analytical simulation. These two damage thresholds are:

- 1.) Damage occurs where the residual stress exceed 80% of yield (called 80% yield criteria)
- 2.) Damage occurs where the residual stress exceeds 90% of yield (called 90% yield criteria)

It is outside of my expertise to comment on these damage threshold criteria. Furthermore, I have not reviewed any of the nonlinear analyses from which the percentage of damaged area D reported in Tables 6 and 7 of Ref. III.1 were obtained.

The results presented in Tables 6 and 7 of Ref. III.1 are tabulated herein in Tables III-1 and III-2 in which these results are ordered in the order of increasing percentage of damaged area D . Also shown in Tables III-1 and III-2 is the non-exceedance probability NEP corresponding to each of these ordered results as computed from:

$$NEP = \frac{n - 0.5}{N} (100\%) \quad (III-4)$$

where N is the total number of trials and n is the ordered trial number. The results shown in Tables III-1 and III-2 are the basis for both the U damage surface developed in Ref. III.1 and the LN damage surface presented herein in Section III.2.

Ref. III.1 has assumed a uniform distribution of D between a lower bound value D_{90} based on the 90% yield criteria to an upper bound value D_{80} based on the 80% yield criteria. This assumption seems reasonable and will be made herein as well.

III.1.5 Comments on Development of U Damage Surface

As noted earlier, several conservatisms and unconservatisms are embedded into the development of the U damage surface developed in Ref. III.1. These conservatisms and unconservatisms will be briefly discussed in the subsections of this section.

III.1.5.1 Establishment of Upper Bound D_{UB}

Ref. III.1 developed a mean estimate of \bar{D} for each of the trials from:

$$D = \frac{D_{90} + D_{80}}{2} \quad (III-5)$$

which is the appropriate equation for the mean D for a uniform distribution. However, Ref. III.1 ignored the scatter of D about \bar{D} . On average:

$$D_{80} \approx 2 D_{90} \quad (III-6)$$

This scatter of D about \bar{D} should be considered when establishing D_{UB} . Since it was not considered D_{UB} was unconservatively established.

Secondly, D_{UB} was established at the 95% upper confidence limit for the upper bound on D . This upper bound D_{UB} cuts off the uniform distribution at the 5% EP, and assumes 0% EP beyond D_{UB} . In most seismic risk evaluations, the fragility curve or damage surface between

about 1% EP and 5% EP significantly contributes to the mean computed annual risk when the fragility curve or damage surface is convolved with the hazard curve.

For both of the above reasons, D_{UB} has been unconservatively established. For example, Ref. III.1 has established the following values of D_{UB} .

PGV (m/sec)	D_{UB} (%)
2.44	0.630
5.35	1.744

Two of the 14 results reported in Table III-1 exceed $D_{UB} = 0.630\%$ for the 80% yield criteria case. Similarly two of the 14 results reported in Table III-2 are either at or exceed $D_{UB} = 1.744\%$ for the 80% yield criteria case.

III.1.5.2 Use of Uniform Distribution From Zero to D_{UB}

For the U damage surface, Eqn. (III-2) is used to establish EP for any D corresponding to a specified PGV. This uniform distribution is very conservative for the distribution shown in Table III-1 for $PGV = 2.44$ m/sec. The trial results are not uniformly distributed, but are heavily skewed to low D. The distribution shown in Table III-2 for $PGV = 5.35$ m/sec is more nearly uniform and can be reasonably approximated by a uniform distribution.

III.1.5.3 Linear Variation of D With PGV

Eqns. (III-1) and (III-2) assume that D_{UB} and D for any specified EP vary linear with PGV. My experience with sliding and impact problems is that the sliding displacements and impact velocities vary with PGV to a power greater than unity. If my past experience proves correct for the current problem, then this linear variation of D_{UB} and D with PGV may be increasingly unconservative for PGV values greater than 5.35 m/sec. Conversely, some conservatism may be introduced for PGV values between 2.44 m/sec and 5.35 m/sec. I am concerned about the extrapolation of Eqn. (III-1) beyond the range of PGV between about 1.5 m/sec and 6.0 m/sec.

The most important region of a fragility curve or damage surface is typically between EP values of 1% to 50%. Because of their shapes, either a lognormally distributed or normally distributed fragility curve or damage surface will result in EP increasing faster than linear with PGV over this important range. Therefore, these distributions can generally be extrapolated further beyond the range of available data points. My preference is for the lognormal distribution because within my experience, a lot of nonlinear computed fragility results reasonably fit this distribution. However, even this distribution should not be extrapolated too far. Extrapolation beyond the range of 1.5 m/sec to 8.0 m/sec is suspect even using a lognormal distribution.

III.2. Development of Improved Damage Surface Estimation

III.2.1 Approach to Account for Variability of D between D_{80} and D_{90}

Assuming D varies uniformly between D_{80} and D_{90} , the cumulative NEP for various D values can be estimated by the following procedure from the trial results presented in Tables III-1 and III-2 for PGV = 2.44 m/sec and 5.35 m/sec, respectively. First determine the NEP_{TH} for the highest trial in Tables III-1 or III-2 for which D_{80} is less than the specified D. Next, determine all of the trials for which D is between D_{90} and D_{80} . For each of these trials find the percentage associated with being less than D assuming a uniform distribution. Then, the NEP associated with the specified D is given by:

$$NEP = NEP_{TH} + \frac{100\%}{N} \sum \left(\frac{D - D_{90}}{D_{80} - D_{90}} \right) \quad (III-7)$$

where N is the total number of trials, and the summation is performed only for the trials where D is between D_{90} and D_{80} . Lastly, the exceedance probability EP is given by:

$$EP = 100\% - NEP \quad (III-8)$$

The NEP or EP for D values less than the lowest D_{90} or greater than the highest D_{80} in Table III-1 for PGV = 2.44 m/sec or Table III-2 for PGV = 5.35 cannot be estimated by the above procedure. There are insufficient numbers of trials to cover these D values. The NEP for D below the lowest D_{90} is less than the lowest NEP in the tables, and the NEP for D higher than the highest D_{80} is greater than the highest NEP in the tables. Values of NEP for D in these regions are estimated by judgment.

Table III-3A presents the estimated EP values obtained for various D from the data in Tables III-1 and III-2 using the above procedure. Table III-3A becomes the data base for establishing the damage surface.

III.2.2 Improved Approximation of Damage Surface

A lognormally distributed approximation of the damage surface was fit by trial and error to the exceedance probability EP data shown in Table III-3A. The following lognormal distribution was found to provide a good fit to Table III-3A:

Lognormal Distribution Parameters

Median :	$PGV_{50} = (5.7 \text{ m/sec})D^{0.5}$	
Log. Std. Dev.:	$\beta = 0.28D^{-0.5} \leq 0.8$	(III-9)
Truncation Point:	$EP = 1\%$	

A practical problem associated with the use of the lognormal distribution is that it will predict small EP values even at very low PGV values. For sliding and impact problems, the extreme lower tail of the lognormal distribution should not be used because damage won't occur for low PGV values. A practical solution to this problem is to truncate the lognormal

distribution at an EP of about 1.0%. Below this level EP should be taken as zero. Nonlinear analyses performed for lower PGV levels would enable this truncation point to be better defined. However, the above recommendation has proven to be adequate for all risk assessments of which I am aware that have included sliding and impact fragilities.

Table III-3B show the EP predicted by the lognormal LN damage surface defined by the parameters in Eqn. (III-9). Good agreement exists between Table III-3B and Table III-3A except for the $D = 0.03\%$ and $PGV = 2.44$ m/sec case. The agreement for this case could be improved by use of a more complex equation for the logarithmic standard deviation β . However, this improvement was considered to be unnecessary because the computed risk is insensitive to EP when EP exceeds about 70%. Therefore, even for $D = 0.03\%$ and $PGV = 2.44$ m/sec, the fit is more than adequate.

III.2.3 Comparison of Uniform U Damage Surface With Table 3A

Table III-3C shows the EP predicted by the uniform U damage surface used in Ref. III.1 for the same cases shown in Table III-3A. The agreement is not as good as that obtained from the LN damage surface approximation.

For $PGV = 5.35$ m/sec, the U damage surface provides a good approximation to the Table III-3A results except for D greater than about 1.67% where the U damage surface estimate of EP becomes seriously unconservative. This unconservatism could have significant unconservative consequences for estimating the annual probability of exceeding higher values of D .

For $PGV = 2.44$ m/sec, the U damage surface approximation significantly overestimates EP for D between 0.06% and 0.56%. However, a more significant issue is that the U damage surface significantly underestimates EP for D greater than 0.60%.

This unconservatism at higher D values can be easily corrected by changing Eqn. (III-1) to slightly increase D_{UB} . The unconservatism shown when comparing Table III-3C with Table III-3A is eliminated when:

$$D_{UB} = 0.436(PGV) - 0.305 \quad (III-10)$$

is used instead of Eqn. (III-1). The resulting D_{UB} values become:

PGV (m/sec)	D_{UB} (%)
2.44	0.759
5.35	2.028

These D_{UB} values lie at about the EP = 1% level based upon the data presented in Table III-3A. They also adequately exceed the highest D_{80} values shown in Tables III-1 and III-2.

II.2.4 Extension of Damage Surface to Other PGV Values

Nonlinear analyses have only been performed for PGV of 2.44 m/sec and 5.35 m/sec. However, it is necessary to extend the candidate damage surfaces over as broad a range of PGV values and D values as is credible. Table III-4 extends the estimated damage surface over the range of PGV from 1.5 m/sec to 8.0 m/sec, and D from 0.03% to 2.0%. This range is the maximum range over which I believe it is credible to extend the nonlinear results summarized in Tables III-1 and III-2.

Table III-4 shows the exceedance probabilities EP predicted by both the uniform U damage surface proposed in Ref. III.1 and the lognormal LN damage surface proposed in Section 2.2. Over the majority of the damage surface region covered by Table III-4, the U damage surface approximation provides a conservatively biased estimate of EP. In my judgment, the amount of conservative bias is not sufficient to seriously over predict the annual probability of exceeding any specified D when this damage surface is convolved with a seismic hazard curve.

However, there are a few regions where the U damage surface is significantly unconservative. These regions are identified by a dash under the U predicted values. These under prediction regions could have an important unconservative effect on predicted annual probability of exceeding a specified D because they all occur at low EP values within the range that generally significantly influences the annual probability of exceedance. These underlined under predictions of EP should be eliminated by the following suggestions.

First, the U damage surface proposed in Ref. III.1 should not be extended to PGV values greater than about 6.0 m/sec. Extension to higher PGV values is likely to become seriously unconservative for the reason discussed in Section 1.5.3.

Secondly, the upper bound D_{UB} should be defined by Eqn. (III-10) instead of Eqn. (III-1). This change will resolve the issues discussed in Section 1.5.1.

III.3. Recommendations

III.3.1 Recommendations Concerning LN Damage Surface Representation

The LN damage surface representation defined by Eqn. (III-9) is judged to provide an good description of the damage surface over the entire range of PGV and D values covered by Table III-4. This range covers:

$$\begin{aligned} 1.5\text{m/sec} &\leq \text{PGV} \leq 8.0 \text{ m/sec} \\ 0.03\% &\leq D \leq 2.0\% \end{aligned} \tag{III-11}$$

Extension of this LN damage surface representation beyond the range of Eqn. (III-11) becomes questionable unless additional nonlinear analyses are performed.

An additional 15 nonlinear analyses conducted at a PGV of approximately 1.0 m/sec should be sufficient to enable a modified LN damage surface to be extended down to about 0.5 m/sec for $D = 0.03\%$ and larger. However if percent damage areas less than 0.03% are also

required, it will be necessary to perform nonlinear analyses at two PGV levels below 2.44 m/sec. The existing nonlinear analysis results are not helpful in defining the important region of the damage surface from EP = 1% to 70% for D less than 0.03%.

It is unlikely that the damage surface needs to be extended beyond PGV of 8.0 m/sec because such a high PGV is not very credible at least in my judgment. However, it might be necessary to define the damage surface for percent damage area D greater than 2%. Nonlinear analyses would have to be conducted at a ground motion significantly above PGV of 5.35 m/sec to enable the damage surface to be extended above D = 2.0%. Ideally, the PGV for these additional analyses should be selected so that the nonlinear simulations produced D in the range of 1.5% to 10% if D needs to be extended beyond 2%.

III.3.2 Recommendations Concerning U Damage Surface Representation

The primary advantage of the U damage surface representation presented in Ref. III.1 is the ease with which it can be used. With one correction, this U damage surface representation is judged to provide a more than adequate representation of the damage surface over the following range:

$$\begin{aligned} 1.5\text{m/sec} &\leq \text{PGV} \leq 6.0 \text{ m/sec} \\ 0.03\% &\leq D \leq 2.0\% \end{aligned} \quad \text{(III-12)}$$

The one recommended correction is that D_{UB} used in Eqn. (III-2) should be computed by Eqn. (III-10) as opposed to Eqn. (III-1) recommended in Ref. III.1.

It is very questionable whether a linear equation such as either Eqn. (III-1) or (III-10) can be extended to cover a range of PGV values larger than about a factor of four. Therefore if the PGV range defined in Eqn. (III-12) must be extended, it is questionable whether the simplification of the U damage surface representation format can be maintained over a broader PGV range.

References

III.1 Seismic Consequences Abstraction Report, Draft, Rev00C, June 2003

**Table III-1: Percentage Damaged Area D
Obtained From Nonlinear Analyses for
PGV = 2.44 m/sec**

NEP (%)	D(%)	
	80% Yield Criteria	90% Yield Criteria
3.57	.050	.025
10.71	.057	.026
17.86	.060	.032
25.0	.092	.043
32.14	.099	.046
39.29	.11	.057
46.43	.27	.13
53.57	.30	.13
60.71	.43	.20
67.86	.46	.22
75.0	.53	.23
82.14	.53	.23
89.29	.64	.24
96.43	.71	.29

**Table III-2: Percentage Damaged Area D
Obtained From Nonlinear Analyses for
PGV = 5.35 m/sec**

NEP (%)	D(%)	
	80% Yield Criteria	90% Yield Criteria
3.57	.099	.071
10.71	.14	.074
17.86	.53	.25
25.0	.57	.30
32.14	.82	.39
39.29	.96	.50
46.43	1.03	.53
53.57	1.06	.53
60.71	1.28	.60
67.86	1.28	.60
75.0	1.49	.74
82.14	1.67	.89
89.29	1.74	.92
96.43	1.84	1.03

**Table III-3: Exceedance Probabilities EP for
Various Damage Area Percentages D and
Peak Ground Velocities PGV**

Table III-3A: Nonlinear Data Results From Tables III-1 and III-2

PGV (m/sec)	D(%)										
	.03	.06	.12	.25	.50	.75	1.00	1.25	1.5	1.75	2.0
2.44	97.6	77.4	60.7	46.0	11.1	1.5	X	X	X	X	X
5.35	X	98.5	91.5	89.3	75.8	55.8	35.1	19.8	10.2	4.4	2.0

Table III-3B: Lognormal LN Damage Surface Approximation

PGV (m/sec)	D(%)										
	.03	.06	.12	.25	.50	.75	1.00	1.25	1.5	1.75	2.0
2.44	87.1	75.7	60.4	39.1	10.2	1.5	0	0	0	0	0
5.35	98.3	95.3	89.4	87.0	76.3	59.8	41.0	24.2	12.9	5.2	1.9

Table III-3C: Uniform U Damage Surface Approximation

PGV (m/sec)	D(%)										
	.03	.06	.12	.25	.50	.75	1.00	1.25	1.5	1.75	2.0
2.44	95.2	90.5	80.9	60.3	20.6	0	0	0	0	0	0
5.35	98.3	96.6	93.1	85.7	71.3	57.0	42.7	28.3	14.0	0	0

**Table III-4: Exceedance Probability EP Extended Over
A Wide Range of PGV**

PGV (m/sec)		Damage Area Percent D_p (%)											
		.03	.06	.12	.25	.5	.75	1.0	1.25	1.5	1.75	2.0	
1.5	LN	69.9	53.6	36.6	12.6	0	0	0	0	0	0	0	0
	U	88.9	77.7	55.5	<u>7.2</u>	0	0	0	0	0	0	0	0
2.0	LN	81.1	67.3	50.6	26.4	3.8	0	0	0	0	0	0	0
	U	93.5	87.0	74.0	45.8	<u>0</u>	0	0	0	0	0	0	0
3.0	LN	91.7	83.0	69.9	53.6	22.8	6.2	1.1	0	0	0	0	0
	U	96.4	92.9	85.8	70.4	40.8	11.1	<u>0</u>	0	0	0	0	0
4.0	LN	95.9	90.6	81.1	72.8	49.2	25.8	10.3	3.1	0	0	0	0
	U	97.6	95.1	90.2	79.6	59.3	38.9	18.5	<u>0</u>	0	0	0	0
5.0	LN	97.9	94.5	87.7	84.2	70.7	51.6	32.0	16.6	7.4	2.6	0	0
	U	98.1	96.3	92.6	84.5	68.9	53.4	37.9	22.4	6.8	<u>0</u>	0	0
6.0	LN	98.8	96.6	91.8	90.8	84.2	72.7	57.3	40.5	25.4	14.0	6.8	0
	U	98.5	97.0	94.0	87.5	74.9	62.4	49.8	37.3	24.7	12.2	<u>0</u>	0
7.0	LN	99.3	97.8	94.3	94.6	91.8	86.0	76.8	64.6	50.5	36.3	23.8	0
	U	98.7	97.5	95.0	89.5	79.0	68.4	57.9	<u>47.4</u>	<u>36.9</u>	<u>26.4</u>	<u>15.8</u>	0
8.0	LN	99.6	98.5	96.0	96.0	95.8	93.2	88.7	81.8	72.4	61.0	48.5	0
	U	98.9	97.8	95.7	90.9	81.9	72.8	63.8	<u>54.7</u>	<u>45.6</u>	<u>36.6</u>	<u>27.5</u>	0

ATTACHMENT IV

SPREADSHEET FOR DRIP SHIELD DAMAGE ABSTRACTION FROM ROCKFALL

This spreadsheet contains the calculations that produce the drip shield damage abstraction for rock blocks in the nonlithophysal zones, as described in Section 6.6.1 of this report.

This spreadsheet is not reproduced here because it is very complex, with large tables and many graphics. This Attachment summarizes the contents of the 15 worksheets in the spreadsheet, including sources of input information and the outputs from the calculations. The reader is referred to the electronic file on CD-ROM to view the details of the calculations.

The following worksheets are included:

- (1) rockfall 1e-7
- (2) block information 1e-7
- (3) rockfall 1e-6
- (4) block information 1e-6
- (5) selected blocks
- (6) Impact information
- (7) intermediate pivot calculation
- (8) impact information by case
- (9) 1e-7 CDF fit
- (10) 1e-7 CDF chart
- (11) 1e-6 CDF fit
- (12) 1e-6 CDF chart
- (13) statistics
- (14) mode_PGV
- (15) frac_no_fail PGV

The inputs, outputs, and formulas used in each worksheet are described below.

(1) rockfall 1e-7

This worksheet is a copy of the results presented in DTN: MO0301MWD3DE27.003 and shows the overall amount of rockfall on a case by case basis for each combination of ground motion time history and synthetic fracture pattern. No new calculations have been done.

(2) block information 1e-7

This worksheet is a copy of the results presented in DTN: MO0301MWD3DE27.003 and shows the details of rockfall on a case by case basis for each combination of ground motion time history and synthetic fracture pattern. No new calculations have been done.

(3) rockfall 1e-6

This worksheet is a copy of the results presented in DTN: MO0305MWDNLRKF.001. and shows the overall amount of rockfall on a case by case basis for each combination of ground motion time history and synthetic fracture pattern. No new calculations have been done.

(4) block information 1e-6

This worksheet is a copy of the results presented in DTN: MO0305MWDNLRKF.001. and shows the details of rockfall on a case by case basis for each combination of ground motion time history and synthetic fracture pattern. No new calculations have been done.

(5) selected blocks

Here, the blocks selected for detailed structural response calculations and the results of these calculations are presented. The first two columns are a summary of Table 10 in this report, and the last 3 columns are a summary of Table 11 in this report. The only calculation is shown in Column 3, where the natural logarithm of column 2 is calculated. The Figure IV-1 shows the coordinate system for the finite-element grid. Note the rockfall angles.

(6) impact information

In this worksheet, the block information for the 1e-6 and 1e-7 cases are combined for convenience. Then, the information from "selected blocks" worksheet is used to calculate the damage due to rockfall for all other cases by log-linear interpolation. Figure IV-2 shows the angle sectors used to assign each impact angle to one of the classes given in the "selected blocks" worksheet.

Note that the spreadsheet coordinate system origin (Figure IV-2, see below) is at the vertical and horizontal center of the dripshield, whereas the finite element grid coordinate system origin (Figure IV-1) is at the horizontal center and bottom of the dripshield. Bins are created around the three discrete rockfall angles by bisection. The angles that define the bins are shown in Figure IV-2. Column O shows the class assignments based on each impact angle. In column P, the patch area is log-linear interpolated for the given kinetic energy level (column N) and the angle information (column O) from the six points given in the "selected blocks" worksheet. In column Q, the number of rockfall events with damage for each case is computed by simple summation.

(7) intermediate pivot calculation

In this worksheet, the pivot table feature of Excel is used to sum the total damaged patch area for all events for a given case (column AV).

(8) impact information by case

This worksheet presents the total damaged patch area on a case by case basis for both the 1e-6 per year and 1e-7 per year hazard levels. Column C shows the damaged patch area in m² (same as column AV in previous worksheet). This is converted into a percentage of the total area in Column D by dividing by 38.2667 m², which is the surface area of the drip shield (BSC 2003g, Section 5.5.1).

Also, summary statistics for the failed area calculations are calculated using the mean, median, standard deviation, min and max functions of Excel.

These statistics are also reported in Table 12 of the main text.

(9) 1e-7 CDF fit

This worksheet fits a triangular CDF to the logarithm of the percent failed patch area. Column A contains the patch area for the 1e-7 per year hazard level case. Column B contains the logarithm of Column A. Column C contains the fitted CDF. Column D contains the actual CDF, and column E is the difference between columns

C and D. The triangular distribution is assigned a minimum value of -3 (i.e., minimum percent failed patch area is 0.001%) and a maximum value of 2 (i.e., maximum percent failed patch area is 100%). The mode is unknown and estimated by minimizing the squares of column E using the "Solver" tool in excel. These calculations are shown in the block shaded in yellow.

Here - Actual CDF = rank / (n+1),

where rank = rank of observation in ascending order and n = number of observations.

Also, the f_no_fail is the fraction of cases with no failure, computed by counting the number of cases with zero failed patch area, and dividing by the number of observations.

(10) 1e-7 CDF chart

This worksheet compares the actual CDF to the fitted CDF. It is the source for Figure 10 in the main text.

(11) 1e-6 CDF fit

This worksheet fits a triangular CDF to the logairthm of the percent failed patch area.

Column A contains the patch area for the 1e-6 per year hazard level case. The methodology is the same as that used in the worksheet "1e-7 CDF fit".

(12) 1e-6 CDF chart

This worksheet compares the actual CDF to the fitted CDF. It is the source for Figure 9 in the main text.

(13) statistics

This worksheet summarizes the statistics of the fits for the 1e-7 and 1e-6 cases.

The information is taken from the worksheets "1e-7 CDF fit" and "1e-6 CDF fit".

Also included are the assumed damage for the 5e-5 per year hazard level case, as discussed in Section 6.6.1.4.

(14) mode_PGV

This worksheet shows a graph of the mode of percent failed area versus PGV using information from the previous worksheet. Also shown is the power-law fit to the damage using the "add trendline" option of Excel.

(15) mode_PGV

This worksheet shows a graph of the fraction of undamaged cases versus PGV using information from the previous worksheet. Also shown is the power-law fit to the damage using the "add trendline" option of Excel.

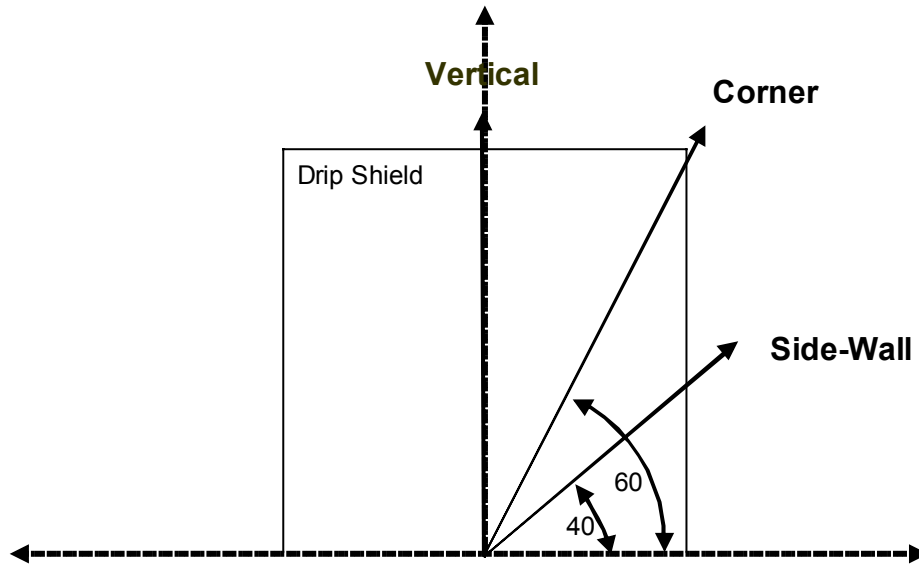


Figure IV-1. Coordinate System for the Finite-Element Grid

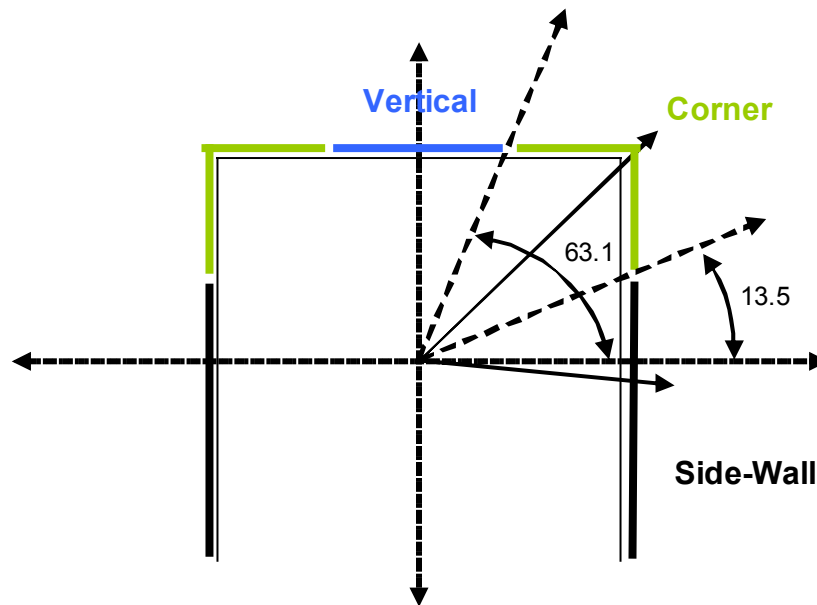


Figure IV-2. Spreadsheet Coordinate System

INTENTIONALLY LEFT BLANK

ATTACHMENT V

**REVIEW COMMENTS ON RESPONSE SURFACE FOR DRIP SHIELD DAMAGE
FROM ROCKFALL IN NONLITHOPHYSAL ZONE**

by R. P. Kennedy

**Review Comments on Response Surface
for Drip Shield Damage from Rockfall in
Nonlithophysal Zone²**

R.P. Kennedy
July 2003

V.1. Introduction

This report presents my review comments on the response surface for drip shield damage from rockfall in nonlithophysal zone developed and presented in Section 6.6.1 of Ref. V.1.

Damage is defined in terms of the percentage of damaged area D . The response surface defines the exceedance probability EP that the defined percentage of damaged area D might be exceeded as a function of the peak ground velocity PGV ,

V.1.1 Symbols and Units Used Herein

D	=	Percentage of damaged area (%)
D_M	=	Mode of D (%)
EP	=	Exceedance Probability (%)
EP_0	=	Zero damage exceedance probability (%)
EP_D	=	Damage area exceedance probability conditional on damage occurring (%)
NEP	=	Non-Exceedance Probability (%)
NEP_0	=	Zero damage non-exceedance probability (%)
NEP_D	=	Damage area non-exceedance probability conditional on damage occurring (%)
PGV	=	Peak ground velocity (m/sec)

V.1.2 Response Surface Recommended in Ref. V.1

Ref. V.1 recommends that the non-exceedance probability NEP_0 (%) for no damage be computed as a function of PGV (m/sec) by:

$$NEP_0 = 60.1\%(PGV)^{-0.735} \quad (V-1a)$$

Thus, the exceedance probability EP_0 for no damage is:

$$EP_0 = 100\% - NEP_0 \quad (V-1b)$$

Given the condition that damage occurs, Ref. V.1 recommends that the mode (most likely) percentage of damaged area D_M be computed from:

² Section numbers, table numbers, equation numbers, and reference numbers have been changed by adding a "V" to distinguish this attachment from the main body of the text. No other changes have been made to the content of this independent review, beyond these editorial changes.

$$D_M = 0.0088\%(PGV)^{3.7767} \quad (V-2)$$

Furthermore, Ref. V.1 recommends that a log-triangular distribution be used to define the conditional probability density function (PDF) on the percentage of damaged area D given the condition that damage occurs. This PDF is zero at -3 ($D = 0.001\%$) and at $+2$ ($D = 100\%$) and is maximum at D_M . Thus defining:

$$Y_M = \text{Log}(D_M) \quad (V-3a)$$

$$Y = \text{Log}(D) \quad (V-3b)$$

the conditional exceedance probability EP_D and non-exceedance probability NEP_D for any percentage of damaged area D are given by:

$$\underline{-3 < Y \leq Y_M}$$

$$NEP_D = \frac{20\%(Y + 3)^2}{Y_M + 3} \quad (V-4a)$$

$$EP_D = 100\% - NEP_D$$

$$\underline{2 > Y \geq Y_M}$$

$$EP_D = \frac{20\%(2 - Y)^2}{2 - Y_M} \quad (V-4b)$$

$$NEP_D = 100\% - EP_D$$

Lastly, the exceedance probability EP for any given damage area percentage D at a specified PGV is given by:

$$EP = (EP_0)(EP_D) \quad (V-5)$$

V.2. Review Comment

V.2.1 Comment on Drip Shield Damage Criteria

Ref. V.1 assumes that the drip shield is damaged over any areas where the computed residual stress due to rockfall impact exceeds 50% of yield. Considering the large uncertainty on what residual stress level might ultimately lead to damage, I don't believe that a single deterministic percentage of yield residual stress value should be used to define the damage area. Instead, uncertainty bounds and a distribution function between these bounds should be estimated for the residual stress associated with damage. Based on the discussion in Ref. V.1, the deterministic 50% of yield criteria appears to be very conservative.

V.2.2 Comment on Ref. V.1 Damage Surface Equations

The Ref. V.1 damage surface equations (summarized herein in Section 1.2) were based on nonlinear time history analyses for rockfalls associated with the following two ground motion levels:

$$\begin{aligned} \text{PGV} &= 2.44 \text{ m/sec} \\ \text{PGV} &= 5.35 \text{ m/sec} \end{aligned} \quad (\text{V-6})$$

The results are summarized in Worksheets (9) and (11) of the Excel Spreadsheet defined in Attachment IV of Ref. V.1. These results are ordered from lowest to highest percentage of damaged area D.

I have three comments on the development of the damage surface equations given in Ref. V.1.

First, I believe that it would be preferable for the NEP and EP for each of the ordered trial result tabulated in Worksheets (9) and (11) be computed from:

$$\begin{aligned} \text{NEP} &= \frac{n - 0.5}{N} (100\%) \\ \text{EP} &= 100\% - \text{NEP} \end{aligned} \quad (\text{V-7})$$

where N is the total number of trials (60 in worksheet (9) for PGV = 5.35 m/sec, and 51 in Worksheet (11) for PGV = 2.44 m/sec) and n is the ordered trial number.

Secondly, although Ref. V.1 does compare the conditional NEP_D computed by Eqn. (V-4) versus the tabulated data, no overall comparison is made for EP computed from Eqn. (V-5) versus the Worksheet data. Therefore, it is difficult for the reviewer to judge the overall adequacy of the Ref. V.1 damage surface even at PGV of 2.44 m/sec and 5.35 m/sec. In order to rectify this deficiency, I have compared the data base results (Da) with Ref. V.1 with the predicted (Pr) EP for various D in Table V-1. I recommend that Ref. V.1 should contain a table similar to Table V-1.

Third, even though the Ref. V.1 damage surface equation was developed only from multiple analyses at PGV of 2.44 m/sec and 5.35 m/sec, no PGV bounds are placed on the proposed damage surface.

I make some recommendations in Section V.3 concerning the Ref. V.1 damage surface for drip shield damage from rockfall in nonlithophysal zone.

V.3. Recommendations

For PGV = 2.44 m/sec, Table V-1 shows good agreement with the data for the Ref. V.1 predicted damage surface for all D from zero to 30%. For PGV = 5.35 m/sec, the agreement is also good up to D of about 1.5%. Above D of about 1.5%, the predicted damage surface becomes very conservative. This over prediction of EP occurs within a potentially important

region (EP between 1% and 50%) of the damage surface. It could lead to significant overestimation of the annual probability of exceeding higher D percentages. So long as this potential conservatism is acceptable, I consider the Ref. V.1 damage surface to be more than adequate within the following range of PGV values.

Data is only available to define the damage surface at PGV values of 2.44 m/sec and 5.35 m/sec. Without data at other PGV values, I judge that it is highly suspect to extend the predicted damage surface beyond the range of:

$$1.5 \text{ m/sec} \leq \text{PGV} \leq 6.0 \text{ m/sec} \quad (\text{V-8})$$

References

V.1. *Seismic Consequences Abstraction Report, Rev00E, Draft, July 2003*

Table V-1: Exceedance Probabilities EP for Various Damage Area Percentages D and Peak Ground Velocities PGV

PGV (m/sec)		Damage Area Percent D _p (%)								
		0	0.01	0.03	0.10	.30	1.0	3.0	10.0	30.0
2.44	Da	75.5	69.9	53.9	45.9	41.1	20.4	10.9	7.0	1.2
	Pr	68.8	63.1	56.3	45.9	33.8	21.2	12.3	5.3	1.5
5.35	Da	80.8	79.3	68.3	65.8	64.8	48.0	17.2	7.5	2.3
	Pr	82.5	78.0	72.7	64.8	55.1	42.3	<u>28.5</u>	<u>12.6</u>	<u>3.5</u>

Da = Data
Pr = Predicted

INTENTIONALLY LEFT BLANK

ATTACHMENT VI

**REVIEW COMMENTS ON RESPONSE SURFACE FOR DRIP SHIELD DAMAGE
FROM VIBRATORY GROUND MOTION**

by R. P. Kennedy

Review Comments on Response Surface for Drip Shield Damage from Vibratory Ground Motion³

R.P. Kennedy
July 2003

VI.1. Introduction

This report presents my review comments on the response surface for drip shield damage from vibratory ground motion developed and presented in Section 6.6.3 of Ref. VI.1.

Damage is defined in terms of the percentage of damaged area D . The response surface defines the exceedance probability EP that the defined percentage of damaged area D might be exceeded as a function of the peak ground velocity PGV .

VI.1.1 Symbols and Units Used Herein

D	=	Percentage of damaged area (%)
D_{UB}	=	Upper bound on D (%) as a function of PGV
EP	=	Exceedance Probability (%)
NEP	=	Non-Exceedance Probability (%)
PGV	=	Peak ground velocity (m/sec)
U	=	Uniform damage surface defined by Eqns. (VI-1) and (VI-2)
LN	=	Lognormal damage surface defined by Eqn. (VI-4)

VI.1.2 Response Surface Recommended in Ref. VI.1

Ref. VI.1 defines an upper bound D_{UB} (%) on D as a function of PGV (m/sec) by:

PGV Value (m/s)	D_{UB} %
0.0	0
0.55	0
2.44	2.68
5.35	50
20	50

(VI-1)

At any given PGV , Ref. VI.1 assumes the percentage of damaged area D (%) is uniformly distributed between zero and D_{UB} . Thus, the exceedance probability EP (%) for any specified D conditional on the given PGV is defined by:

³ Section numbers, table numbers, equation numbers, and reference numbers have been changed by adding a "VI" to distinguish this attachment from the main body of the text. No other changes have been made to the content of this independent review, beyond these editorial changes.

$$EP = \left[1 - \frac{D}{D_{UB}} \right] (100\%) \quad (VI-2)$$

The damage surface defined by Eqns. (VI-1) and (VI-2) will be called herein the “Uniform damage surface and will be represented in the attached tables by the symbol U. In the following sections, I will present my review comments on this at each of the PGV values tabulated in Eqn. (VI-1).

VI.2 Damage Surface At PGV=2.44m/sec

VI.2.1 Comment on Drip Shield Damage Criteria Used At PGV=2.44m/sec

Ref. VI.1 assumes that the drip shield is damaged over any areas where the computed residual stress due to rockfall impact exceeds 50% of yield. Considering the large uncertainty on what residual stress level might ultimately lead to damage, I don’t believe that a single deterministic percentage of yield residual stress value should be used to define the damage area. Instead, uncertainty bounds and a distribution function between these bounds should be estimated for the residual stress associated with damage. Based on the discussion in Ref. VI.1, the deterministic 50% of yield criteria appears to be very conservative.

VI.2.2 Comment on Uniform Damage Surface Equations At PGV = 2.44 m/sec

The percentage damage area D was computed in 14 simulations performed using PGV=2.44m/sec ground motion records. The results are presented in Table 14 of Ref. VI-1. These results are shown herein in Table VI-1 ordered from the lowest to highest D. Also shown in Tables VI-1 is the non-exceedance probability NEP corresponding to each of these ordered results as computed from:

$$NEP = \frac{n - 0.5}{N} (100\%) \quad (VI-3)$$

where N is the total number of trials and n is the ordered trial number.

Table VI-2 compares these data results with percent damage areas predicted from the Uniform distribution U at PGV=2.44m/sec. It can be seen that the Uniform distribution defined in Ref. VI.1 is very conservative for percent damage areas D from about 0.50 percent and higher. It could lead to significant overestimation of the annual probability of exceeding D percentages greater than 0.50 percent.

A much better fit at PGV=2.44m/sec is provided by the following lognormal distribution:

Lognormal LN

Median:	$D_{50} = 0.55\%$	(VI-4)
Log. Std. Dev.:	$\beta = 0.85$	

Table VI-2 also shows the damage area percentage predicted by this Lognormal distribution LN. This Lognormal distribution predicts the simulation results well, although it also tends to overpredict the exceedance probability EP for D greater than about 1.25 percent. However, this overprediction is much less than for the U distribution.

If the conservatism of the Uniform distribution U is unacceptable, one should consider using the Lognormal distribution at $PGV=2.44\text{m/sec}$.

VI.3 Damage Surface At $PGV=5.35\text{m/sec}$ and Higher

Five simulations were performed for ground motions with $PGV=5.35\text{m/sec}$. Ref.-VI.1 reports that large plastic deformations of the drip shield and separation between drip shields on the order of 10 to 25 percent of the length of the drip shield occurred in each of the simulations.

This limited data is not a very adequate basis for estimating the exceedance probability EP for various percent damage areas D at $PGV=5.35\text{m/sec}$. All that one can really say is that D will be large.

The upper bound $D_{UB}=50$ percent in Table 15 of Ref. VI-1 is probably reasonable at $PGV=5.35\text{m/sec}$. However, a Uniform distribution, with a lower bound of zero is not reasonable in my opinion. Considering increased corrosion rates due to high residual stresses as well as drip shield separation, I would expect a lower bound on a Uniform distribution should be in excess of 10 percent at $PGV=5.35\text{m/sec}$. A more detailed review of the results of the five simulations might allow this lower bound to be better established.

Considering both increased corrosion rates and drip shield separations, I would expect both the upper bound and lower bound on a Uniform distribution for D to further increase as PGV is increased above 5.35m/sec . I have no idea as to how one might estimate this further increase. However, the percent damage areas at $PGV=5.35\text{m/sec}$ for the drip shield might be sufficiently high that further increases in D may not have much impact on the overall risk assessment. The primary conclusion is that the drip shields are likely to be severely damaged at a $PGV=5.35\text{m/sec}$ or higher.

VI.4 Damage Surface At $PGV=0.55\text{m/sec}$

Ref. VI.1 assumes no damage occurs to the drip shield at a PGV of 0.55m/sec . This assumption should be validated by performing a few simulations using $PGV=0.55\text{g}$ ground motion.

References

VI.I *Seismic Consequences Abstraction Report, Draft, Rev00E, July 2003*

**Table VI-1: Percentage Damaged Area D
Obtained From Nonlinear Analyses for
PGV = 2.44 m/sec**

NEP(%)	D(%)
3.57	0.12
10.71	0.14
17.86	0.26
25.0	0.26
32.14	0.27
39.29	0.30
46.43	0.50
53.57	0.65
60.71	0.67
67.86	0.98
75.0	1.12
82.14	1.19
89.29	1.25
96.43	2.13

**Table VI-2: Exceedance Probabilities EP for
Various Damage Area Percentages D at
PGV=2.44m/sec**

	D%								
	0.12	0.25	0.50	0.75	1.00	1.25	1.50	1.75	2.00
Data	96.4	82.7	53.6	37.4	31.1	10.7	8.7	6.7	4.6
Uniform U	95.5	90.7	<u>81.3</u>	<u>72.0</u>	<u>62.7</u>	<u>53.4</u>	<u>44.0</u>	<u>34.7</u>	<u>25.4</u>
Lognormal LN	96.3	82.3	54.5	35.8	24.1	16.7	11.9	8.6	6.4

INTENTIONALLY LEFT BLANK

ATTACHMENT VII

SPREADSHEET FOR FAULT DISPLACEMENT DAMAGE ABSTRACTION

Assessment of Waste Package Failure Due To Fault Displacement

This spreadsheet summarizes the supporting calculations for Section 6.8 of this report.

Table VII-1. - Drip Shield Clearance Calculation (all units in mm) (basis for Table 19)

		<u>Source or Formula</u>
Drift diameter (Dd)	5500	BSC 2003i
Invert thickness (Ti)	806	BSC 2003i
Drip Shield Height - Exterior (Hdse)	2886	BSC 2003f
Drip Shield Height - Interior (Hdsi)	2716	BSC 2003f
Clearance above Drip Shield (Hdsc)	1808	= Dd - Hdse - Ti

**Table VII-2. Waste Package to Drip Shield Clearance (basis for Table 20)
(all units in mm - WP dimensions from BSC 2003j, Table 1)**

<u>Package</u>	<u>Diameter</u>	<u>Length</u>	<u>Clearance</u>
44-BWR	1674	5165	1042
24-BWR	1318	5105	1398
21-PWR	1644	5165	1072
12-PWR	1330	5651	1386
Naval-Long	1949	6065	767
Naval-Short	1949	5430	767
5DHLW/DOE SNF --Short	2110	3590	606
5DHLW/DOE SNF --Long	2110	5217	606
2-MCO/2-DHLW	1814	5217	902

The formula for calculating the clearance is given by Hdsi - Diameter

Table VII-3. Maximum Allowable Fault Displacement (in mm) (basis for Table 21)

Two values are provided - with and without drift collapse. In both cases, the behavior of the invert and pallet is approximated by treating the emplacement pallet as collapsed into the invert. No further collapse of the invert is accounted for. With drift collapse, maximum allowable displacement = $H_{dsi} - \text{Diameter}$
 Without drift collapse, maximum allowable displacement = $H_{dsi} - \text{Diameter} + H_{dsc}$
 where H_{dsc} equals 1808-mm (see Table VII-2).

Package	with collapse	w/o collapse
44-BWR	1042	2850
24-BWR	1398	3206
21-PWR	1072	2880
12-PWR	1386	3194
Naval-Long	767	2575
Naval-Short	767	2575
5DHLW/DOE SNF - Short	606	2414
5DHLW/DOE SNF - Long	606	2414
2-MCO/2-DHLW	902	2710

Table VII-4. Fault Displacement For Mean Hazard Curves (in cm) (basis for Table 23) Based on Probabilistic Seismic Hazard Analyses (PSHA) (CRWMS M&O 1998)

DTN: MO0004MWDRIFM3.002).

The values for the 1st two probabilities are from Table 8-1 of the cited reference. The values for the latter three probabilities are obtained from interpolation within DTN MO0004MWDRIFM3.002 and in Figures 8-2 through 8-14 for the appropriate fault.

Fault	Mean Annual Exceedance Probability (-)				
	1.00E-04	1.00E-05	1.00E-06	1.00E-07	1.00E-08
1 - Bow Ridge	<0.1	7.8	72	220	600
2 - Solitario Canyon (60 m offset)	<0.1	32.0	190	500	>1000
3 - Drill Hole Wash	<0.1	<0.1	17	80	240
4- Ghost Dance	<0.1	<0.1	13	58	160
5 - Sundance	<0.1	<0.1	6	42	~145
6 - Unnamed	<0.1	<0.1	13	70	210
7a	<0.1	<0.1	2	20	~75
7b	<0.1	<0.1	1	6	9
7c	<0.1	<0.1	0.1	<1	<1
7d	<0.1	<0.1	<0.1	<0.1	<0.1
8a	<0.1	<0.1	2	20	~75
8b	<0.1	<0.1	1	6	9
8c	<0.1	<0.1	0.1	<1	<1
8d	<0.1	<0.1	<0.1	<0.1	<0.1
9	<0.1	0.1	11	70	200

Table VII-5. Intersections of Known Faults With Emplacement Drifts (basis for Table 22)

Output from the Multi-scale TH model (DTN: LL030704623122.031, tspa03.mesh03-150w) provides information on location of fault zones within each emplacement drift tunnel along with whether that location is within the lower lithophysal zone or not. To correlate this information to the specific fault in question, the location coordinates must be compared to a map of the geologic fault locations (e.g., BSC 2003o). The results of this comparison are summarized below. For each fault, the specific tunnels impacted in the lower lithophysal and other zones are listed.

Abandoned Wash Fault (comes off Ghost Dance fault)

- Only intersects drifts 5-15 through 5-27, which are in the contingency area

Sundance Fault

<i>lower lith</i>	<i>other</i>
1-8	none
1-7	
1-6	

Drill Hole Wash Fault

<i>lower lith</i>	<i>other</i>
3-2	2-17E
3-1	2-16E
2-10W	2-15E
2-9W	2-14E
2-8W	2-13E
2-7W	2-12E
2-6W	2-11E
2-5W	2-10E
	2-9E

Pogany Wash Fault

<i>lower lith</i>	<i>other</i>
2-2W	2-7E
2-1W	2-6E
2-5E	
2-4E	
2-3E	
2-2E	
2-1E	

Sevier Wash Fault

<i>lower lith</i>
2-2E

**Table VII-6. Design Basis Waste Package Dimensions and Inventory (basis for Table 24)
(dimensions repeated from Table VII-2; waste package inventory from BSC 2003k, Table 11)**

WP Configuration	WP Length (m)	WP Diameter (m)	Nominal Quantity
21 PWR with APs	5.165	1.644	4299
21 PWR with CRs	5.165	1.644	95
12 PWR AP Long	5.651	1.330	163
44 BWR with APs	5.165	1.674	2831
24 BWR with APs	5.105	1.318	84
5 DHLW Short/1 DOE SNF Short	3.590	2.110	1147
5 DHLW Long/1 DOE SNF Long	5.217	2.110	1406
5 DHLW Long/1 DOE SNF Short	5.217	2.110	31
5 HLW Long Only	5.217	2.110	679
2-MCO/2-DHLW	5.217	1.814	149
Naval-Short	5.430	1.949	144
Naval-Long	6.065	1.949	156

NOTES: The diameter of DHLW packages and HLW package is taken to be that of the DHLW packages in Table VII-2. The length of the DHLW Short package is taken to be that of the 5 DHLW/DOE SNF - Short package in Table VII-2. The length of the DHLW Long and HLW Long packages is taken to be that of the 5 DHLW/DOE SNF - Long package in Table VII-2.
AP = absorber plate; CR = control rod

Table VII-7. Simplified Groups of Waste Packages (basis for Table 25)

<u>WP</u> <u>Configuration</u>	Average	Total	<u># packages</u>	<u>%</u>
	<u>Length (m)</u>	<u>Length (m)</u>		
PWR	5.1824	23616.123	4557	41.9%
BWR	5.1633	15050.935	2915	26.7%
Naval	5.760	1728.06	300	3.1%
HLW	4.670	15934.235	3412	28.3%
Total		56329.353	11184	100.0%

Total Length is given by package length times number of packages, summed over each package type in the group.

Average length is given by Total length / Total number of packages in group.

% = Total length for that group / Total length for all groups.

The PWR group includes the 21 PWR AP, 21 PWR CR, and 12 PWR AP Long packages.

The BWR group includes the 44 BWR AP and the 24 BWR AP packages.

The Naval group includes the Naval-Short and Naval-Long packages.

The HLW group includes all packages containing HLW.

Table VII-8. Fault Exceedance Probabilities That Cause Failure in the Lower Lithophysal Zone (basis for Table 27)

Using Figures 8-2 through 8-14 of the PSHA, along with the maximum allowable fault displacements for each simplified waste package group as summarized in Table VII-3, one can determine the fault displacement event probability required to cause failure for each waste package type. This is done as follows:

- the allowable fault displacement is given by the value from Table VII-3 (w/ drift collapse)
- using Figures 8-4 (Drill Hole Wash), 8-6 (Sundance), and 8-8 (site 7a) the probability associated with that magnitude of fault displacement is determined from the mean hazard curve
- this is done for each waste package group
- note that relative to the accuracy of these figures, the BWR and PWR groups are shown with the same probability
- The Drill Hole Wash results apply to Pagany Wash and Sevier Wash.

Fault	HLW	Naval	BWR	PWR
Sundance	$< 5 \times 10^{-8}$	$< 4 \times 10^{-8}$	$< 3 \times 10^{-8}$	$< 3 \times 10^{-8}$
Drill Hole Wash	$< 2 \times 10^{-7}$	$< 1 \times 10^{-7}$	$< 6 \times 10^{-8}$	$< 6 \times 10^{-8}$
Pagany Wash	$< 2 \times 10^{-7}$	$< 1 \times 10^{-7}$	$< 6 \times 10^{-8}$	$< 6 \times 10^{-8}$
Sevier Wash	$< 2 \times 10^{-7}$	$< 1 \times 10^{-7}$	$< 6 \times 10^{-8}$	$< 6 \times 10^{-8}$
7a/8a	$< 2 \times 10^{-8}$	N/A	N/A	N/A

Table VII-9. Expected Number of Waste Packages Emplaced on Faults In Lower Lithophysal Zone (basis for Table 28)

Table VII-5 can be used to determine the total number of waste packages impacted by each fault in the lower lith (based on number of fault intersections with each tunnel). The results of Table VII-7 can then be used to calculate the expected number of waste packages of each type (simplified grouping) that would be on a fault. These results are summarized below.

	<u>Total</u>	<u>PWR</u>	<u>BWR</u>	<u>Naval</u>	<u>HLW</u>
Sundance	3	1.26	0.80	.09	0.85
Drill Hole, etc.	16	6.71	4.28	.49	4.53
7a/8a	117.3	49.18	31.34	3.60	33.18

Table VII-10. Expected Waste Packages Failures Versus Mean Annual Exceedance Probability (basis for Table 29)

The results of Table VII-8 and Table VII-9 can now be combined to provide the expected number of packages failed versus probability.

Annual Exceed. Probability (1/yr)	Expected Number of Waste Package Failures				
	PWR	BWR	Naval	HLW	Total
> 2×10^{-7}	0	0	0	0	0
1×10^{-7} to 2×10^{-7}	0	0	0	4.53	4.53
6×10^{-8} to 1×10^{-7}	0	0	0.49	4.53	5.02
5×10^{-8} to 6×10^{-8}	6.71	4.28	0.49	4.53	16.00
4×10^{-8} to 5×10^{-8}	6.71	4.28	0.49	5.37	16.85
3×10^{-8} to 4×10^{-8}	6.71	4.28	0.58	5.37	16.94
2×10^{-8} to 3×10^{-8}	7.97	5.08	0.58	5.37	19.00
1×10^{-8} to 2×10^{-8}	7.97	5.08	0.58	38.56	52.18

INTENTIONALLY LEFT BLANK

ATTACHMENT VIII

**REPRESENTATION OF ALEATORY AND EPISTEMIC UNCERTAINTY IN THE
CALCULATION OF EXPECTED DOSE FROM SEISMIC EVENTS AT THE
PROPOSED YUCCA MOUNTAIN FACILITY FOR THE DISPOSAL OF HIGH LEVEL
RADIOACTIVE WASTE**

BY J. C. HELTON

Representation of Aleatory and Epistemic Uncertainty in the Calculation of Expected Dose from Seismic Events at the Proposed Yucca Mountain Facility for the Disposal of High Level Radioactive Waste

J. C. Helton

Department of Mathematics and Statistics, Arizona State University, Tempe, AZ 85287-1804 USA

and

Department 6849, MS 0779
Sandia National Laboratories
Albuquerque, NM 87185-0779 USA

VIII.1 INTRODUCTION

The following presentation provides a conceptual description of the calculation of expected doses (mrem/yr) to reasonably maximally exposed individuals (RMEIs) that result from potential seismic events at the proposed Yucca Mountain (YM) facility for the disposal of high-level radioactive waste.^{1, 2} A conceptual and representational distinction is made between the effects and implications of aleatory and epistemic uncertainty in the assessment of the effects of seismic events at the YM facility, with aleatory uncertainty arising from the many possible seismic events that could occur over a time period of interest (e.g., 0 to 10,000 yr) and epistemic uncertainty arising from a lack of knowledge with respect to quantities used in the characterization of aleatory uncertainty or in the calculation of doses given the occurrence of a seismic event.³⁻⁶ Due to the low likelihood of seismic events at the YM facility, traditional, integration-based importance sampling is introduced as a means to facilitate the computational determination of expected doses (Ref.7, Section 4.3.1).

The presentation is organized as follows. Initially, the calculation of expected doses that result from aleatory uncertainty in the occurrence and properties of seismic events is considered (Sect. VIII.2). Such doses are defined by an integral over possible seismic events, and importance sampling is introduced as a means to accelerate the convergence of numerical approximations to this integral. Then, the calculation of expected doses that result from both aleatory uncertainty and epistemic uncertainty is considered (Sect. VIII.3). These doses are defined by a double integral, with one integral over the possible seismic events that could occur and the other integral over imprecisely known analysis inputs. Thus, one integral relates to aleatory uncertainty, and the other integral relates to epistemic uncertainty. Two different, sampling-based strategies for the numerical evaluation of the double integral that defines expected dose from aleatory and epistemic uncertainty are described, and the prior use of these strategies in the determination of expected dose from igneous events at the YM facility is indicated. Finally, the presentation ends with a discussion of the representation of expected doses when synergisms between multiple seismic events are possible (Sect. VIII.4).

This presentation is very formal, with expected doses being defined by integrals over various spaces related to aleatory and epistemic uncertainty. However, it is important to recognize that every integral and every quantity used in association with an integral in this presentation is an entity that must be defined, dealt with, and numerically evaluated in the actual computational implementation of a performance assessment for the YM facility. The formal representations given here can be used as a starting point in documentation that clearly connects the overall structure of analyses of expected doses from seismic events at the YM facility with descriptions that provide the necessary finer detail required for the complete and unambiguous specification of the individual parts of such an analysis. In particular, documentation can be written that provides two-way mapping (i.e., from general to specific and also from specific to general) between the overall structure of an analysis and detailed descriptions of specific parts of that analysis.

For example, dose to the RMEI at time τ from a seismic event at time t with a peak ground velocity of v appears simply as a function $D(\tau | t, v)$ in the integrals that define expected dose in this presentation. This usage clearly

indicates how the dose $D(\tau|t, \nu)$ to the RMEI enters into the calculation of expected dose but tells nothing about how this dose is actually calculated. In a complete documentation of the analysis, a formal description of the overall analysis would provide a forward reference to where $D(\tau|t, \nu)$ was defined, and the location at which $D(\tau|t, \nu)$ was defined would provide a backward reference to the description of the overall analysis that clearly indicated the use of $D(\tau|t, \nu)$ in the calculation of expected dose and other summary quantities of interest. Further, complete analysis documentation would also describe the numerical procedures used to estimate both $D(\tau|t, \nu)$ and the integrals involving $D(\tau|t, \nu)$ that determine expected dose. In this way, the interested individual would be provided with a road map to the complete analysis that clearly tied general structure, specific detail, and numerical procedures together.

VIII.2 EXPECTED DOSE FROM ALEATORY UNCERTAINTY

The development of results in this section and the next section (Sect. VIII.3) relating to expected doses from seismic events at the YM facility is based on the following three assumptions: (i) dose to the RMEI at time τ (yr) from a seismic event occurring prior to τ depends only on the time of occurrence t (yr) and peak ground velocity (PGV) ν (m/s) at the waste drifts associated with that seismic event (see Assumption 5.4), (ii) the occurrence of a seismic event has no effect on the dose to the RMEI that derives from any subsequent seismic event, and (iii) the occurrence of seismic events follows a Poisson process (see Assumption 5.5) characterized by a function $\lambda_A(\nu)$ (1/yr) of PGV ν (Fig. VIII-1), where $\lambda_A(\nu)$ is the annual exceedance frequency for a PGV of size ν and

$$prob_A [n|\Delta t, \lambda_A(\nu)] = \left\{ \frac{[\lambda_A(\nu) \Delta t]^n}{n!} \right\} \exp[-\lambda_A(\nu) \Delta t] \quad (\text{VIII.2.1})$$

is the probability that exactly n seismic events with a PGV exceeding ν occur over a time interval of length Δt (yr) (Ref. 8, pp. 172-173). The synergisms between multiple seismic events are considered in Section VIII.4, so it is not included as formal assumption in Section 5 of the main body of this report.

With respect to notation, this presentation will use a subscript A to designate quantities that relate primarily to aleatory uncertainty and, beginning in Sect. VIII.3, a subscript E to designate quantities that relate primarily to epistemic uncertainty. For notational convenience, it is also assumed that

$$D(\tau|t, \nu) = \text{dose (mrem/yr) to the RMEI at time } \tau \text{ from a seismic event at time } t \text{ with a PGV of } \nu \quad (\text{VIII.2.2})$$

and that $D(\tau|t, \nu) = 0$ mrem/yr for $\tau < t$. In the computational implementation of an actual analysis for the YM facility, the function $D(\tau|t, \nu)$ would be a complex model implemented through the linked operation of several computer programs. However, the functional representation in Eq. (VIII.2.2) is all that is needed for the present discussion.

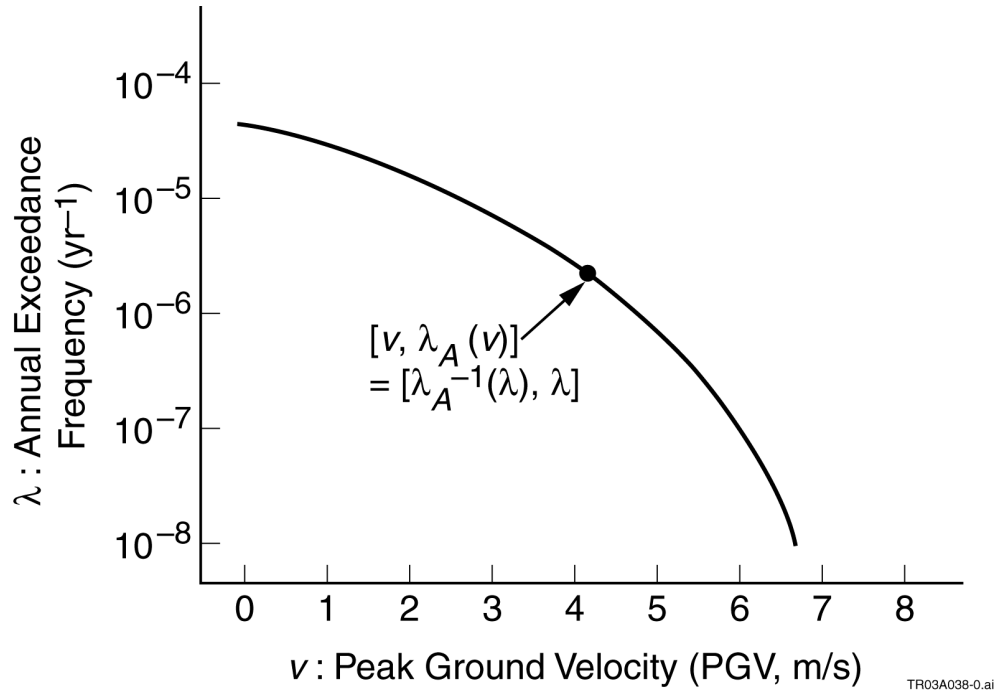


Fig. VIII-1. Representation of aleatory uncertainty in PGV at disposal drifts induced by seismic events, with (i) $[v, \lambda_A(v)]$ representing a point on the exceedance frequency curve, where v is a PGV from the abscissa and $\lambda_A(v)$ is the corresponding exceedance frequency on the ordinate, and (ii) $[\lambda_A^{-1}(\lambda), \lambda]$ representing the same point on the exceedance frequency curve, where λ is the exceedance frequency from the ordinate and $\lambda_A^{-1}(\lambda)$ is the corresponding PGV on the abscissa.

The Poisson process characterized by $\lambda_A(v)$ results in an uncountably infinite number of possible dose curves $[D(\tau|t, v)]$, with one curve resulting for each possible occurrence time, PGV pair $[t, v]$ (Fig. VIII-2). One way to summarize these dose curves is by calculating an expected dose at each time τ . Given the preceding assumptions, the expected dose $E_A[D(\tau|t, v)]$ to the RMEI at time τ from seismic events is given by

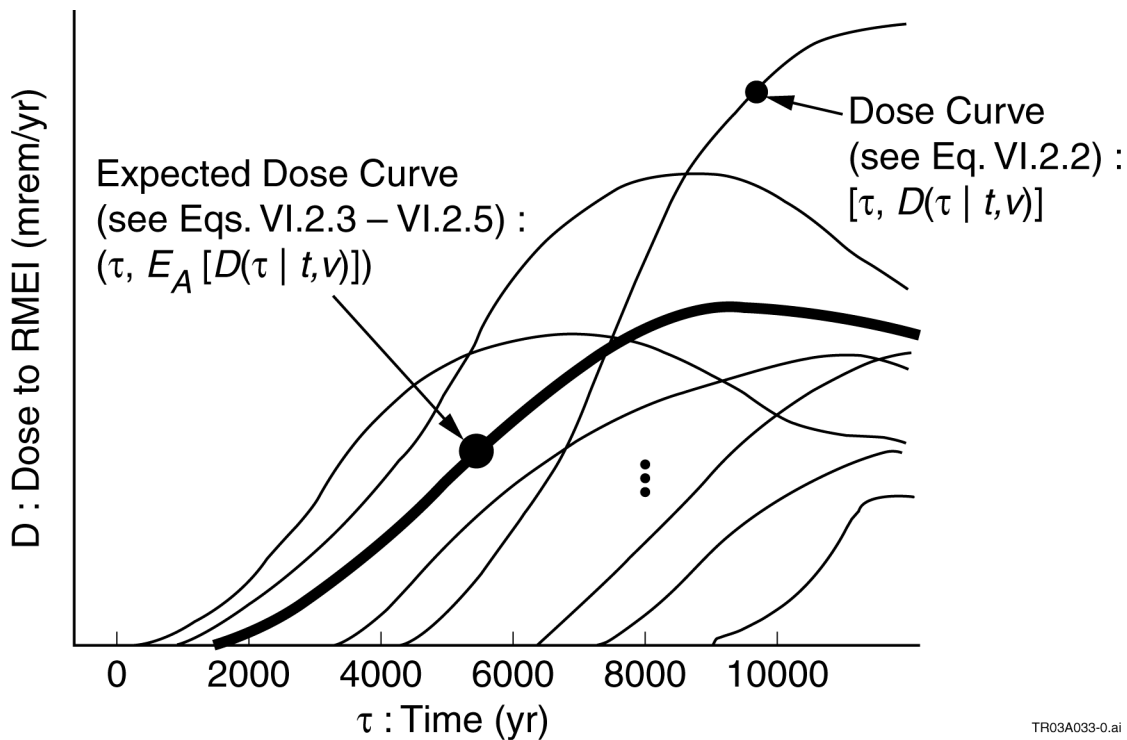
$$E_A[D(\tau|t, v)] = \int_{tMIN}^{\tau} \int_{vMIN}^{vMAX} D(\tau|t, v) [-d\lambda_A(v)/dv] dv dt \quad (VIII.2.3)$$

$$= \int_{tMIN}^{\tau} \int_{\lambdaMIN}^{\lambdaMAX} D(\tau|t, \lambda_A^{-1}(\lambda)) d\lambda dt \quad (VIII.2.4)$$

where (i) $[tMIN, tMAX]$ defines the time interval under consideration (e.g., $tMIN = 0$ yr, $tMAX = 10,000$ yr) and $tMIN < \tau \leq tMAX$, (ii) $[vMIN, vMAX]$ and $[\lambdaMIN, \lambdaMAX]$ define the ranges of PGVs and exceedance frequencies for PGVs, respectively, with $\lambda_A(vMIN) = \lambdaMAX$ and $\lambda_A(vMAX) = \lambdaMIN$ (e.g., $vMIN = 0.388$ m/s, $vMAX = 10.73$ m/s, $\lambdaMIN = 10^{-8}$ yr⁻¹, $\lambdaMAX = 10^{-4}$ yr⁻¹), (iii) the double integral in Eq. (VIII.2.3) is defined by the limit of the approximating sums

$$\begin{aligned}
 E_A [D(\tau | t, v)] &\cong \sum_{i=1}^{nTM} \sum_{j=1}^{nPGV} D(\tau | t_i, v_j) [\lambda_A(v_{j-1}) - \lambda_A(v_j)] \Delta t_i \\
 &= \sum_{i=1}^{nTM} \sum_{j=1}^{nPGV} D(\tau | t_i, v_j) \left[-\frac{\lambda_A(v_j) - \lambda_A(v_{j-1})}{\Delta v_j} \right] \Delta v_j \Delta t_i \\
 &\cong \sum_{i=1}^{nTM} \sum_{j=1}^{nPGV} D(\tau | t_i, v_j) [-d\lambda_A(v)/dv] \Delta v_j \Delta t_i
 \end{aligned}
 \tag{VIII.2.5}$$

with $tMIN = t_0 < t_1 < \dots < t_{nTM} = \tau$, $vMIN = v_0 < v_1 < \dots < v_{nPGV} = vMAX$, $\Delta t_i = t_i - t_{i-1}$, and $\Delta v_j = v_j - v_{j-1}$, and (iv) the double integral in Eq. (VIII.2.4) follows from a change of variables in the integral involving PGV in Eq. (VIII.2.3). The validity of the integral representations for $E_A[D(\tau | t, v)]$ in Eqs. (VIII.2.3) and (VIII.2.4) depends on either assumption (ii) indicated in the first paragraph of this section being true or $\lambdaMAX(\tau - tMIN)$ being sufficiently small to render the likelihood of two or more seismic events over the time interval $[tMIN, \tau]$ inconsequential (see Eq. (VIII.2.1)).



TR03A033-0.ai

Fig. VIII-2. Possible time-dependent dose curves $[\tau, D(\tau | t, v)]$ (see Eq. (VIII.2.2)) to RMEI due to seismic events of different PGVs occurring at different times (note: due to the delays associated with groundwater transport, nonzero doses commence at a time subsequent to the occurrence of the initiating seismic events) and associated mean dose curve $(\tau, E_A[D(\tau | t, v)])$ (see Eqs. (VIII.2.3) – (VIII.2.5)).

As shown in Eqs. (VIII.2.3) and (VIII.2.4), expected dose $E_A[D(\tau | t, v)]$ is defined by double integrals involving time and PGV (i.e., Eq. (VIII.2.3)) or time and exceedance frequency λ (i.e., Eq. (VIII.2.4)). Thus, in concept, techniques for the numerical evaluation of integrals (e.g., appropriate forms of Simpson’s rule or the trapezoidal rule) could be used to estimate $E_A[D(\tau | t, v)]$. An alternative approach to the estimation of $E_A[D(\tau | t, v)]$ is to use a Monte Carlo procedure for the evaluation of the integrals in Eqs. (VIII.2.3) and (VIII.2.4) (Ref. 7, Sect. 4.2.2), with this alternative approach currently favored for use in performance assessment (PA) for the YM facility.

The integral in Eq. (VIII.2.4) is used for illustration; analogous procedures can be applied to the integral in Eq. (VIII.2.3). Specifically, the representation for $E_A[D(\tau|t, \nu)]$ in Eq. (VIII.2.4) can be reformulated as

$$E_A[D(\tau|t, \nu)] = \int_{tMIN}^{tMAX} \int_{\lambda MIN}^{\lambda MAX} D(\tau|t, \lambda_A^{-1}(\lambda)) d\lambda dt \quad (\text{VIII.2.6})$$

$$= \int_{tMIN}^{tMAX} \int_{\lambda MIN}^{\lambda MAX} \left[\frac{D(\tau|t, \lambda_A^{-1}(\lambda))}{\lambda IMP(\lambda) t IMP(t)} \right] \lambda IMP(\lambda) t IMP(t) d\lambda dt \quad (\text{VIII.2.7})$$

$$\cong \sum_{i=1}^{nIMP} \left[\frac{D(\tau|t_i, \lambda_A^{-1}(\lambda_i))}{\lambda IMP(\lambda_i) t IMP(t_i)} \right] / nIMP \quad (\text{VIII.2.8})$$

where (i) Eq. (VIII.2.6) is an immediate reformulation of Eq. (VIII.2.4) based on the convention that $D(\tau|t, \nu) = 0$ mrem/yr for $\tau < t$ and is introduced so that the importance sampling procedure described in Eqs. (VIII.2.7) and (VIII.2.8) can sample on $[tMIN, tMAX]$ rather than on $[tMIN, \tau]$, (ii) Eq. (VIII.2.7) is the standard important sampling transformation used in the Monte Carlo evaluation of an integral with $\lambda IMP(\lambda)$ and $t IMP(t)$ positive valued density functions defined on $[\lambda MIN, \lambda MAX]$ and $[tMIN, tMAX]$ (Ref. 7, Sect. 4.3.1), and (iii) Eq. (VIII.2.8) is the importance sampling approximation to the integral defining $E_A[D(\tau|t, \nu)]$, and hence to $E_A[D(\tau|t, \nu)]$, obtained with a random or Latin hypercube sample $[t_i, \lambda_i]$, $i = 1, 2, \dots, nIMP$, generated from $[tMIN, tMAX] \times [\lambda MIN, \lambda MAX]$ in consistency with the definitions of the density functions $t IMP(t)$ and $\lambda IMP(\lambda)$.^{9, 10} It is important to recognize that the distributions used in importance sampling have nothing to do with the treatment of uncertainty; they are simply numerical devices used to accelerate the convergence of Monte Carlo integration procedures and have no effect on the value of the integral being evaluated.

As examples, $\lambda IMP(\lambda)$ and $t IMP(t)$ are often assumed to correspond to uniform or loguniform distributions. Specifically, uniform and loguniform importance sampling distributions for λ result in $\lambda IMP(\lambda)$ being defined by

$$\lambda IMP_u(\lambda) = \begin{cases} 1/(\lambda MAX - \lambda MIN) & \text{for } \lambda MIN \leq \lambda \leq \lambda MAX \\ 0 & \text{otherwise} \end{cases} \quad (\text{VIII.2.9})$$

and

$$\lambda IMP_{lu}(\lambda) = \begin{cases} 1/[\lambda \ln(\lambda MAX/\lambda MIN)] & \text{for } \lambda MIN \leq \lambda \leq \lambda MAX \\ 0 & \text{otherwise,} \end{cases} \quad (\text{VIII.2.10})$$

respectively. The density functions $t IMP_u(t)$ and $t IMP_{lu}(t)$ are defined analogously for uniform and loguniform sampling, respectively, on $[tMIN, tMAX]$.

For uniform sampling on $[\lambda MIN, \lambda MAX]$ and $[tMIN, tMAX]$ in consistency with the density functions $\lambda IMP_u(\lambda)$ and $t IMP_u(t)$, the approximation to $E_A[D(\tau|t, \nu)]$ in Eq. (VIII.2.8) becomes

$$E_A[D(\tau|t, \nu)] \cong \left[\frac{(\lambda MAX - \lambda MIN)(t MAX - t MIN)}{nIMP} \right] \sum_{i=1}^{nIMP} D(\tau|t_i, \lambda_A^{-1}(\lambda_i)). \quad (\text{VIII.2.11})$$

For loguniform sampling on $[\lambda MIN, \lambda MAX]$ and $[tMIN, tMAX]$ in consistency with the density functions $\lambda IMP_{lu}(\lambda)$ and $t IMP_{lu}(t)$, the approximation to $E_A[D(\tau|t, \nu)]$ in Eq. (VIII.2.8) becomes

$$E_A[D(\tau|t, \nu)] \cong \left[\frac{\ln(\lambda MAX/\lambda MIN) \ln(t MAX/t MIN)}{nIMP} \right] \sum_{i=1}^{nIMP} t_i \lambda_i D(\tau|t_i, \lambda_A^{-1}(\lambda_i)). \quad (\text{VIII.2.12})$$

Other definitions for $\lambda IMP(\lambda)$ and $t IMP(t)$ result in analogous approximations to $E_A[D(\tau|t, \nu)]$.

The development of $E_A[D(\tau|t, v)]$ ends with a reminder that $E_A[D(\tau|t, v)]$ does not correspond to an actual dose received by the RMEI. Rather, $E_A[D(\tau|t, v)]$ is the expected (i.e., average) value of the infinitely many possible doses that the RMEI could receive at time τ from the infinitely many possible seismic events that could (but probably will not) occur before time τ . In particular, $E_A[D(\tau|t, v)]$ is the result of reducing all these possible doses and their associated “likelihood” to a single number through the integration processes described in Eqs. (VIII.2.3) and (VIII.2.4).

The character and likelihood of the actual doses that the RMEI could receive is preserved when the results of the analysis are presented as a distribution rather than as an expected value (Fig. VIII-3). Exactly the same information is used in the development of distributions for dose and expected values for dose; the only difference is in the details of the processing of this information. For example, the complementary cumulative distribution function (CCDF) for dose to the RMEI at time τ is defined by

$$prob_A[D(\tau|t, v) > D] = \int_{t_{MIN}}^{\tau} \int_{v_{MIN}}^{v_{MAX}} \delta_D[D(\tau|t, v)] [-d\lambda_A(v)/dv] dv dt \quad (VIII.2.13)$$

$$= \int_{t_{MIN}}^{\tau} \int_{\lambda_{MIN}}^{\lambda_{MAX}} \delta_D[D(\tau|t, \lambda_A^{-1}(\lambda))] d\lambda dt, \quad (VIII.2.14)$$

where $prob_A[D(\tau|t, v) > D]$ is the probability that the RMEI will receive a dose at time τ (i.e., $D(\tau|t, v)$) that exceeds a dose of size D and the indicator function δ_D is defined by

$$\delta_D[D(\tau|t, v)] = \begin{cases} 1 & \text{if } D(\tau|t, v) > D \\ 0 & \text{otherwise.} \end{cases} \quad (VIII.2.15)$$

Except for the indicator function δ_D , the integrals defining $E_A[D(\tau|t, v)]$ in Eqs. (VIII.2.3) and (VIII.2.4) and the integrals defining $prob_A[D(\tau|t, v) > D]$ in Eqs. (VIII.2.13) and (VIII.2.14) are the same. Thus, the same evaluations of $D(\tau|t, v)$ that are used to estimate $E_A[D(\tau|t, v)]$ can also be used to estimate $prob_A[D(\tau|t, v) > D]$. In particular, the expected dose associated with the distribution defined by the CCDF in Fig. VIII-3 is the quantity $E_A[D(\tau|t, v)]$ defined in Eqs. (VIII.2.3) – (VIII.2.4); thus, the expected dose curve ($\tau, E_A[D(\tau|t, v)]$) in Fig. VIII-2 is a summary of the result of reducing distributions of the form shown in Fig. VIII-3 to expected values.

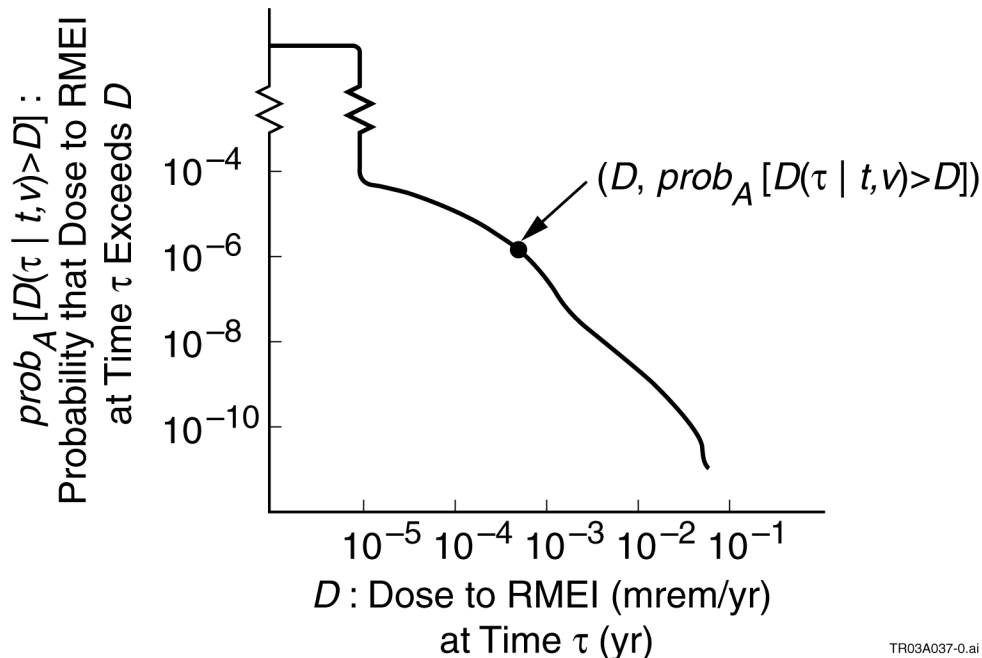


Fig. VIII-3. Illustration of complementary cumulative distribution function (CCDF) of dose (mrem/yr) to RMEI at time τ (yr) i.e., a plot of $(D, prob_A [D(\tau | t, \nu) > D])$.

As noted earlier, the integral representations for $E_A[D(\tau | t, \nu)]$ in Eqs. (VIII.2.3) and (VIII.2.4) are only valid if either (i) the occurrence of a seismic event has no effect on the dose to the RMEI that derives from any subsequent seismic event or (ii) $\lambda_{MAX}(\tau - t_{MIN})$ is sufficiently small to render the likelihood of two or more seismic events over the time interval $[t_{MIN}, \tau]$ inconsequential. A stronger restriction is required for the validity of the integral representations of $prob_A [D(\tau | t, \nu) > D]$ in Eqs. (VIII.2.13) and (VIII.2.14). In particular, these representations are valid only if (ii) above is satisfied. This constraint is necessary because the indicator function δ_D in Eqs. (VIII.2.13) and (VIII.2.14) is applied to the dose resulting from a single seismic event and thus the additive effects of two or more seismic events occurring before time τ is not incorporated into $prob_A [D(\tau | t, \nu) > D]$. The appropriate formalism for the incorporation of the synergisms that could possibly exist in the determination of dose subsequent to multiple seismic events is discussed in a later section (Sect. VIII.4).

VIII.3 ALEATORY AND EPISTEMIC UNCERTAINTY

The preceding section (Sect. VIII.2) introduces the calculation of expected dose $E_A[D(\tau | t, \nu)]$ at time τ from seismic events to the RMEI. The indicated expectation is over events that can occur in the future. As indicated in the Introduction (Sect. VIII.1), uncertainty with respect to what can occur in the future is referred to as aleatory uncertainty, and in the example of the preceding section, its probabilistic nature was characterized by the function $\lambda_A(\nu)$. Specifically, aleatory uncertainty arises from the many possible seismic events that could occur over a time period of interest (e.g., 0 to 10,000 yr). If only aleatory uncertainty was present and $D(\tau | t, \nu)$ and $\lambda_A(\nu)$ were known with complete certainty, then the expected dose $E_A[D(\tau | t, \nu)]$ would derive solely from aleatory uncertainty and could be calculated with complete certainty.

Unfortunately, quantities such as $D(\tau | t, \nu)$ and $\lambda_A(\nu)$ can never be known with complete certainty in a PA as complex as the one that must be carried out for the YM facility. As a result, there is significant state of knowledge uncertainty with respect to how $D(\tau | t, \nu)$ and $\lambda_A(\nu)$ should be defined (Fig. VIII-4). This type of uncertainty is referred to as epistemic uncertainty to distinguish it from the previously introduced concept of aleatory uncertainty. Specifically, epistemic uncertainty arises from a lack of knowledge with respect to quantities used in the

characterization of aleatory uncertainty or in the calculation of doses or other effects given the occurrence of a seismic event.

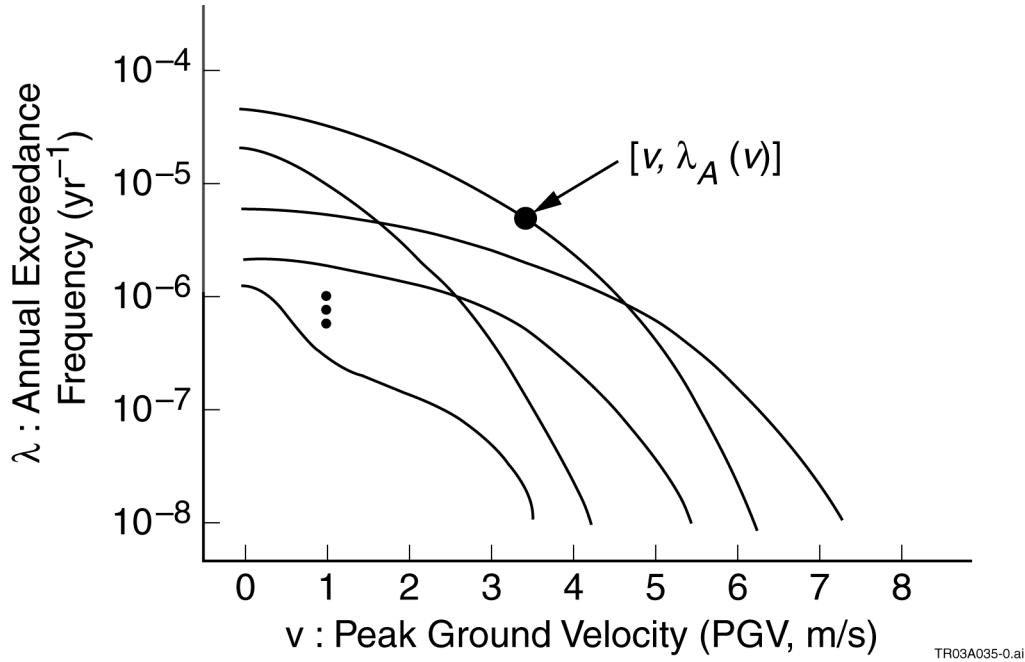


Fig. VIII-4. Illustration of multiple exceedance frequency curves $\lambda_A(v)$ resulting from epistemic uncertainty in PGV at disposal drifts induced by seismic events.

The notation introduced in the previous section (Sect. VIII.2) for $D(\tau | t, v)$ and $\lambda_A(v)$ can be expanded to explicitly display a dependence on imprecisely known quantities. Specifically, $D(\tau | t, v)$ and $\lambda_A(v)$ can be represented by $D(\tau | t, v, \mathbf{e}_D)$ and $\lambda_A(v | \mathbf{e}_A)$, where

$$\mathbf{e}_D = [e_{D1}, e_{D2}, \dots, e_{D,nD}] \tag{VIII.3.1}$$

is a vector of imprecisely known variables required in the determination of $D(\tau | t, v)$, and

$$\mathbf{e}_A = [e_{A1}, e_{A2}, \dots, e_{A,nA}] \tag{VIII.3.2}$$

is a vector of imprecisely known variables required in the definition of $\lambda_A(v)$. The fundamental idea is that the analysis has been developed to the point that it is believed that the elements of \mathbf{e}_A and \mathbf{e}_D should have fixed values and that appropriate analysis results would be obtained if these fixed values were known. Unfortunately, the appropriate values for these quantities are not known with certainty, and so there is epistemic uncertainty with respect to what their values should be. The elements of \mathbf{e}_A and \mathbf{e}_D can be interpreted generally enough to include imprecisely known functions and designators for alternative models. For notational convenience,

$$\mathbf{e} = [\mathbf{e}_A, \mathbf{e}_D] = [e_1, e_2, \dots, e_{nE}] \tag{VIII.3.3}$$

can be used to represent the vector of all imprecisely known variables.

Inclusion of a dependence on $\mathbf{e} = [\mathbf{e}_A, \mathbf{e}_D]$ results in the representations for $E_A[D(\tau | t, v)]$ in Eqs. (VIII.2.3) and (VIII.2.4) having the form

$$E_A [D(\tau | t, v, \mathbf{e})] = \int_{t_{MIN}}^{\tau} \int_{v_{MIN}}^{v_{MAX}} D(\tau | t, v, \mathbf{e}_D) [-d\lambda_A(v | \mathbf{e}_A) / dv] dv dt \quad (VIII.3.4)$$

$$= \int_{t_{MIN}}^{\tau} \int_{\lambda_{MIN}}^{\lambda_{MAX}} D(\tau | t, \lambda_A^{-1}(\lambda | \mathbf{e}_A), \mathbf{e}_D) d\lambda dt \quad (VIII.3.5)$$

The preceding notation emphasizes that the possible values for $\mathbf{e} = [\mathbf{e}_A, \mathbf{e}_D]$ result in different possible values for $\lambda_A(v | \mathbf{e}_A)$, $D(\tau | t, v, \mathbf{e}_D)$ and thus $E_A[D(\tau | t, v, \mathbf{e})]$. As \mathbf{e}_D only affects the calculation of dose and \mathbf{e}_A only affects the distributions that characterize aleatory uncertainty in t and v , $E_A[D(\tau | t, v, \mathbf{e}_D) | \mathbf{e}_A]$ or $E_A[D(\tau | t, v) | \mathbf{e}_A, \mathbf{e}_D]$ are probably more conceptually correct notational representations for expected dose from aleatory uncertainty than $E_A[D(\tau | t, v, \mathbf{e})]$; however, for notational simplicity, the use of $E_A[D(\tau | t, v, \mathbf{e})]$ to represent this dose will be retained. Fortunately, the integrals in Eqs. (VIII.3.4) and (VIII.3.5) remove all ambiguity with respect to exactly what is represented by $E_A[D(\tau | t, v, \mathbf{e})]$.

Analyses for the YM facility, like most large PAs, use probability to characterize epistemic uncertainty. Specifically, distributions

$$D_1, D_2, \dots, D_{nE} \quad (VIII.3.6)$$

are specified for the elements of \mathbf{e} , where D_k is the distribution assigned to e_k . Correlations and other restrictions involving pairs or larger groups of variables are also possible. These distributions and any associated restrictions provide a numerical quantification of what is known about individual variables and also the necessary starting structure to propagate this knowledge through the overall analysis. For notational convenience, the set of all possible values for \mathbf{e} associated with the distributions in Eq. (VIII.3.6) will be represented by the set \mathbb{E} (i.e., \mathbb{E} is the sample space or universal set associated with epistemic uncertainty) and the corresponding density function defined on \mathbb{E} will be represented by $d_{\mathbb{E}}(\mathbf{e})$.

Each element \mathbf{e} of \mathbb{E} gives rise to a value for the expected dose $E_A[D(\tau | t, v, \mathbf{e})]$ indicated in Eqs. (VIII.3.4) and (VIII.3.5) (Fig. VIII-5). One way of describing the (epistemic) uncertainty in $E_A[D(\tau | t, v, \mathbf{e})]$ is to determine and present the range of values for $E_A[D(\tau | t, v, \mathbf{e})]$ that results from all possible values of \mathbf{e} contained in \mathbb{E} . This is the simplest of all approaches to uncertainty analysis and is typically referred to as interval analysis.

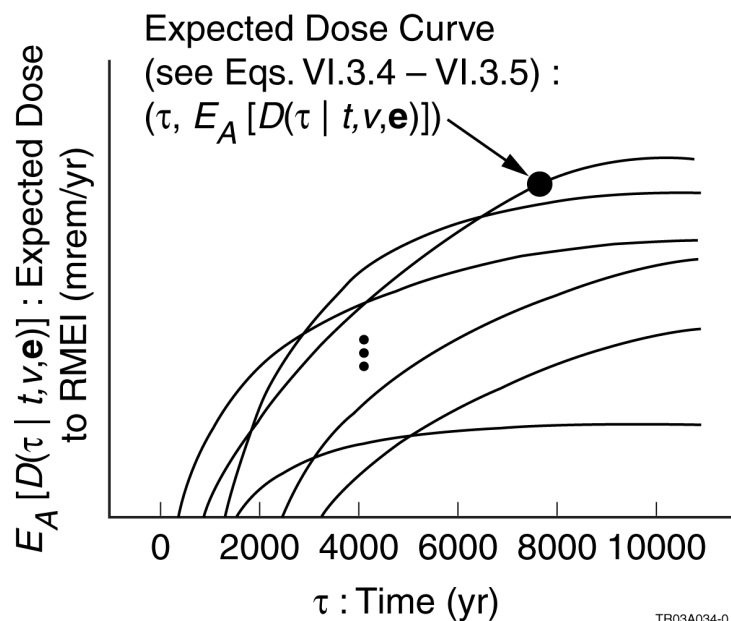


Fig. VIII-5. Illustration of expected dose curves to RMEI resulting from epistemic uncertainty (i.e., plots of $(\tau, E_A[D(\tau | t, v, \mathbf{e})])$ for $0 \leq \tau \leq 10,000$ yr and different values of \mathbf{e} ; see Eqs. (VIII.3.4) – (VIII.3.5)).

The specification of the distributions in Eq. (VIII.3.6) provides the necessary information to carry out more sophisticated uncertainty assessments than simple interval analysis. More specifically, the distributions in Eq. (VIII.3.6) provide the basis for calculating both the expected value and the distribution of $E_A[D(\tau | t, v, \mathbf{e})]$ that arise from possible values for \mathbf{e} (Fig. VIII-6). In particular, the expected value $E_E(E_A[D(\tau | t, v, \mathbf{e})])$ of $E_A[D(\tau | t, v, \mathbf{e})]$ over epistemic uncertainty is given by

$$E_E \left(E_A \left[D(\tau | t, v, \mathbf{e}) \right] \right) = \int_{\mathbf{E}} E_A \left[D(\tau | t, v, \mathbf{e}) \right] d_E(\mathbf{e}) dE \tag{VIII.3.7}$$

$$= \int_{\mathbf{E}} \left[\int_{t_{MIN}}^{t_{MAX}} \int_{v_{MIN}}^{v_{MAX}} D(\tau | t, v, \mathbf{e}_D) \left[-d\lambda_A(v | \mathbf{e}_A) / dv \right] dv dt \right] d_E(\mathbf{e}) dE \tag{VIII.3.8}$$

$$= \int_{\mathbf{E}} \left[\int_{t_{MIN}}^{t_{MAX}} \int_{\lambda_{MIN}}^{\lambda_{MAX}} D(\tau | t, \lambda_A^{-1}(\lambda | \mathbf{e}_A), \mathbf{e}_D) dv dt \right] d_E(\mathbf{e}) dE, \tag{VIII.3.9}$$

where \mathbf{E} and $d_E(\mathbf{e})$ are defined in conjunction with Eq. (VIII.3.6) and dE corresponds to an increment of volume from \mathbf{E} .

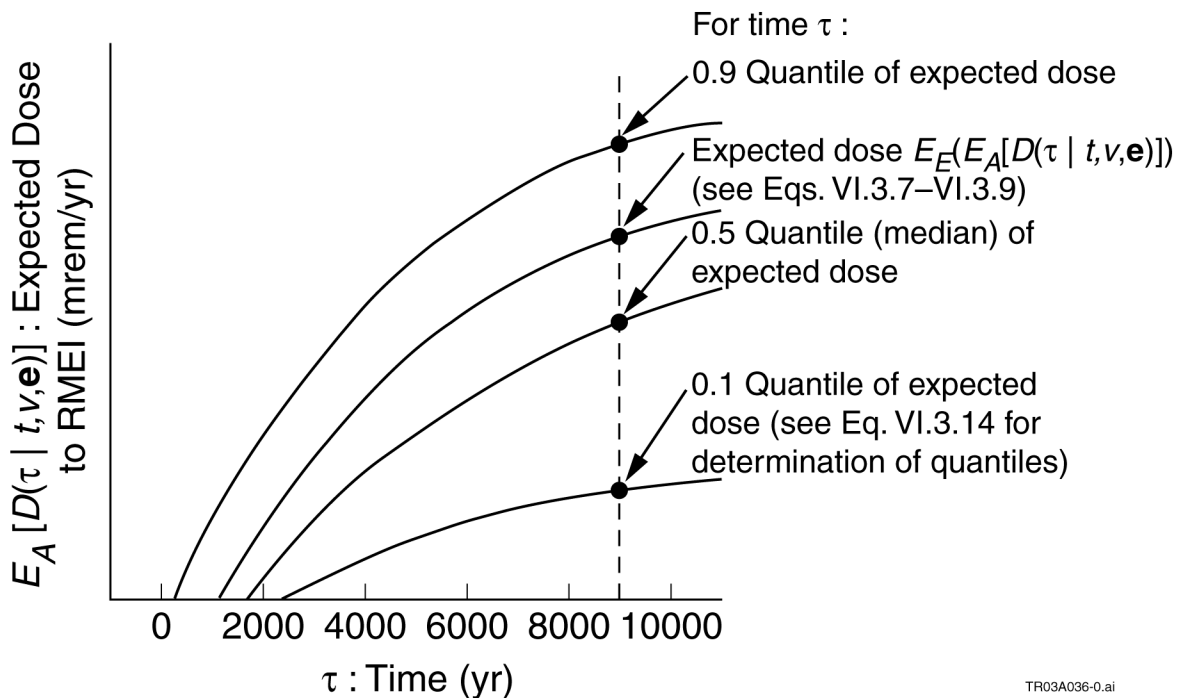


Fig. VIII-6. Illustration of expected and selected quantile curves for distribution of expected (over aleatory uncertainty) dose curves resulting from epistemic uncertainty (i.e., the indicated expected and quantile curves derive from the epistemic uncertainty in \mathbf{e} and result from integration over the set \mathbf{E} of possible values for \mathbf{e}).

Similarly, the epistemic (i.e., degree of belief) probability $prob_E(E_A[D(\tau|t, v, \mathbf{e})] > E)$ of exceeding an expected dose to the RMEI of size E is given by

$$prob_E(E_A[D(\tau|t, v, \mathbf{e})] > E) = \int_{\mathbf{E}} \delta_E(E_A[D(\tau|t, v, \mathbf{e})]) d_E(\mathbf{e}) dE \quad (\text{VIII.3.10})$$

$$= \int_{\mathbf{E}} \delta_E \left[\int_{t_{MIN}}^{t_{MAX}} \int_{v_{MIN}}^{v_{MAX}} D(\tau|t, v, \mathbf{e}_D) [-d\lambda_A(v|\mathbf{e}_A)/dv] dv dt \right] d_E(\mathbf{e}) dE \quad (\text{VIII.3.11})$$

$$= \int_{\mathbf{E}} \delta_E \left[\int_{t_{MIN}}^{t_{MAX}} \int_{\lambda_{MIN}}^{\lambda_{MAX}} D(\tau|t, \lambda_A^{-1}(\lambda|\mathbf{e}_A), \mathbf{e}_D) d\lambda dt \right] d_E(\mathbf{e}) dE, \quad (\text{VIII.3.12})$$

where the indicator function δ_E is defined by

$$\delta_E(E_A[D(\tau|t, v, \mathbf{e})]) = \begin{cases} 1 & \text{if } E_A[D(\tau|t, v, \mathbf{e})] > E \\ 0 & \text{otherwise} \end{cases} \quad (\text{VIII.3.13})$$

and plays the same role as the indicator function δ_D in Eqs. (VIII.2.13) and (VIII.2.14). The q th quantile (e.g., 0.1, 0.5, 0.9) for $E_A[D(\tau|t, v, \mathbf{e})]$ is obtained by solving the equation

$$q = prob_E(E_A[D(\tau|t, v, \mathbf{e})] > E) \quad (\text{VIII.3.14})$$

for E (see Fig. VIII-6).

Two computational strategies for the estimation of $E_E(E_A[D(\tau|t, v, \mathbf{e})])$ are presented. The first strategy involves first approximating the integral over \mathbf{E} and then approximating the integrals that define $E_A[D(\tau|t, v, \mathbf{e})]$. The second strategy involves treating $E_E(E_A[D(\tau|t, v, \mathbf{e})])$ as being defined by a single integral over the high dimensional space \mathbf{AE} defined by

$$\begin{aligned} \mathbf{AE} &= [t_{MIN}, t_{MAX}] \times [\lambda_{MIN}, \lambda_{MAX}] \times \mathbf{E} \\ &= \{ \mathbf{ae} : \mathbf{ae} = [t, \lambda, \mathbf{e}], t_{MIN} \leq t \leq t_{MAX}, \lambda_{MIN} \leq \lambda \leq \lambda_{MAX}, \mathbf{e} \in \mathbf{E} \} \end{aligned} \quad (\text{VIII.3.15})$$

and then approximating this integral without drawing a distinction between the parts that derive from aleatory uncertainty and the parts that derive from epistemic uncertainty.

In Strategy 1, a random or Latin hypercube sample

$$\mathbf{e}_k = [\mathbf{e}_{Ak}, \mathbf{e}_{Dk}] = [e_{1k}, e_{2k}, \dots, e_{n_{E,k}}], k = 1, 2, \dots, nS, \quad (\text{VIII.3.16})$$

is generated from \mathbf{E} in consistency with the distributions indicated in Eq. (VIII.3.6). Then, $E_E(E_A[D(\tau|t, v, \mathbf{e})])$ is approximated by

$$E_E(E_A[D(\tau|t, v, \mathbf{e})]) \cong \sum_{k=1}^{nS} E_A[D(\tau|t, v, \mathbf{e}_k)] / nS. \quad (\text{VIII.3.17})$$

To complete the approximation of $E_E(E_A[D(\tau|t, v, \mathbf{e})])$, approximations $\hat{E}_A[D(\tau|t, v, \mathbf{e}_k)]$ to $E_A[D(\tau|t, v, \mathbf{e}_k)]$ for $k = 1, 2, \dots, nS$ must be developed. Possibilities for the determination of $\hat{E}_A[D(\tau|t, v, \mathbf{e}_k)]$ include (i) use of the

importance sampling procedures indicated in conjunction with Eqs. (VIII.2.6) – (VIII.2.12) and (ii) development of computationally efficient procedures that depend on specific properties of the problem under consideration. Once the approximations $\hat{E}_A [D(\tau|t, v, \mathbf{e}_k)]$ to $E_A[D(\tau|t, v, \mathbf{e}_k)]$ are determined,

$$E_E \left(E_A \left[D(\tau|t, v, \mathbf{e}) \right] \right) \cong \sum_{k=1}^{nS} \hat{E}_A \left[D(\tau|t, v, \mathbf{e}_k) \right] / nS \quad (\text{VIII.3.18})$$

provides the final approximation to $E_E(E_A[D(\tau|t, v, \mathbf{e})])$.

With Strategy 1, the same numerical results used to estimate $E_E(E_A[D(\tau|t, v, \mathbf{e})])$ can also be used to estimate $\text{prob}_E(E_A[D(\tau|t, v, \mathbf{e})] > E)$. Specifically,

$$\text{prob}_E \left(E_A \left[D(\tau|t, v, \mathbf{e}) \right] > E \right) = \sum_{k=1}^{nS} \delta_E \left(\hat{E}_A \left[D(\tau|t, v, \mathbf{e}_k) \right] \right) / nS, \quad (\text{VIII.3.19})$$

where the indicator function δ_E is defined in Eq. (VIII.3.13). Strategy 1 also provides the mapping

$$\left(\mathbf{e}_k, \hat{E}_A \left[D(\tau|t, v, \mathbf{e}_k) \right] \right), k = 1, 2, \dots, nS, \quad (\text{VIII.3.20})$$

between uncertain analysis inputs (i.e., the \mathbf{e}_k) and analysis results (i.e., the $\hat{E}_A [D(\tau|t, v, \mathbf{e}_k)]$) that can be explored with a variety of sensitivity analysis procedures to determine the effects of individual uncertain analysis inputs on expected dose.¹¹

In Strategy 2, a random or Latin hypercube sample

$$\mathbf{ae}_k = [t_k, \lambda_k, \mathbf{e}_{Ak}, \mathbf{e}_{Dk}] = [t_k, \lambda_k, e_{1k}, e_{2k}, \dots, e_{nE,k}], k = 1, 2, \dots, nS, \quad (\text{VIII.3.21})$$

is generated from \mathbf{AE} (see Eq. (VIII.3.14)) in consistency with whatever sampling distributions are assigned to t and λ (see Eqs. (VIII.2.6) – (VIII.2.12)) and also in consistency with the distributions indicated in Eq. (VIII.3.6) for the elements of $\mathbf{e} = [\mathbf{e}_A, \mathbf{e}_D]$. Then, $E_E(E_A[D(\tau|t, v, \mathbf{e})])$ as represented in Eq. (VIII.3.9) is approximated by

$$E_E \left(E_A \left[D(\tau|t, v, \mathbf{e}) \right] \right) \cong \sum_{k=1}^{nS} \left[\frac{D(\tau|t_k, \lambda_A^{-1}(\lambda_k | \mathbf{e}_{Ak}), \mathbf{e}_{Dk})}{\lambda_{IMP}(\lambda_k) t_{IMP}(t_k)} \right] / nS, \quad (\text{VIII.3.22})$$

where $\lambda_{IMP}(\lambda)$ and $t_{IMP}(t)$ are the sampling distributions for λ and t (see Eqs. (VIII.2.9) – (VIII.2.12)). In particular,

$$E_E \left(E_A \left[D(\tau|t, v, \mathbf{e}) \right] \right) \cong \left[\frac{(\lambda_{MAX} - \lambda_{MIN})(t_{MAX} - t_{MIN})}{nS} \right] \sum_{k=1}^{nS} D(\tau|t_k, \lambda_A^{-1}(\lambda_k | \mathbf{e}_{Ak}), \mathbf{e}_{Dk}), \quad (\text{VIII.3.23})$$

if $\lambda_{IMP}(\lambda)$ and $t_{IMP}(t)$ correspond to uniform distributions on $[\lambda_{MIN}, \lambda_{MAX}]$ and $[t_{MIN}, t_{MAX}]$ (see Eqs. (VIII.2.9) and (VIII.2.11)), and

$$E_E \left(E_A \left[D(\tau|t, v, \mathbf{e}) \right] \right) \cong \left[\frac{\ln(\lambda_{MAX}/\lambda_{MIN}) \ln(t_{MAX}/t_{MIN})}{nS} \right] \sum_{k=1}^{nS} t_k \lambda_k D(\tau|t_k, \lambda_A^{-1}(\lambda_k | \mathbf{e}_{Ak}), \mathbf{e}_{Dk}) \quad (\text{VIII.3.24})$$

if $\lambda IMP(\lambda)$ and $tIMP(t)$ correspond to loguniform distributions on $[\lambda MIN, \lambda MAX]$ and $[tMIN, tMAX]$ (see Eqs. (VIII.2.10) and (VIII.2.12)). Analogous approximations also hold for $E_E[E_A[D(\tau|t, v, \mathbf{e})]]$ as represented in Eq. (VIII.3.8).

With Strategy 2, it is not possible to estimate the expected doses $E_A[D(\tau|t, v, \mathbf{e})]$ to the RMEI for different values of \mathbf{e} . This inability results from the concurrent variation of the aleatory variables t_k and $v_k = \lambda_A^{-1}(\lambda_k | \mathbf{e}_{Ak})$ and the epistemic variables $e_{1k}, e_{2k}, \dots, e_{nE,k}$ associated with $\mathbf{e}_k = [\mathbf{e}_{Ak}, \mathbf{e}_{Dk}]$ in the determination of the doses

$$D\left(\tau|t_k, \lambda_A^{-1}(\lambda_k | \mathbf{e}_{Ak}), \mathbf{e}_{Dk}\right), k = 1, 2, \dots, nS, \quad (\text{VIII.3.25})$$

to the RMEI that are calculated for each sample element \mathbf{ae}_k (see Eq. (VIII.3.21)) in Strategy 2. Specifically, because dose to the RMEI is known for only one pair $[t_k, v_k]$ of time, PGV values for each vector $\mathbf{e}_k = [\mathbf{e}_{Ak}, \mathbf{e}_{Dk}]$ of epistemic variable values, it is not possible to estimate the integral over time and PGV that defines the expected dose $E_A[D(\tau|t, v, \mathbf{e}_k)]$ associated with \mathbf{e}_k . As a result, Strategy 2 does not provide a basis to estimate the uncertainty in expected dose $E_A[D(\tau|t, v, \mathbf{e})]$ to the RMEI as defined by $prob_E[E_A[D(\tau|t, v, \mathbf{e})] > E]$ in Eqs. (VIII.3.10) – (VIII.3.12).

Strategy 2 does allow an estimate of the uncertainty in the dose to the RMEI due to both aleatory and epistemic uncertainty. In particular, this uncertainty is characterized by the probability

$$prob_{EA}\left[D(\tau|t, v, \mathbf{e}_D) > D\right] = \int_E \int_{tMIN}^{tMAX} \int_{vMIN}^{vMAX} \delta_D\left[D(\tau|t, v, \mathbf{e}_D)\right] \left[-d\lambda_A(v|\mathbf{e}_A)/dv\right] d_E(\mathbf{e}) dv dt dE \quad (\text{VIII.3.26})$$

$$= \int_E \int_{tMIN}^{tMAX} \int_{\lambda MIN}^{\lambda MAX} \delta_D\left[D\left(\tau|t, \lambda_A^{-1}(\lambda|\mathbf{e}_A), \mathbf{e}_D\right)\right] d_E(\mathbf{e}) dv dt dE \quad (\text{VIII.3.27})$$

$$\cong \sum_{k=1}^{nS} \left[\frac{\delta_D\left[D\left(\tau|t_k, \lambda_A^{-1}(\lambda_k|\mathbf{e}_{Ak}), \mathbf{e}_{Dk}\right)\right]}{\lambda IMP(\lambda_k) tIMP(t_k)} \right] / nS, \quad (\text{VIII.3.28})$$

where (i) the indicator function δ_D is defined in Eq. (VIII.2.15), (ii) the density functions $\lambda IMP(\lambda)$ and $tIMP(t)$ are the same as indicated in conjunction with Eqs. (VIII.2.6 – VIII.2.12), and (iii) the sample elements $\mathbf{ae}_k = [t_k, \lambda_k, \mathbf{e}_{Ak}, \mathbf{e}_{Dk}]$, $k = 1, 2, \dots, nS$, correspond to the sample in Eq. (VIII.3.21). The preceding probability defines the CCDF for dose to the RMEI (i.e., $D(\tau|t, v, \mathbf{e}_D)$) that derives from both aleatory and epistemic uncertainty and is very different from the probability $prob_E[E_A[D(\tau|t, v, \mathbf{e})] > E]$ defined in Eqs. (VIII.3.10) – (VIII.3.12), which defines the CCDF for expected dose to the RMEI (i.e., $E_A[D(\tau|t, v, \mathbf{e})]$) that derives from epistemic uncertainty.

Strategy 2 provides the following mapping from analysis inputs to analysis results:

$$\left[\mathbf{ae}_k, D\left(\tau|t_k, v_k, \mathbf{e}_{Dk}\right)\right], k = 1, 2, \dots, nS, \quad (\text{VIII.3.29})$$

where $v_k = \lambda_A^{-1}(\lambda_k | \mathbf{e}_{Ak})$. Like the mapping in Eq. (VIII.3.20) associated with Strategy 1, this mapping can be explored with a variety of sensitivity analysis procedures¹². However, the interpretation of any results obtained in such a sensitivity analysis would be very different from the interpretation of results obtained from a sensitivity analysis of the mapping in Eq. (VIII.3.20) for two reasons. First, the mapping in Eq. (VIII.3.20) obtained with Strategy 1 involves expected dose to the RMEI (i.e., $E_A[D(\tau|t, v, \mathbf{e})]$) while the mapping in Eq. (VIII.3.29) obtained with Strategy 2 involves dose to the RMEI (i.e., $D(\tau|t, v, \mathbf{e})$). Hence, the dependent variables under study are not

the same. Second, the mapping obtained with Strategy 1 involves only epistemic uncertainty while the mapping obtained with Strategy 2 involves both epistemic uncertainty and aleatory uncertainty. Thus, the uncertainty spaces being sampled from (i.e., \mathbf{E} and \mathbf{AE}) are fundamentally different.

If implemented correctly and with sufficiently large sample sizes to assure convergence, both strategies will produce the same value for the expected dose $E_E(E_A[D(\tau|t, v, \mathbf{e})])$. Strategy 1 has the advantage that it permits uncertainty and sensitivity studies of the effects of epistemic uncertainty on the expected dose to the RMEI (i.e., $E_A[D(\tau|t, v, \mathbf{e})]$); such studies are not possible with Strategy 2. Strategy 2 has the advantage that it is likely to be more computationally efficient (i.e., require fewer evaluations of $D(\tau|t, v, \mathbf{e})$) in the determination of $E_E(E_A[D(\tau|t, v, \mathbf{e})])$ than Strategy 1.

Both computational strategies are used in the determination of expected dose to the RMEI from igneous events at the YM facility. In particular, the expected dose $E_E(E_A[D(\tau|t, v, \mathbf{e})])$ from the eruptive component of igneous events is calculated with Strategy 1, and the expected dose $E_E(E_A[D(\tau|t, v, \mathbf{e})])$ from the groundwater release component of igneous events is calculated with Strategy 2. Thus, when viewed at a sufficiently high-level, the calculation of expected doses $E_E(E_A[D(\tau|t, v, \mathbf{e})])$ from seismic events, the eruptive component of igneous events, and the groundwater component of igneous events is conceptually the same, although the uncertain variables, the representation of aleatory uncertainty, and the dose models are at least partially different for these three cases.

VIII.4 EXPECTED DOSE FROM ALEATORY AND EPISTEMIC UNCERTAINTY INCLUDING SYNERGISMS

The computational procedures for the calculation of expected doses presented in the two preceding sections (Sects. VIII.2, VIII.3) are predicated on the assumption that the occurrence of a seismic event has no effect on doses that derive from any subsequent seismic event. Further, the computational procedures presented for the determination of distributions of doses do not include the possibility of multiple seismic events occurring before a given time. This section briefly presents the formal representations for expected dose and distribution of expected dose that includes the possibility of synergisms between multiple seismic events on dose subsequent to these events.

For this representation, the occurrence of multiple seismic events between $tMIN$ and $tMAX$ is assumed to be possible. The properties of a sequence of seismic event occurring between $tMIN$ and $tMAX$ is represented by a vector

$$\mathbf{a} = [\mathbf{a}_1, \mathbf{a}_2, \dots, \mathbf{a}_{nO}], \quad (\text{VIII.4.1})$$

where

$$\mathbf{a}_i = [\mathbf{a}_{i1}, \mathbf{a}_{i2}, \dots, \mathbf{a}_{i,nP}] \quad (\text{VIII.4.2})$$

is the vector of properties (e.g., time of occurrence, PGV, extent of rock fall, ...) that, in essence, defines the i^{th} seismic event occurring between $tMIN$ and $tMAX$. If time of occurrence and PGV are the only two defining characteristics of a seismic event, then \mathbf{a}_i would be defined by

$$\mathbf{a}_i = [t_i, v_i], \quad (\text{VIII.4.3})$$

where t_i and v_i are the time of occurrence and PGV associated with the i^{th} seismic event, and \mathbf{a} would be defined by

$$\begin{aligned} \mathbf{a} &= [\mathbf{a}_{i1}, \mathbf{a}_{i2}, \dots, \mathbf{a}_{nO}] \\ &= [t_1, v_1, t_2, v_2, \dots, t_{nO}, v_{nO}]. \end{aligned} \quad (\text{VIII.4.4})$$

For completeness, \mathbf{a}_0 can be used to represent the degenerate vector (i.e., the vector with no components) that corresponds to no seismic events occurring between $tMIN$ and $tMAX$. Then, the set \mathbf{A} containing \mathbf{a}_0 and all possible vectors \mathbf{a} of the form indicated in Eq. (VIII.4.1) corresponds to the universe (i.e., sample space) of all possible sequences of seismic events that could occur over the time interval $[tMIN, tMAX]$.

Aleatory uncertainty with respect to the potential occurrence of the sequences of seismic events represented by the elements of \mathbf{A} is characterized by a probability distribution defined on \mathbf{A} . For notational convenience, this distribution is represented by its density function $d_A(\mathbf{a})$, where the probability $prob_A(\mathbf{U})$ of a subset \mathbf{U} of \mathbf{A} is given by

$$prob_A(\mathbf{U}) = \int_{\mathbf{U}} d_A(\mathbf{a}) dA. \quad (\text{VIII.4.5})$$

For example, if the elements of \mathbf{A} are of the form indicated in Eq. (VIII.4.4), then $d_A(\mathbf{a})$ could derive from a function $\lambda_A(v)$ of the form considered in the two preceding sections (Sects. VIII.2, VIII.3).

The expected dose $E_A[D(\tau|\mathbf{a})]$ to the RMEI at time τ would then be defined by

$$E_A[D(\tau|\mathbf{a})] = \int_{\mathbf{A}} D(\tau|\mathbf{a}) d_A(\mathbf{a}) dA, \quad (\text{VIII.4.6})$$

where

$$D(\tau|\mathbf{a}) = \text{dose (mrem/yr) to the RMEI at time } \tau \text{ from the sequence of seismic events represented by } \mathbf{a}. \quad (\text{VIII.4.7})$$

The representation for $D(\tau|\mathbf{a})$ allows the potential for synergistic interactions involving two or more seismic events. Similarly, the probability $prob_A[D(\tau|\mathbf{a}) > D]$ that the dose to the RMEI at time τ will exceed a dose of size D is given by

$$prob_A[D(\tau|\mathbf{a}) > D] = \int_{\mathbf{A}} \delta_D[D(\tau|\mathbf{a})] d_A(\mathbf{a}) dA, \quad (\text{VIII.4.8})$$

where

$$\delta_D[D(\tau|\mathbf{a})] = \begin{cases} 1 & \text{if } D(\tau|\mathbf{a}) > D \\ 0 & \text{otherwise.} \end{cases} \quad (\text{VIII.4.9})$$

Unlike the representation for $prob_A[D(\tau|t, v)]$ in Eqs. (VIII.2.13) and (VIII.2.14), in which $\mathbf{a} = [t, v]$ corresponds to a single seismic event and $D(\tau|t, v)$ corresponds to the dose from this single event, the preceding representation for $prob_A[D(\tau|\mathbf{a}) > D]$ incorporates the possibility that \mathbf{a} corresponds to multiple seismic events and that $D(\tau|\mathbf{a})$ is affected by some form of interaction (i.e., synergism) involving these events.

As before, epistemic uncertainty is assumed to exist in the elements of a vector $\mathbf{e} = [\mathbf{e}_A, \mathbf{e}_D]$ of the form defined in Eq. (VIII.3.3) with (i) this uncertainty characterized by probability distributions D_1, D_2, \dots, D_{nE} for the elements of \mathbf{e} as indicated in Eq. (VIII.3.6), (ii) the set of all possible values for \mathbf{e} constituting a set \mathbf{E} , and (iii) the distributions D_1, D_2, \dots, D_{nE} giving rise to a density function $d_E(\mathbf{e})$ defined on \mathbf{E} . With the introduction of epistemic uncertainty in the elements of \mathbf{e} , dose $D(\tau|\mathbf{a}, \mathbf{e}_D)$ to the RMEI is a function of \mathbf{e}_D , and expected dose $E_A[D(\tau|\mathbf{a}, \mathbf{e})]$ to the RMEI arising from aleatory uncertainty is a function of both \mathbf{e}_A and \mathbf{e}_D . In particular, the

density function $d_A(\mathbf{a}|\mathbf{e}_A)$ and also possibly the sample space $\bar{A}(\mathbf{e}_A)$ associated with aleatory uncertainty can change as a function of \mathbf{e}_A . As a result, expected dose $E_A[D(\tau|\mathbf{a}, \mathbf{e})]$ arising from aleatory uncertainty now has the form

$$E_A[D(\tau|\mathbf{a}, \mathbf{e})] = \int_{\bar{A}(\mathbf{e}_A)} D(\tau|\mathbf{a}, \mathbf{e}_D) d_A(\mathbf{a}|\mathbf{e}_A) dA, \quad (\text{VIII.4.10})$$

and the expected value $E_E(E_A[D(\tau|\mathbf{a}, \mathbf{e})])$ of $E_A[D(\tau|\mathbf{a}, \mathbf{e})]$ over epistemic uncertainty has the form

$$E_E(E_A[D(\tau|\mathbf{a}, \mathbf{e})]) = \int_{\mathbf{E}} E_A[D(\tau|\mathbf{a}, \mathbf{e})] d_E(\mathbf{e}) dE \quad (\text{VIII.4.11})$$

$$= \int_{\mathbf{E}} \left[\int_{\bar{A}(\mathbf{e}_A)} D(\tau|\mathbf{a}, \mathbf{e}_D) d_A(\mathbf{a}|\mathbf{e}_A) dA \right] d_E(\mathbf{e}) dE. \quad (\text{VIII.4.12})$$

The preceding results are analogous to those in Eqs. (VIII.3.4) and (VIII.3.5) and Eqs. (VIII.3.7) – (VIII.3.9) with a more general dependence on the properties of the seismic events under consideration now incorporated into the representation of dose and expected dose.

The probability $prob_E(E_A[D(\tau|\mathbf{a}, \mathbf{e})] > E)$ that an expected dose of size E will be exceeded is now given by

$$prob_E(E_A[D(\tau|\mathbf{a}, \mathbf{e})] > E) = \int_{\mathbf{E}} \delta_E(E_A[D(\tau|\mathbf{a}, \mathbf{e})]) d_E(\mathbf{e}) dE \quad (\text{VIII.4.13})$$

$$= \int_{\mathbf{E}} \delta_E \left(\int_{\bar{A}(\mathbf{e}_A)} D(\tau|\mathbf{a}, \mathbf{e}_D) d_A(\mathbf{a}|\mathbf{e}_A) dA \right) d_E(\mathbf{e}) dE, \quad (\text{VIII.4.14})$$

where

$$\delta_E(E_A[D(\tau|\mathbf{a}, \mathbf{e})]) = \begin{cases} 1 & \text{if } E_A[D(\tau|\mathbf{a}, \mathbf{e})] > E \\ 0 & \text{otherwise.} \end{cases} \quad (\text{VIII.4.15})$$

The preceding result is analogous to the results in Eqs. (VIII.3.10) – (VIII.3.12) except, as already explained, a more general dependence of dose on the properties of seismic events is allowed.

Computational Strategies 1 and 2 described in the preceding section (Sect. VIII.3) for the evaluation of expected dose $E_E(E_A[D(\tau|\mathbf{a}, \mathbf{e})])$ with $\mathbf{a} = [t, v]$ can also be applied to the evaluation of expected dose with the more complex forms introduced in this section for \mathbf{a} and the dose that derives from \mathbf{a} . The procedures are conceptually the same for both cases and will not be repeated here. However, the same caveats as presented at the end of Sect. VIII.3 still apply. Further, if the probabilistic structure of the set \bar{A} is complicated, the actual construction of iterated integrals and associated density functions for integration over \bar{A} can be a difficult task.

VIII.5 REFERENCES

1. U.S. DOE (U.S. Department of Energy). 2002. *Yucca Mountain Science and Engineering Report*, DOE/RW-0539-1, Rev. 1. Las Vegas, NV: U.S. Department of Energy. [155943]
2. U.S. DOE (U.S. Department of Energy). 2002. *Yucca Mountain Site Suitability Evaluation*, DOE/RW-0549. Las Vegas, NV: U.S. Department of Energy. [156958]
3. Kaplan, S. and B.J. Garrick. 1981. "On the Quantitative Definition of Risk," *Risk Analysis*. Vol. 1, no. 1, pp. 11-27. [100557]
4. Helton, J.C. 1994. "Treatment of Uncertainty in Performance Assessments for Complex Systems," *Risk Analysis*. Vol. 14, no. 4, pp. 483-511. [107739]
5. Paté-Cornell, M.E. 1996. "Uncertainties in Risk Analysis: Six Levels of Treatment," *Reliability Engineering and System Safety*. Vol. 54, no. 2-3, pp. 95-111. [107499]
6. Helton, J.C. 1997. "Uncertainty and Sensitivity Analysis in the Presence of Stochastic and Subjective Uncertainty," *Journal of Statistical Computation and Simulation*. Vol. 57, no. 1-4, pp. 3-76. [107496]
7. Rubinstein, R.Y. 1981. *Simulation and the Monte Carlo Method*. New York: John Wiley & Sons. [163476]
8. Hahn, G.J. and S.S. Shapiro. 1967. *Statistical Models in Engineering*. New York: John Wiley & Sons. [146529]
9. McKay, M.D., R.J. Beckman, and W.J. Conover. 1979. "A Comparison of Three Methods for Selecting Values of Input Variables in the Analysis of Output from a Computer Code," *Technometrics*. Vol. 21, no. 2, pp. 239-245. [127905]
10. Helton, J.C. and F.J. Davis. 2002. *Latin Hypercube Sampling and the Propagation of Uncertainty in Analyses of Complex Systems*, SAND2001-0417. Albuquerque, NM: Sandia National Laboratories. [163475]
11. Helton, J.C. and F.J. Davis. 2000. *Sampling-Based Methods for Uncertainty and Sensitivity Analysis*, SAND99-2240. Albuquerque, NM: Sandia National Laboratories. [156572]